Nanofibrous fibrinogen scaffolds

Towards an understanding of the self-assembly mechanisms and an application as a biomaterial

Dissertation

Zur Erlangung des Doktorgrades in den Naturwissenschaften (Dr. rer. nat.)

Fachbereich 1 (Physik, Elektrotechnik)

Universität Bremen

Karsten Stapelfeldt

Termin des Kolloquiums: 02.10.2020

Erstgutachterin: Prof. Dr. Dorothea Brüggemann

Zweitgutachterin: Prof. Dr. Monika Fritz

Table of contents

List of abbreviations

a.u.	Absorbance unit
AEBSF	4-(2-aminoethyl)benzenesulfonyl fluoride hydrochloride
APTES	(3-Aminopropyl)triethoxysilane
DMEM	Dulbecco's modified Eagle's medium
ECM	Extracellular matrix
EDC	1-Ethyl-3-(3-dimethylaminopropyl)carbodiimid
EDTA	Ethylenediaminetetraacetic acid
FPA	Fibrinopeptide A
FPB	Fibrinopeptide B
HEPES	4-(2-hydroxyethyl)-1-piperazineethanesulfonic acid
NHS-ester	N-Hydroxysuccinimide-ester
N-terminus	Amino-terminus
PBAT	Polybutylene adipate terephthalate
PBS	Phosphate buffered saline
PDMS	Polydimethylsiloxan
PLA	Polylactic acid
Plas	Plasmin
PS	Polystyrene
RGD-sequence	Arginine, glycine, aspartate sequence
SDS PAGE	Sodiumdodecylsulfate polyacrylamide gel electrophoresis
SEM	Scanning electron microscope
ThT	Thioflavine T
Uro	Urokinase
UV	Ultraviolet

I. List of figures

II. List of tables

III. Summary

The plasma protein fibrinogen is a crucial protein in hemostasis and wound healing. Upon vascular injury fibrinogen is enzymatically converted into insoluble fibrin nanofibers. After injury the enzyme thrombin cleaves off two small fibrinopeptides from soluble fibrinogen, which exposes binding sites that allow the polymerization into fibrin nanofibers that form a blood clot which seals the wound.

Because of its *in vivo* functions as a blood clot and a provisional extracellular matrix fibrinogen is a promising candidate for the fabrication of novel biomaterials designed for wound treatment. The main idea of current research is to obtain nanofibers from fibrinogen which have similar morphology and characteristics as fibrin nanofibers, but which are prepared *in vitro* without the enzymatic cleavage by thrombin. One main technique to obtain nanofibers from biological materials is electrospinning, which however has some drawbacks especially for the production of protein fibers. Because of these drawbacks, some methods have been described which utilize self-assembly of fibrinogen into nanofibers for example in special buffers or on hydrophobic surfaces. The self-assembly of fibrinogen into nanofibers, which occurs even without enzymatic activation, is an interesting and not completely understood phenomenon.

Therefore, in the course of this thesis, the self-assembly of fibrinogen was studied, by drying fibrinogen in the presence of different ions. It was shown that dependent on the presence of ions fibrinogen fibers formed during the drying process when fibrinogen concentrations in the physiologically relevant range of 2 to 5 mg/ml were applied. The self-assembly of fibrinogen was observed in the presence of different ions and at pH values of 7 to 9. Interestingly, the analyzed self-assembly was a surface independent process and drying of fibrinogen resulted in fibrous scaffolds on hydrophilic glass and gold as well as on various hydrophobic polymers.

Since the fibrinogen fiber scaffolds prepared by self-assembly reached dimensions up to several cm^2 and required comparably low concentrations of fibrinogen, a novel method to fabricate fibrinogen scaffolds by self-assembly was developed. However, the self-assembly during drying in the presence of ions was a reversible process and the prepared fibrinogen fibers were not stable upon rehydration, which is a problem for further experiments or a

potential future application. Therefore, different crosslinking procedures were analyzed for their potential to stabilize the fibrinogen scaffolds. It was shown that treatment with formaldehyde or glutaraldehyde vapor resulted in a reliable crosslinking of the fibrinogen scaffold and maintained the fibrous structure.

In a second main experimental part of this thesis changes in secondary structure during the fibrinogen self-assembly were analyzed using circular dichroism. It was shown that the formation of fibrinogen fibers was accompanied by a transition of α-helical into β-sheet structures. The native content of 23 % α-helical and 28 % β-sheet structures was shifted to 19 % and 32 %, respectively. Remarkably, the change in secondary structure was reversible when crosslinked fibers were rehydrated. An additional thioflavin T staining revealed that the observed change in secondary structure was not due to the formation of β-amyloid structures.

Since an understanding of fibrinogen self-assembly allows preparation of fibrinogen scaffolds which could be used in the future as a biomaterial for tissue engineering and wound healing application, the bioactivity of self-assembled scaffolds was studied in the third main part of this thesis. In experiments carried out for 35 days it was shown that the long-term degradation of fibrinogen scaffolds was dependent on the crosslinking time in formaldehyde vapor. Furthermore, the long-term incubations revealed that single enzymes like plasmin or thrombin had no additional effect on the fibrinogen scaffold stability while a combination of plasmin and urokinase resulted in an accelerated degradation.

The results of this thesis allow some insight into the mechanism of fibrinogen, which seems to rely on the exclusions of water during the drying process and on the effect that ions have on the hydration shell of the fibrinogen molecule. Overall the fibrinogen self-assembly can be used on many surfaces materials, requires low fibrinogen concentration and can be carried out at physiological pH, which makes fibrinogen self-assembly a potential alternative to other fabrication techniques for fibrinogen biomaterials. In addition, the results of the secondary structure analysis and the bioactivity investigation indicate that the fibrinogen remained intact and bioactive during the self-assembly process. Therefore, fibrinogen scaffolds prepared by the newly developed method of salt-induced self-assembly have a high potential for cell culture tests and even future application in wound healing.

IV. Zusammenfassung

Das Plasmaprotein Fibrinogen ist ein entscheidendes Protein bei der Blutstillung und Wundheilung. Bei Gefäßverletzungen wird Fibrinogen enzymatisch in unlösliche Fibrin-Nanofasern umgewandelt. Nach einer Verletzung spaltet das Enzym Thrombin vom löslichen Fibrinogen zwei kleine Fibrinopeptide ab, wodurch Bindungsstellen freigelegt werden, die die Polymerisation zu Fibrin-Nanofasern ermöglichen, die ein Blutgerinnsel bilden, welches die Wunde verschließt.

Aufgrund seiner *in vivo*-Funktionen als Blutgerinnsel und als provisorische extrazelluläre Matrix ist Fibrinogen ein vielversprechender Kandidat für die Herstellung neuartiger Biomaterialien zur Wundbehandlung. Die Hauptidee der aktuellen Forschung besteht darin, aus Fibrinogen Nanofasern zu gewinnen, die eine ähnliche Morphologie und ähnliche Eigenschaften wie Fibrin-Nanofasern aufweisen, die jedoch *in vitro* ohne die enzymatische Spaltung durch Thrombin hergestellt werden. Eine Haupttechnik zur Gewinnung von Nanofasern aus biologischen Materialien ist das Elektrospinnen, das jedoch insbesondere für die Herstellung von Proteinfasern einige Nachteile hat. Wegen dieser Nachteile sind einige Methoden beschrieben worden, bei denen die Selbstorganisation von Fibrinogen zu Nanofasern genutzt wird, zum Beispiel in speziellen Puffern oder auf hydrophoben Oberflächen. Die Selbstorganisation von Fibrinogen zu Nanofasern, die auch ohne enzymatische Aktivierung stattfindet, ist ein interessantes und noch nicht vollständig verstandenes Phänomen.

Deshalb wurde im Rahmen dieser Arbeit die Selbstorganisation von Fibrinogen untersucht, indem Fibrinogen in Gegenwart verschiedener Ionen getrocknet wurde. Es konnte gezeigt werden, dass in der Anwesenheit von Ionen Fibrinogenfasern entstehen, die während des Trocknungsprozesses gebildet werden, wenn Fibrinogenkonzentrationen im physiologisch relevanten Bereich von 2 bis 5 mg/ml genutzt werden. Die Selbstorganisation von Fibrinogen wurde in Gegenwart verschiedener Ionen und bei pH-Werten von 7 bis 9 beobachtet. Interessanterweise war die analysierte Selbstorganisation ein oberflächenunabhängiger Prozess, und die Trocknung von Fibrinogen führte zu faserigen Gerüsten auf hydrophilem Glas und Gold sowie auf verschiedenen hydrophoben Polymeren.

Da die durch Self-Assembly hergestellten Fibrinogen-Fasergerüste Abmessungen bis zu mehreren cm^2 erreichten und vergleichsweise niedrige Fibrinogenkonzentrationen benötigten, wurde eine neue Methode zur Herstellung von Fibrinogengerüsten durch Selbstorganisation entwickelt. Die Selbstorganisation während des Trocknens in Gegenwart von Ionen war jedoch ein reversibler Prozess, und die präparierten Fibrinogenfasern waren bei der Rehydratation nicht stabil, was ein Problem für weitere Experimente oder eine potentielle zukünftige Anwendung darstellt. Daher wurden verschiedene chemische Quervernetzungsverfahren auf ihr Potenzial zur Stabilisierung der Fibrinogengerüste analysiert. Es zeigte sich, dass die Behandlung mit Formaldehyd- oder Glutaraldehyddampf zu einer zuverlässigen Vernetzung des Fibrinogen-Gerüsts führte und die Faserstruktur erhalten blieb.

Im zweiten experimentellen Hauptteil dieser Arbeit wurden Veränderungen der Sekundärstruktur während der Fibrinogen-Selbstorganisation mittels Zirkulardichroismus analysiert. Es konnte gezeigt werden, dass die Bildung von Fibrinogenfasern mit einem Übergang von α-helikalen in β-Faltblattstrukturen einhergeht. Der native Gehalt von 23 % α-helikal und 28 % β-Blattstrukturen wurde zu 19 % bzw. 32 % verschoben. Bemerkenswert ist, dass die Veränderung der Sekundärstruktur reversibel war, wenn vernetzte Fasern rehydriert wurden. Eine zusätzliche Thioflavin T-Färbung zeigte, dass die beobachtete Veränderung der Sekundärstruktur nicht auf die Bildung von β-Amyloidstrukturen zurückzuführen war.

Da das Verständnis der Fibrinogen-Selbstorganisation die Herstellung von Fibrinogengerüsten ermöglicht, die in Zukunft als Biomaterial für Tissue Engineering und Wundheilungsanwendungen eingesetzt werden könnten, wurde im dritten Hauptteil dieser Arbeit die Bioaktivität von selbstorganisierten Gerüsten untersucht. In Experimenten, die über 35 Tage durchgeführt wurden, konnte gezeigt werden, dass der Langzeitabbau von Fibrinogen-Gerüsten von der Vernetzungszeit in Formaldehyddampf abhängig ist. Darüber hinaus zeigten die Langzeitinkubationen, dass einzelne Enzyme wie Plasmin oder Thrombin keinen zusätzlichen Einfluss auf die Stabilität des Fibrinogen-Gerüstes hatten, während eine Kombination von Plasmin und Urokinase zu einem beschleunigten Abbau führte.

Die Ergebnisse dieser Arbeit erlauben einen Einblick in den Mechanismus der Fibrinogen Faserbildung, der scheinbar auf dem Ausschluss von Wasser während des Trocknungsprozesses und auf dem dem Effekt von Ionen auf die Hydratationshülle des Fibrinogenmoleküls beruht. Insgesamt kann die Fibrinogen-Selbstorganisation auf vielen Oberflächenmaterialien verwendet werden, erfordert eine niedrige Fibrinogenkonzentration und kann bei physiologischem pH-Wert durchgeführt werden, was die Fibrinogen-Selbstorganisation zu einer potenziellen Alternative zu anderen Herstellungstechniken für Fibrinogen-Biomaterialien macht. Darüber hinaus deuten die Ergebnisse der Sekundärstrukturanalyse und der Bioaktivitätsuntersuchung darauf hin, dass das Fibrinogen während der Selbstorganisation intakt und biologisch aktiv blieb. Daher verfügen Fibrinogengerüste, die mit dem neu entwickelten Verfahren der salzinduzierten Selbstorganisation hergestellt wurden, über ein großes Potential für zellbiologische Untersuchungen oder sogar zukünftige Anwendungen in der Wundheilung.

1. Motivation

The sealing of a wound in the human body is facilitated by the enzymatic conversion of the soluble plasma protein fibrinogen into fibrin nanofibers. Therefore, fibrin has attracted great attention to be applied in wound treatment and has become an interesting material for the field of tissue engineering. In addition, one approach in tissue engineering is to prepare fibrinogen fibers *in vitro* without an enzymatic activation by electrospinning fibrinogen solution. However, this approach requires organic solvents and high voltage that possibly have negative effects on the bioactivity of the fibers. Therefore, some recent publications have also presented methods, which induced the formation of fibrinogen nanofibers without enzymatic activation in solution or as a surface reaction. This remarkable property of fibrinogen was termed self-assembly and it was discussed to use self-assembled fibrinogen fibers for tissue engineering and wound healing applications. However, the mechanism behind fibrinogen self-assembly remains elusive. Some studies focused on the exposure of fibrinogen solution to hydrophobic surfaces as the main driving force while others investigated the self-assembly at low pH values or in the presence of ethanol. Most of these studies proposed a change in secondary structure as an underlying mechanism of fibrinogen self-assembly, but no detailed investigation of structural changes was conducted. In most of these studies the samples of self-assembled fibrinogen were dried for analysis. The drying of the fibrinogen is an important factor that has been largely neglected. Only a few studies discussed that changes in ionic strength and drying effects during the preparation of fibrinogen samples could have an additional effect on fibrinogen self-assembly, but did not identify, which of these factors is the actual driving force that results in the organization of fibrinogen molecules into fibers. Without a fundamental understanding of the self-assembly process it is not possible to tailor self-assembled fibrinogen scaffolds towards selected applications in tissue engineering because neither the assembly process nor the bioactivity of the fibrinogen fibers can be sufficiently controlled or evaluated.

The main scientific motivation of this thesis is to gain insight into the fundamental principles of fibrinogen self-assembly. One key question is whether drying of fibrinogen solutions is sufficient to induce fibrinogen self-assembly. Therefore, in this thesis fibrinogen self-assembly induced by drying was systemically investigated for the first time

in respect of factors like presence of ions, ion composition, fibrinogen concentration, pH, surface material or humidity. The results obtained allow formulating a potential mechanism of drying induced fibrinogen self-assembly, which might also help to explain self-assembly of fibrinogen fibers observed in other studies.

Furthermore, changes in the secondary structure of fibrinogen were analyzed to elucidate the role of conformational changes during fibrinogen self-assembly. For the first time, with the data obtained it will be possible to discuss the role of conformational changes during fibrinogen self-assembly proposed in other studies based on the foundation of measured results.

Overall, the systematic investigation of factors contributing to fibrinogen self-assembly will provide a framework, which will allow specific use of self-assembly as a process for the preparation of fibrinogen scaffolds as bio- and tissue engineering materials. Furthermore, the detailed analysis of single parameters will provide a first basis for potential application of tailored self-assembled fibrinogen for selected tissue engineering approaches, like for example wound healing.

This is closely related to the second and more application-driven motivation of this thesis: To evaluate whether self-assembled fibrinogen scaffolds are suitable biomaterials for tissue engineering or wound healing applications. This evaluation also relies on the fundamental understanding of the self-assembly process and the associated conformational changes. Additionally, other factors like fiber yield and the dimension of the obtained fibrinogen fiber scaffolds as well as their stability in an aqueous environment are crucial. These application relevant factors will also be addressed in this thesis, which will allow an assessment of the practical feasibility of fibrinogen self-assembly in tissue engineering applications.

Another important question that should precede an application of self-assembled fibrinogen is whether fibrinogen maintains its biological activity. The structural analysis gives some indication about the biological activity. In addition, the bioactivity of self-assembled fibrinogen will be addressed using binding and degradation experiments with biologically relevant partners or enzymes in this thesis. This will allow a first interpretation whether fibrinogen stays biologically active during the self-assembly processes and provide a

foundation for future cell culture experiments and a potential future application of fibrinogen as a biomaterial.

The findings presented in this thesis will shed light on the fundamental mechanism of fibrinogen self-assembly and the biological activity of self-assembled fibrinogen nanofibers. A basic understanding of fibrinogen self-assembly can be a future basis for the tailored fabrication of fibrinogen biomaterials for applications in tissue engineering.

2. Introduction

2.1. The extracellular matrix

In native tissue cells are surrounded by a nanofibrous network of proteins and proteoglycans termed extracellular matrix (ECM). One of the main functions of the ECM is the structural and support of tissue and cells by offering a three-dimensional architecture with various binding sites for cells. Many ECM components offer sequences to which cells can bind via integrins like for example the RGD sequence; a sequence of the tree amino acids arginine, glycine and aspartate (Kular et al., 2014). However, the function of the ECM is not limited to a passive role as a static scaffold. The ECM is subject to constant remodeling by the cells in it and likewise influences cellular migration, differentiation and proliferation (Kular et al., 2014). The ECM does affect cellular behavior by providing biochemical clues of the single ECM components or their degradation products. Furthermore, the ECM also influences cells by mechanical signaling. Some ECM proteins include cryptic binding sites whose availability depends on the tensile state and a partial unfolding of the molecule. At the same time the fiber formation of many ECM components is also dependent of the tensile state of the tissue. Cell on the other hand can sense as well as induce mechanical forces, which makes the ECM an topographical, biochemical and biomechanical regulatory environment (Vogel, 2018).

The most abundant ECM protein is collagen. The ubiquitous protein is present in almost all tissues and over 20 different collagens have been characterized. In various tissues different types of collagen are present. For example, the ubiquitous major form collagen type I is found in almost all kinds of tissue, while type III collagen is mainly found in the walls of blood vessels (Bosman and Stamenkovic, 2003). One of the functions of collagen is to provide mechanical strength to tissues, which are exposed to pressure, shear or tensile forces like for example skin, the walls of blood vessels, bone or tendons (Bosman and Stamenkovic, 2003). The mechanical strength of the collagen in the ECM of these tissues is due to its fibrous morphology. The collagen molecule itself has an elongated triple-helical structure and in the collagen types occurring in tissues the collagen molecules are arranged in fibrils. Only the collagen type I, II, III, V and XI assemble into fibrils while other

collagen types are often of regulatory function (Bosman and Stamenkovic, 2003; Kular et al., 2014).

Elastin is another important ECM component, which as the name implicates gives tissue its elasticity. It is mainly found in connective tissue and in the walls of blood vessels. Elastin is produced by crosslinking its soluble precursor tropoelastin by the enzyme lysyloxidase. The final elastin in tissue is a crosslinked polymer that is extremely stable and lasts for the entire lifetime of the host. Although crosslinked elastin is highly stable, it has large domains of repetitive hydrophobic amino acids. The dynamic interactions of the hydrophobic domains give the crosslinked elastin polymer its elasticity (Debelle and Tamburro, 1999).

The protein fibronectin is another important component of the native ECM. Fibronectin is a ubiquitous protein that is present in the ECM of almost all tissues. *In vivo* fibronectin is assembled into fibrous networks by a cell driven process. Cells bind to the RGD sequence of fibronectin via integrins. The interaction of cells and fibronectin is a process that is essential from the first embryonal development to the matured tissue. Interestingly, the fibronectin fiber network of the ECM also matures with age and function of the respective tissue. Fibronectin fibers are present as small elastic fibers that are still rearrangeable as well as matured insoluble fibers of larger sizes. The functions of fibronectin range from structural functions and cellular support of cells due to the strong integrin binding to signaling and migratory functions for cells. Furthermore, the fibronectin network plays a crucial role in the assembly, regulation and organization of other ECM components like for example collagen.

In the case of a wound the skin is penetrated and the underlying tissue is damaged. This does not only mean that cells in the wounded area are lost, but also that the ECM is damaged and that the various functions of the different ECM components are impaired. During the wound healing process the functions of the ECM are carried out by a provisional matrix out of fibrin.

2.2. Wound healing

The human body has a great capability to withstand and regenerate injuries. In case of a wound the blood released during hemorrhage has its own integrated mechanism to seal the site of injury and to prevent further blood loss. During vascular lesion the soluble plasma protein fibrinogen is enzymatically converted to fibrin. The fibrin forms a meshwork of nanofibers, which aggregate with blood platelets to seal the wound. The meshwork of fibrin fibers serves as a provisional ECM and temporarily replaces many functions of the native ECM (Clark, 2001).

The sealing of the wound is only the very first step of wound healing. Although, wound healing is a continuous process of overlapping events it is generally divided into four phases: Hemostasis, inflammation, proliferation and remodeling (Guo and DiPietro, 2010). The Hemostasis is the initial formation of a blood clot by the conversion of fibrinogen into fibrin fibers and the attachment of platelets, which stops the bleeding. The initial hemostasis is completed in the first hours after wounding and sometimes can be prolonged up to the first three days. Nevertheless, the fibrin network, which is formed during hemostasis, is also crucial for later stages of the wound healing process (Braiman-Wiksman et al., 2016). The second phase of wound healing, the inflammation, occurs simultaneously with hemostasis. Neutrophil immune cells from the blood invade into the wound space. The main function of the inflammatory response is to protect the wound site from potential infections with pathogens but an additional function is the secretion of cytokines, which attract and stimulate the proliferation of fibroblasts (Cumming et al., 2009).

The third phase is the proliferation phase in which fibroblasts and epithelial cells from the surrounding tissue start to migrate and proliferate into the wound site and start to regenerate the lost tissue. During this phase the fibrin clot serves as a scaffold for the cells, which continually replace the fibrin with collagen. The proliferation phase starts in the first days after the wound is inflicted and continues for weeks up to several months after the wounding (Braiman-Wiksman et al., 2016). The final remodeling phase can continue for month or even years and is defined by a maturation of the regenerated tissue towards native tissue (Guo and DiPietro, 2010). An overview about the phases of wound healing is given in Figure 1.

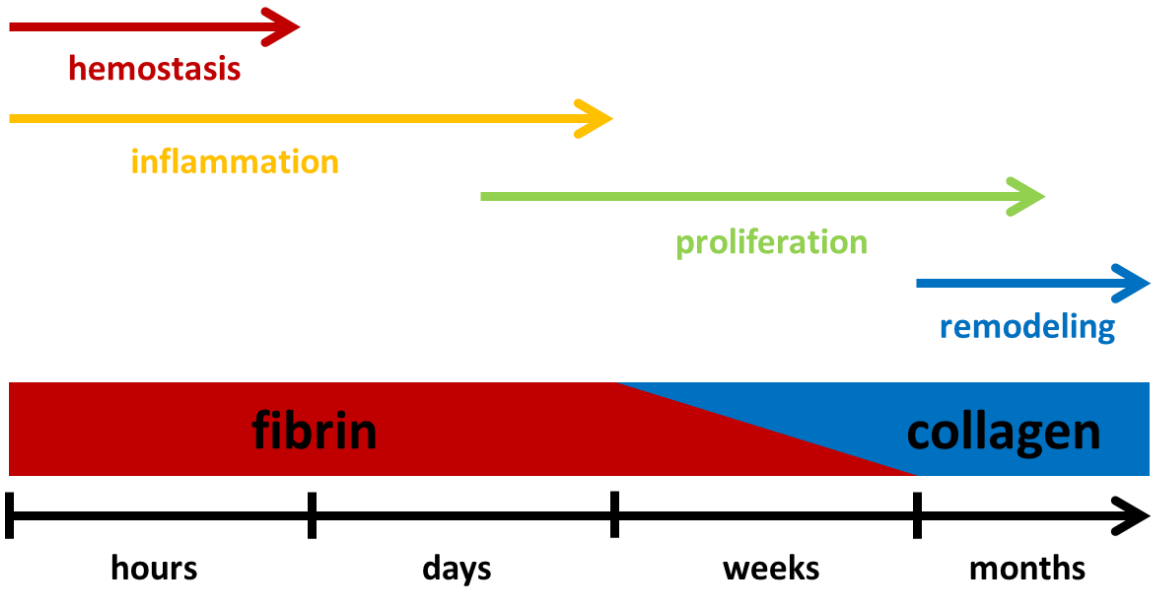

Figure 1: Time scale of wound healing. The process of wound healing is divided into four overlapping phases. The hemostasis during the first hours after wounding is accompanied by the inflammation phase that lasts up to days. During hemostasis the wound is sealed with fibrin. In the proliferation phase fibroblasts migrate into the wound space and start to replace the fibrin with collagen. During the remodeling phase the wound tissue matures towards native tissue.

The crucial initial event of hemostasis is formation of the fibrin clot out of the soluble plasma protein fibrinogen. Therefore, the fibrinogen molecule and its enzymatically conversion into fibrin are discussed in the next chapter.

2.3. Fibrinogen and fibrin

Fibrinogen is a plasma protein, which circulates in the blood with a concentration of 2-5 mg/ml making fibrinogen the third most abundant serum protein after albumin and globulin. Fibrinogen is produced in the liver and circulates in the blood stream with a half-life time of roughly two days (Stein et al., 1978).

The main reason for the abundance of fibrinogen in the bloodstream is its crucial function in blood clotting and in the subsequent wound healing processes. In case of a wound fibrinogen is activated by the enzyme thrombin and the fibrinogen molecules assemble into fibrin nanofibers, which close the wound. This tightly regulated process is termed coagulation (Mosesson, 2005).

2.3.1. Molecular Structure of fibrinogen

Fibrinogen is a dimeric macromolecule with a molecular weight of 340 kDa. It is composed of two Aα-chains, two Bβ-chains and two γ-chains (Kattula et al., 2017; Mosesson, 2005). One set of Aα-, Bβ- and γ-chains forms a coiled coil triple-helix structure, respectively. The different chains of the half molecule are linked by disulfide bridges at the borders of the coiled coil structure. The N-termini of the single chains of the two half molecules are linked together by disulfide bridges and form the center of the fibrinogen molecule, the so called E-domain (Huang et al., 1993). The C-termini of the Bβ- and γ-chains of each half molecule form a β-nodule and a γ-nodule rich in β-sheet structures. The β- and γ- nodule are referred to as D-domain (Zuev et al., 2017). In the fibrinogen molecule two D-domains of the half molecules face in opposite directions at the periphery. The two D-domains are linked by coiled coil triple-helix structures to the central E-domain and give rise to a three nodular geometry of the fibrinogen molecule with an overall length of 45 nm (Figure 2 A). This three nodular shape of the fibrinogen molecule was confirmed *in vitro* using electron and atomic force microscopy (Fowler and Erickson, 1979; Protopopova et al., 2015). To each D-domain an α-C domain is linked with a flexible connector. The α-C domains are usually folded back from the D-domain to the central E-domain as depicted in Figure 2 A (Zuev et al., 2017).

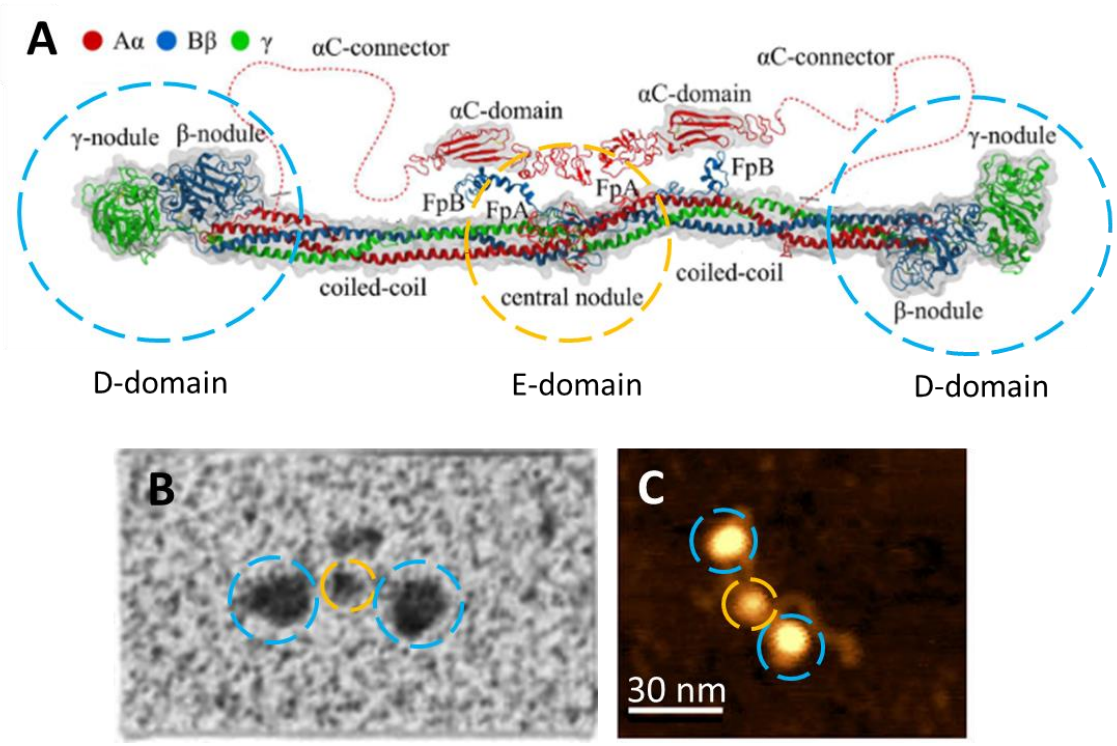

Figure 2: Domain structure of the fibrinogen molecule
A: Fibrinogen molecular structure with the E-domain highlighted in yellow and the D-domains highlighted in blue. The domains mainly consist of β-sheets while the linkers between the domains consist of coiled α-helices. Image modified from (Zuev et al., 2017).
B: Electron microscopic image of a fibrin monomer with the E- and D-domains highlighted. Image modified from (Weisel and MEDVED, 2001).
C: Atomic force microscopy image of a fibrinogen molecule with the E- and D-domains highlighted. Image modified from (Protopopova et al., 2015).

Even though, the secondary structure of fragments of human fibrinogen was determined by X-ray diffraction (Spraggon et al., 1997; Yee et al., 1997) and a complete structure has been confirmed (Kollman et al., 2009), the structure and role of the C-terminal region of the Aα-chain remained elusive for a long time. This is due to flexible high-repeat regions linking the C-terminal nodule of the Aα-chain to the rest of the molecule. This high-repeat regions increase the flexibility of the Aα-chain, which makes crystallization and thereby X-ray analyses challenging (Kollman et al., 2009).

Interestingly, the flexibility of the αC-terminus has been indirectly observed even earlier in electron microscopy. For some molecules a second nodular central domain was observed, whose location varied (Weisel et al., 1985). Later studies revealed that the fibrinogen molecule is often present in a conformation, in which the high repeat linker and the C-terminal α-nodule are folded back in a way that allows close contact to the central E-

domain (Weisel and Medved, 2001). Nevertheless, the C-terminal α-nodules have also been found in various other constellations with respect to the central E-domain and it is very likely that the fibrinogen molecules in solution or in the blood stream have highly flexible αC-termini, which change their conformation constantly (Protopopova et al., 2015; Weisel et al., 1993; Weisel et al., 1985). Nevertheless, it has been discussed that dependent on the pH the αC-domains have preferred positions in respect to the central E-domain. At a physiological pH of 7.4 the αC-domains are likely to be in a compact position close to the E-domain, while at high pH an extended confirmation with the αC-domains elongated towards the periphery is likely (Figure 3). The most probable positions of the αC-domain at different pH values are also reflected in differences of the hydrodynamic diameter of the fibrinogen molecule (Wasilewska et al., 2009).

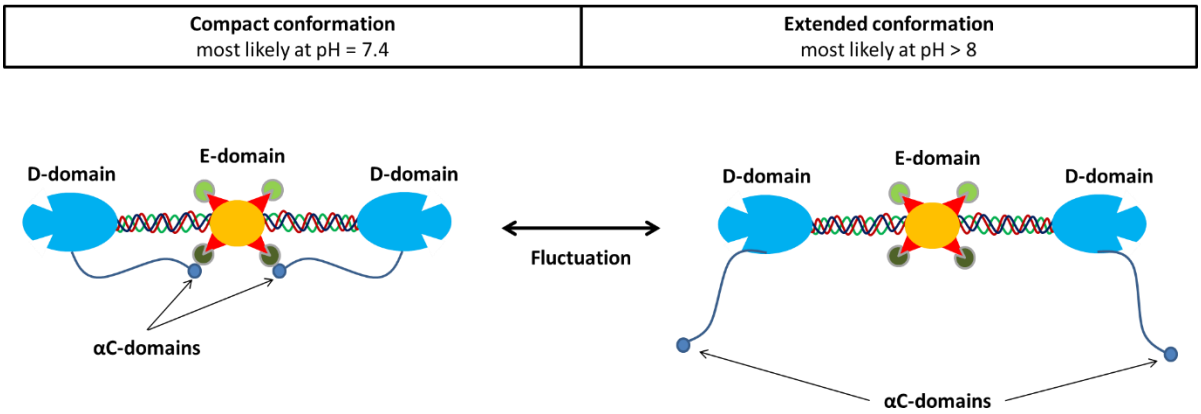

Figure 3: Conformational fluctuations of fibrinogens αC-domains.
The flexible αC-domains of fibrinogen can fluctuate between a compact conformation with the αC-domains in close contact to the central E-domain and between an extended conformation. At pH 7.4 the compact conformation of the αC-domains is more likely, while at pH values higher than 8 and extended conformation. However both conformation and intermediate states are possible due to the high flexibility of the αC-domains.

However, the high repeat linker chain of the αC-terminus is not an unordered structure. This sequence of the protein is rich in tandem repeats of prolin. It has been discussed that these repeated amino acids could form an extended poly-L-proline helix structure (Weisel and MEDVED, 2001). Similar structures have been observed in collagen or cell surface proteins and are discussed to be highly flexible due to the hydrogen bridges in the helix. The function of similar structures was described to yield in a high flexibility and also to assist protein-protein-interaction (Williamson, 1994; Zuev et al., 2017).

The highly flexible αC-termini of fibrinogen have been shown to be important for later stages of fibrinogen interaction and for the crosslinking of single fibrin fibers (Collet et al., 2005; Zuev et al., 2017).

Two other structural components of fibrinogen, which have a crucial function in the assembly of fibrinogen molecules into fibrin fibers, are the fibrinopeptides A and B. They are located at the central E-domain at the N-termini of the Aα-chain and the Bβ-chain, what is also indicated by the nomenclature (Blombäck and Blombäck, 1972). Although the fibrinopeptides A and B are very short α-helical domains consisting of only 16 or 12 amino acids, respectively, they prevent the association of fibrinogen molecules to fibrin by masking binding sites at the central E-domain (Mosesson, 2005). If fibrinopeptides A and B are cleaved off by the proteolytic enzyme thrombin, these binding sites become exposed allowing the association of fibrinogen molecules into fibrin fibers, as described in the next chapter (Mosesson, 2005; Weisel et al., 1993).

2.3.2. Conversion of fibrinogen into fibrin nanofibers

The emergency of a wound requires a fast wound closure response *in vivo*. However, under non-hemorrhage circumstances fibrinogen in the blood should not be converted to fibrin at all cost. The formation of fibrin in an intact blood vessel could clock the blood vessels and lead to insufficient perfusion of vital organs or even death (Fowkes et al., 1993). Therefore, it is crucial that the activation of fibrinogen by thrombin is tightly regulated. Thrombin is the core enzyme of the blood clotting process, which under normal non-hemorrhage conditions, is only present in its inactive precursor form, so called prothrombin. The activation of prothrombin is achieved by two linked pathways referred to as coagulation cascade (Figure 4). The enzymes involved in this cascade are historically named as factors with a roman numeral. Since most of the factors are proteases, which are present in their inactive form, the convention is to add the suffix ‘a’ to the factor name, if the factor is activated during the coagulation cascade (Palta et al., 2014).

The first pathway for thrombin activation is the extrinsic pathway. In case of a tissue wound, which also damages a blood vessel, blood will be permeating into the damaged tissue. Factor III (tissue factor), which is bound to the sub-endothelial tissue becomes

exposed to the blood. Factor VII (Proconvertin), which is present in the blood, can now bind to factor III initiating the FIII/FVIIa complex. This complex hydrolyses factor X (Stuart-Prower factor) to factor Xa. Factor Xa in combination with factor V hydrolyses factor II (Prothrombin) to factor IIa (Thrombin) (Figure 4).

The second pathway to activate thrombin is the intrinsic pathway. In this pathway, the blood plasma components factor XII (Hageman factor), high-molecular-weight kininogen and prekallikrein form a complex with a negatively charged surface for example the collagen of the tissue, which is exposed during the injury of a blood vessel. The activation complex can also be formed intrinsically at the wall of a blood vessel without an injury of the surrounding tissue. This complex converts factor XI to factor Xia, which activates factor IX, which in turn converts factor VIII to factor VIIIa. Factor VIIIa activates factor X, which similarly to the extrinsic pathway leads to the activation of thrombin (Dahlbäck, 2000; Palta et al., 2014).

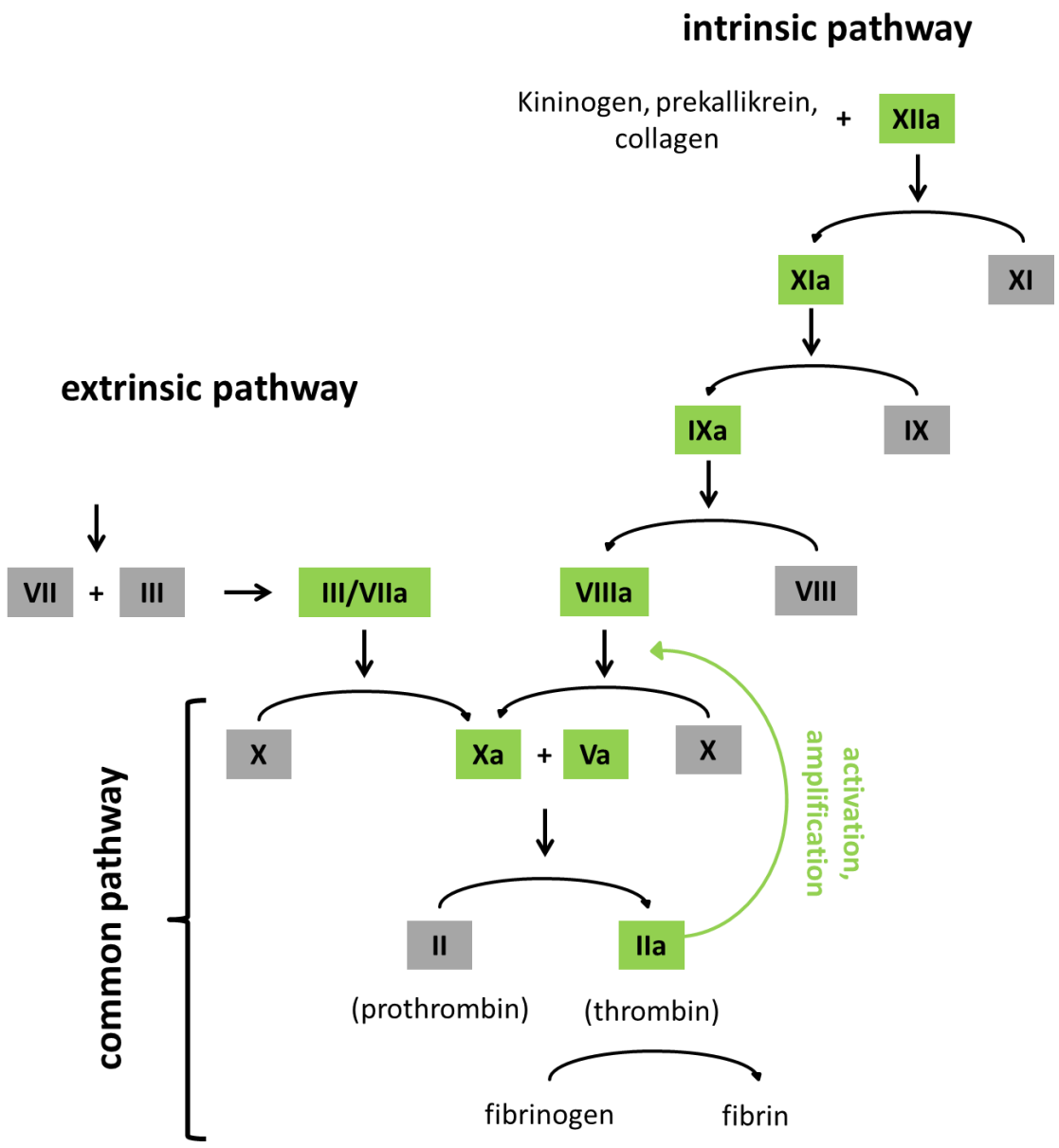

Figure 4: Extrinsic and intrinsic pathway of the blood coagulation cascade
The core enzyme of the coagulation cascade, thrombin, is activated by either the intrinsic or the extrinsic pathway. Thrombin converts fibrinogen into fibrin and additionally amplifies the coagulation cascade.

Interestingly, the activated thrombin can activate factor VIII in a positive feedback loop. This feedback reaction leads to a rapid amplification of the thrombin activity at the site of injury and ensures a quick assembly of the fibrin blood clot (Palta et al., 2014).

It has been discussed that an additional role of the intrinsic pathway is the amplification of the coagulation cascade. It is remarkable that the intrinsic and the extrinsic pathway are activated by similar initial events. Both pathways can be triggered by the formation of a

complex made out of proenzymes in the blood and a tissue component which is not present in the blood at all. For the extrinsic pathway the complex is formed out of tissue factor and factor VII, for the intrinsic pathway the complex can consist of collagen and factor XII (Dahlbäck, 2000).

Additionally, the activation of the intrinsic or the extrinsic pathway is also crucial for the regulation of the blood coagulation cascade. One of the most important inhibitors of the coagulation cascade is antithrombin, which can inhibit almost all proteases of the coagulation cascade (Palta et al., 2014). The inhibition activity of antithrombin is even increased by the presence of heparin on the surface of vascular epithelium cells, which results in a strong inhibition of the free coagulation enzymes in the blood plasma of an intact blood vessel. However, in case of a vascular lesion less heparin is present and the coagulation enzymes form complexes with the underlying tissue becoming less accessible for inhibition by antithrombin. This efficient regulatory mechanism allows a strong restriction of coagulation in the blood plasma without any spontaneous coagulation or fibrin formation while promoting rapid and local thrombin activation and fibrin formation at the injury site (Rosenberg, 1989; Weitz et al., 1990).

When thrombin is activated by the coagulation cascade, it utilizes soluble fibrinogen from the blood plasma as the major component for fibrin fiber formation. Thrombin cleaves off fibrinopeptide A from the N-terminus of the α-chain of fibrinogen, which makes a polymerization site accessible, which is called E_A or also referred to as knob A. The E_A-polymerization site is a gly-pro-arg-val motive starting at the seventeenth amino acid residue of the newly formed fibrin α-chain N-terminus. Similarly to fibrinopeptide A, a thrombin-catalyzed cleavage of fibrinopeptide B exposes gly-his-arg-pro motives at the E-domain-located terminus of the β-chain, which are correspondingly termed E_B or knob B (Chernysh et al., 2012).

After exposure, the E-domain polymerization sites bind to complementary binding sites at the D-domain referred to as hole A or hole B (Figure 5 A). These so called knob-hole interactions are a noncovalent binding mechanism between the D-domain of one fibrinogen molecule and the E-domain of an adjacent molecule, which results in a half staggered alignment of fibrin monomers giving rise to the double stranded fibrin protofibrils forming

the fibrin clot (Chernysh et al., 2012). The half-staggered alignment of fibrin monomers in the forming double stranded protofibril can be observed by atomic force microscopy like depicted in Figure 5 B.

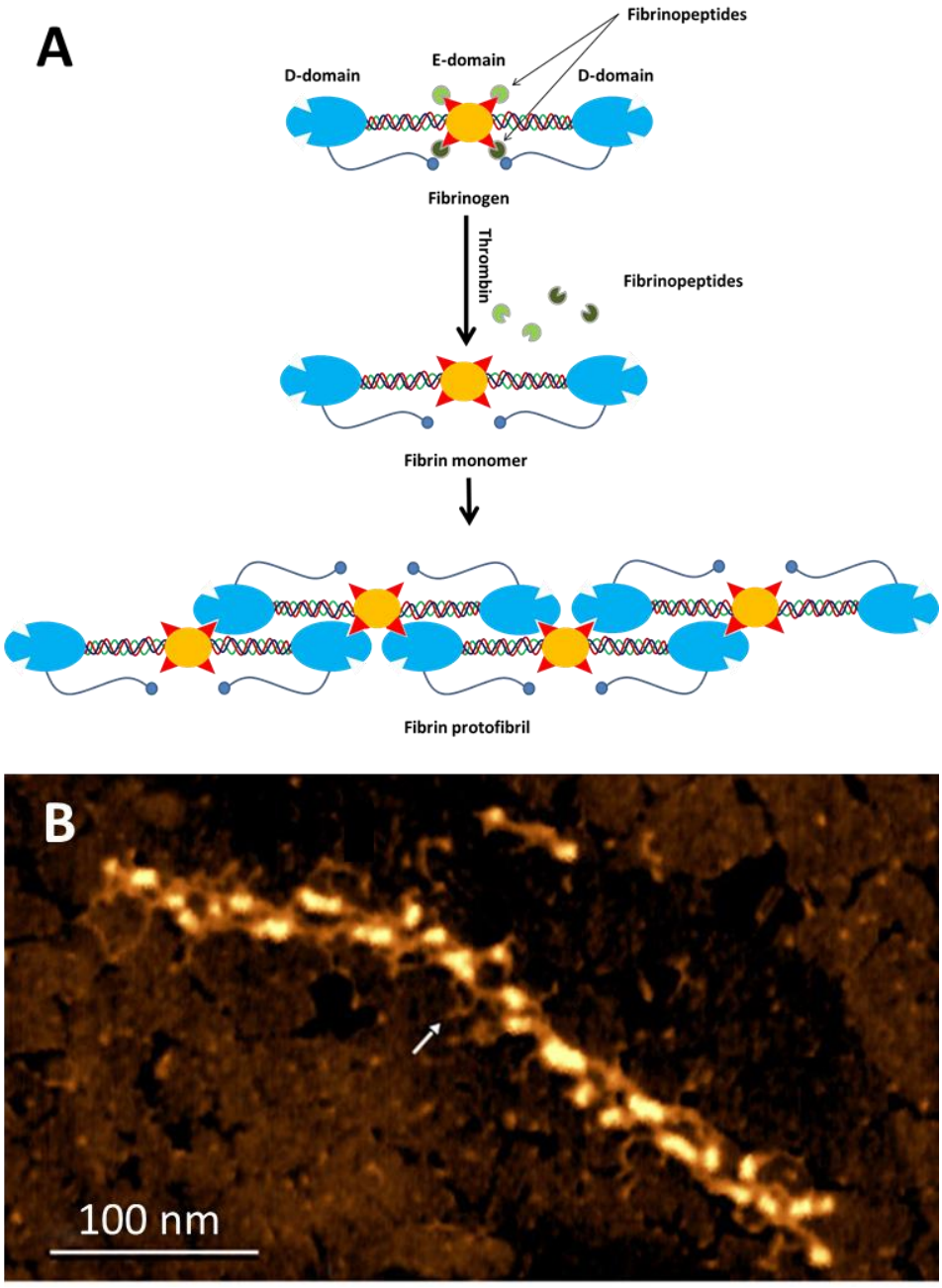

Figure 5: Formation of a fibrin protofibril

A: Schematic representation of double stranded protofibril formation. After cleavage of the fibrinopeptides by thrombin the fibrin monomers align in a half staggered configuration due to knob-hole interactions.
B: Atomic force microscopy image of a fibrin protofibril. Image modified from (Protopopova et al., 2015).

Under normal *in vivo* conditions both fibrinopeptides A and B are cleaved off by thrombin. However, the cleavage of fibrinopeptide A is a fast process while the cleavage of fibrinopeptide B is delayed (Pechik et al., 2006). Interestingly, the venom of some vipers, like for example *Agkistrodon halys halys,* contains proteases, which initiate fibrinogen polymerization and therefore rapid blood clotting by exclusively cleaving fibrinopeptide A (Weisel et al., 1993). Fibrin prepared with those proteases lacks only fibrinopeptide A and appears as a more ordered fiber network while showing a low lateral aggregation of the protofibrils. In contrast, fibrin prepared with thrombin lacks both fibrinopeptides A and B and seems more antiperiodic and unordered with a high lateral aggregation of the protofibrils. This has led to the conclusion that the cleavage of fibrinopeptide A is sufficient for polymerization, but that the delayed cleavage of fibrinopeptide B plays an important role in the overall organization of the polymerized protofibrils, which is crucial for the mechanical properties and the later crosslinking events of the fibrin clot (Weisel et al., 1993).

Crosslinking of the fibrin clot

Since fibrin protofibrils are held together by noncovalent interactions the *in vivo* maturation of the fibrin clot requires further crosslinking of the fibrin protofibril network to increase mechanical stability and to provide a permanent wound closure. Crosslinking *in vivo* is catalyzed by the enzyme transglutaminase, also referred to as factor XIII or fibrin stabilizing factor. Transglutaminase is activated by thrombin in the presence of Ca^{2+}-ions. This elucidates the central regulatory role of thrombin during blood clotting. Thrombin is not only responsible for the formation of fibrin protofibrils, but additionally the key activator of subsequent crosslinking events in the fibrin clot (Lorand, 2001). The activated transglutaminase catalyzes the formation of a peptide bond between the ε-amino group of a lysine residue and the γ-glutamyl group of a glutamine residue (Lorand et al., 1968).

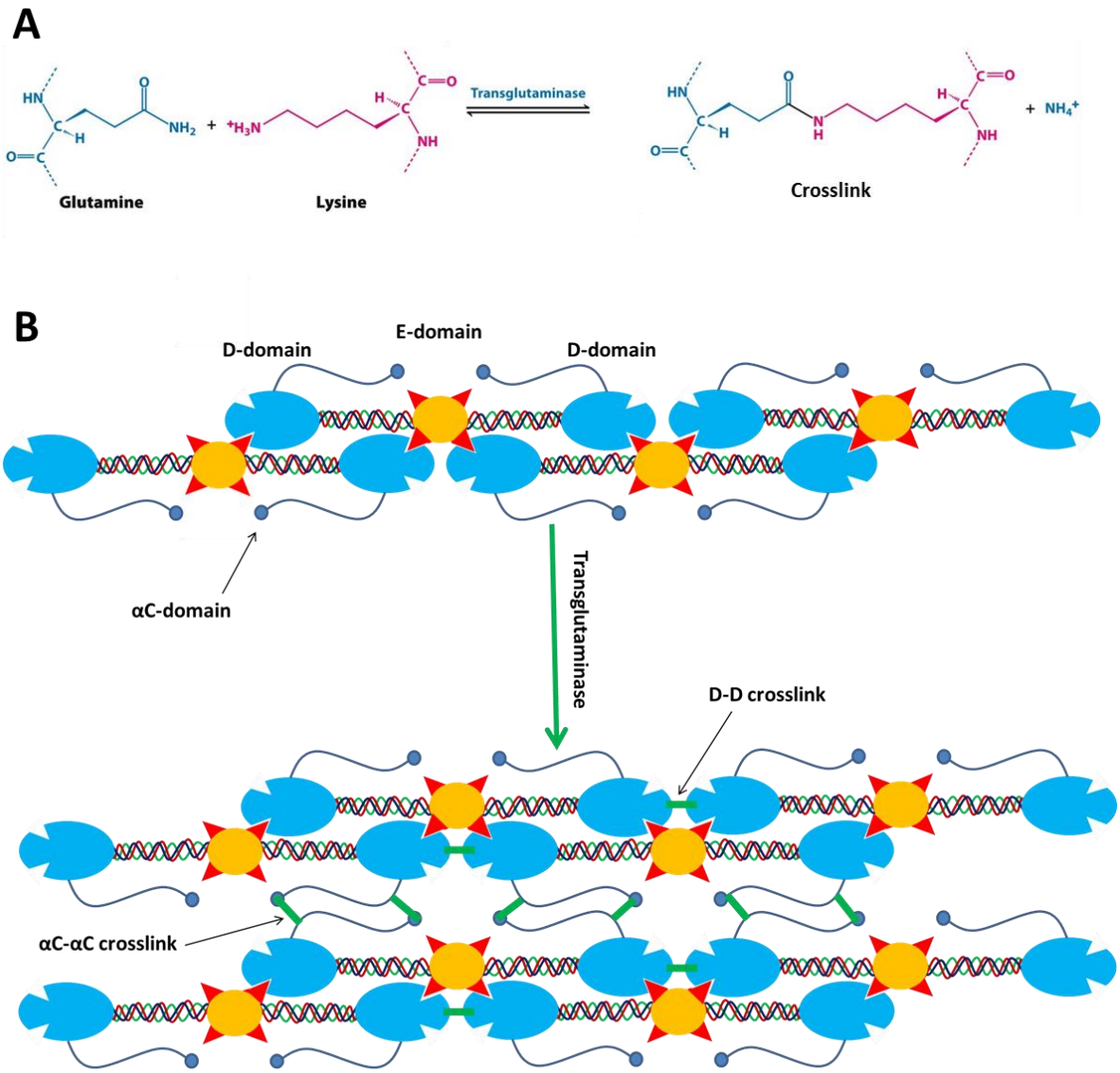

Figure 6: Transglutaminase crosslinking of fibrin protofibrils
A: Reaction scheme of the transglutaminase catalyzed crosslinking of a glutamine and a lysine residue. Image modified from (Berg et al., 2012).
B: Transglutaminase crosslinking of two fibrin protofibrils. The protofibrils are crosslinked via their flexible α-C domains. Additionally, transglutaminase crosslinks the fibrin monomers of one protofibril via their D-domains.

It was shown that transglutaminase binds to the αC-domains of fibrin protofibrils. After thrombin activation, the αC-domains of the fibrin monomer are no longer adhered to the central E-domain, but are in a flexible state making them available for intermolecular interactions. However, the first crosslinks catalyzed by transglutaminase occur between a lysine residue at the D-domain of a fibrin monomer and a glutamine residue at the D-domain of an adjacent fibrin monomer, which results in the covalent stabilization of fibrin

monomers in the fibrin protofibril. Crosslinking of the fibrin monomers increases the viscoelastic modulus and the clot resistance against enzymatic degradation (Lorand, 2001).

In a second slower reaction, transglutaminase catalyzes crosslinking of lysine and glutamine residue at the αC-domains of adjacent fibrin protofibrils. This second crosslinking reaction covalently links the different protofibrils via the flexible αC-domains forming the matured fibrin network. The αC-domains of the protofibrils maintain their flexibility even after crosslinking. However, due to steric hindrance they are less likely to be found in contact with the E-domain. This is sometimes considered as change in tertiary structure although the overall conformation of the αC-domains remains flexible and fluctuating (Mosesson, 2005).

It is remarkable that the same crosslinking reaction increases the mechanical stability to fibrin by covalently linking the fibrin monomers in the protofibrils, while also maintaining the elasticity of the fibrin network by crosslinking different fibrin protofibrils over their flexible αC domains (Ariëns et al., 2002).

Although the transglutaminase-catalyzed crosslinking of the fibrin protofibrils is well understood, it should not be neglected that transglutaminase crosslinking can also occur between the forming fibrin clot and other proteins. It is highly probable that during wound healing transglutaminase plays an additional role in the crosslinking of the fibrin clot to the surrounding tissue (Muszbek et al., 1999).

2.3.3. Fibrin as a provisional extracellular matrix

If tissue is wounded or if larger parts of the tissues are lost none of the native ECM components remains intact or even present in the site of injury. The fibrin fiber network serves as a wound closure, but it also fulfills the function of a provisional ECM into which cells from the surrounding tissue migrate and regenerate and replace the lost tissue (Clark, 2001). Fibrinogen has RGD binding sites to which cells can bind via integrins. In addition, many cells are also able to bind fibrinogen without integrin receptors. Fibrin also has specific binding sites for fibroblast growth factor and for endothelial cell growth factor, which regulate the cellular migration and proliferation during later stages of the wound

healing. This makes the fibrin a structural support between cells, which also has regulatory functions (Laurens et al., 2006).

In addition to cells and growth factors, fibrin also binds to other blood plasma proteins, which are integrated into the fibrin network during hemostasis. Especially plasma fibronectin, a soluble form of fibronectin related to tissue fibronectin, is co-assembled into the fibrin network in high concentrations (Laurens et al., 2006). Fibronectin binds to a fibrin at a specific binding site located in the α-C domain of fibrin while other domains of fibrin are not able to bind fibronectin. Interestingly fibrinogen does not bind fibronectin, which indicates that the binding site at the α-C domain of fibrinogen is not accessible because the α-C domain of fibrinogen is in contact with the central E-domain of the molecule (Makogonenko et al., 2002). Fibronectin also binds to collagen, which makes it an important linker between the fibrin clot and the periwound tissue collagen as well as an important regulator of collagen deposition in the fibrin clot during the proliferation phase (Lenselink, 2015).

Similar to fibronectin the glycoprotein vitronectin is incorporated into the blood clot during hemostasis. Both proteins act as an additional amplification for cell adhesion in the forming blood clot because both contain many RGD sequences to which cells can bind (Laurens et al., 2006). Furthermore, fibronectin and vitronectin are chemically crosslinked to the fibrin fiber network by the transglutaminase reaction, which also crosslinks the fibrin fibers during the maturation of the fibrin clot (Laurens et al., 2006). Interestingly, fibrinogen has an additional binding site for transglutaminase, which is not the site of active crosslinking. Transglutaminase is bound to this exosite in its inactive form. This way transglutaminase is already incorporated into the blood clot during the first stage of hemostasis where it can be activated to crosslink the fibrin fibers as well as binding partners of fibrin (Hornyak and Shafer, 2002).

Another binding partner of fibrin is heparin. Heparin binds to a specific binding site at the new N-terminus of the fibrin β-chain where fibrinopeptide B was cleaved of by thrombin during the fibrin formation. Heparin hardly binds to fibrinogen since fibrinopeptide B is still present and blocks the binding site due to steric hindrance (Odrljin et al., 1996b). The heparin binding site of fibrin has two functions. Heparin is involved in the inhibition of

thrombin by forming a complex with antithrombin and activating it. By binding of heparin to fibrin, this formation of an inhibitory complex does not take place and thrombin remains active. This way the presence of fibrin ensures a continuous formation of more fibrin in the blood clot and keeps thrombin in its active form by binding the heparin (Hogg and Jackson, 1989). Furthermore, many cells as for example endothelial cells present heparin like molecules at their cell surface and can use the heparin binding site of fibrin. The heparin binding site is one of the major integrin independent binding sites for cells in the fibrin clot (Odrljin et al., 1996a).

In addition to the scaffold function of fibrin and its central role in the binding of cells and the factors mentioned above, the fibrin clot temporarily also has to fulfill the function of ECM elasticity. This function is accomplished by the coiled coil linker domains, which connect the central E-domain with the D-domains. The α-helical coiled coil structures are refolded into β-sheets upon stretching of the fibrin, which results in a high elasticity (Lim et al., 2008; Litvinov et al., 2012a). Another important factor contributing to the high elasticity of the fibrin clot is the transglutaminase crosslinking of the fibrin protofibrils. The protofibrils are crosslinked via their flexible α-C domains, which allows single protofibrils to displace in respect to each other and thereby extend the fibrin clot (Helms et al., 2012).

Degradation of fibrin

For the remodeling of the provisional fibrin matrix into a collagen matrix by the cell types introduced in the next section, it is necessary that cells can degrade the fibrin fibers. A partial degradation is required to enhance the invasion of cells into the fibrin matrix, while during remodeling of the fibrin clot the fibrin has to be gradually degraded and replaced with collagen until the wound tissue is completely converted into native tissue without fibrinogen present. The main mechanism used by cells to degrade fibrin is the proteolytic digestion by plasmin, which is termed fibrinolysis (Kane, 1984). Plasmin is a protease, which cleaves fibrin monomers into various smaller fragments in a gradual process and thereby destroys the fibrous structure of the fibrin clot (Pizzo et al., 1972).

Plasmin is present in the bloodstream in its inactive precursor form plasminogen. During the formation of the fibrin clot plasminogen is incorporated into the emerging fibrin fiber network. Cells migrating into the fibrin clot can activate the deposited plasminogen by

means of tissue plasminogen activator. Interestingly, activated plasmin itself converts plasminogen into plasmin in a positive feedback loop. The activation of plasmin can also be achieved or enhanced by exogenous factors that are not involved in the *in vivo* activation. One major exogenous activator of plasmin is the enzyme urokinase, which is produced by epithelial cells of the urinary tract and has a similar activating function like the tissue plasminogen activator. Urokinase is also used for the activation of plasminogen in clinical applications (Kane, 1984).

Plasmin-catalyzed fibrinolysis is the main *in vivo* pathway for fibrin degradation, but it was shown that cells *in vitro* can also use matrix metalloproteinases, which degrade collagen *in vivo*, to degrade fibrin. The cellular degradation of fibrinogen catalyzed by matrix metalloproteinases is only observed in cells, which lack the capability to utilize plasmin or for *in vitro* systems, where the plasmin activation is inhibited. This shows that the matrix metalloproteinase system is not the main *in vivo* degradation path for fibrin (Hotary et al., 2002).

The conversion of plasminogen to activated plasmin is not limited to the fibrin clot. Some activation of plasmin also occurs in the bloodstream as a mechanism to dissolve potential aggregations of fibrinogen or fibrin in the blood vessel and to prevent thrombosis (Ambrus et al., 1962). Overall, plasmin is the key counterpart to thrombin, which disassembles the fibrin formed by thrombin and additionally prevents aggregations of fibrin or fibrinogen.

2.3.4. Cellular interactions with the fibrin clot

Platelets

The first cellular components, which interact with the fibrin network, are blood platelets. Platelets are cellular fragments, which have no nucleus and are derived from megakaryocytes. Platelets have a disc-like shape if they are present in the bloodstream (Palta et al., 2014). As soon as they bind to the site of a blood vessel injury and to the collagen of the underlying tissue, they undergo a transition to a star-shaped morphology (Caen and Michel, 1972). These activated platelets aggregate simultaneously with the formation of fibrin at the injury site. The first blood clot is sometimes also referred to as

platelet plug. Integrin $\alpha_{IIb}\beta_3$-, a receptor that binds to fibrin, is present in the platelet membrane and allows a tight binding of activated platelets to the forming fibrin network. Only the combination of a fibrin network and platelets forms a mechanically stable barrier to seal the injury site and to prevent blood loss (Mosesson, 2005).

The presence of thrombin activates platelets while activated platelets further activate the coagulation cascade by providing an additional assembly surface for the initial complexes of coagulation factors. Moreover, activated platelets release calcium ions, which further increase the activity of most enzymes in the coagulation cascade (Monroe et al., 2002; Palta et al., 2014). In later stages of the matured blood clot the platelets start to secrete a platelet derived growth factor, a cytokine, which activates the migration and proliferation of fibroblasts and endothelial cells (Palta et al., 2014).

Fibroblasts

Roughly, five days after injury, fibroblasts start to migrate into the fibrin clot from the surrounding tissue. This process is accelerated by the platelet-derived growth factor and by fibroblast growth factor-2, which binds to fibrin. Fibroblasts themselves can also bind to fibrin via integrin $\alpha_{IIb}\beta_3$. Thereby, the fibrin network provides a provisional extracellular matrix allowing migration and proliferation of fibroblasts (Laurens et al., 2006). However, it has been shown that the morphological characteristics like fiber thickness or the number of branching points of the fibrin network have a strong influence on fibroblast binding and proliferation (Sporn et al., 1995).

Binding to fibrin can trigger fibroblasts to switch into the myofibroblast phenotype. These myofibroblasts are rich in actin fibers and can contract similarly to muscle cells (Laurens et al., 2006). It is assumed that the contractile force of the myofibroblast plays a key role in the mechanics of the mature blood clot and in keeping the wound closed (Laurens et al., 2006).

Another main role of the fibroblasts migrating into the blood clot is the synthesis and deposition of collagen fibers, which usually start in the first days post wounding. At the same time fibroblasts are capable to digest the fibrin network, thereby gradually replacing the fibrin fibers of the provisional extracellular matrix with collagen fibers and creating the

matrix of a regenerated tissue in the proliferative and the remodeling phase (Laurens et al., 2006).

Endothelial cells

In case of large injuries, small blood vessels in the tissue might also be destroyed. New blood vessels in the clot and regenerating tissue are formed by endothelial cells, which also migrate to the site of injury from the surrounding tissue (Hinsbergh et al., 2001). Endothelial cells digest the fibrin network by secreting plasmin and matrix metalloproteinases. The local degradation of the fibrin network allows an accelerated migration of endothelial cells and forms cavities in the fibrin network. The endothelial cells reorganize in those cavities and start the formation of new blood vessels in a complex process, which is called angiogenesis (Laurens et al., 2006).

Remarkably, the process of angiogenesis is strongly influenced by the morphology of the fibrin network. Dense fibrin networks with a low porosity only allow slow angiogenesis while fibrin with a high porosity alleviates blood vessel formation (Annemie Collen et al., 1998). It was even demonstrated that in fibrin with artificial cavities, endothelial cells utilized those preexisting cavities and formed blood vessels in them. For large blood clots an early start of angiogenesis is important to ensure the supply with oxygen and nutrients for the regenerating tissue (Laurens et al., 2006).

2.4. Tissue engineering using fibrin and fibrinogen

The rapidly growing interdisciplinary field of tissue engineering utilizes the current knowledge about the structure and function of living tissue to generate artificial tissue with biomimetic characteristics. Tissue engineering aims to create artificial tissue replacements, which mimic the morphological architecture and biochemical environment of natural ECM. The aim is to establish reproducible *in vitro* methods to generate artificial scaffolds for medical applications like for example as tissue replacements or as wound healing grafts (Chaudhari et al., 2016).

These replacements are fabricated either by using decellularized donor tissue or by preparing either synthetic or natural ECM materials in a way that mimics native tissue architecture and function (Fisher and Mauck, 2013). When these scaffolds are applied to a

defect, they serve as ECM replacement that promotes healing of the defect as depicted in Figure 7.

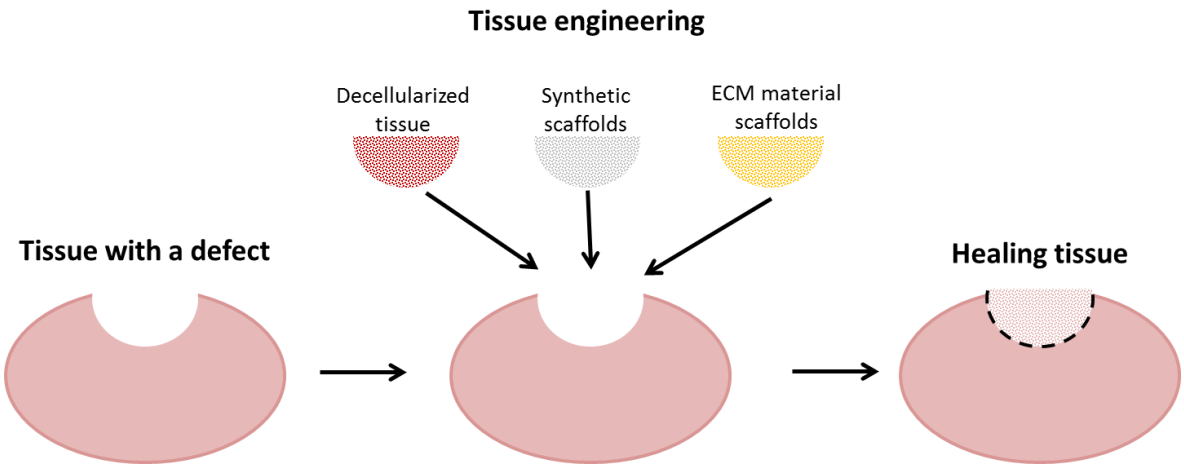

Figure 7: Scaffold types used in tissue engineering.
Tissue engineering aims to treat tissue defects by a provisional scaffold, which provides the functions of the native tissue ECM. Common scaffolds for this purpose are decellularized tissue, synthetic scaffolds or ECM material scaffolds.

An ideal tissue engineering scaffold would have the same nanofibrous morphology and a similar biochemistry as the ECM in native tissue. In addition, the material should be biocompatible, non-immunogenic and biodegradable. Although decellularized tissues fulfill most of these requirements and have been successfully used in tissue engineering, the availability and preparation of such custom-made tissues is often complicated. Moreover, the risk of immunogenic responses is high, when decellularized tissue is transferred into a patient. Therefore, efforts have been made to utilize synthetic materials for the fabrication of tissue engineering scaffolds, since such scaffolds are widely available and a controlled fabrication might lead to tissue engineering scaffolds allowing a better control of the cellular response (Lutolf and Hubbell, 2005). However, synthetic materials often lack the desired biochemical properties or even have a low biocompatibility, which led to the idea of using the native materials present in the ECM for tissue engineering. These natural material scaffolds often contain purified ECM components like collagen or fibronectin, which have the inherent biochemistry and biocompatibility but do not provide all functions of native ECM. However, there is no clear-cut definition of synthetic or ECM materials used in tissue engineering and combinations of both material classes have been tested (O'Brien, 2011).

Especially for the engineering of biomaterial scaffolds to replace lost tissue or for wound healing applications it seems reasonable to use fibrin or its soluble precursor fibrinogen. The enzymatic conversion of fibrinogen into fibrin can easily be utilized to obtain fibrin scaffolds for tissue engineering applications. Therefore, fibrin-based materials have been tested for the treatment of wounds and have successfully been applied in clinical procedures long before the term tissue engineering was introduced (Sierra, 1993). Although fibrin-based materials show the remarkable qualities of native fibrin and are inherently suited for wound treatment, the novel discipline of tissue engineering has recently focused on the production of materials from the fibrin precursor molecule fibrinogen. Interestingly, fibrinogen can be processed into (nano-)fibrous biomaterials either by electrospinning or under versatile self-assembly conditions. However, the question how useful these fibrinogen scaffolds are from a fabrication or from an application point of view is still under discussion and it still has to be determined whether such fibrinogen fibers are a reasonable alternative or a possible addition to fibrin materials.

2.4.1. Fibrin as a biomaterial for tissue engineering

Since fibrin can be easily prepared *in vitro* by incubating fibrinogen with the enzyme thrombin and the resulting fibrin scaffold inherently has the required biochemistry and morphology for cellular interactions, it is one of the first successfully used biomaterials in tissue engineering, especially in applications to prevent bleeding and promote wound healing (Brown and Barker, 2014; Janmey et al., 2009).

The first idea to use fibrin in the treatment of wounds was discussed by Bergel in 1909. More than 100 years ago Bergel realized that the use of the native material for wound closure would not only provide an initial wound closure, but would also help in subsequent tissue regeneration (Bergel, 1909). Since the 1940s, fibrin and the process of fibrin formation were understood well enough to fabricate gels or patches of fibrin *in vitro,* which were applied as wound healing materials (Sierra, 1993). Newer approaches even try to directly embed cells into those preformed fibrin scaffolds. Fibrin gels have been used *in vitro* to induce stem cell differentiation (Catelas et al., 2006). Furthermore, fibrin patches loaded with stem cells have been developed for stem cell delivery (Zhang et al., 2006). Even a co-culture fibrin scaffold with one layer containing fibroblasts and a second layer

containing keratinocytes stacked on top has been established. This two-layer cellular skin equivalent scaffold has been successfully tested in an animal model already (Mazlyzam et al., 2007). Additional advantages of fibrin for biomaterial applications are that the gelation time, porosity, fiber thickness and mechanical properties can be controlled by adjusting the thrombin concentration, the addition of transglutaminase or changes of the pH (Brown and Barker, 2014; Janmey et al., 2009).

In addition to prefabricated *in vitro* fibrin scaffolds, there is a second and more common way to apply fibrin as a biomaterial. Clinically, fibrin is often applied in the form of fibrin sealant or so called fibrin glue. For this application highly concentrated fibrinogen and thrombin solutions are supplied in different vials, which are mixed and immediately sprayed or dripped onto the tissue (Albala and Lawson, 2006). Such fibrin sealants have been widely applied in Europe since the 1970s and have been approved in the United States in the late 1990s (Brown and Barker, 2014). In addition to the applications of fibrin sealant for dermal and burning wounds (Mittermayr et al., 2006), fibrin glue has also been utilized for many other clinical and surgical applications. For example, fibrin sealant has been used to connect larger blood vessels (Dascombe et al., 1997; Shireman and Greisler, 1998) as well as in microsurgical blood vessel reconnection (Andree et al., 2008), which makes fibrin sealant a very useful tool in vascular surgery. Furthermore, fibrin sealants have been employed in hernia repair (Fortelny et al., 2008; Santoro et al., 2007) and in neuro-surgery (Bjarkam et al., 2008).

In summary, the easy handling and the unmatched biocompatibility of fibrin make it an ideal biomaterial for clinical applications and it is not surprising that fibrin-based materials are already used in most fields of modern surgery (Albala and Lawson, 2006).

2.4.2. Fibrinogen as biomaterial for tissue engineering

The rise of the relatively new scientific field of tissue engineering was accompanied by the interesting new idea to prepare fibrous scaffolds out of the fibrin precursor fibrinogen. Many methods have been described to produce fibrinogen nanofibers *in vitro* without the addition of the enzyme thrombin. Since the fibrinogen molecules in those fibers still comprise fibrinopeptides A and B, these fibers cannot be considered to be fibrin. Although

fibrin nanofibers are a biocompatible material, which is inherently suitable for tissue engineering, new methods to produce fibrinogen nanofibers *in vitro* have been established with the aim to use fibrinogen nanofibers as a potential alternative to fibrin fibers for tissue engineering (Rajangam and An, 2013).

Fibrinogen fiber formation in solution

The formation of fibrinogen nanofibers without thrombin can be achieved by different self-assembly methods. Two methods for the *in vitro* preparation of fibrinogen fibers in solution have been described by Wei and coworkers. Fibrinogen fiber formation has been induced by incubation of fibrinogen in acidic pH (Wei et al., 2008a) or in ethanol solution (Wei et al., 2008b). Upon incubation in an acidic pH of 2 or incubation in 80% ethanol the formation of fibrinogen fibers was observed. For acid-induced fibrinogen fiber formation, a conformational change and a partial denaturation were proposed as a potential mechanism of self-assembly. Furthermore, it was speculated about an amyloid-like nature of the fibrinogen fibers (Wei et al., 2008a). Similarly for ethanol-induced fibrinogen fiber formation conformational changes were discussed as a potential mechanism (Wei et al., 2008b). However, in both studies no further investigation of the fibrinogen conformation or formation of amyloid structures was conducted. Amyloids are stacked and self-propagating β-sheet motives, which result in long and unbranched fibers, which are insoluble (Toyama and Weissman, 2011). The formation of β-amyloid structures occurs during the assembly of some natural polymers like for example silk and has been discussed to be involved in many self- assembly processes of nanofibers for biomaterial application (Wei et al., 2017). Nevertheless, the transition of many proteins into insoluble amyloid fibers is accompanied by a loss in protein function and many diseases are linked to the formation of amyloid structures, which are also referred to as protein misfolding diseases (Chiti and Dobson, 2006). Amyloid misfolding of fibrinogen has been reported as hereditary fibrinogen amyloidosis, a genetic disease in which beta amyloid fibrinogen agglomerates in organs due to a mutation in the primary structure of fibrinogen (Picken, 2010). Wei and coworkers used fibrinogen without any mutations in their studies, which makes a potential amyloid formation unlikely. Additionally, the harsh pH value of 2 potentially denatured fibrinogen completely (Marguerie, 1977), which makes a profound interpretation of the self-assembly processes presented by Wei and coworkers challenging. A major drawback for the use of

these methods in tissue engineering is that the yield of fibrinogen fibers is very low and the preparation of applicable scaffolds seems unfeasible. In addition, the harsh pH or ethanol treatments most likely involved, have adverse effects on the bioactivity and biocompatibility of the newly formed fibrinogen fibers.
Nevertheless, the ethanol induced fibrinogen self-assembly described by Wei and coworkers was used in one further study to generate alternating sheets of graphene and fibrinogen fibers in a layer by layer approach (Wang et al., 2014).

Another method to induce the self-assembly of fibrinogen in aqueous solution was recently described by Hämisch and coworkers. The ionic strength of a fibrinogen and NaCl solution was decreased by diluting the solution, which resulted in an aggregation of fibrinogen in the solution as confirmed by light scattering. Additionally, the formation of aggregates upon a drop in ionic strength was confirmed using AFM. Interestingly, the formation of fibrinogen aggregates was fastest with the lowest final ionic strength. However, if the fibrinogen aggregated in a fibrous form was not confirmed (Hämisch et al., 2019).

Fibrinogen fiber formation on hydrophobic surfaces

Self-assembly of fibrinogen has also been observed as a surface reaction. Especially hydrophobic surfaces like for example nanostructured graphite (Reichert et al., 2009), trioctylmethylamine (Koo et al., 2012), gold surfaces (Chen et al., 2009) or polystyrene (Zhang et al., 2017) have been reported to induce the self-assembly of fibrinogen fibers.

The mechanism inducing self-assembly on hydrophobic surfaces is not obvious. An orientation of fibrinogen molecules on the surface and an exposure of cryptic binding sites on the α-C domains of the molecule has been discussed in some studies (Chen et al., 2009; Koo et al., 2010; Reichert et al., 2009), although a concrete mechanism has not been revealed to date. One factor that makes the investigation of the mechanism of surface induced fibrinogen fiber formation challenging is the change in concentration and ionic strength during the drying of the samples, which was postulated to have an additional effect on the fiber formation (Reichert et al., 2009).

A more recent study has investigated the adhesion of fibrinogen molecules to a polyethylene single crystal at different pH values. It was shown that fibrinogen formed fibrous agglomerates upon adsorption to the polyethylene surface at a pH of 7.4. At a pH of 9.2 only single molecules adsorbed to the surface. However, it has to be noted, that the samples at a pH 7.4 were prepared in a buffer containing Na^{+}-ions, while for the samples at a pH of 9.2 a buffer containing Ca^{2+}-ions was used. This is likely to have a strong additional influence on fibrinogen adsorption (Helbing et al., 2016).

Dubrovin and coworkers conducted another interesting recent atomic force microscopy study of fibrinogen fiber formation on hydrophobic surfaces, which investigated the fibrinogen self-assembly on highly oriented pyrolytic graphite modified with anoligoglycine-hydrocarbon. This treatment makes the graphite surface slightly more hydrophilic (10° of static contact angle). It was shown that fibrinogen adsorption to the modified surface resulted in the gradual formation of fibrinogen fibrils within several minutes. The formation of fibrinogen fibrils was accompanied by an unfolding of different fibrinogen domains and a reduction of sample height, which indicates a change in fibrinogen conformation (Dubrovin et al., 2019).

The biocompatibility and bioactivity of fibers prepared by self-assembly on hydrophobic surfaces has not been determined, although the milder way to induce self-assembly implicates better biological functions as compared to ethanol- or acid-induced assembly. The major drawback of the self-assembly on hydrophobic surfaces also lies in the poor fiber yield. For the fabrication of tissue engineering scaffolds, the fiber formation is to scarce and the hydrophobic surface limits the formation of a two-dimensional fiber network. Although fibrinogen fibers prepared on hydrophobic surfaces are not applied in tissue engineering, the research of fibrinogen self-assembly on hydrophobic surfaces has strong implications for potential surface coatings of implant materials. If an implant is designed to have contact with blood, like for example a stent, an agglomeration of fibrinogen fibers can have unwanted and even fatal consequences like thrombosis (van Kampen et al., 1979). This can potentially be avoided by coating the implant with a surface that shows a low fibrinogen adsorption and fiber formation (Zhang et al., 2017).

Fibrinogen fiber formation by extrusion

Recently, extrusion through hydrophilic aluminum oxide nanopores has been introduced as a new method to prepare nanofibers from various biopolymers including fibrinogen (Raoufi et al., 2016). It was discussed that during the extrusion of a viscous fibrinogen solution through a nanopore shear forces are present, which partially unfold the fibrinogen molecule. A conformational change during the extrusion process has been confirmed for the ECM protein fibronectin, which makes a confirmation change during fibrinogen extrusion plausible (Raoufi et al., 2015). However, the extrusion approach mostly results in bundles of fibers instead of porous scaffolds with nanofibers and the outcome can vary, which makes extrusion of fibrinogen not suitable for the fabrication of tissue engineering scaffolds.

2.4.2.1. Electrospinning of fibrinogen fibers

None of the techniques mentioned above is reliable enough or has sufficient fiber yield to produce dense fibrinogen fiber networks, which could be applied for tissue engineering. However, as a well-established technique, electrospinning facilitates the preparation of nanofibers on a large scale *in vitro* and can be used for fibrinogen (Wnek et al., 2003).

Electrospinning was originally designed for the production of non-biological polymer nanofibers, but has been introduced as a tool to prepare nanofibers from many different biological materials. The usual setup for electrospinning consists of a grounded collector and a metallic needle as a spinneret, which are connected to a high voltage power supply like schematically shown in Figure 8 (Li and Xia, 2004).

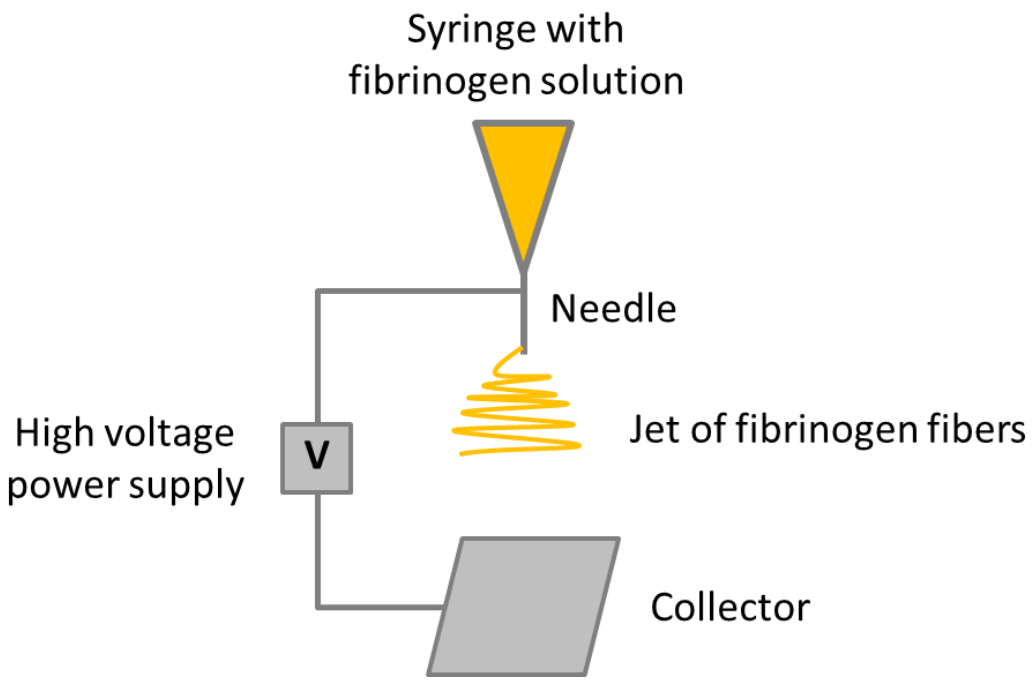

Figure 8: Scheme of an electrospinning setup
For electrospinning, a polymer solution is extruded through a needle to which a high voltage is applied. Due to charge effects, the polymer solution overcomes the surface tension and a liquid jet of polymer nanofibers is ejected towards the collector.

When a polymer is dissolved in an organic solvent and pressed through the spinneret while a high voltage is applied (1 to 30 kV), the drop of polymer solution at the tip of the spinneret will become highly charged. Due to the repulsion of the induced surface charges, the drop changes its shape to a so called Taylor cone. If the electric field is strong enough, the electrostatic forces can overcome the surface tension of the drop and a small liquid jet is ejected towards the collector. Since the organic solvent evaporates, thin threads of the polymer fibers are deposited on the collector (Li and Xia, 2004; Teo and Ramakrishna, 2006). Electrospinning is a versatile method since the fiber diameters can be controlled by adjusting the polymer concentration, the voltage and the distance between the spinneret and the collector. Moreover, by using a movable collector it is possible to control the fiber orientation and even obtain aligned fiber scaffolds (Teo and Ramakrishna, 2006). The well controllable fiber morphology provided by electrospinning and obtained scaffold dimensions made this technique attractive for the fabrication of nanofibers from various biopolymers like collagen (Matthews et al., 2002), silk fibroin (Min et al., 2004) or chitosan (Ohkawa et al., 2004). However, especially the electrospinning of proteins has been controversially discussed, because the organic solvents commonly used, like for example

1,1,1,3,3,3-hexafluoro-2-propanol, have been shown to denature proteins (Kundu and Kishore, 2004). Circular dichroism studies of the secondary structure in electrospun protein fibers have shown that collagen was completely denatured by the organic solvent and the high voltages during the electrospinning process. The electrospun fibers had lost 99% of their native secondary structure (Zeugolis et al., 2008).

Despite the denaturation problem, electrospinning has also been used to produce fibers from fibrinogen, which was first described by Wnek and coworkers (Wnek et al., 2003). Wnek achieved fibrinogen fibers with a wide diameter range of 80 to 700 nm, which organized into fibrous networks with dimensions of several cm^2. The production of large-scale scaffolds seemed like a first step to produce fibrinogen fibers that could be applied for tissue engineering. However, the fibrinogen had to be dissolved in 1,1,1,3,3,3-hexafluoro-2-propanol. If this solvent or the electrospinning process affects the secondary structure or even denatures the fibrinogen has not been addressed (Wnek et al., 2003). During electrospinning of fibrinogen, the fiber diameter and orientation can be controlled by adjusting the voltage, the fibrinogen concentration and the collector. These advantages led to follow up studies, which characterized the mechanics and the liquid flow permeability of fibrinogen fiber scaffolds, but did not investigate structural changes, biological function or cell interactions (McManus et al., 2006; Sell et al., 2008a)

Later, the feasibility of electrospun scaffolds for tissue engineering applications was tested in two studies without a prior investigation of structural changes of the fibrinogen during electrospinning. These experiments showed that fibroblasts as well as smooth muscle cells proliferated on electrospun fibrinogen nanofibers and even started to deposit collagen over a time course of 14 days. Therefore, the authors of the studies concluded that electrospun fibrinogen nanofibers are bio-mimicking, still biologically active and have great potential for applications in tissue engineering (McManus et al., 2007b; McManus et al., 2007a). However, this conclusion should be treated with caution. Since both proliferation studies failed to include crucial control groups, a final conclusion about cell proliferation cannot be made. The fact that fibroblasts as well as smooth muscle cells started to deposit collagen on electrospun fibrinogen fibers is likewise no proof for bioactivity or biocompatibility since it is long known that fibroblasts and smooth muscle cells deposit collagen even on standard polystyrene cell culture surfaces (Amento et al., 1991; Diegelmann et al., 1979).

Despite these undiscussed questions electrospun fiber materials were further developed by modification with different crosslinking agents (Sell et al., 2008b). It was shown that the mechanical properties could be altered and the degradation time of electrospun fibrinogen nanofibers could be delayed. Nevertheless, glutaraldehyde crosslinking and 1-ethyl-3-(3-dimethylaminopropyl) carbodiimide hydrochloride crosslinking had negative effects on the biocompatibility of the electrospun fibrinogen fibers indicated by a poor collagen deposition (Sell et al., 2008b).

The first study that actually investigated secondary structure changes in fibrinogen fibers induced by electrospinning was conducted by Carlisle and coworkers (Carlisle et al., 2009). In this study the structural changes of fibrinogen upon dissolving in 1,1,1,3,3,3-hexafluoro-2-propanol were analyzed using circular dichroism spectroscopy. It was shown that the content of α-helices increased from 25% to 60% in the spinning solution. Interestingly, this massive change of secondary structure was interpreted as a proof that fibrinogen stayed largely folded in the spinning solution. Unfortunately, only the structure of fibrinogen in the spinning solution before the actual electrospinning process was analyzed (Carlisle et al., 2009). The structure of fibrinogen in the electrospun fiber therefore stays elusive. One attempt to overcome the drawbacks of the organic solvent was the electrospinning of fibrinogen in a mixture of formic and acetic acid. The secondary structure of the resulting fibers was analyzed using Fourier-transform infrared spectroscopy. Fibers prepared in the acidic solvent showed no differences in secondary structure when compared to fibers prepared with the 1,1,1,3,3,3-hexafluoro-2-propanol solvent (Mirzaei-Parsa et al., 2018).

Electrospun ccomposites of fibrinogen and poly-lactic acid fibers have been used to investigate the effects of electrospun fibrinogen scaffolds on stem cell differentiation (Forget et al., 2016). Interestingly, the chondrogenic differentiation of mesenchymal stem cells was favorable on randomly oriented fibers rather than on aligned fibers and a thin two-dimensional scaffold proved to be more useful for differentiation than a thicker three-dimensional scaffold (Forget et al., 2016).

In another recent study, electrospun fibrinogen fibers were also applied to guide endothelial cell migration (Gugutkov et al., 2013). This study analyzed the primary structure of electrospun fibrinogen by SDS PAGE. With this method, it was shown that the peptide

backbones of the Aα-, Bβ- and γ-chains were still intact after electrospinning. However, this method did not allow any conclusion about the secondary structure of fibrinogen in electrospun fibers. In summary, electrospinning is one of the most applied techniques for the production of fibrinogen fibers, because of its well-characterized fabrication process, adjustable fiber dimensions and scaffold porosities. However, there is a lack of studies, which focus on the secondary structure of the electrospun fibrinogen fibers. It is remarkable that the secondary structure, which is responsible for all the advantageous properties of fibrinogen including the promotion of cell adhesion, biocompatibility and bioactivity, has been widely neglected during the establishment of electrospun fibrinogen fibers as a biomaterial for future tissue engineering applications.

2.5. Aim of the thesis

This thesis aims at a fundamental understanding of fibrinogen fiber assembly under *in vitro* conditions in a cell- and enzyme-free environment. Towards novel concepts in wound healing therapy it is of particular interest, how the presence of different salts and varying environmental conditions influences the assembly of fibrinogen into fibrillar networks.

The first key question will be how different environmental conditions induce fibrillogenesis of fibrinogen and which morphological characteristics the fiber assemblies exhibit. Therefore, the influence of different ion species, variations in ionic strength, fibrinogen concentration or pH value, different drying conditions as well as different substrate materials on fibrinogen assembly will be investigated. First, the morphological characteristics of fibrinogen scaffolds will be studied to identify key parameters, which induce fibrillogenesis. The findings of these studies will be used to propose a fundamental mechanism for fibrinogen self-assembly under *in vitro* conditions.

Another focus of this thesis will be the protein conformation in self-assembled fibrinogen nanofibers. To answer the second key question whether fibrinogen self-assembly *in vitro* is accompanied by conformational changes, the results from morphological analysis will be correlated with secondary structure analysis. This project part also aims at the question whether fibrinogen self-assembly *in vitro* is associated with the formation of pathogenic amyloid fibrils.

Finally, the biofunctionality of self-assembled fibrinogen nanofibers will be in the focus of this thesis. After key parameters for *in vitro* assembly of fibrinogen into nanofibers have been identified it will be the next aim to investigate the fiber ability to bind to other molecules. Moreover, the degradation characteristics of self-assembled fibrinogen fibers under the influence of varying enzymes will be studied. The results of this project part will be important to answer the question whether fibrinogen fibers, assembled under *in vitro* conditions, are biologically active.

The expected results of this dissertation will be used to gain insight into the fundamental mechanisms of fibrinogen fiber formation *in vitro*. The expected findings will also provide a first indication of the potential use of self-assembled fibrinogen fibers in future wound healing applications.

3. Background of the main analytical techniques

In order to understand the self-assembly of fibrinogen, the presence and the morphology of fibrinogen fibers prepared under various *in vitro* conditions was analyzed using scanning electron microscopy. To gain an insight into potential changes in secondary structure during fibrinogen self-assembly, the fibrinogen samples were analyzed using circular dichroism spectroscopy. Therefore, a detailed introduction into the background of these two techniques is given in this chapter.

3.1. Scanning electron microscopy

The principal of scanning electron microscopy is similar to optical microscopy only that a focused electron beam is used instead of a light beam for imaging. The electrons are generated by either a field emission or a thermionic cathode. When a high voltage of usually 0.1 to 50 kV is applied, the electrons are accelerated towards the anode. This primary electron beam is generated in high vacuum and can be focused by a set of (electro)magnetic lenses (Figure 9). When the focused primary electron beam hits a point of the specimen surface, electrons of the specimen with low exit energy are emitted, which is also referred to as inelastic scattering. These secondary electrons are collected by a positively biased collector and an intensity value for this point of the specimen is calculated based on the number of detected secondary electrons. By scanning the sample point by point, an image of the specimen can be generated. Since secondary electrons show an enhanced emission on edges and small particles, the position of the detector generates artificial shadow contrast at deeper positions and a topographical image of the specimen surface with a high depth of focus can be achieved. Secondary electrons can only be emitted from a depth of a few nanometers of the specimen surface. In combination with the focus of the electron beam this allows a resolution of 1-10 nm (Pfützner, 2012; Reimer, 1998).

In addition to secondary electrons, backscattered electrons are also detected in a scanning electron microscope. Backscattered electrons are high-energy electrons of the primary electron beam, which are reflected upon collisions with atoms of the specimen, which is also referred to as elastic scattering. Since the number of these collisions and the penetration depth into the specimen can vary, backscattered electrons are decelerated

individually and have a broad energy spectrum. Therefore, detection of the backscattered electrons has a higher information depth and a large exit area, which leads to a lower resolution (Figure 9). On the other hand, the number of collisions of the backscattered electrons is dependent on the atomic density of the specimen, which makes it possible to distinguish between different specimen materials (Reimer, 1998; Schatten, 2011).

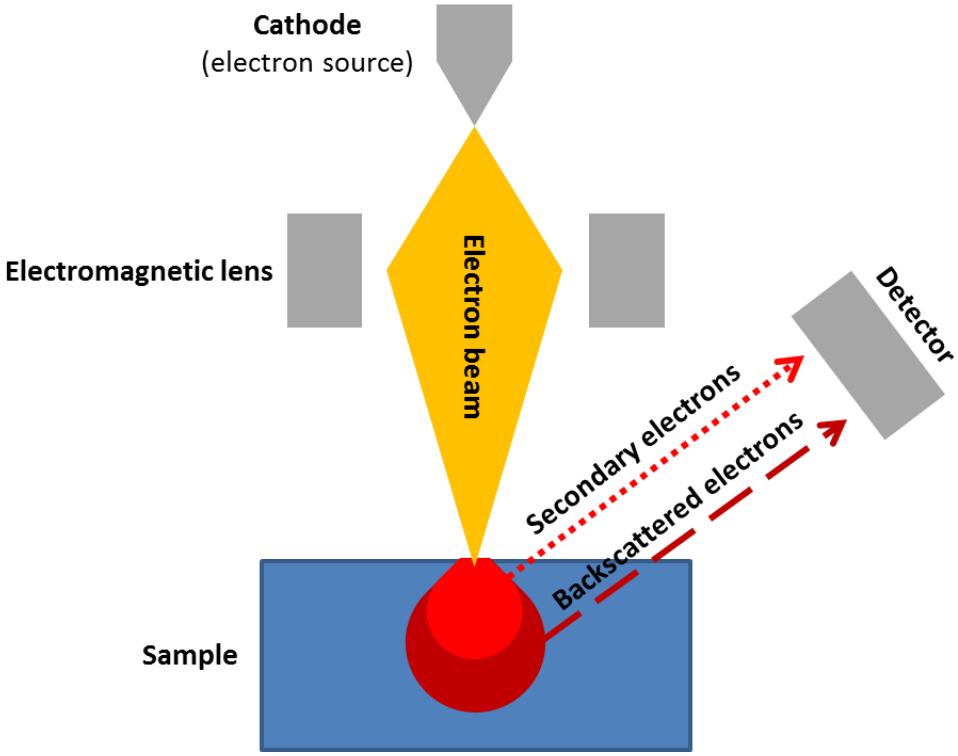

Figure 9: Schematic setup of an electron microscope.
An electron beam is generated from a cathode and focused using an electromagnetic lens. When the electron beam gets in contact with a sample, electrons from the sample surface are released. Secondary electrons with a low exit energy are emitted from a low depth, while backscattered electrons with a higher exit energy can be released from deeper parts of the sample. Dependent on their exit energy secondary and backscatter electrons can be detected.

The majority of biological samples is analyzed by detecting secondary electrons. Biological materials usually contain water, which would interfere with an electron microscopically analysis. If an uncontrolled drying does not result in a sufficient dehydration of the sample, commonly used treatments are freeze-drying or critical point drying. In addition, many samples are fixated using aldehyde crosslinking and subsequently dehydrated stepwise using an ethanol exchange while maintaining the native morphology (Goldstein et al., 1981). Since most organic materials have rather insulating characteristics, it is necessary to coat the sample with a few nanometer thin layer of a conductive material like gold or to

work with low acceleration voltages (Schatten and Pawley, 2008). The insulation properties of biological materials also cause an accumulation of electrons at the sample surface leading to charge effects. At the same time, secondary electrons of uncoated samples can be released from a certain depth of the sample, which decreases the resolution, when working with unsputtered samples (Schatten and Pawley, 2008). These drawbacks are overcome by sputtering the sample with a layer of gold or another heavy metal. Secondary electrons of sputter-coated samples are mostly released from the metal layer, which prevents charging of the biological material beneath. On the other hand, the coating of biological samples only results in an indirect image of the sample morphology, since only the morphology of the metal layer on the specimen surface is detected. This makes the sample preparation and the coating procedure a crucial factor for the electron microscopically analysis of biological samples (Schatten, 2011).

3.2. Circular Dichroism Spectroscopy

Like for other spectroscopy techniques the main underlying principle of circular dichroism spectroscopy is the measurement of the absorbance of light with a certain wavelength as defined by Lambert-Beer's law:

$$A = \log\left(\frac{I_0}{I}\right) = \varepsilon c l$$

Here A is the absorbance, which is defined as the logarithm of the ratio of incoming light intensity (I_0) and the outgoing intensity (I). The absorbance can also be calculated by multiplying the concentration c (in M) by the path length l (in cm) with a material specific extinction coefficient ε (in M^{-1} cm^{-1}) (Berova et al., 2000).

The measurement of absorption and the determination of concentration by spectroscopy are mostly used for components in solution, but can also be used for solids. Every spectroscopic method has two crucial prerequisites: The exact knowledge of the path length, which for solutions is determined by the used cuvette and a homogenous distribution of the measured material in the sample (Mark, 1991).

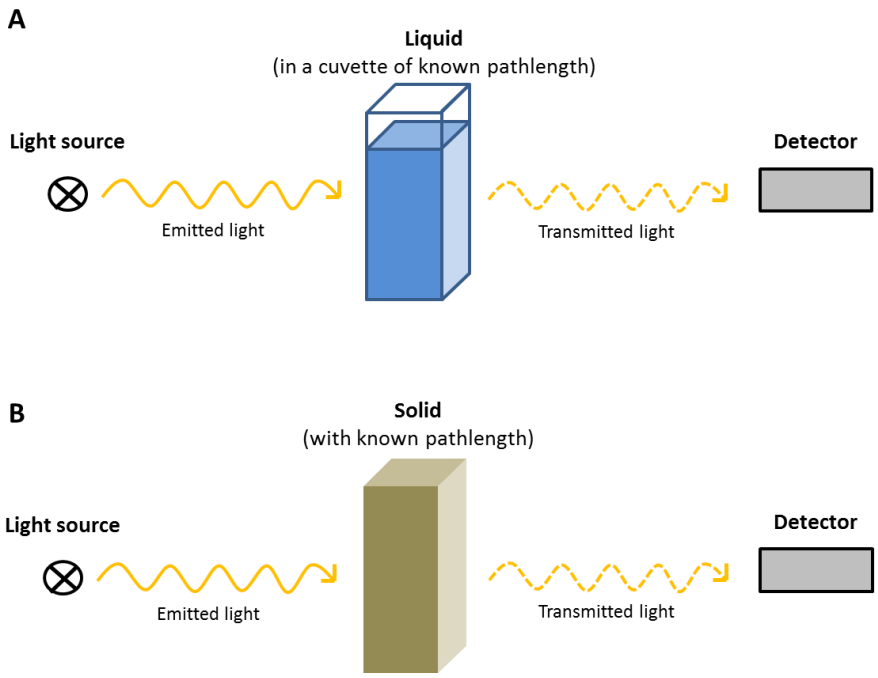

Figure 10: Schematic setup of liquid and solid state spectroscopy.
Spectroscopy relies on the analysis of absorbance of light of a certain wavelength. The absorbance of a liquid in a cuvette (A) or a solid (B) can be measured by detecting the transmitted light. For a further interpretation of the absorbance the exact path length of the sample has to be known.

The second basic principle of circular dichroism spectroscopy are differences in the absorption of left handed and right handed circular polarized light by chiral molecules. Chirality is a geometrical term for molecules, which cannot be superposed on their mirror images (Berova et al., 2000).

Polarization of light

Light is an electromagnetic wave, in which the field vectors of the electrical and magnetical components are vertically shifted to each other. Both vectors are perpendicular to the propagation direction of the wave. The direction of field vectors is random in natural light. When natural light passes through a polarizer only one field vector direction remains in respect to the propagation of the wave and linear polarized light can be observed by the receiver (Foster et al., 2018).

If two linearly polarized light waves are perpendicular to each other and their phase is shifted, circular polarized light is generated. The sum of the field vectors of both waves will be a field vector with a constant magnitude, but the direction of this field vector will change

over time in a rotational manner. From the point of the receiver the wave will describe a helix around the propagation direction, which can either be clockwise (right hand circular polarization) or counterclockwise (left hand circular polarization) (Foster et al., 2018).

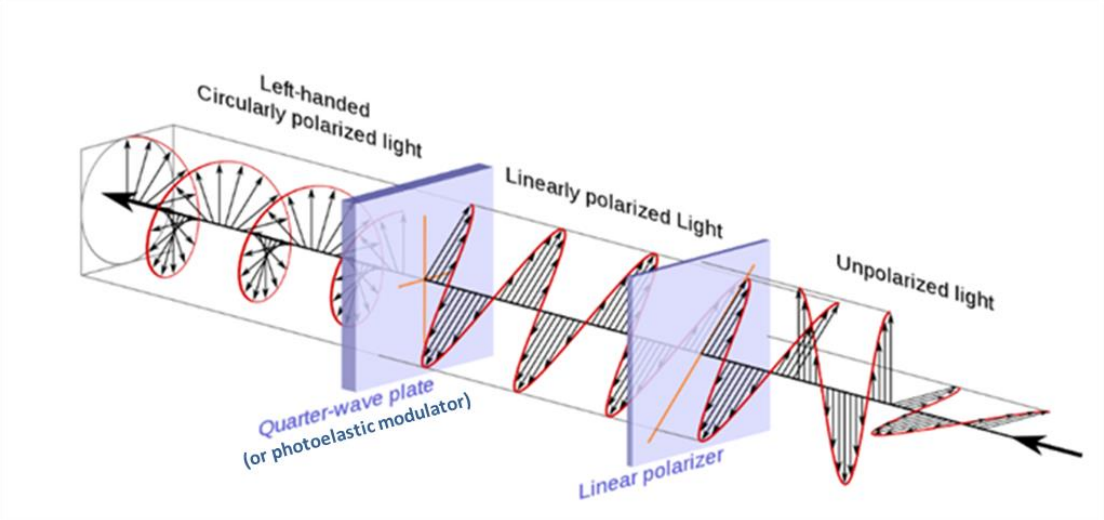

Figure 11: Polarization of light
Unpolarized light with random electrical field vector orientations is converted to linear polarized light with only one field vector orientation by beaming it through a polarizer. By beaming linear polarized light through a quarter-wave plate, circular polarized light can be generated. In circular polarized light, the electrical field vectors rotated in a helix around the direction of propagation. Image modified from https://byjus.com/physics/polarization-of-light/ 11.2019

Experimentally circularly polarized light can be generated by passing linearly polarized light through a birefringent material. Common birefringent materials to generate circularly polarized light are quarter-wave plates, through which linearly polarized light is transmitted at a 45° angle. This splits the light into two perpendicular polarization directions, which move through the wave plate at different speeds. Thereby, the phases of the two transmitted waves are shifted, which results in circularly polarized light (Greenfield, 2006; Kemp, 1969). The circularly polarized light used for circular dichroism spectroscopy is often generated by the use of photo elastic modulators. Photo elastic modulators commonly used are blocks of quartz glass attached to a piezoelectric actuator. Controlled high frequency vibrations of the piezoelectric actuator induce birefringent properties in the quartz glass, which turns the quartz block into a tunable wave plate like depicted in Figure 12 (Greenfield, 2006; Kemp, 1969; Wang et al., 2019).

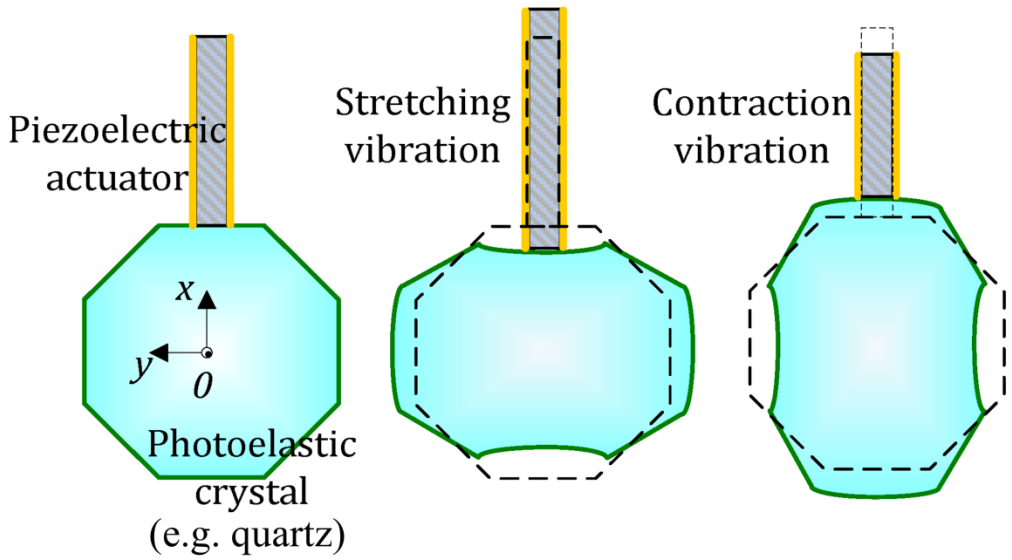

Figure 12: Scheme of a photoelastic modulator.
A piezoelectric actuator excites vibrations in a photoelastic crystal like for example quartz. This vibration is accompanied by variations in the birefringence of the photoelastic crystal, which changes the phase and polarization of incident light. (Figure modified from (Wang et al., 2019).

Absorbance of circularly polarized light by chiral molecules

Since circularly polarized light itself is chiral, right or left-handed polarized light of the same wavelength is absorbed differently by chiral molecules. This effect can either be described as a difference in absorbance or as a modification of Lambert-Beer's law with different extinction coefficients for right or left-handed polarized light (Kelly et al., 2005).

$$\Delta A = A_L - A_R$$

$$\Delta A = (\varepsilon_L - \varepsilon_R)cl$$

Another way to describe the difference in the absorbance of right or left-handed polarized light is to combine the electrical field vectors of the different orientations. If the absorbance of right and left-handed circularly polarized light is different, the resulting field vectors have an elliptical orientation like depicted in Figure 13.

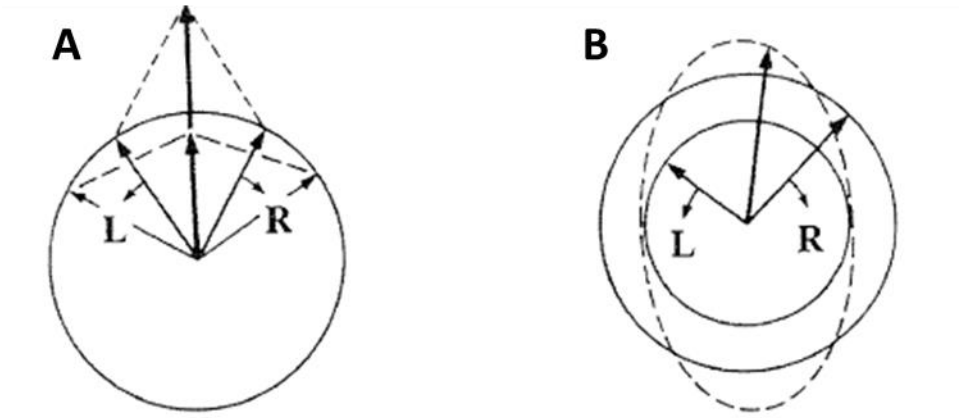

Figure 13: Elliptical orientation of field vectors.
If the electrical field vectors of right and left circular polarized light with the same amplitude are combined, the result is plane polarized (**A**). If the field vectors of the right and left circular polarized light have different magnitudes, the result is epileptically polarized. Figure modified from (Kelly et al., 2005).

This ellipticity can be described as the tangent angle θ of the combinations of the right-handed (E_R) and the left-handed (E_L) electrical field vectors (Kelly et al., 2005).

$$\tan\theta = \frac{E_R - E_L}{E_R + E_L}$$

By converting the ellipticity into radians, the relationship between ellipticity θ and the difference in absorbance ΔA can be described as follows:

$$\theta = 32.98\,\Delta A$$

Circular dichroism spectroscopy of proteins

In circular dichroism spectroscopy of proteins, the ellipticity is often normalized to the number of amino acids N and described as mean residue ellipticity (θ_{MRE}):

$$\theta_{MRE} = \frac{100 * \theta}{N * c * l}$$

Circularly polarized light is absorbed by the protein backbone. The electrons of the oxygen, carbon and nitrogen atoms of the peptide group form a delocalized π-electron system, which absorbs UV light in a wavelength range of 180 to 250 nm (Greenfield, 1996).

After excitation the transition of electrons from π-bonding orbitals to π-antibonding orbitals ($\pi \rightarrow \pi^*$) is possible for the electrons of the C=O bond as well as for the free electrons at the

nitrogen atom, because the free electron pair of the nitrogen is a mesomeric part of the π-electron system. Additionally, excitation of the free electrons of the oxygen to π-antibonding orbitals ($N \rightarrow \pi^*$) is also possible (Kelly et al., 2005). All three atoms of the peptide group lay in one plane and no bond rotation is possible due to the π-electron system. The only bonds that can freely rotate in the protein backbone are the bonds to the adjacent chiral carbon atoms next to the peptide group. The two dihedral angles of the π-electron systems on the bonds of the chiral α-carbon atom are termed φ and ψ. The rotations of these two bonds are the only possibilities to change the conformation of the protein backbone, which is termed secondary structure. Some compositions of φ and ψ angles are more energetically favorable and found more often in nature while others are impossible due to steric hindrance like calculated and illustrated in the Ramachandran plot (Ramakrishnan and Ramachandran, 1965). The favorable angle compositions arise from the possibility of hydrogen bonds between different peptide groups and thereby also stacking of the π-electron systems. This gives rise to two main secondary structures found in proteins (see Figure 14).

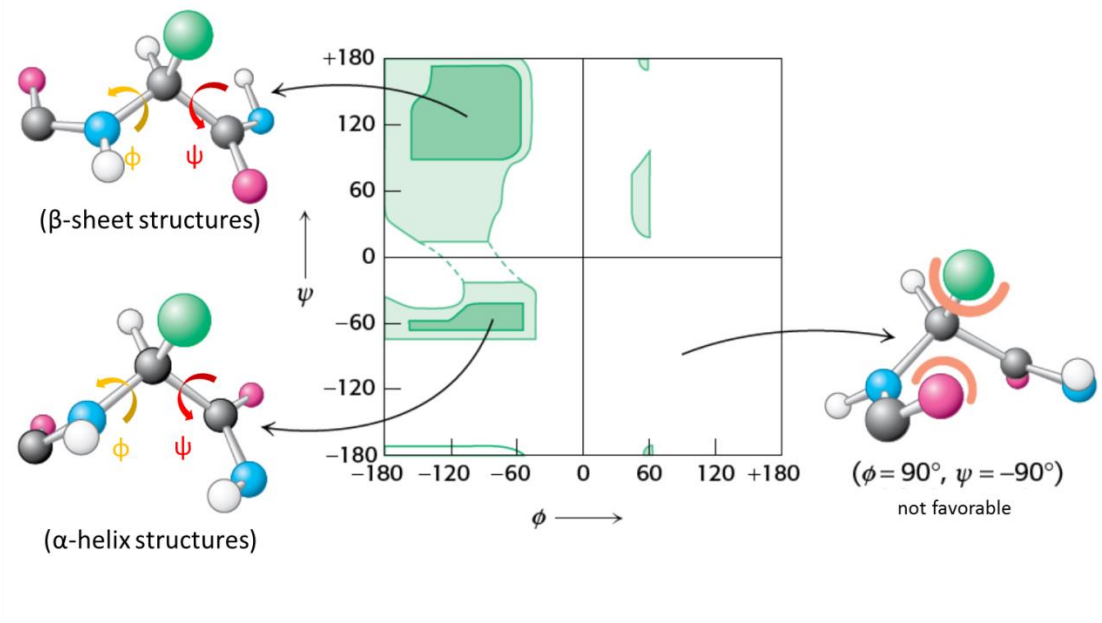

Figure 14: Ramchandran plot of possible ϕ and ψ angles in a protein backbone.
The dihedral angles of the freely rotating bonds in the protein backbone determine the secondary structure. Due to steric hindrance, not all angle combinations are favorable. The two main groups of possible angle combinations are observed in α-helical or β-sheet conformations of the protein backbone. Figure modified from (Berg et al., 2012).

The first major secondary structure that is found in proteins is the α-helix, where angles φ and ψ are around -60° and 45°, respectively. This results in a total angle of around -105° from one amino acid residue to the next and ultimately leads to a right-handed helical structure with 3.6 amino acids per turn. The α-helix is stabilized by hydrogen bridges between one peptide group and the fourth peptide group downstream in the protein backbone, which is located in the next turn of the helix slightly shifted (Berg et al., 2012). The second predominant secondary structure found in proteins are β-sheets with φ and ψ angles of -135° and 135°. This allows a concertina-like shape in long strands wherein the hydrogen bridges form between peptide groups of neighboring strands (Berg et al., 2012).

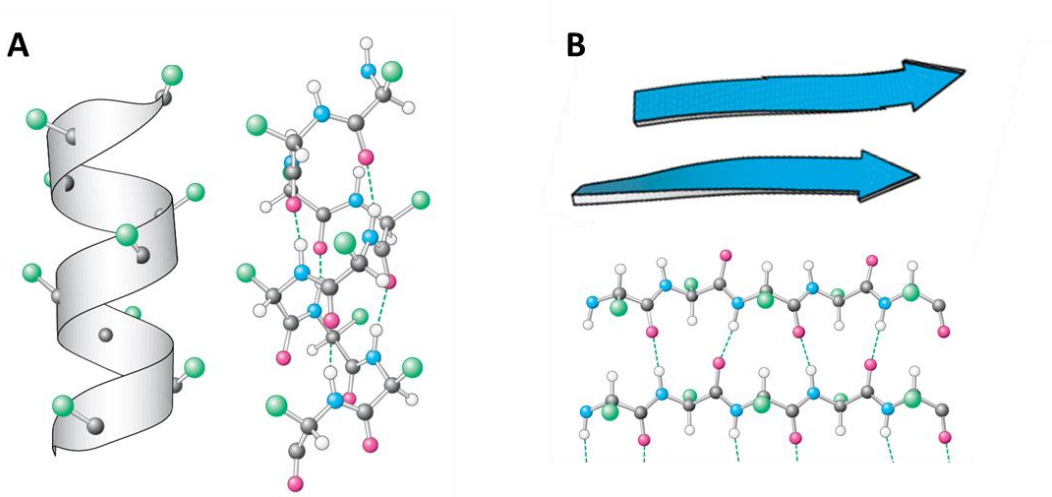

Figure 15: Schematic and molecular representation of α-helix and β-sheet structures in the protein backbone.
In a α-helix the hydrogen bridges are formed between one peptide group and the fourth downstream peptide group (**A**). In a beta sheet structure, hydrogen bridges are formed between the peptide groups of neighboring strands (**B**). Figure modified from (Berg et al., 2012).

One can envision the protein backbone as a pearl chain of small π-electron systems. Dependent on how the chain is folded, the π-electron systems have a different orientation to each other. This influences the ratios of left and right-handed circularly polarized light absorbed by different conformations. Furthermore, the orientation of π-electron systems also has an influence on inductive effects between the single systems, which influences the energy required to excite the π-electron and thereby changes the wavelength, which is absorbed by the system. Therefore, α-helix and β-sheet structures show different circular dichroism spectra, which are characteristic for the respective secondary structure. Circular dichroism spectra of a α-helix show a local maximum in ellipticity at 192 nm and two

separate minima at 208 and 222 nm. In contrast, circular dichroism spectra of a β-sheet only show a maximum in ellipticity at 195 nm, a shoulder at 212 nm and a minimum at 216 nm (Berova et al., 2000).

Since most proteins contain different secondary structures, the measured circular dichroism spectra often contain different structural signals. One also has to consider the circular dichroism spectroscopy does not provide a measurement of the structure of a single protein molecule, but it yields a measurement of an ensemble of many molecules of the same protein. Hence, many algorithms have been developed to determine individual secondary structure components from a circular dichroism spectrum. These algorithms predicted the secondary structure from a circular dichroism spectrum based on variable selection or singular value decomposition of reference spectra from proteins with a known structure. However, most of these algorithms failed , which consist of a combination of α-helices and β-sheets or have a high content of β-sheets in general. In this thesis the BeStSel web server was used to analyze circular dichroism spectra, since it accurately distinguishes different structural components and therefore reliably estimates the secondary structure (Micsonai et al., 2018; Micsonai et al., 2015).

The BeStSeL web server determines secondary structure based on a circular dichroism spectrum by fitting a linear combination of eight different basis spectra. Each basis spectrum is representative for one secondary structure component. The basis spectra are based on a set of 73 reference spectra of proteins with a known structure. Since these basis spectra also contain spectra for beta sheet structures of different twists and orientations, a more reliable structure analysis of proteins containing α-helices and β-sheets is possible. In addition, each basis spectrum is optimized separately and combined to the fitting procedure by a least square method. (Micsonai et al., 2018).

Solid state circular dichroism spectroscopy

In this thesis the circular dichroism of planar or fibrous fibrinogen scaffolds was measured in a dried state. Even though circular dichroism spectroscopy is mostly used as a method for the analysis of proteins in solution, the analysis of a protein in a solid state is also possible like for most other spectroscopic methods (Harada and Kuroda, 2002). When working with dried protein samples it has to be considered that the dried protein is possibly

not homogenously distributed. This results in turbidity and dispersion of light. In a non-homogenous solid there is even the risk of birefringence or even macroscopic anisotropy, which potentially results in measurement artifacts (Kuroda and Honma, 2000); (Castiglioni et al., 2009). Some approaches in sold state circular dichroism use grinded solids in Nujol mulls (refined mineral oil) to overcome the heterogeneity induced light dispersion effects. However, the use of this approach leads to refraction and scattering effects at the grain boundaries (Kuroda and Honma, 2000).

When working with solid-state samples prepared by drying, an additional challenge is the heterogeneity in sample thickness, which makes a correct determination of the path length difficult. In addition, heterogeneity in sample thickness can become problematic when only a small part of the sample is scanned during circular dichroism. One method to minimize these effects is to measure the sample in different orientation or if possible to measure different parts of the sample (Castiglioni et al., 2009).

During the sample preparation for solid stated circular dichroism of dried proteins, the molecules might orient during the drying process giving rise to a highly ordered structure as compared to the randomly orientated protein molecules in solution (Kuroda and Honma, 2000). Due to the drying, the degrees of freedom of a protein molecule especially the rotation and orientation of chemical bonds can become severely restricted. This results in an artificial solid-state chirality of components, which are not chiral in the liquid state, and leads to measurement artifacts. These artifacts in combination with anisotropy might also lead to an overestimation of β-sheet structure content (Harada and Kuroda, 2002) One easy method to exclude those artifacts is to measure the solid state sample from front and backside (Castiglioni et al., 2009; Harada and Kuroda, 2002). Despite these challenges, solid-state circular dichroism spectroscopy is an applied technique to measure secondary structure of proteins. Especially for protein samples, it is advisable to measure the samples from front and back side. Furthermore, an exact determination of sample thickness and heterogeneity with the used concentrations is crucial (Castiglioni et al., 2009; Harada and Kuroda, 2002). Like for any measurement technique, an additional analysis with other methods is advisable to validate the results obtained using solid state circular dichroism spectroscopy and allow a profound interpretation of the structural data obtained.

4. Methods

4.1. Preparation of fibrinogen, buffers and solutions

All aqueous buffers and solutions were prepared using deionized water from a TKA Gen Pure water purification system (Thermo Fisher Scientific, Schwerte, Germany).

4.1.1. Buffer preparation

For self-assembly studies, different aqueous buffer systems were used. Solutions of 10 mM NH_4HCO_3 (Roth, Karlsruhe, Germany), 20 mM sodium citrate (Sigma, Steinheim, Germany), 750 mM NaCl (AppliChem, Darmstadt, Germany), 20 or 750 mM KCl (Roth, Karlsruhe, Germany), were prepared by dissolving the desired concentration in deionized water. In addition, solutions of 50 mM NaH_2PO_4 (Roth, Karlsruhe, Germany), 50 mM Na_2HPO_4 (Roth, Karlsruhe, Germany), 50 mM KH_2PO_4 (AppliChem, Darmstadt, Germany) and 50 mM K_2HPO_4 (AppliChem, Darmstadt, Germany) were prepared. Sodium and potassium phosphate buffers were prepared by either mixing 50 mM NaH_2PO_4 and 50 mM Na_2HPO_4 solution or mixing 50 mM KH_2PO_4 and 50 mM K_2HPO_4 solution to obtain buffers with a pH of 7.4. The pH was monitored using a pH meter (Roth, Karlsruhe, Germany). Sodium phosphate buffers were also prepared with pH values of 5, 6, 7, 8 or 9. Five times concentrated phosphate buffered saline (5x PBS) with pH values of 5, 6, 7, 8 or 9 was prepared by adding 700 mM of NaCl into the previously prepared sodium phosphate buffers. To obtain 5x PBS with a pH of 7.4 commercially available PBS tablets (Thermo Fisher, Schwerte, Germany) were used. One PBS tablet was dissolved in 100 ml of deionized water.

HEPES buffered saline was prepared by adjusting a solution of 10 mM 2-(4-(2-Hydroxyethyl)-1-piperazinyl)-ethansulfonsäure (HEPES; Acròs organics, New Jersey, USA) to a pH of 7.4. 150 mM NaCl (AppliChem, Darmstadt, Germany) and 5 mM $CaCl_2$ (Sigma, Steinheim, Germany) were added to the HEPES solution.

The buffers used for sodium dodecyl sulfate polyacrylamide gel electrophoresis (SDS PAGE) were all purchased from Thermo Fisher (Thermo Fisher, Schwerte, Germany). The SDS sample buffer contained 106 mM Tris HCl, 141 mM Tris Base, 2% LDS, 10%

Glycerol, 0.51 mM EDTA, 0.22 mM SERVA Blue G250 and 0.175 mM Phenol Red. The SDS running buffer contained 5 mM Tris(hydroxymethyl)-aminomethane, 5 mM tricine and 0.005% sodium dodecyl sulfate. For the washing of the SDS page gels a solution of 40 % methanol (VWR, Darmstadt, Germany) and 10 % acetic acid (VWR, Darmstadt, Germany) was prepared. The staining of the SDS page gel was carried out in the same solution containing 0.1 % (w/v) coomassie brilliant blue (Sigma, Steinheim, Germany).

4.1.2. Fibrinogen solutions

Fibrinogen solutions were obtained by dissolving commercially available fibrinogen powder (100% clottable Merck, Darmstadt, Germany) in 10 mM NH_4HCO_3 or in 20 mM sodium citrate solution. The fibrinogen solution in citrate was used without further treatments.

Fibrinogen in 10 mM NH_4HCO_3 solution was obtained by dialysis by preparing 10 to 20 ml fibrinogen solution with a starting concentration of 20 mg/ml in 15 ml tubes (Sarstedt, Nümbrecht, Germany). After 30 min, when the fibrinogen had completely dissolved, the solution was pipetted into a cellulose membrane dialysis tubing with a 14 kDa cut-off (Sigma, Steinheim, Germany), which had been washed three times for 10 min in ultrapure water. The dialysis tubing was sealed using 70 mm dialysis tubing closures (Sigma, Steinheim, Germany). The solution of fibrinogen was dialyzed overnight against 1 l of 10 mM NH_4HCO_3 under constant stirring.

To determine the concentration after dialysis the absorbance at 280 nm was measured using a Nanodrop spectrometer (Thermo Fisher, Schwerte, Germany). For the calculation of the fibrinogen concentration, the extinction coefficient was determined by measuring the absorbance of different concentrations of undialyzed fibrinogen solutions (Figure 16).

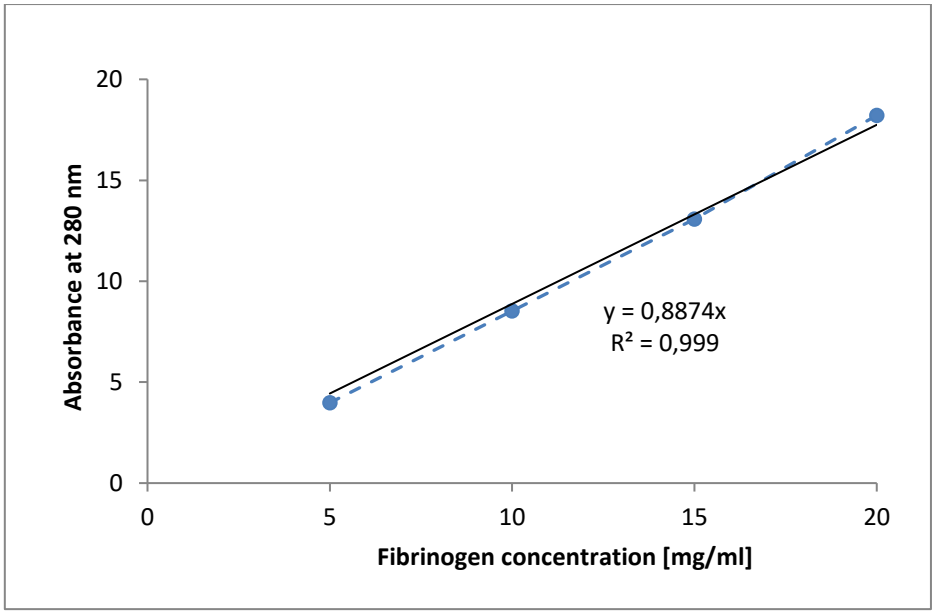

Figure 16: Calibration curve of fibrinogen absorbance
The absorbance at 280 nm was determined for 5, 10, 15 and 20 mg/ml fibrinogen in 10 mM NH_4HCO_3 solution and plotted. The increment of the obtained calibration curve is the specific extinction coefficient of fibrinogen at 280 nm, which was found to be 0.8874 $(mg/ml)^{-1} * cm^{-1}$.

The concentration of fibrinogen in the solution was calculated by using the Lambert-Beer law with the measured absorbance at 280 nm and the determined extinction coefficient of 0.8874 $(mg/ml)^{-1} * cm^{-1}$.

Lambert-Beer law:

$$A_{280\,nm} = \varepsilon_{280\,nm} * c * l$$

The measured concentration of the dialyzed fibrinogen solution was used to dilute the solution to a concentration of 10 mg/ml. The 10 mg/ml fibrinogen stock solutions were aliquoted in Safe lock tubes (Eppendorf, Wesseling-Berzdorf, Germany) and stored at -20°C in a freezer (Liebherr, Biberach an der Riß, Germany).

4.2. Substrate preparation

The main substrate, on which fibrinogen samples were prepared, were round glass cover slips with a diameter of 15 mm (VWR, Darmstadt, Germany). For all following experiments the glass slides were cleaned by immersion in piranha solution, which was

freshly prepared by mixing 95% sulfuric acid (VWR, Darmstadt, Germany) with 30% hydrogen peroxide solution (VWR, Darmstadt, Germany) in a 3:1 ratio. The glass slides were placed in a polyoxymethylene sample holder and immersed in the priranha solution for 5 min. Directly after cleaning in the piranha solution the samples were washed three times with one litre of deionized water from a Genepure water purification system (Thermo Fisher Scientific, Schwerte, Germany). The cleaned glass slides were stored in deionized water. Directly before use, the glass slides were dried under nitrogen flow. The piranha cleaning treatment made the glass slides highly hydrophilic, which became visible when 1 µl drop of deionized water was placed on a dried piranha cleaned slide (Figure 17).

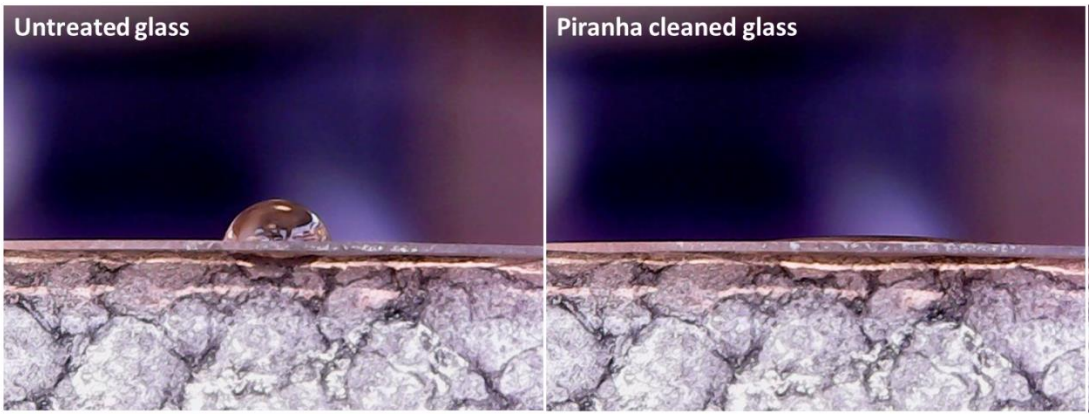

Figure 17: Hydrophilicity of an untreated and a piranha cleaned glass slide
1 µl of deionized water was added onto an untreated or onto a piranha cleaned glass slide. On untreated glass, the drop stayed at one spot while on piranha cleaned glass the drop rapidly covers the surface as a thin layer.

For circular dichroism experiments, Suprasil quartz cuvettes (Hellma UK Ltd.) with path lengths of 0.01, 0.1 or 0.5 mm were used as substrates. The cuvettes were cleaned in an UV−ozone cleaner (BioForce Nanosciences Inc., Salt Lake City, United States) for 1 h.

Other substrate materials used in this thesis were: Polylactic acid (PLA) and polybutylene adipate terephthalate (PBAT) (kindly provided by Prof. Dr. Jörg Müssig, HSB City University of Applied Sciences, Bremen) as well as polystyrene (PS; Sarstedt, Nümbrecht, Germany), polydimethylsiloxane (PDMS; Distrelec GmbH, Bremen, Germany and parafilm (Thermo Fisher Scientific, Schwerte, Germany) substrates, which were directly used without further treatment.

Surface modification of glass substrates

For some experiments the surface of glass slides was modified either by coating it with gold or by modifying it using a silanization with (3-Aminopropyl)triethoxysilane (APTES). Gold-coated glass slides were prepared by sputter coating untreated 15 mm diameter glass slides in an EM ACE600 high vacuum sputter coater (Leica Microsystems, Wetzlar, Germany) with a 5 nm adhesion layer of chromium and subsequently with 50 nm of gold. Substrates modified with (3-Aminopropyl)triethoxysilane (APTES) were prepared by immersion of piranha cleaned glass slides into a mixture of 5% APTES (Sigma, Steinheim, Germany) and 95% ethanol (VWR, Darmstadt, Germany) for 16 h under constant stirring. For this procedure a custom-made PLA glass slide holder was used, which was fabricated using a MakerBot replicator 3D printer (MakerBot industries, New York, United States). After modification, the substrates were washed three times in 200 ml pure ethanol and dried for storage.

4.3. Assembly of fibrin and fibrinogen scaffolds

Fibrin samples were used as reference samples for fibrinogen self-assembly experiments and were prepared on piranha-cleaned glass slides using NH_4HCO_3, phosphate buffer or PBS by the addition of thrombin. 200 µl 10 mg/ml fibrinogen in 10 mM NH_4HCO_3 were incubated with 10 U Thrombin. Additionally, 200 µl 10 mg/ml fibrinogen in 10 mM NH_4HCO_3 were incubated with 10 U Thrombin in the presence of 10 mM phosphate buffer. For thrombin incubations in the presence of PBS, 5 mg/ml fibrinogen, 5 mM NH_4HCO_3 and 2.5x PBS were incubated with 5 U Thrombin. The samples were incubated at 37°C on a heating plate for 1 h and subsequently dried at room temperature.

Fibrinogen scaffolds in citrate solution were prepared by pipetting 200 µl of a 5 mg/ml fibrinogen solution in 20 mM citrate onto a piranha cleaned glass slide and dried overnight at ambient conditions.

All other fibrinogen samples were prepared following the routine depicted in Figure 18. 100 µl of 10 mg/ml fibrinogen in 10 mM NH_4HCO_3 solution were pipetted onto piranha cleaned glass slides (Figure 18 A). In a second step, 100 µl of 5x PBS were added (Figure 18 B), which resulted in final concentrations of 5 mg/ml fibrinogen, 5 mM NH_4HCO_3

solution and 2.5x PBS before the drying procedure (Figure 18 C). For reference samples, on which fibrinogen was dried only in the presence of NH_4HCO_3, 100 µl deionized water were added during step B. This resulted in final concentrations of 5 mg/ml fibrinogen and 5 mM NH_4HCO_3 solution before the drying process started.

For other samples either 100 µl of 50 mM phosphate buffer or 100 µl of 5x PBS were added, which resulted in final concentrations of 5 mg/ml fibrinogen, 5 mM NH_4HCO_3 solution and either 25 mM phosphate buffer or 2.5x PBS.

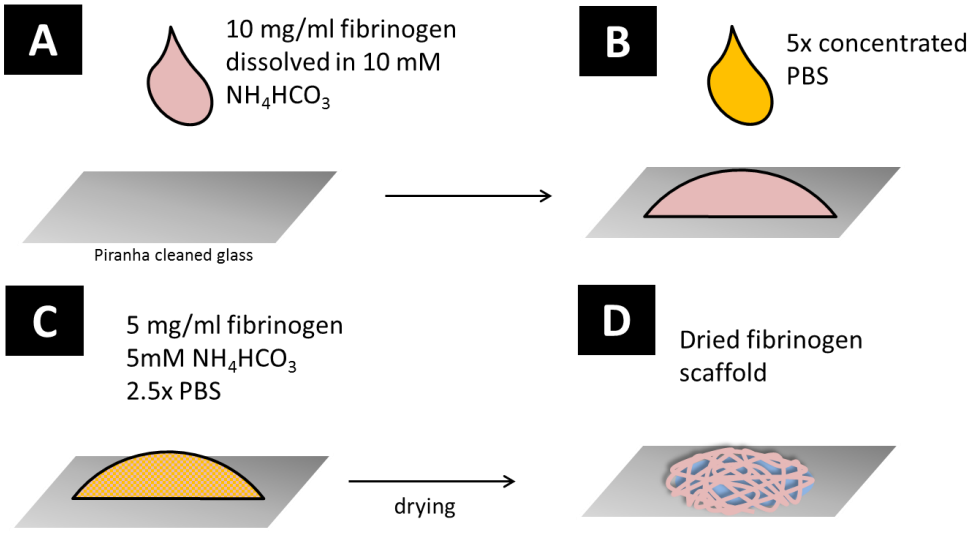

Figure 18: Schematic representation of the fibrinogen sample preparation with addition of PBS
In a first step, fibrinogen in NH_4HCO_3 solution is placed on a piranha cleaned glass slide (A). In a second step, the PBS is added (B). The mix of fibrinogen, NH_4HCO_3 and PBS (C) is dried overnight and a fibrinogen scaffold is obtained (D).

All other fibrinogen scaffolds were prepared by variations of the standard routine shown in Figure 18. In addition to piranha cleaned glass as a substrate, the fibrinogen samples were also prepared on gold coated surfaces, in cleaned quartz glass cuvettes (the total sample volume was adjusted to 40 µl), on APTES modified glass, PLA, PS, PBAT, PDMS or on parafilm surfaces.

The fibrinogen concentration of the stock solution applied in step A was varied in a way that final fibrinogen concentrations of 0, 1, 2, 3, 4 or 5 mg/ml were present on the sample.

In step B, other compositions of salt solutions were added as well. Different concentrations of PBS were added resulting in final concentrations of 0x, 0.5x, 1x, 2.5x or 5x PBS. Analogous to PBS, sodium phosphate buffer was used with final concentrations of 0 mM, 5 mM, 10 mM, 25 mM or 50 mM. In addition, 2.5x PBS or 25 mM sodium phosphate buffer were applied with pH values of 5, 6, 7, 8 or 9. Another variation of step B was the addition of single PBS components. Salt solution were added instead of PBS to achieve final concentrations of 375 mM NaCl, 10 mM KCl, 375 mM KCl, or 25 mM potassium phosphate buffer.

For control experiments using the protease inhibitor 4-(2-aminoethyl)benzenesulfonyl fluoride hydrochloride (AEBSF), fibrinogen and PBS were prepared according to the standard procedure shown in Figure 18. However, in these experiments the PBS was supplemented with 0.1 or 1 mM of commercially available AEBSF solution (Sigma, Steinheim, Germany).

Larger fibrinogen scaffolds were prepared by using a 24 x 24 mm Menzel glass slides, (VWR, Darmstadt, Germany), which were piranha cleaned. On this substrate 200 µl of 10 mg/ml fibrinogen in 10 mM NH_4HCO_3 were mixed with 200 µl of 5x PBS and dried under ambient conditions.

The last step in the standard preparation of fibrinogen scaffolds is the drying process (Figure 18 D), which was carried out under ambient conditions for most samples. However, selected sets of samples were also dried under controlled temperature and humidity in a self-made incubation chamber. The samples were dried overnight inside the humidity chamber with a constant temperature of 25°C. On different days, samples were prepared with relative humidities of 10, 20, 30, 40 or 50%. All samples for circular dichroism measurements were prepared in the humidity chamber at a constant temperature of 25°C and a humidity of 30%.

Construction of a humidity chamber

The humidity chamber was constructed using a Styrofoam box, in which the humidity could be regulated by flushing in dry compressed air or compressed air, which was humidified by streaming it through a water bath. The humidity and temperature inside the

box were measured using a digital TI HDC1080 sensor (Watterott, Leinefelde-Worbis, Germany). A Raspberry Pi computer (Raspberry PI (trading) limited, Cambridge, United Kingdom) was used to actuate magnetic valves (RPE, Carbonate, Italy) based on the measured humidity to flush the chamber with dry or humidified compressed air to achieve the desired humidity. In addition, the temperature data from the sensor were used to regulate the temperature inside the incubation chamber using a heating film (Thermo technologies, Rohrbach, Germany) and a Peltier element (Conrad electronics, Hirschau, Germany). An overview of the setup of the humidity chamber is given in Figure 19.

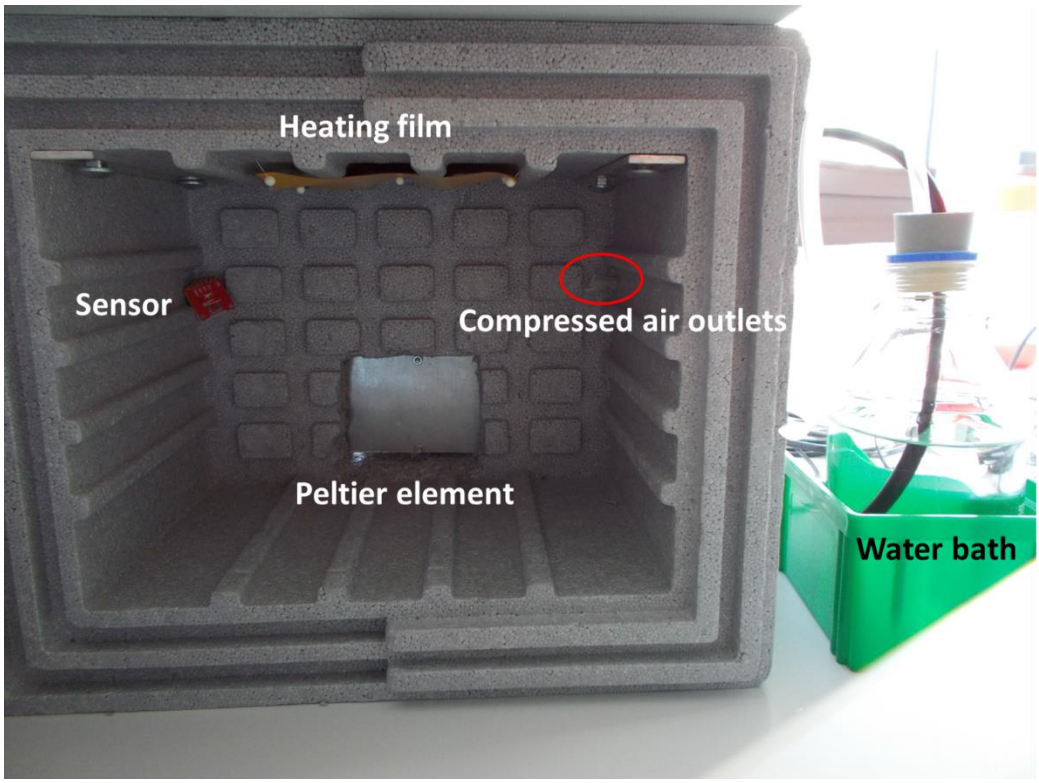

Figure 19: Inside view of the humidity chamber
The humidity and temperature inside the chamber are measured by the sensor. A Raspberry Pi computer, which is located inside a metal casing above the box, regulates the humidity by flushing in dry compressed air or compressed air, which was humidified by flushing it through a water bath. A heating film and a Peltier element are used to adjust the temperature.

4.3.1. Measurements of turbidity

One set of samples, where 5 mg/ml fibrinogen in 5 mM NH_4HCO_3 were dried in the presence of 2.5x PBS on a piranha cleaned glass slide under ambient conditions, was imaged during the drying process using a digital microscope (Meade Instruments, Irvine,

United States). The images were taken in bright field mode over a time course of 2 h to investigate changes in the turbidity of the sample.

Analysis of sample coverage using bright field imaging and ImageJ

The fibrinogen scaffolds prepared by drying in the presence of different phosphate buffer or PBS concentrations were analyzed for the total sample coverage. For this analysis bright field images of the dried samples were recorded using a digital microscope. For the analyses of the total sample coverage, the open source Java software ImageJ was used. Bright field pictures of the samples were converted to black and white images and a threshold was set manually so that only the opaque parts of the samples were analyzed (Figure 20). The coverage of the selected area was calculated using the *analyze particles* function in ImageJ. The coverage was calculated in percent of the total sample surface. Differences in coverage of samples prepared with different buffer concentrations were analyzed for significance by ANOVA followed by the Tukey post hoc-test using the GraphPad Prism software (GraphPad Software, San Diego, United States).

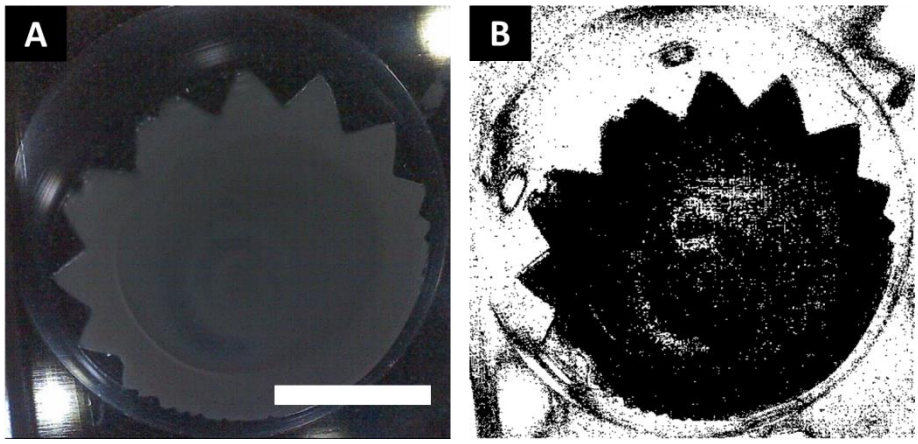

Figure 20: Representation of determination of sample coverage using ImageJ
A bright field image of the fibrinogen scaffold on the piranha cleaned glass substrate (A) was converted into a black and white image and a threshold was applied to highlight the area covered by the scaffold. The total area of the scaffold and the coverage of the glass substrate were calculated. Scale bar represents 5 mm.

4.4. Stabilization and crosslinking of fibrinogen samples

Stabilization of fibrinogen scaffolds

Three different approaches were investigated to further increase the resistance of the fibrinogen scaffolds to hydrolysis in aqueous environment. For a treatment with methanol vapor, the samples were incubated overnight in a methanol (VWR, Darmstadt, Germany) vapor atmosphere. The methanol vapor atmosphere was generated by putting the sample in a beaker and adding a petri dish filled with 1 µl of methanol per cm^3 of beaker volume. The beaker was sealed using parafilm and kept at room temperature overnight, which allowed methanol to evaporate and generate a methanol-saturated atmosphere inside of the sealed beaker. The other two stabilization approaches were UV treatment and UV treatment in the presence of riboflavin. Samples for UV treatment in the presence of riboflavin were prepared with PBS, which contained 2 mM riboflavin (Sigma, Steinheim, Germany). Both types of samples were exposed to UV light generated by an UV lamp (MS Laborgeräte, Heidelberg Germany) for 1 h.

Crosslinking of fibrinogen scaffolds

Seven different crosslinking approaches were tested for the potential to increase the stability of fibrinogen scaffolds and will be described in detail below. The tested crosslinking procedures were transglutaminase treatment, EDC crosslinking (1-Ethyl-3-(3-dimethylaminopropyl)carbodiimide), genipin crosslinking as well as crosslinking in liquid glutaraldehyde or glutaraldehyde vapor and crosslinking in liquid formaldehyde or formaldehyde vapor. All crosslinking methods link fibrinogen molecules by covalent bonds, but the functional groups, which are crosslinked, and the crosslinking reactions are different. Therefore, the mechanisms of the applied crosslinking reactions are demonstrated in Figure 21.

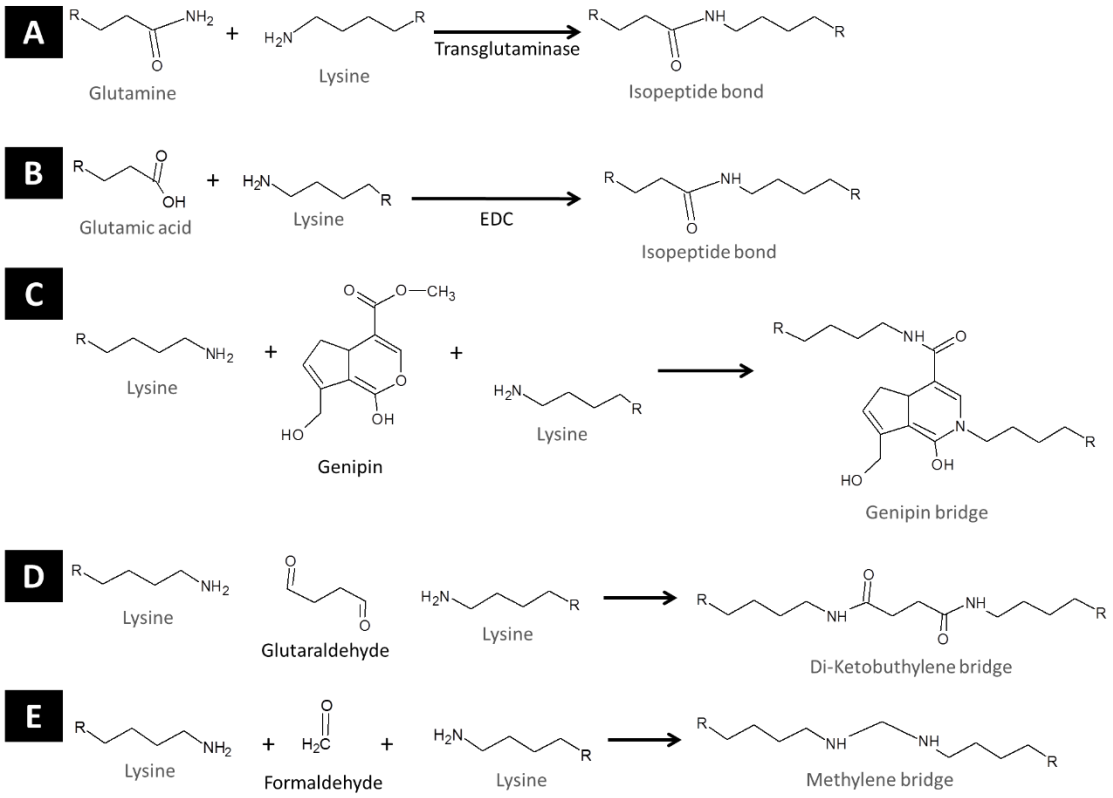

Figure 21: Reaction mechanisms of different crosslinking agents
A: A glutamine and a lysine residue can be crosslinked by the enzyme transglutaminase, which results in an isopeptide bond. The transglutaminase itself is not integrated in the crosslinked structure.
B: A glutamic acid residue and a lysine residue can be crosslinked by 1-Ethyl-3-(3-dimethylaminopropyl)carbodiimid (EDC), which results in an isopeptide bond. The EDC itself is not integrated in the crosslinked structure.
C: Two lysine residues can react with different groups of one genipin molecule. This reaction covalently links the lysine residue via a genipin bridge.
D: Two lysine residues can react with the two aldehyde groups of one glutaraldehyde molecule. This reaction covalently links the lysine residues via a di-ketobuthylene bridge.
E: Two lysine residues can successively react with the aldehyde group of one formaldehyde molecule and the resulting imine group. This reaction covalently links the lysine residues via a methylene bridge.

For transglutaminase crosslinking 200 µl of 5 U/ml transglutaminase (Thermo Fisher Scientific, Schwerte, Germany) in PBS were pipetted onto the fibrinogen scaffolds and incubated for 1 h at 37°C on a heating plate (IKA, Staufen, Germany). After the incubation, the transglutaminase solution was carefully removed and the samples were dried under ambient conditions.

For EDC crosslinking 200 µl 50 mM 1-Ethyl-3-(3 dimethylaminopropyl)carbodiimid (Sigma, Steinheim, Germany) in deionized water were added to the fibrinogen scaffolds for

30 min. The crosslinking solution was carefully removed and the samples were dried in ambient conditions.

For genipin crosslinking. the dried scaffolds were incubated for 1 h in 200 µl 30 mM genipin (Sigma, Steinheim, Germany). The crosslinking solution was carefully removed and the samples were dried in ambient conditions.

An approach based on glutaraldehyde solution and a glutaraldehyde vapor crosslinking were used. For glutaraldehyde solution crosslinking the dried fibrinogen scaffolds were exposed to 200 µl of an aqueous solution of 2% glutaraldehyde (AppliChem, Darmstadt, Germany) for 30 min. The crosslinking solution was carefully removed and the samples were dried in ambient conditions. For glutaraldehyde vapor crosslinking, the samples were placed in a beaker together with a petri dish filled with 1 µl of 50% glutaraldehyde solution per cm^3 of beaker volume. The beaker was sealed with parafilm and the samples were incubated overnight in the glutaraldehyde vapor atmosphere.

Formaldehyde crosslinking was tested similarly in a solution-based and a vapor-based crosslinking approach. For formaldehyde solution crosslinking, the dried fibrinogen scaffolds were exposed to 200 µl of an aqueous solution of 4% formaldehyde (AppliChem, Darmstadt, Germany) for 30 min. The crosslinking solution was carefully removed and the samples were dried in ambient conditions. For formaldehyde vapor crosslinking, the samples were placed in a beaker together with a petri dish filled with 1 µl of 37% formaldehyde solution per cm^3 of beaker volume. The beaker was sealed with parafilm and the samples were incubated overnight in the formaldehyde vapor atmosphere.

4.4.1. Washing and detachment of fibrinogen scaffolds

Fibrinogen scaffolds prepared without stabilization treatment or crosslinking were either washed twice in 200 µl of deionized water or washed one time in 10 mM NH_4HCO_3 or PBS. The supernatant was carefully pipetted of the samples after 5 min of washing. The samples were subsequently dried in ambient conditions. The fibrinogen scaffolds that were used for stabilization treatments were washed for 5 min using 200 µl of ultrapure water. After washing, the samples were dried in ambient conditions.

Fibrinogen scaffolds crosslinked by the described procedures were carefully washed three times with 2 ml of deionized water for 5 min. Some of the samples partially detached during the washing procedure and it was taken care that the detached parts remained on the sample while pipetting off the washing fractions. All samples were subsequently dried under ambient conditions. For some formaldehyde crosslinked samples, the detachment was investigated by washing vigorously three times with 2 ml of deionized water until the fibrinogen scaffold had completely detached. For the detachment experiments, scaffolds crosslinked on piranha cleaned glass slides and on APTES modified glass slides were used.

4.5. Scanning electron microscopy

To analyze the morphology of dried fibrinogen scaffolds SEM analysis was carried out. Samples for top view SEM analysis were mounted on a flat SEM holder. Before imaging in the SEM, all samples were sputter coated with a 7 nm gold layer in a Bal-Tec SCD 005 sputtering system (Leica Microsystems, Wetzlar, Germany). The sputtered samples were analyzed in a Zeiss Auriga field emission device (Carl Zeiss, Oberkochen, Germany) using acceleration voltage of 3 kV and the SE2 detector for imaging.

In addition to the SEM top view analysis, cross-sections of samples were imaged. The cross-sections were prepared by carefully fixating the samples in a pair of forceps and scratching the backside of the glass substrate using a diamond cutter. The glass was broken with a pair of forceps while avoiding compression of the fibrinogen scaffold on the top of the glass substrate. The broken substrates were fixated in a 90° angle on a SEM holder and the cross-section was also sputtered with a 7 nm gold layer in a Bal-Tec SCD 005 sputtering system. SEM imaging of the samples was carried out using the SE2 detector and acceleration voltage of 3 kV. The scaffold thickness was analyzed on three independently prepared cross-section samples using ImageJ. For each sample, five images of cross-sections were measured at five different positions of each image.

Calculation fiber diameter using Image J

From the SEM images, the fiber thickness was calculated using the open source software ImageJ with the BoneJ plugin. The SEM images were cropped to exclude areas, which showed large agglomerations of fibers. A threshold was manually set to highlight the fibers.

Then the ImageJ plugin BoneJ was used to analyze the fiber thickness. The BoneJ plugin calculates the fiber thickness by filling the threshold image with circles of maximal diameter and determining the average diameter of the circles. Especially in areas where fibers are overlaying or aggregate, this can lead to an overestimation of fiber thickness (Figure 22). The fiber diameter analysis was carried out with SEM images of three independently prepared samples and at least four images per sample were analyzed. The average fiber diameters and the standard deviations were calculated using Microsoft Excel.

Figure 22: Representation of fiber diameter analysis using ImageJ
A SEM image of fibrinogen fibers was cropped (A) and a threshold was manually applied (B). The ImageJ plugin BoneJ was used to measure the fiber thickness by integrating circles of the highest possible diameter and averaging the diameters.

4.6. Structural analysis of self-assembled fibrinogen

In the second main experimental part, the secondary structure of self-assembled fibrinogen scaffolds was analyzed using circular dichroism spectroscopy. A Chirascan spectrometer (Applied Photophysics, United Kingdom) was used to measure the circular dichroism spectra of all samples over a wavelength range of 190 to 250 nm using intervals of 1 nm. For each sample, the circular dichroism spectra were measured in three repeats, which were averaged and smoothed with a Savitsky-Golay filter using smoothing windows of 5 to 10 data points. From the ellipticity represented in the circular dichroism spectra the mean residue ellipticity (θ_{MRE}) was calculated by normalizing the ellipticity to the number of amino acids N, the fibrinogen concentration (c) and the path length (l):

$$\theta_{MRE} = \frac{\theta}{N * c * l}$$

For the necessary calculation of fibrinogen concentration, the absorbance at wavelength 214 nm was additionally determined. The fibrinogen concentrations were calculated

according to the method described by (Kuipers and Gruppen, 2007). Some samples were measured in a liquid state while the main fibrinogen scaffold samples were measured dry using solid-state circular dichroism spectroscopy. The calculation of the used extinction coefficients and the path length for solid-state samples will be introduced in the next section. For samples, which were measured in liquid, the path lengths of the respective cuvettes were used.

4.6.1. Circular dichroism measurements of fibrinogen solution and fibrin

To gain a first understanding of the secondary structure the circular dichroism spectrum of fibrinogen in solution was recorded. 10 µl of 5 mg/ml fibrinogen in 5 mM NH_4HCO_3 solution were measured in a 0.01 mm path length cuvette. After baseline correction for the 5 mM NH_4HCO_3 solution, the mean residue ellipticity of fibrinogen was calculated from the averaged circular dichroism spectra obtained in three independent experiments.

For comparison, the circular dichroism spectrum of fibrin was recorded. The fibrin hydrogel was directly prepared in a 0.01 mm cuvette by incubating 5 mg/ml fibrinogen in 5 mM NH_4HCO_3 solution in the presence of 25 U/ml thrombin for 15 min at room temperature. Since the cleaved fibrinopetides A and B and the thrombin were still present in the formed fibrin, the circular dichroism spectrum of fibrin also had to be corrected for the signal generated by fibrinopeptides A and B as well as thrombin. The circular dichroism spectra of 14 mM fibrinopeptide A or 14 mM fibrinopeptide B in 5 mM NH_4HCO_3 were both measured in 0.5 mm path length cuvettes. The spectrum of thrombin was measured with 25 U/ml thrombin in 5 mM NH_4HCO_3 in a 0.1 mm path length cuvette (Figure 23).

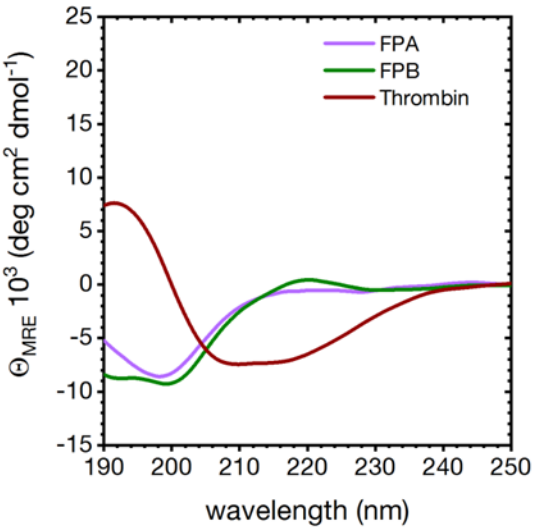

Figure 23: Circular dichroism spectra of fibrinopeptides and thrombin
The spectra of 14 mM fibrinopeptide A (FPA) or 14 mM fibrinopeptide B (FPB) in 5 mM NH_4HCO_3 were both measured in 0.5 mm path length cuvettes. The spectrum of thrombin was measured with 25 U/ml thrombin in 5 mM NH_4HCO_3 in a 0.1 mm path length cuvette. The graph has been published in the supplementary information of (Stapelfeldt et al., 2019b).

With the data obtained for thrombin and the fibrinopeptides, the fibrin spectrum was corrected and the mean residue ellipticity of fibrin was calculated from the averaged circular dichroism spectra obtained in three independent experiments.

Both the mean residue ellipticity of fibrinogen in solution and fibrin were analyzed for the content of secondary structure motives using the BeStSel web server (Micsonai et al., 2018; Micsonai et al., 2015). The secondary structure motives were summed up in α-helical structure and β-sheet structure. All other secondary structure motives were categorized as other.

4.6.2. Circular dichroism measurements of dried fibrinogen scaffolds

The circular dichroism spectra of fibrinogen scaffolds prepared with different concentrations, pH values or humidities were analyzed in a dried state. In order to calculate the mean residue ellipticity, the fibrinogen concentration had to be determined. Therefore, the extinction coefficient and the path length of the dried samples are required. Using the experimentally determined extinction coefficients and the path lengths described in the following, the mean residue ellipticity of the dried samples was calculated. For each investigated parameter, the circular dichroism spectra obtained in three independent

experiments were averaged. The secondary structure contents were analyzed using the BeStSel web server.

Determination of the extinction coefficient

To determine the extinction coefficient of dried fibrinogen, fibrinogen solutions were dried either in the absence or in the presence of PBS. For samples dried without PBS, fibrinogen concentrations of 0.4, 1, 1.5, 2, 2.5, 4 and 5 mg/ml were analyzed. For samples dried with PBS, fibrinogen concentrations of 0.4, 1, 1.5, 2, 3, 4 and 5 mg/ml were analyzed. The samples were directly dried in 0.01 mm quartz cuvettes and the absorbance at 214 nm was measured in the circular dichroism spectrometer (Figure 24).

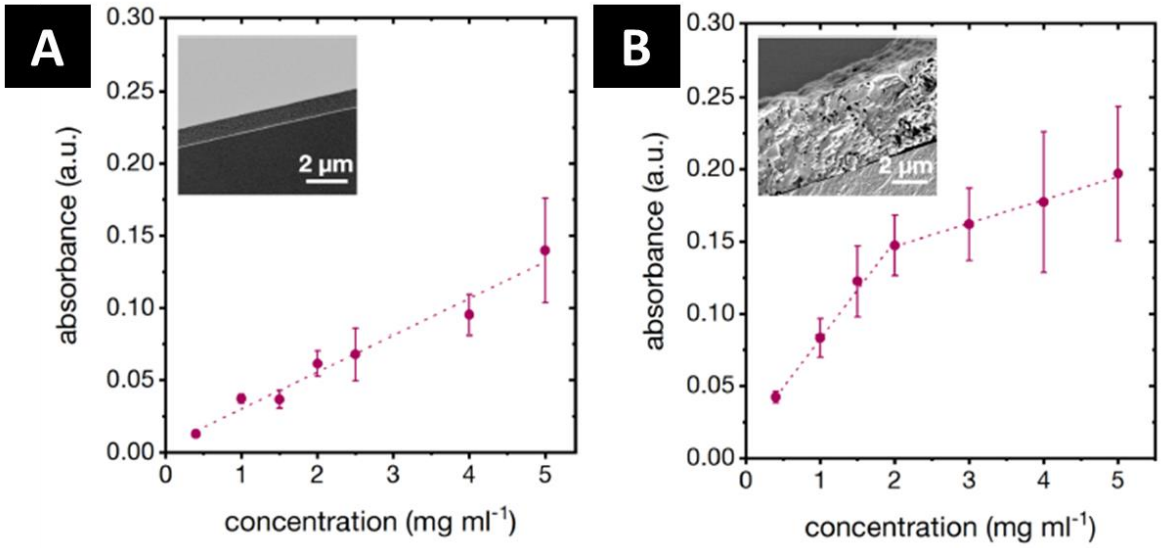

Figure 24: Calibration curves for the determination of the fibrinogen extinction coefficient at 214 nm
Different concentrations of fibrinogen were dried in the absence (A) or in the presence of PBS (B) and the absorbance was measured at 214 nm. Insets show cross-sections from SEM analysis of the dried fibrinogen scaffolds. Image modified from the supplementary information of (Stapelfeldt et al., 2019b).

The increment of the calibration curve of fibrinogen samples prepared without PBS was used to calculate the extinction coefficient of 160,837,851 M^{-1} * cm^{-1}. For samples prepared in the presence of PBS, two distinct absorbance regimes with different slopes were observed. Therefore, two different extinction coefficients were calculated. For concentrations of 0.4 to 2 mg/ml fibrinogen the extinction coefficient was 462,591,577 M^{-1} * cm^{-1}. For concentrations of 3 to 5 mg/ml fibrinogen the extinction coefficient was 125,155,759 M^{-1} *cm^{-1}. The calculated extinction coefficients were used for

the calculations of the mean residue ellipticity in all experiments carried out with dried samples.

Determination of the path length of dried fibrinogen samples

The path length of the dried fibrinogen samples was calculated by extrapolating the measured thicknesses of the cross-sectional SEM analyses of fibrinogen samples prepared on glass (Table 1).

Table 1: Path length of fibrinogen scaffolds
The thickness of fibrinogen scaffolds used in circular dichroism experiments was extrapolated from the thickness of fibrinogen scaffold cross-sections.

	path length of fibrinogen scaffolds (µm)	
fibrinogen concentration (mg/ml)	fibrinogen without PBS	fibrinogen with PBS
1	1.1	1.1
2	1.2	1.1
3	1.1	2.7
4	1.1	2.2
5	1.3	2

Crosslinked and rehydrated fibrinogen scaffolds

Circular dichroism measurements of crosslinked and rehydrated fibrinogen scaffolds were performed in APTES modified cuvettes. Cleaned 0.01 mm quartz cuvettes were modified with APTES by incubating them overnight in a 5% APTES 95% ethanol mixture. The cuvette was subsequently washed three times for 5 min in absolute ethanol.

Fibrinogen scaffolds were prepared in the APTES modified cuvettes by drying 40 µl of 5 mg/ml fibrinogen in 5 mM NH_4HCO_3 with 2.5x PBS present. The samples were dried overnight at 25 °C and a constant relative humidity of 30%. The circular dichroism spectra of the dried scaffolds were measured before crosslinking.

The dried fibrinogen scaffolds prepared in an APTES modified cuvette were subsequently crosslinked by formaldehyde vapor treatment in a parafilm sealed beaker for 2 h. The formaldehyde vapor was generated from 1 µl of 37% formaldehyde solution per cm^3 of beaker volume. After crosslinking, the samples were washed in ultrapure water and dried.

The circular dichroism spectra of the dried and crosslinked samples were measured. Additionally, crosslinked and washed samples were measured in a rehydrated state where 40 µl of deionized water were added to the cuvette before closing it and measuring the circular dichroism spectrum.

For the samples prepared on APTES, the crosslinked samples or the crosslinked and rehydrated samples, the mean residue ellipticity was calculated from the averaged circular dichroism spectra obtained in three independent experiments. The extinction coefficients and the path lengths determined in the previous sections were used. The secondary structure contents were calculated using the BeStSel web server.

4.7. Long-term degradation of self-assembled fibrinogen scaffolds

In the third main experimental part of this thesis, the long-term degradation of fibrinogen scaffolds was studied. In addition to the degradation in aqueous solution, the degradation of fibrinogen scaffolds was analyzed in the presence of the enzymes thrombin, plasmin or urokinase. The fibrinogen degradation potential of the enzymes was analyzed in solution before the enzymes were used for long-term degradation experiments on crosslinked fibrinogen scaffolds.

4.7.1. Enzymatic degradation of fibrinogen in solution

Solutions of 1 mg/ml fibrinogen were incubated overnight at 37°C either in DMEM (Dulbecco's Modified Eagle's Medium; Sigma, Steinheim, Germany) or in HEPES buffered saline. Either no enzyme was present during the incubation or 0.01 U/ml plasmin (Sigma, Steinheim, Germany), 1 µg/ml urokinase (Merck, Darmstadt, Germany) or a combination of 0.01 U/ml plasmin and 1 µg/ml urokinase were applied. After incubation, the samples were analyzed using gel electrophoresis. The degradation of fibrinogen by plasmin was reported by (Pizzo et al., 1972), while urkinase was described as an activator of plasminogen (Blasi et al., 1987).

Gel electrophoresis

The enzymatically digested samples were analyzed using sodium dodecyl sulfate polyacrylamide gel electrophoresis (SDS PAGE). 18 µl of each sample were mixed with 5 µl of SDS sample buffer and heated to 70°C for 10 min. After the heating, the samples and pre-stained protein standard were loaded onto a precast Nupage tris acetate gel (Thermo Fisher Scientific, Schwerte, Germany). The gel ran at 150 V (Consort nv, Turnhout, Belgium) for 1 h in a gel chamber filled with SDS running buffer. After electrophoresis, the protein bands within the gel were stained in coomassie solution (Sigma, Steinheim, Germany) on a shaker for 1 h. The gels were washed twice in a solution of 40% methanol, 10% acetic acid and 50% deionized water without coomassie for 1 h, subsequently. In a final washing step the gels were washed with deionized water for 1 h.

Long-term degradation of fibrinogen scaffolds

Fibrinogen scaffolds were prepared by drying 200 µl of 5 mg/ml fibrinogen in 5 mM NH_4HCO_3 solution either in the absence or presence of 2.5x PBS on APTES modified glass slides. The drying was carried out overnight at 25°C and a constant relative humidity of 30%. The samples were crosslinked in formaldehyde vapor in a parafilm sealed beaker. The formaldehyde vapor was generated from 1 µl of 37% formaldehyde solution per cm^3 of beaker volume. One set of samples was crosslinked for 1 h, while a second set of samples was crosslinked for 2 h. After crosslinking, the samples were washed four times in 500 ml deionized water for 15 min. The samples were sterilized using the UV light of a sterile bench (MS Laborgeräte, Heidelberg Germany) for 15 min.

Solutions of 1 U/ml thrombin, 0.01 U/ml plasmin or a combination of 0.01 U/ml plasmin with 1 µg/ml urokinase were prepared in HEPES buffered saline. All enzyme solutions and HEPES buffered saline without any enzymes were sterile filtrated using a Millipore syringe filter (Merck, Darmstadt, Germany).

For each enzyme three samples were placed in individual wells of a 12-well plate (Greiner Bio-One, Frickenhausen, Germany) and 2 ml of enzyme solution per sample were added. Plates were kept at 37°C in an incubator (Heracell, Thermo Fisher Scientific, Schwerte, Germany) for 35 days. Every 7 days 20 µl were taken out for further analysis. The concentrations of fibrinogen, which had been released into the supernatant, were measured

using a Nanodrop spectrometer at a wavelength of 280 nm the same day the samples were taken. The concentrations were calculated using Lambert Beers law and the determined extinction coefficient of fibrinogen like described above. To calculate the total amount of fibrinogen released into the supernatant, the exact volume of supernatant on the sampling day has to be known. Therefore, evaporation controls were prepared by incubating 2 ml of HEPES buffered saline in the incubator and measuring the volume on each sampling day. With the volume and the determined concentration, the total amount of fibrinogen was calculated. For treatments in HEPES buffered saline with thrombin, plasmin or a combination of plasmin and urokinase the experiment was independently repeated three times. After 35 days of incubation, the samples were dried in ambient conditions and the morphology was analyzed in the SEM like described above.

4.8. Binding of fibrinogen and heparin to self-assembled fibrinogen scaffolds

To investigate the binding affinities of fibrinogen and heparin to crosslinked fibrinogen scaffolds, fibrinogen and heparin were fluorescently labeled using Alexa 488 NHS-ester (Sigma, Steinheim, Germany). 30 µl of 5 mM Alexa 488 NHS-ester were added to 5 ml of 1 mg/ml fibrinogen or 1 mg/ml heparin (Sigma, Steinheim, Germany) in 10 mM NH_4HCO_3 solution and incubated for 1 h in the dark at room temperature. To remove unbound Alexa 448 dye the samples were dialyzed using cellulose membrane tubing with a 14 kDa cut-off, which had been washed three times for 10 min in ultrapure water. The dialysis tubing was sealed using 70 mm dialysis tubing closures. The solutions of fibrinogen were dialyzed two times overnight against 1 l of 10 mM NH_4HCO_3.

Fibrinogen scaffolds for the binding experiment were prepared like described above. 200 µl of 5 mg/ml fibrinogen in 5 mM NH_4HCO_3 solution were dried on APTES modified glass slides either in the absence or the presence of 2.5x PBS. For comparison, samples with bovine serum albumin (BSA, Sigma, Steinheim, Germany) were prepared similarly. 200 µl of 5 mg/ml BSA in 5 mM NH_4HCO_3 solution were dried on APTES modified glass slides either in the absence or the presence of 2.5x PBS. The samples were dried overnight at a temperature of 25°C and a constant relative humidity of 30%. After drying, the samples were crosslinked in formaldehyde vapor in a parafilm sealed beaker for 1 h. The

formaldehyde vapor was generated from 1 µl of 37% formaldehyde solution per cm^3 of beaker volume. After crosslinking, the samples were washed four times in 500 ml deionized water for 15 min. In addition, the binding experiment was also carried out on APTES modified glass slides without any protein scaffolds. The APTES controls were not crosslinked.

For the binding experiment 200 µl of the 7 µg/ml Alexa 488 labeled fibrinogen solution or 70 µg/ml Alexa 488 labeled heparin solution were pipetted onto the samples. The samples were incubated for 1 h at ambient conditions in the dark. After the incubation, the supernatant was harvested and the samples were washed with 200 µl 10 mM NH_4HCO_3 for 1 h. The washing fractions were collected. The fluorescence intensity of the fibrinogen and heparin stock solutions, the intensity of the incubation fractions and the intensity of the washing fractions were measured in a LS 50 fluorimeter (Perkin Elmer, Hamburg, Germany). Excitation wavelengths of 490 nm were used and the emission was measured at a wavelength of 525 nm.

5. Results

Since fibrinogen nanofibers are promising biomaterials for wound healing and tissue engineering applications, a number of techniques have been described to produce fibers out of fibrinogen including some approaches utilizing self-assembly. The aim of this thesis was to study the self-assembly during drying in the presence of ions in order to understand the self-assembly mechanism leading to the formation of fibrinogen fibers. Scanning electron microscopy was used to characterize the morphology of the fibrinogen scaffolds prepared under different parameters that allow conclusions about the mechanism of self-assembly.

In a second main part, the changes in secondary structure, which accompanied self-assembly were studied using circular dichroism. The structural analysis provides additional insight into the mechanism of fibrinogen self-assembly as well as a first indication of the biological activity.

The biological activity of self-assembled fibrinogen was further investigated in the third main part of this thesis, by binding experiments as well as an analysis of the enzymatic long-term degradation.

5.1. Morphology of self-assembled fibrinogen scaffolds

In the first set of experiments of this thesis, fibrinogen the self-assembly of fibrinogen was investigated by analyzing the morphology of fibrinogen dried under various conditions by SEM. The first observation of a fibrinogen self-assembly was made, when 5 mg/ml fibrinogen in 20 mM sodium citrate buffer with a pH of 9 were dried on a piranha cleaned glass slide. SEM analysis revealed that on some parts of the samples fibrinogen nanofibers had formed. The fibrinogen fibers were mainly found at the edges of a ring of the dried citrate (Figure 25).

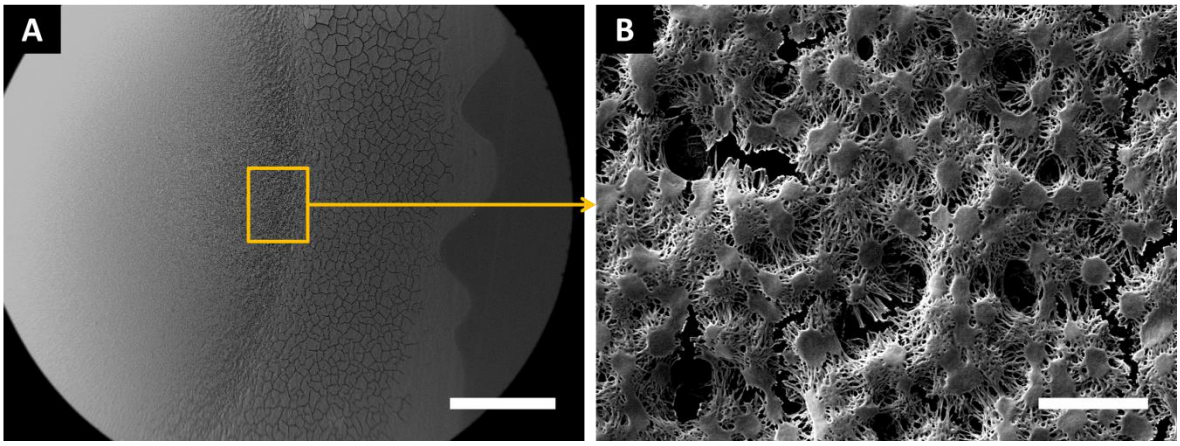

Figure 25: Drying of fibrinogen in citrate buffer results in fibrinogen fibers
5 mg/ml fibrinogen were dried in 20 mM citrate buffer with a pH of 9 on a piranha cleaned glass slide and analyzed in the SEM. A: Overview of the fibrinogen and citrate sample. Fibers were only observed at the highlighted inner border of the dried citrate. Scale bar 1000 µm. B: Magnification of the fibrinogen fiber scaffold formed at the inner border of the dried citrate. Scale bar 10 µm.

The observed fibrinogen fibers set out from central points without fibers in a star-shaped morphology with fibrinogen fiber diameters in the range of 50 to 150 nm. The star-shaped fiber accumulations formed a dense fibrinogen scaffold at the inner border of the dried citrate. On other parts of the sample, no fibers were observed.

5.1.1. Assembly of fibrinogen scaffolds, comparison to fibrin

To identify other buffers, which could also induce fibrinogen self-assembly upon drying, fibrinogen was dissolved in NH_4HCO_3 solution and dried in the presence or absence of phosphate buffer or PBS. For morphological comparison of the self-assembled fibers with fibrin fibers, fibrin scaffolds were prepared by incubating fibrinogen with thrombin in similar buffer systems.

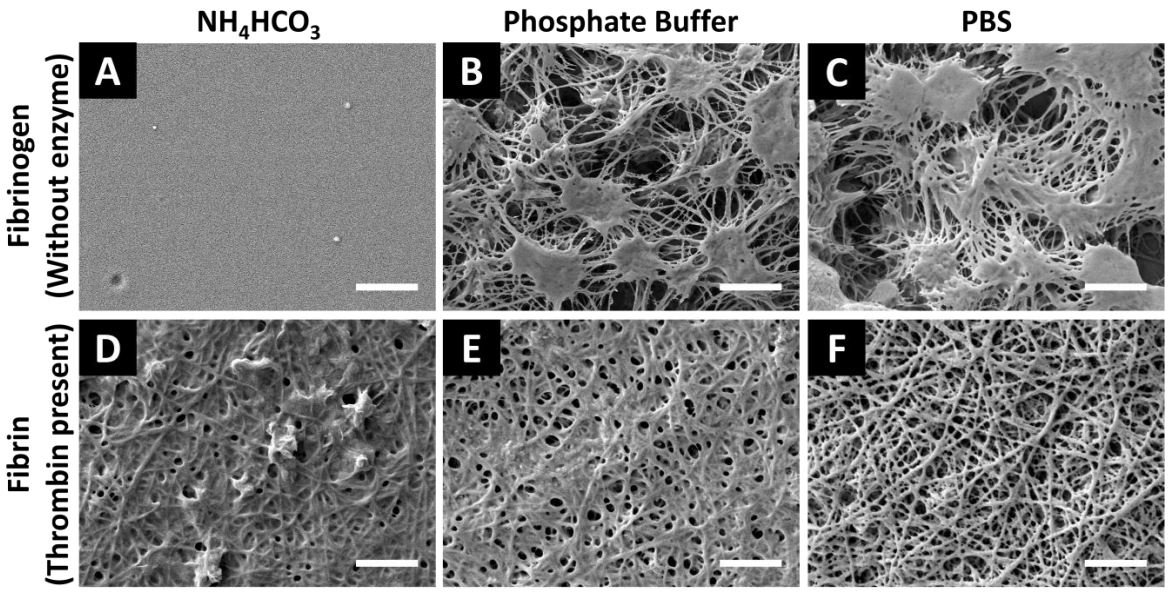

Figure 26: Self-assembly of fibrinogen in phosphate buffer and PBS compared to fibrin
A-C: 5 mg/ml fibrinogen in 5 mM NH_4HCO_3 were dried on a piranha cleaned glass slide without the addition of any enzyme and analyzed in the SEM. For B and C 25 mM phosphate buffer (pH 7.4) or 2.5x PBS (pH 7.4) were present during the drying process respectively, which led to the self-assembly of fibrinogen fibers.
D: Fibrin fibers prepared by incubating 10 mg/ml fibrinogen in 10 mM NH_4HCO_3 with 10 U of thrombin for 1 h at 37°C. Fibrin fibers were subsequently dried and analyzed in the SEM.
E: Fibrin fibers prepared by incubating 10 mg/ml fibrinogen in 10 mM phosphate buffer with 10 U of thrombin for 1 h at 37°C. Fibrin fibers were subsequently dried and analyzed in the SEM.
F: Fibrin fibers prepared by incubating 5 mg/ml fibrinogen in 5 mM NH_4HCO_3 and 2.5x PBS with 5 U of thrombin for 1 h at 37°C. Fibrin fibers were subsequently dried and analyzed in the SEM.
All scale bars represent 2 µm.

When fibrinogen was dried in the presence of NH_4HCO_3 alone, planar fibrinogen layers without any fibrous structures were observed. The additional presence of PBS or phosphate buffer during drying resulted in fibrinogen nanofiber meshes with characteristic star-shaped morphologies with concentrated central points similar to the morphology already observed for fibrinogen and citrate (Figure 26 A-C). However, the coverage and the distribution of fibers on the sample differed, which will be presented in detail in following chapters. The morphology of the self-assembled fibrinogen fibers differed from the morphology of fibrin fibers prepared with thrombin. In similar buffer systems, fibrin fibers prepared with thrombin showed a more homogeneous morphology as well as an even distribution. A star-shaped morphology with pronounced central points was not observed in fibrin (Figure 26 D-F).

Influence of the thrombin inhibitor AEBSF on fibrinogen self-assembly

To exclude the involvement of a potential trace contamination of thrombin in the self-assembly process, a control experiment utilizing AEBSF was conducted. AEBSF is a strong inhibitor for serine proteases, which covalently binds to the active center and thereby inactivates potential trace amounts of thrombin. For the control experiment, fibrinogen self-assembly was induced by drying in the presence of PBS with addition of AEBSF.

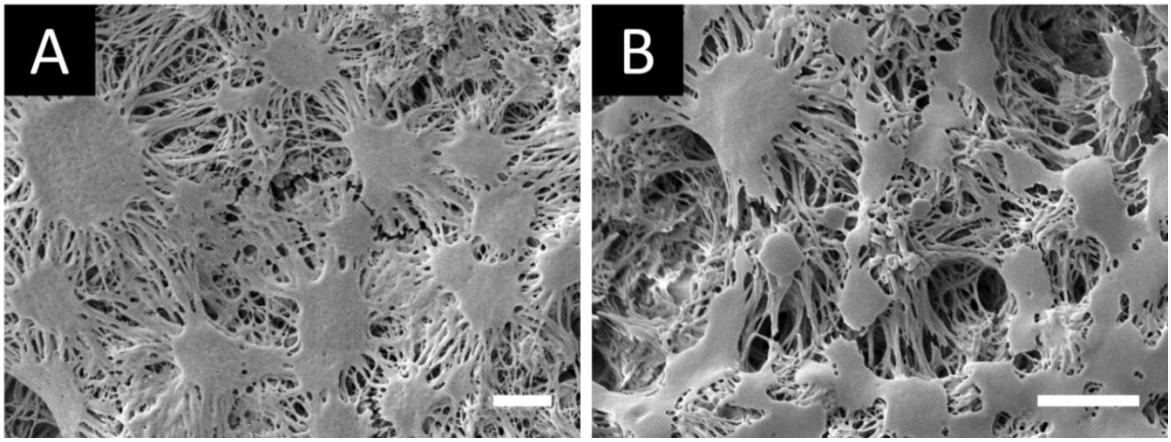

Figure 27: Self-assembly of fibrinogen scaffolds in the presence of AEBSF
Fibrinogen nanofibers were assembled by drying a 5 mg/ml fibrinogen in 5 mM NH_4HCO_3 in the presence of 2.5x PBS (pH 7.4) and 0.1 mM (A) or 1 mM (B) AEBSF on a piranha cleaned glass slide. Subsequent SEM analyses revealed that even in the presence of the thrombin inhibitor AEBSF fiber formation occurred. Scale bars represent 2 µm. Image from (Stapelfeldt et al., 2019a) supplementary material.

Self-assembly of fibrinogen fibers upon drying in PBS still occurred when 0.1 mM or even 1 mM AEBSF were present (Figure 27). The assembly process was not inhibited by the presence of AEBSF and the star-shaped morphology of the self-assembled fibrinogen was not affected.

Macroscopic changes in turbidity during fibrinogen self-assembly

Macroscopically, the drying process of fibrinogen in the presence of PBS or phosphate buffer was accompanied by the formation of crystals and by a change in turbidity as exemplarily shown for fibrinogen and PBS.

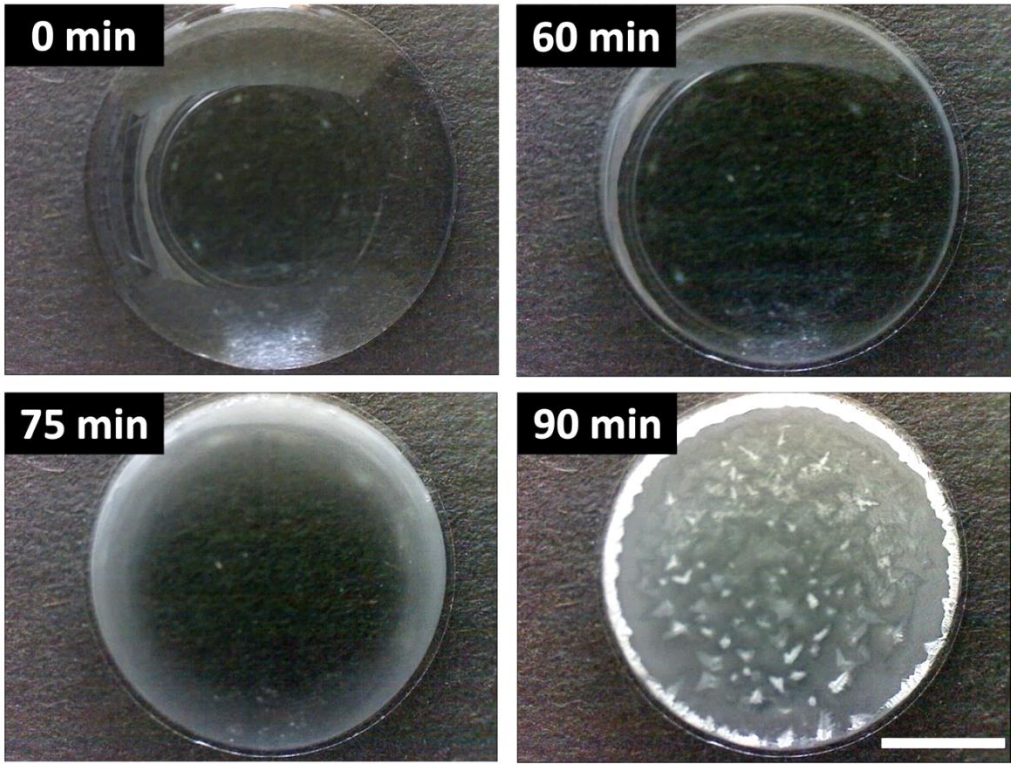

Figure 28: Time series of the fibrinogen drying process
5 mg/ml fibrinogen in 5 mM NH_4HCO_3 were dried in the presence of 2.5x PBS on a piranha cleaned glass slide and imaged using a digital microscope. An initial change in turbidity was observed after 60 min. After 90 min macroscopic PBS crystals started to form. Scale bar represents 5 mm. From the supplementary information of (Stapelfeldt et al., 2019a).

When fibrinogen solution was dried in the presence of PBS, an initial change in turbidity was observed after 60 min at the edges of the sample. After 75 min, the turbid outer ring of the still wet sample had grown. Finally, after 90 min the sample was almost completely dried, which was accompanied by the formation of macroscopic PBS crystals. The spaces between the PBS crystals were covered by an opaque layer (Figure 28).

For fibrinogen, which was dried in NH_4HCO_3 without phosphate buffer or PBS, no change in turbidity was observed and the dried samples remained completely transparent.

5.1.2. Influence of fibrinogen concentration

Different concentrations of fibrinogen in NH_4HCO_3 solution were dried in the presence of either phosphate buffer or PBS. A distinct fibrinogen concentration threshold of fiber formation was observed in both buffer systems.

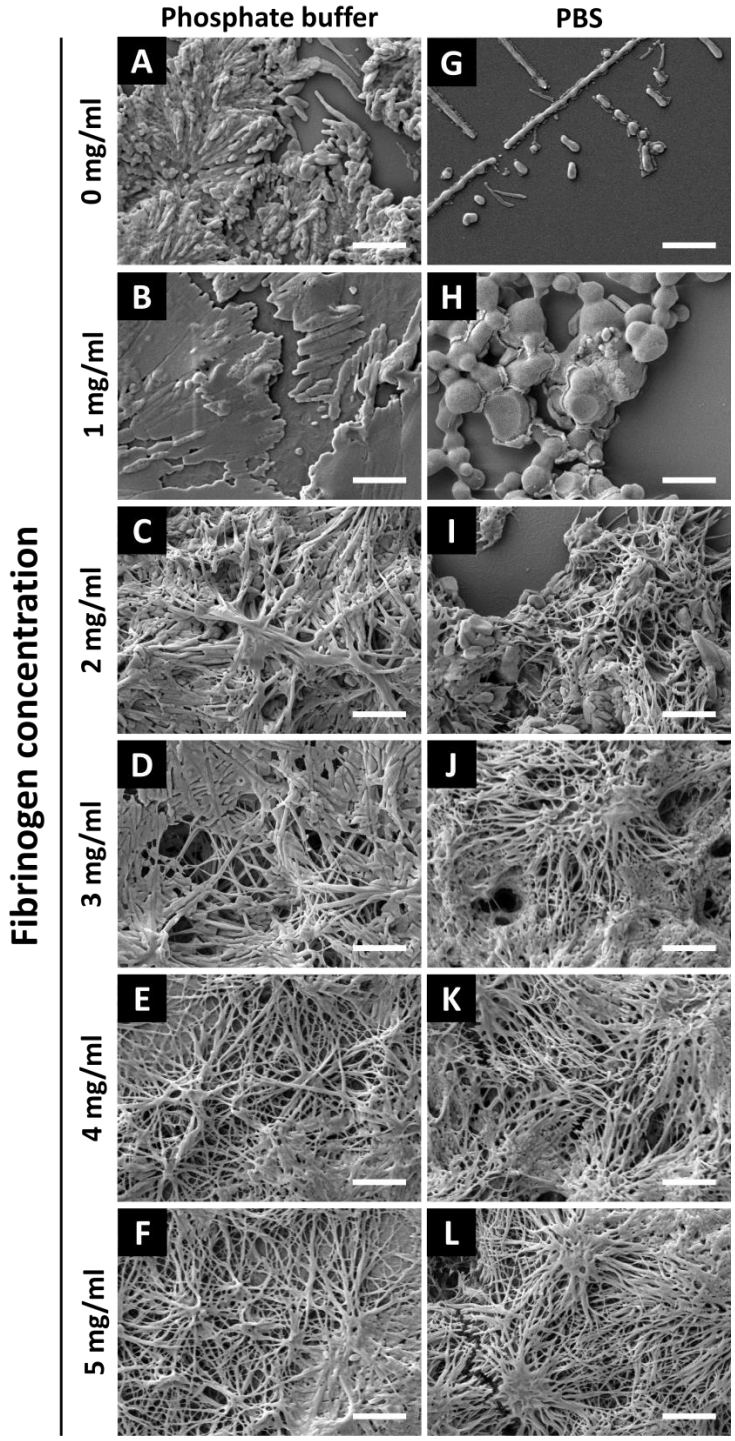

Figure 29: Self-assembly of different fibrinogen concentrations in the presence of phosphate buffer or PBS
Concentrations ranging from 0 to 5 mg/ml fibrinogen in 5 mM NH_4HCO_3 were dried in the presence of phosphate buffer (A-F) or PBS (G-L) on piranha cleaned glass slides. Both posphate buffer and PBS were prepared with a pH of 7.4. SEM analyses showed that fibrinogen fiber formation occurs with fibrinogen concentrations of 2 mg/ml or higher in both buffers. All scale bars represent 2 µm. Panels of this figure have been published in (Stapelfeldt et al., 2019a).

Without fibrinogen no fibers were observed and only crystals of the used phosphate buffer or PBS were present on the dried sample (Figure 29 A and G). When a final concentration of 1 mg/ml fibrinogen was dried in the presence of phosphate buffer or PBS, no fibers were observed (Figure 29 B and H). However, in the samples prepared with PBS globular aggregates were found, when a concentration of 1 mg/ml fibrinogen was used.

When an initial concentration of 2 mg/ml fibrinogen was dried in the presence of phosphate buffer or PBS, fiber formation was observed (Figure 29 C and I). For both buffer systems, the fibers were only found in some spots on the sample. With concentrations of 3 to 5 mg/ml fibrinogen, scaffold formation with increasing densities of fibers was observed for phosphate buffer and PBS (Figure 29 D-F and J-L).

The SEM images of all samples prepared with fibrinogen concentrations that led to fiber self-assembly, were analyzed for the average fiber diameter using ImageJ. The samples of each condition showed a range of various fiber diameters, which are displayed as mean and standard deviations (Figure 30; Table 2).

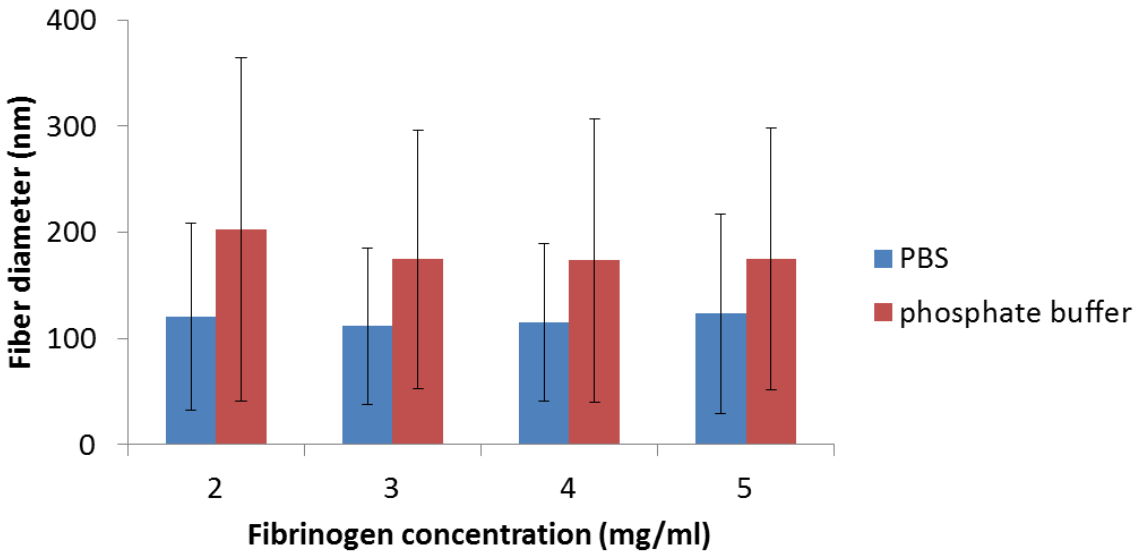

Figure 30: Average diameter of fibrinogen fibers assembled with different fibrinogen concentrations in phosphate buffer or PBS
SEM images of fibrinogen fibers prepared by drying different fibrinogen concentrations in the presence of phosphate buffer or PBS were analyzed for the average fiber diameter using ImageJ. Fiber diameters of three independent samples were averaged and are displayed as mean and standard deviation.

Table 2: Average diameter of fibers assembled with different fibrinogen concentrations.
The fiber diameters of fibers prepared by drying different concentrations of fibrinogen in the presence of phosphate buffer or PBS were analyzed using ImageJ. Using the SEM images of three independent samples, average fiber diameters were determined and are displayed as mean and standard deviation.

	average fiber diameter (nm)	
Fibrinogen concentration (mg/ml)	**Phosphate buffer**	**PBS**
2	203 ± 162	121 ± 88
3	175 ± 122	112 ± 74
4	174 ± 133	115 ± 74
5	175 ± 123	123 ± 94

All fibrinogen concentrations, which resulted in fiber assembly by drying in the presence of phosphate buffer, showed fibers with a similar average diameter in the range of 175 ± 125 nm. Fibers prepared by drying different fibrinogen concentrations in the presence of PBS showed average diameters in a range of 125 ± 75 nm independently from the used concentration. Overall the samples prepared with different fibrinogen concentrations showed a wide range of fiber diameter with a high heterogeneity, which is also reflected in the high standard deviations (Table 2).

To assess if the used fibrinogen had an influence on the overall thickness of the scaffolds in the presence of PBS, cross-sections of all concentrations, which resulted in continuous fiber scaffolds, were prepared. Additionally, cross-sections of planar fibrinogen layers with the same concentrations were prepared. The cross-sections were imaged in the SEM and analyzed using ImageJ.

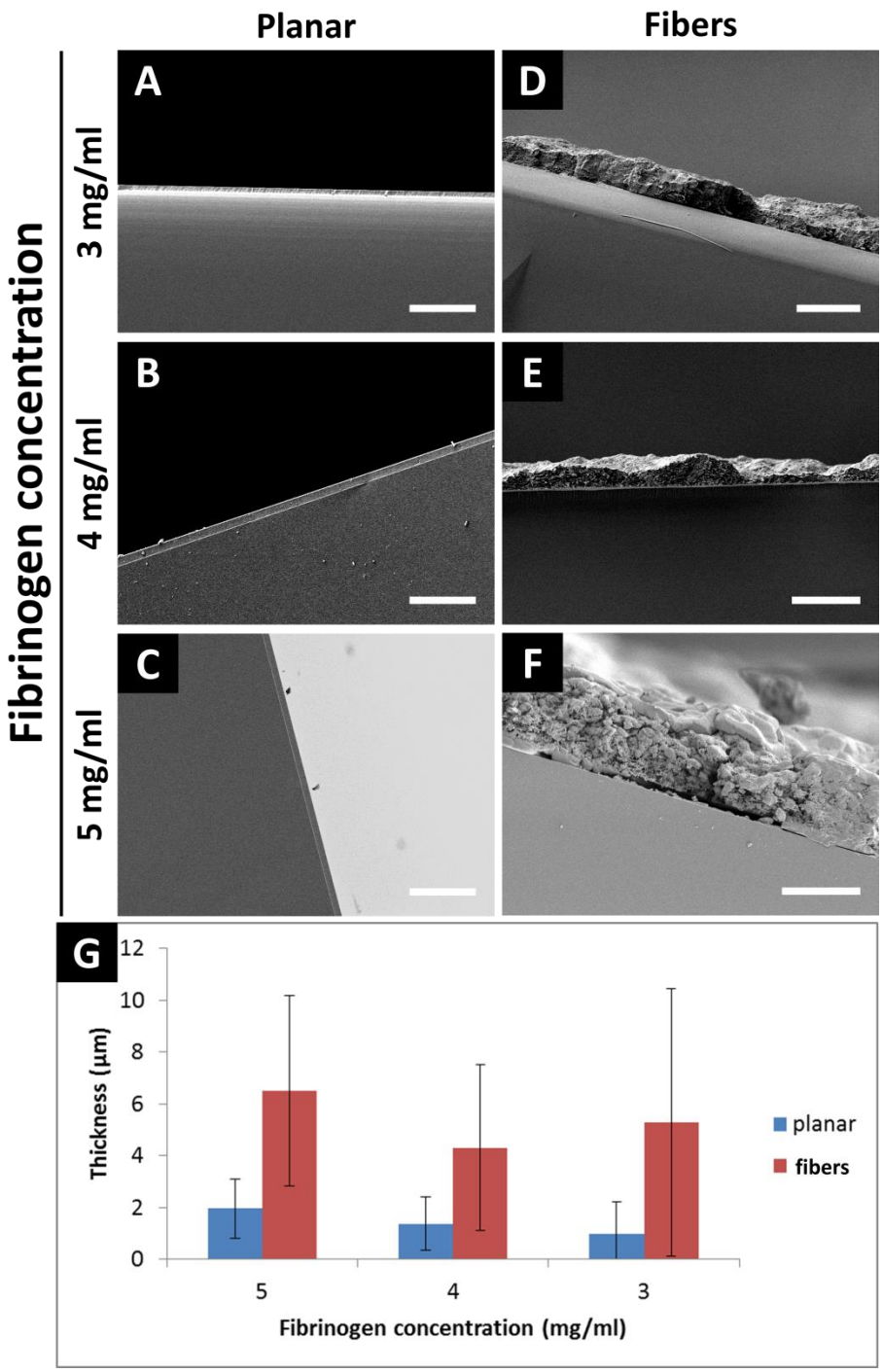

Figure 31: Cross-sections of self-assembled fibrinogen scaffolds

Concentrations ranging from 3 to 5 mg/ml fibrinogen in 5 mM NH_4HCO_3 were dried on piranha cleaned glass slides either without any additions (A-C) or in the presence of PBS (D-F). Cross-sections of the samples were imaged in the SEM and analyzed using ImageJ. Scaffold thicknesses were measured on three independently prepared scaffolds and are displayed as mean and standard deviation (G).

Planar scaffolds showed average thicknesses of 1.5 ± 1 µm (Figure 31 A-C) while fibrous scaffolds had thicknesses of 3 to 12 µm (Figure 31 D-F). Fibers in the scaffolds were observed through the whole scaffold. Due to the high standard deviations, a clear correlation of used fibrinogen concentration and scaffold thickness was not confirmed.

Overall, planar fibrinogen layers had a more uniform thickness. Fibrous fibrinogen scaffolds showed a high heterogeneity in thicknesses, which is reflected in the high standard deviations of average scaffold thickness. Large differences could even be observed at very close positions (Figure 31 E).

5.1.3. Effect of varying buffer concentrations

Fibrinogen in NH_4HCO_3 solution was dried in the presence of different phosphate buffer or PBS concentrations. When no phosphate buffer or PBS was added, only planar layers (Figure 32 A and F) formed similar to the previously observed samples, on which fibrinogen was dried solely in the presence of NH_4HCO_3. However, all concentrations of phosphate buffer (Figure 32 B-E) or PBS (Figure 32 G-J), which were applied during the drying process, resulted in the formation of fibrinogen fibers. Even the presence of 5 mM phosphate buffer or 0.5x PBS, was sufficient to induce self-assembly of fibrinogen into fibers.

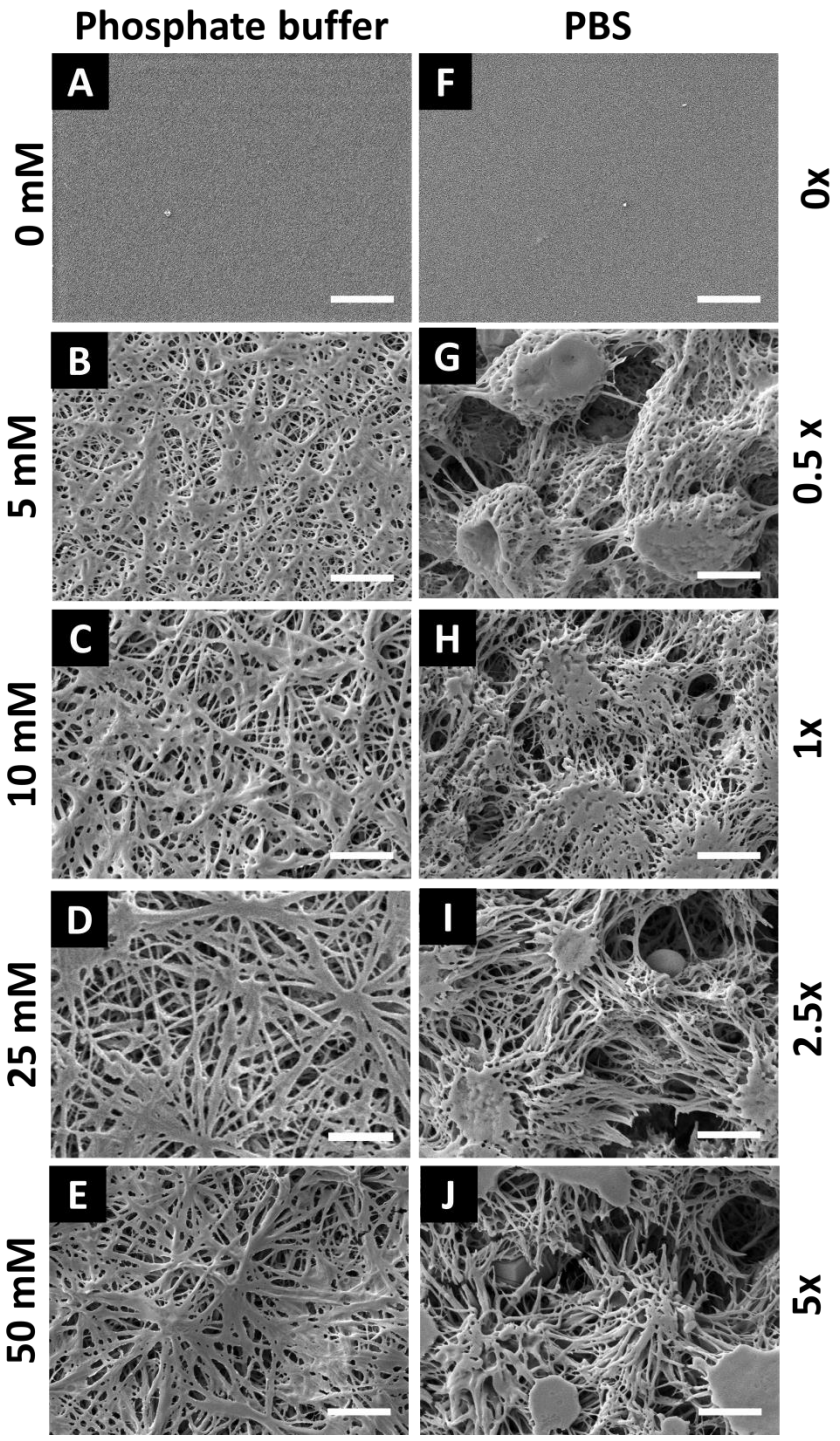

Figure 32: Self-assembly of fibrinogen scaffolds in the presence of different phosphate buffer or PBS concentrations.

5 mg/ml fibrinogen in 5 mM NH_4HCO_3 solution were dried on a piranha cleaned glass slide in the presence of different phospate buffer (B to E) or PBS (G to J) concentrations. Both posphate buffer and PBS were prepared with a pH of 7.4. SEM analyses revealed that without the presence of phosphate buffer or PBS no fiber formation occurred (A and F). For all other concentrations tested, fibrinogen nanofibers were observed after drying. Scale bars represent 2 µm. Image from (Stapelfeldt et al., 2019a).

Drying in the presence of low phosphate buffer concentrations (5 and 10 mM) resulted in fibrinogen scaffolds, which only rarely showed the characteristic star-shaped morphology. Instead, the fiber scaffolds showed more loosely aggregated fibers without concentrated central points. Overall, fiber scaffolds prepared with PBS showed more prominent central points with high fiber density and drying in all PBS concentrations resulted in a similar star-shaped morphology.

The SEM images of fibrinogen assembled in different phosphate buffer and PBS concentrations were analyzed with regard to the average fiber diameter using ImageJ. The samples of each condition showed a wide range of various fiber diameters, which are displayed as mean and standard deviation (Figure 33; Table 3).

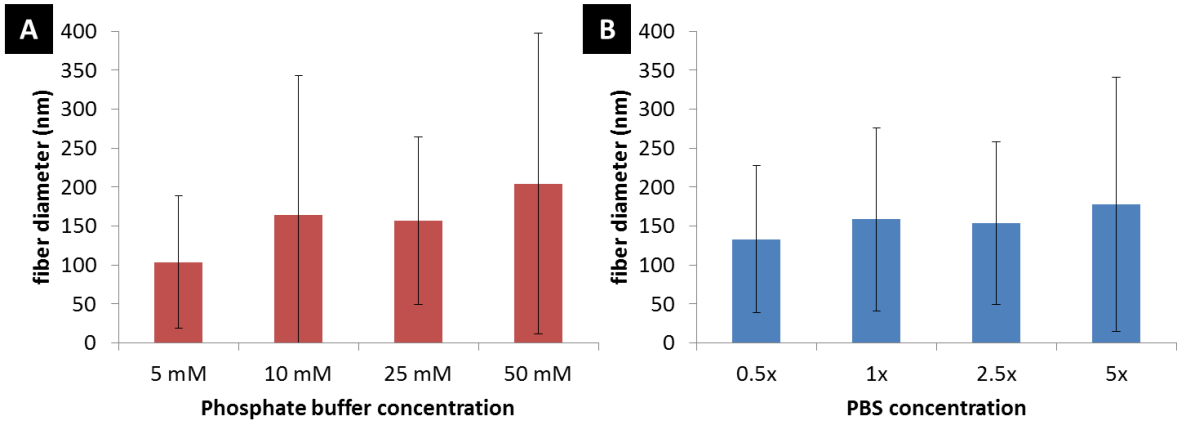

Figure 33: Average diameter of fibrinogen fibers assembled with different phosphate buffer or PBS concentrations

SEM images of fibrinogen fibers prepared by drying in the presence of different phosphate buffer (A) or PBS (B) concentrations were analyzed for the average fiber diameter using ImageJ. Fiber diameters of three independent samples were averaged and are displayed as mean and standard deviation.

Fibers prepared in the presence of 5 mM phosphate buffer showed diameters in a range of 25 to 200 nm, while the diameters of fibers prepared with 10, 25, or 50 mM phosphate buffer ranged from 25 to 350 nm. For fibers prepared in the presence of 0.5x, 1x, or 2.5x PBS fiber diameters in a range of 50 to 250 nm were observed. Only fibers prepared in the presence of 5x PBS showed a broader diameter range of 25 to 350 nm. Overall, the fiber diameters of self-assembled fibrinogen fibers stayed in a wide range and the different concentrations of phosphate buffer had little effect on the observed fiber thickness, which is reflected in the high standard deviation (Table 3).

Table 3: Average diameter of fibers assembled with different buffer concentrations.
The fiber diameters of fibers prepared by drying fibrinogen in the presence of different phosphate buffer or PBS concentrations were analyzed using ImageJ. Using the SEM images of three independent samples average fiber diameters were determined and are displayed as mean and standard deviation.

Phosphate buffer		**PBS**	
concentration (mM)	fiber diameter (nm)	concentration (x)	fiber diameter (nm)
5	104 ± 85	0.5	133 ± 94
10	165 ± 179	1	159 ± 117
25	157 ± 107	2.5	154 ± 104
50	205 ± 193	5	178 ± 163

Although the concentration of phosphate buffer had hardly any effect on the fiber diameter, the macroscopic total coverage of the 15 mm diameter glass slides with fibrinogen scaffolds was dependent on the buffer and the applied buffer concentration (Figure 34).

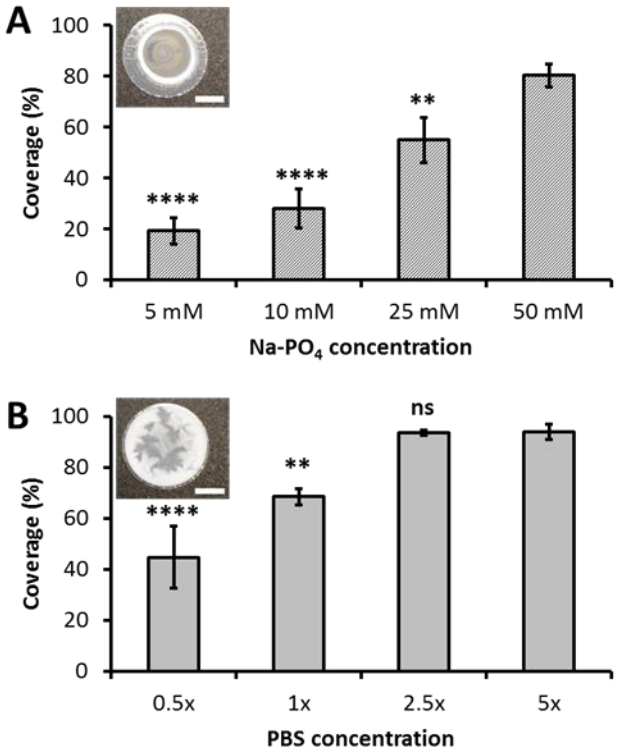

Figure 34: Fibrinogen nanofiber scaffold coverage of 15 mm glass slides in dependence of the buffer concentration used for self-assembly
Fibrinogen nanofibers were prepared by drying a 5 mg/ml fibrinogen in 5 mM NH_4HCO_3 solution in the presence of different concentrations of either (A) phosphate buffer or (B) PBS on a piranha cleaned glass slide. The coverage of the 15 mm glass substrates was measured using a digital microscope. Data represent means and standard deviations of three independently prepared samples for each buffer concentration. The average coverages of the samples with the highest concentration were compared to the other conditions by ANOVA and are indicated by asterisks (****p < 0.0001, **p < 0.001, ns: not significant). Insets show overview images of the 15 mm glass slides with 5 mg/ml fibrinogen dried in the presence of 25 mM phosphate buffer or 2.5x PBS, respectively. Scale bars in insets represent 5 mm. Image from (Stapelfeldt et al., 2019a).

When fibrinogen was dried in the presence of phosphate buffer, the sample coverage was lower as compared to fibrinogen scaffolds prepared in the presence of PBS. Even with the highest phosphate buffer concentration of 50 mM a coverage of only 80% was achieved. When PBS was used to induce fibrinogen fiber formation, coverages higher than 90% were observed with concentrations 2.5x or 5x PBS.

5.1.4. Influence of different salts on fibrinogen assembly

Drying of fibrinogen solutions in NH_4HCO_3 with 2.5x PBS was sufficient to induce fibrinogen self-assembly and resulted in dense fibrinogen scaffolds. 2.5x PBS contains

375 mM NaCl, 10 mM KCl and 25 mM sodium phosphate buffer. Therefore, the individual potential of NaCl and KCl to induce fibrinogen self-assembly upon drying was investigated further. Additionally, fibrinogen in NH_4HCO_3 was dried in the presence of 375 mM KCl and 25 mM potassium phosphate buffer to elucidate, if these ion combinations had an effect on fiber formation, when similar concentrations to the sodium based salts in PBS were used.

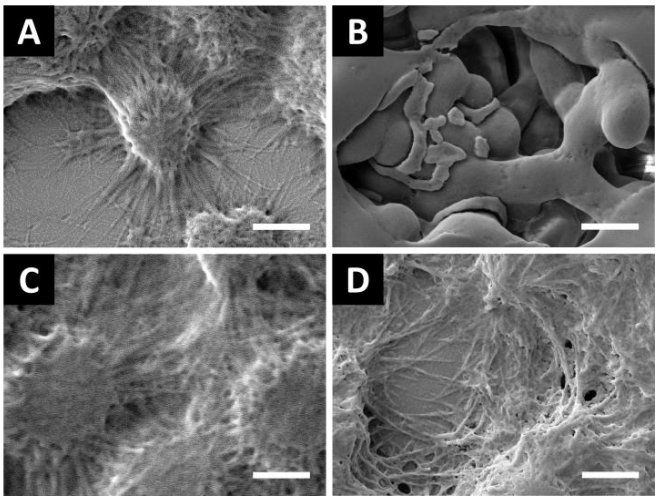

Figure 35: Self-assembly of fibrinogen in the presence of different PBS components
5 mg/ml fibrinogen in 5 nM NH4HCO3 were dried in the presence of (A) 375 mM NaCl, (B) 10 mM KCl, (C) 375 mM KCl or (D) 25 mM K-PO_4 buffer. SEM analyses revealed that nanofibers could be assembled in all buffers, if the salt concentration was at least 25 mM. No fibrinogen fibers formed with 10 mM KCl. Fiber morphology was less defined, when single PBS components were used. Scale bars represent 2 µm. Image from (Stapelfeldt et al., 2019a).

Drying with 375 mM NaCl or KCl was sufficient to induce fibrinogen fiber formation, but with less fibers and a less defined fiber morphology as compared to drying in the presence of PBS (Figure 35 A and C). Nevertheless, with a low concentration of 10 mM KCl no fiber formation was observed (Figure 35 B). Similar to sodium phosphate buffer, drying in the presence of 25 mM potassium phosphate buffer resulted in fibrinogen fibers but with less defined fiber morphology (Figure 35 D).

Although single buffer components were sufficient to induce fibrinogen self-assembly, the overall fiber morphology was most defined when phosphate buffer or PBS were used in 25 mM or 2.5x concentration respectively.

5.1.5. Fibrinogen assembly under varying pH conditions

Drying of fibrinogen solution in the presence of phosphate buffer or PBS with a pH of 7.4 reliably resulted in the self-assembly of fibrinogen fibers. Phosphate buffer can be prepared with different pHs by mixing different ratios of NaH_2PO_4 and Na_2HPO_4. PBS with different pH can be prepared by the addition of NaCl.

Therefore, the PBS has a higher ionic strength as compared to phosphate buffer. However, since phosphate buffer and PBS with low pH have a lower content of sodium, they have a lower ionic strength as compared to phosphate buffer and PBS with high pH (Table 4).

Table 4: Ionic strength of 25 mM phosphate buffer and 2.5x PBS prepared at different pH values.
When phosphate buffers are prepared with different pH values, the total ionic strength is dependent on the pH since different ratios of NaH_2PO_4 and Na_2HPO_4 are used. PBS prepared at different pH values has a higher ionic strength due to the addition of NaCl.

	Ionic strength (mM)	
pH	25 mM phosphate buffer	2.5x PBS
5	26	376
6	32	382
7	62	412
8	72	422
9	74	424

The 25 mM phosphate buffer and 2.5x PBS prepared with pH values of 5 to 9 were used for the drying of fibrinogen solution on piranha cleaned glass slides.

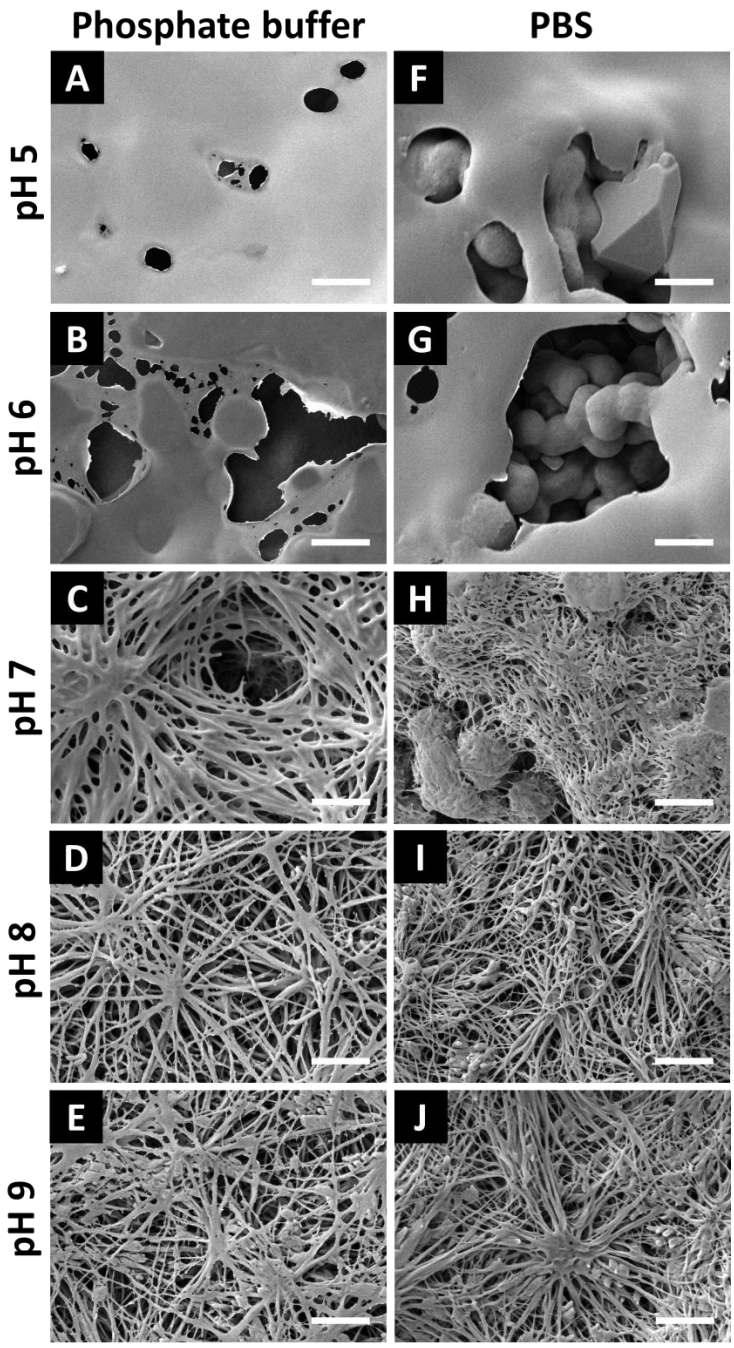

Figure 36: Self-assembly of fibrinogen in the presence of phosphate buffer or PBS with different pH values
5 mg/ml fibrinogen solution in 5 mM NH_4HCO_3 in the presence of either 25 mM Na-PO_4 buffer (A to E) or 2.5x PBS (F to J) were dried under varying pH conditions and subsequently analyzed using SEM. In both buffers the pH was varied from 5 to 9. Fiber formation was only induced for pH 7 to 9, whereas more acidic pH ranges did not yield any nanofibers. Scale bars represent 2 µm. Image from (Stapelfeldt et al., 2019a).

The pH dependence of fiber formation was similar in phosphate buffer and PBS. Both buffers showed a clear threshold pH of 7 for fiber formation. When phosphate buffer with a pH of 5 or 6 was present during drying only planar fibrinogen layers were observed (Figure

36 A and B). PBS with a pH of 5 or 6 resulted in fibrinogen layers and globular aggregates (Figure 27 F and G). Starting with a pH of 7, the presence of phosphate buffer or PBS resulted in the formation of fibrinogen fibers (Figure 36 C-E and H-J). At a pH of 7 combinations of fiber and globular aggregates were observed, especially when PBS was used as buffer. The scaffolds prepared with phosphate buffer or PBS at a pH of 8 showed the most defined fiber scaffolds with thin fibers and a high porosity. At a pH of 9 the fibers prepared in both buffer appeared slightly thicker and the scaffolds were less porous.

To show that the observed morphology of the fibrinogen scaffolds prepared with different pH values was present throughout the scaffold, cross-sections of the samples prepared with PBS were prepared. The cross-sections were imaged at a 90° angle in the SEM.

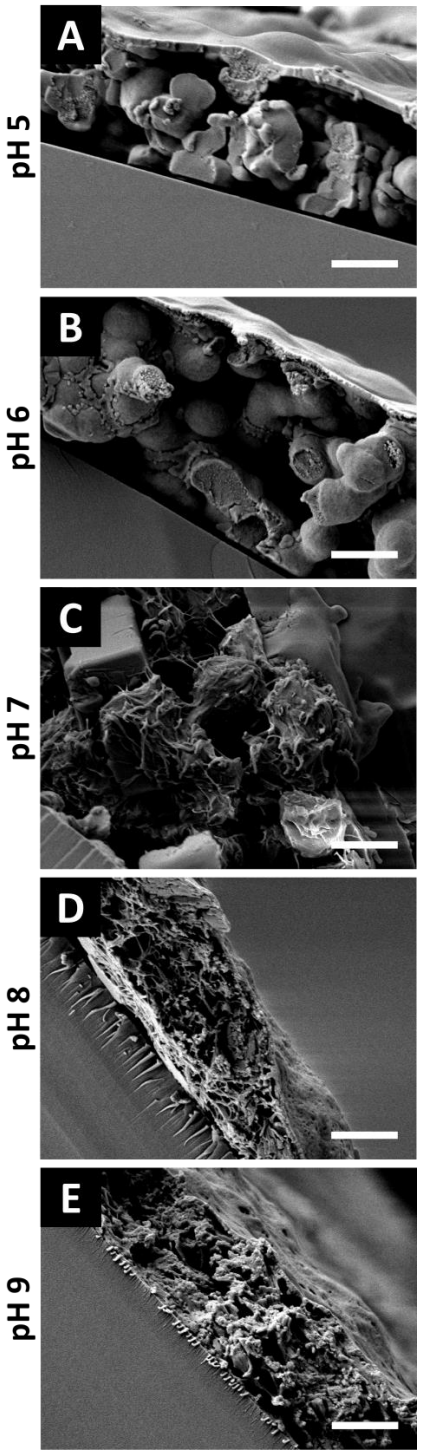

Figure 37: Cross-sections of fibrinogen scaffolds prepared in the presence of PBS with different pH values
5 mg/ml fibrinogen solution in 5 mM NH_4HCO_3 in the presence of 2.5x PBS were dried under pH 5 to 9. Cross-sections of the resulting fibrinogen scaffolds were subsequently prepared and imaged in a 90° angle using SEM. Fiber formation was only induced for pH 7 to 9, whereas more acidic pH ranges resulted in globular aggregates and thin planar layers. Scale bars represent 2 µm.

The cross-sections revealed that the morphology observed in the top view SEM analyses was present throughout the whole scaffold thickness. Scaffolds prepared at a pH of 5 or 6 showed a planar top layer and globular aggregates of fibrinogen without any fibrous structure througout the whole scaffold thickness (Figure 37 A and B). Samples prepared with pH 7, 8 or 9 on the other hand consisted of continious scaffolds of fibrinogen nanofibers throughout the full scaffold thickness (Figure 37 C to E).

5.1.6. Effect of different humidities during fibrinogen assembly

Fibrinogen was assembled into scaffolds by a drying step in the presence of PBS. Therefore, it was of interest to investigate the influence of different relative humidities on the drying and self-assembly process. For this purpose an incubation chamber was constructed, which allowed the assembly of fibrinogen scaffolds under controlled temperature and humidity.

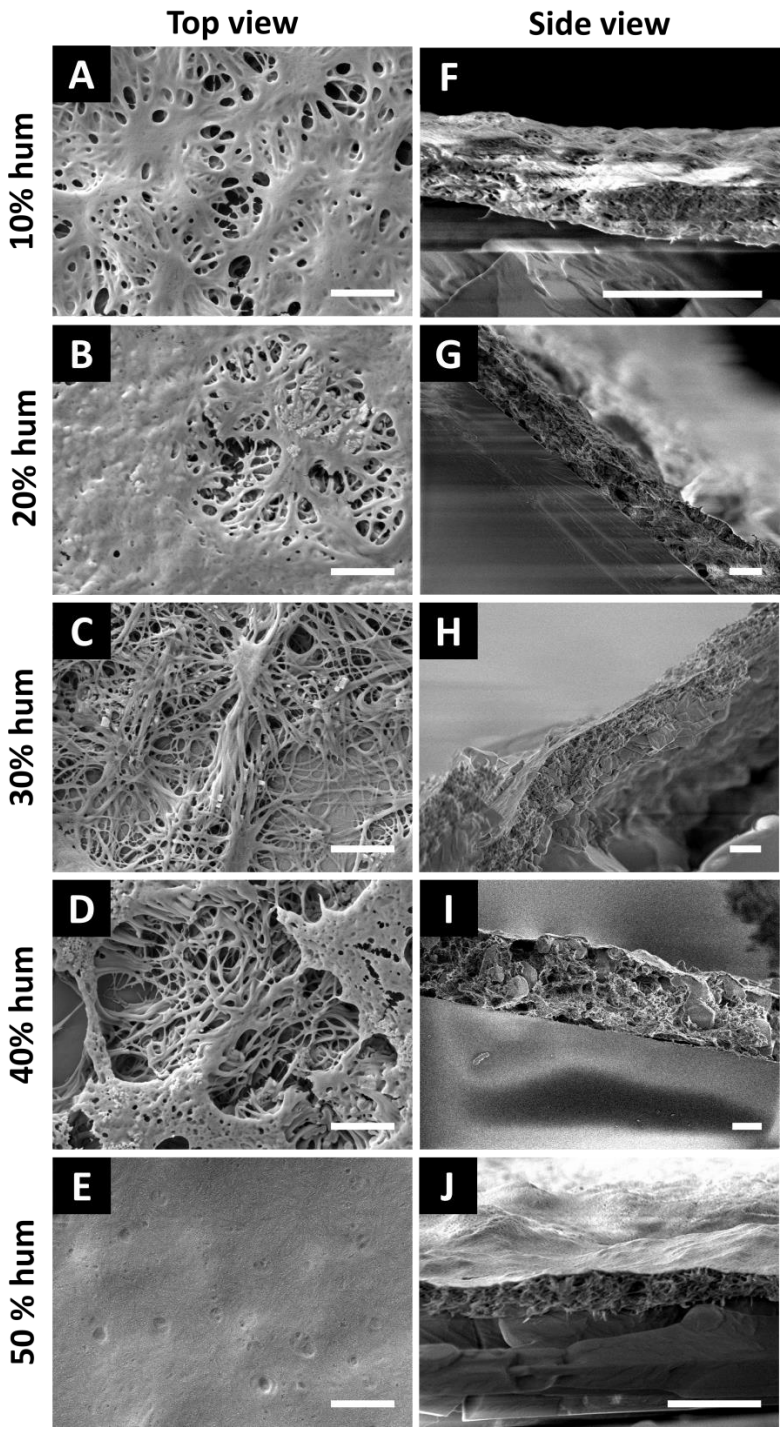

Figure 38: Self-assembled fibrinogen scaffolds prepared at different humidities
5 mg/ml fibrinogen in 5 mM NH_4HCO_3 solution were dried in the presence of 2.5x PBS at different humidities. A-E top view SEM images of the fibrinogen scaffolds. Scale bars represent 2 µm. F-J Side view SEM images of cross-sections of fibrinogen scaffolds. Scale bars represent 10 µm. SEM images F-J were kindly provided by Stephani Stamboroski.

The top view SEM analyses of the fibrinogen scaffolds prepared at different humidities revealed that with relative humidities of 10-40% fibrous scaffolds had formed during the drying process (Figure 38 A-D). However, the samples prepared at a humidity of 50% only showed a planar top layer, on which no fibers could be determined (Figure 38 E). Only an additional analysis of scaffold cross-sections revealed that fiber formation occurred even at 50% humidity. Only the topmost layer of the sample prepared with a humidity of 50% was planar. Underneath this top layer a dense scaffold of fibrinogen fibers was present (Figure 37 J). Furthermore, the cross-sections of the samples prepared at 10% up to 40% humidity showed that the fibrous scaffolds were continuous throughout the whole scaffold thickness.

5.1.7. Assembly of fibrinogen nanofibers on different substrate materials

The fibrinogen self-assembly by drying in the presence of salt buffers described in this thesis was observed on highly hydrophilic piranha cleaned glass slides. Therefore, it was analyzed if the discovered self-assembly process would also occur on gold-sputtered 15 mm glass slides with a higher hydrophobicity.

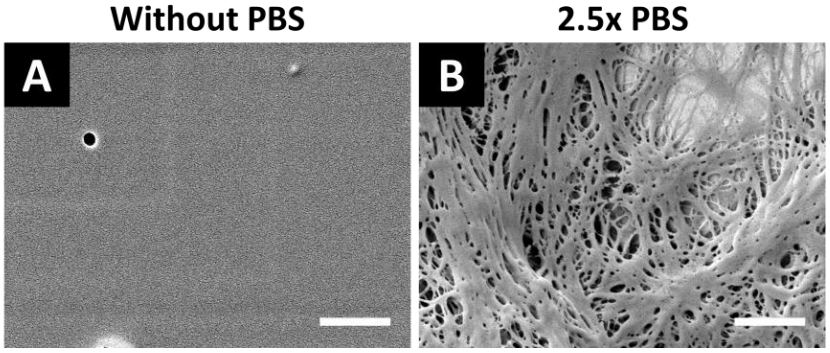

Figure 39: Self-assembly of fibrinogen in the presence of PBS on gold
5mg/ml fibrinogen in 5 mM NH_4HCO_3 solution were either dried without additions or in the presence of 2.5x PBS on a gold coated glass slide. SEM analyses showed that without additions a planar fibrinogen layer had formed. When PBS was present during drying fibrinogen self-assembled into nanofibers.

The fibrinogen self-assembly on gold substrate was analogous to the self-assembly observed on the piranha cleaned glass slides. Without the presence of PBS only planar fibrinogen layers formed (Figure 39 A), while when PBS was present during drying a scaffold of fibrinogen nanofibers was observed (Figure 39 B). The fibrinogen nanofibers

showed a similar star-shaped morphology as compared to the fibers prepared on piranha-cleaned glass.

To further confirm that the drying process of fibrinogen and PBS on gold substrates was analogous to the drying on piranha cleaned glass the fibrinogen concentration and pH dependency experiments were reproduced on gold sputtered substrates.

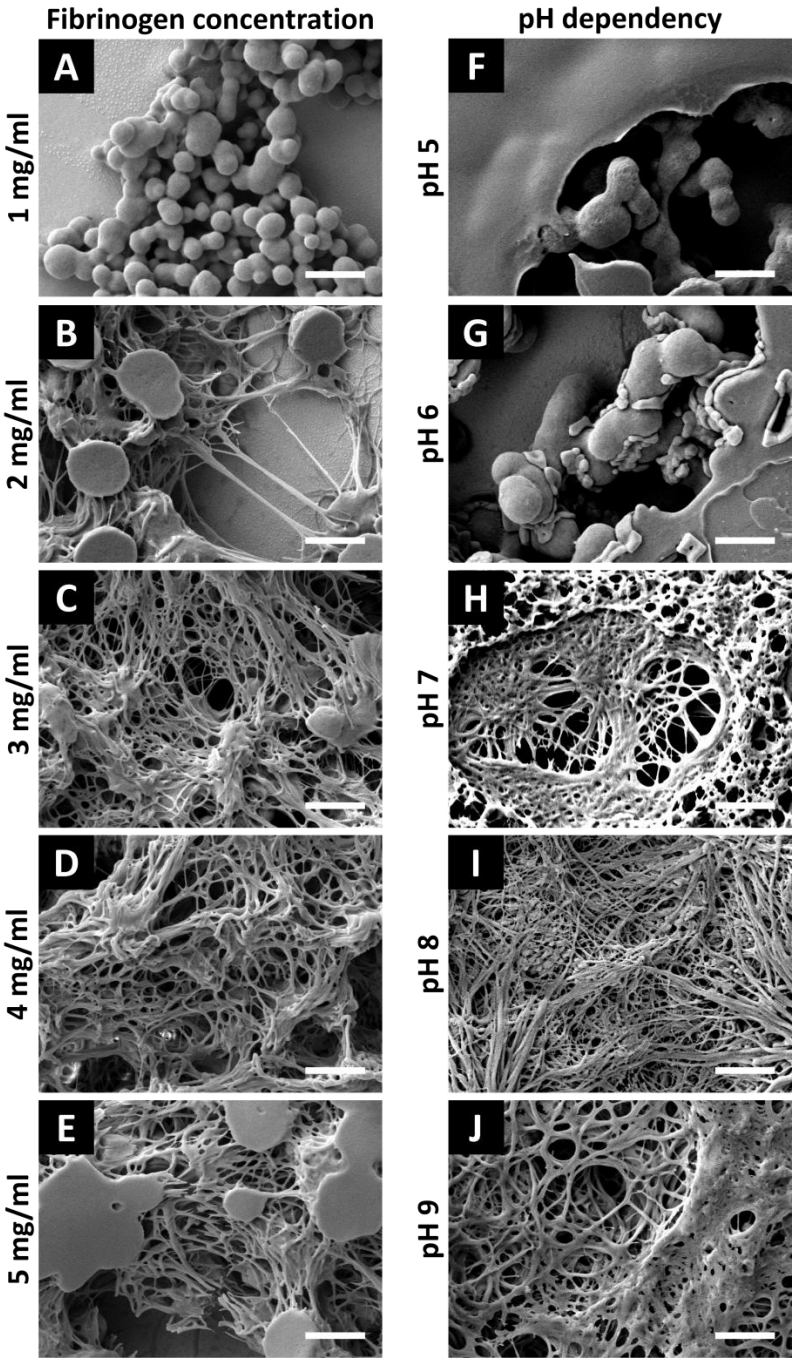

Figure 40: Concentration and pH dependency of fibrinogen self-assembly on gold substrates
Different concentrations of fibrinogen in 5 mM NH_4HCO_3 solution dried in the presence of 2.5x PBS on a gold coated glass slide (A-E). 5 mg/ml fibrinogen in 5 mM NH_4HCO_3 were dried in the presence of 2.5x PBS with different pH values (F-J). SEM analyses revealed that self-assembly occurred with fibrinogen concentrations of 2 mg/ml or higher. With pH values of 5 or 6 no fiber formation was observed while drying in PBS with pH 7, 8 or 9 resulted in fibers. All scale bars represent 2 µm.

On gold substrates, a concentration of at least 2 mg/ml fibrinogen was required to induce fiber formation upon drying in the presence of PBS (Figure 40 B-E). When an initial

concentration of 1 mg/ml fibrinogen was used, no fiber formation was observed (Figure 40 A). These findings are consistent with the observation of fibrinogen self-assembly on piranha cleaned glass slides. When fibrinogen was dried on gold substrates in the presence of PBS with pH values of 5 or 6 no fiber formation was observed (Figure 40 F and G). When the used PBS had a pH value of 7, 8 or 9 fiber formation was observed on gold substrates.

Fibrinogen self-assembly on other substrates

Since the fibrinogen fiber self-assembly induced by drying in the presence of PBS on gold substrate was analogous to the fibrinogen fiber self-assembly on piranha cleaned glass slides, other substrate materials were tested for a fibrinogen self-assembly by drying in the presence of PBS. Fibrinogen in NH_4HCO_3 solution was dried in the presence of PBS on APTES, polylactic acid (PLA), polystyrene (PS), polybutylene adipate terephthalate (PBAT), on parafilm surfaces and on polydimethylsiloxane (PDMS).

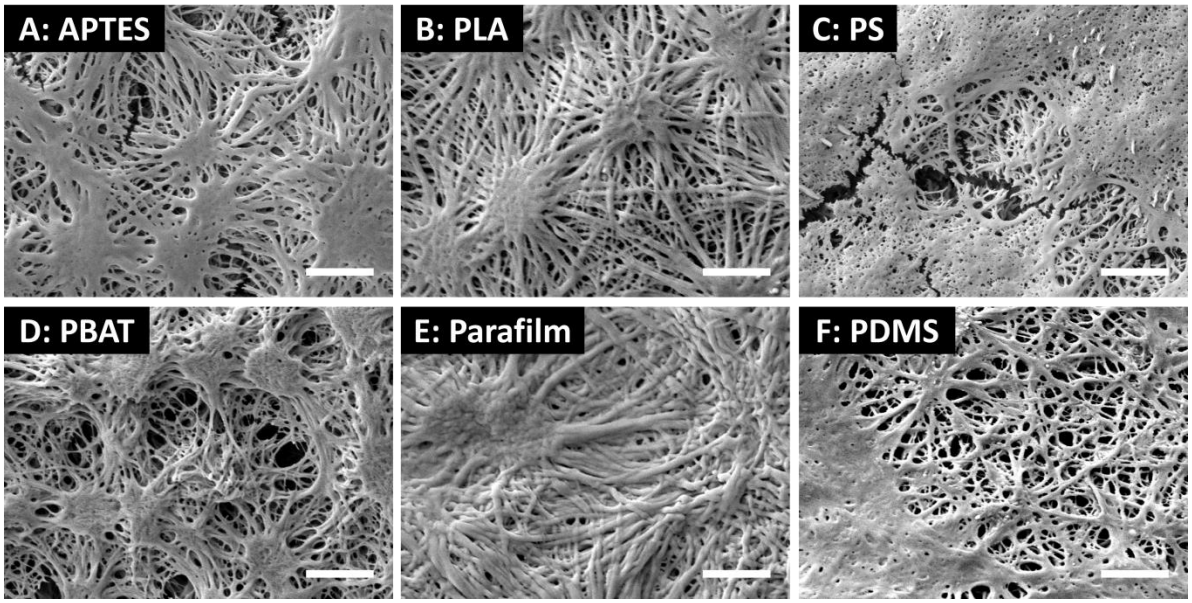

Figure 41: Fibrinogen self-assembly in the presence of PBS on different surface materials
5 mg/ml fibrinogen in 5 mM NH_4HCO_3 were dried in the presence of 2.5x PBS on APTES (A), polylactic acid (B), polystyrene (C), polybutylene adipate terephthalate (D), parafilm surfaces (E) or PDMS (F; here 10 mg/ml fibrinogen were used). SEM analyses revealed that self-assembly of fibrinogen fibers occurred on all tested substrate materials. Scale bars represent 2 µm.

Self-assembly of fibrinogen was observed on all substrate materials, when fibrinogen was dried in the presence of PBS (Figure 41). Although the fiber formation was independent of

the underlying substrate material, fibers showed a less distinct morphology and more aggregation on polystyrene and on polydimethylsiloxane substrates, which showed some non-fibrous areas on the samples (Figure 41 C and F). The fiber scaffolds on APTES modified surfaces, on polylactic acid and on polystyrene showed a star shaped scaffold with distinct fibers and an overall flat morphology (Figure 41 A, B and E). On polybutylene adipate terephthalate surfaces the fibrinogen scaffolds showed a star shaped morphology with a stronger topography.

5.1.8. Fiber stability and crosslinking

For further investigation and for a potential future application of fibrinogen fibers prepared by self-assembly, it is crucial that the fibers are stable in aqueous environment; therefore it was tested how the prepared scaffolds react to rehydration. It was shown that fibrinogen scaffolds prepared by drying in the presence of PBS were not stable in aqueous solution and rapidly redissolved. Fibrinogen solution was dried on piranha cleaned glass slides in the presence of PBS. After the drying procedure, the influence of washing with different solvents and solution was tested.

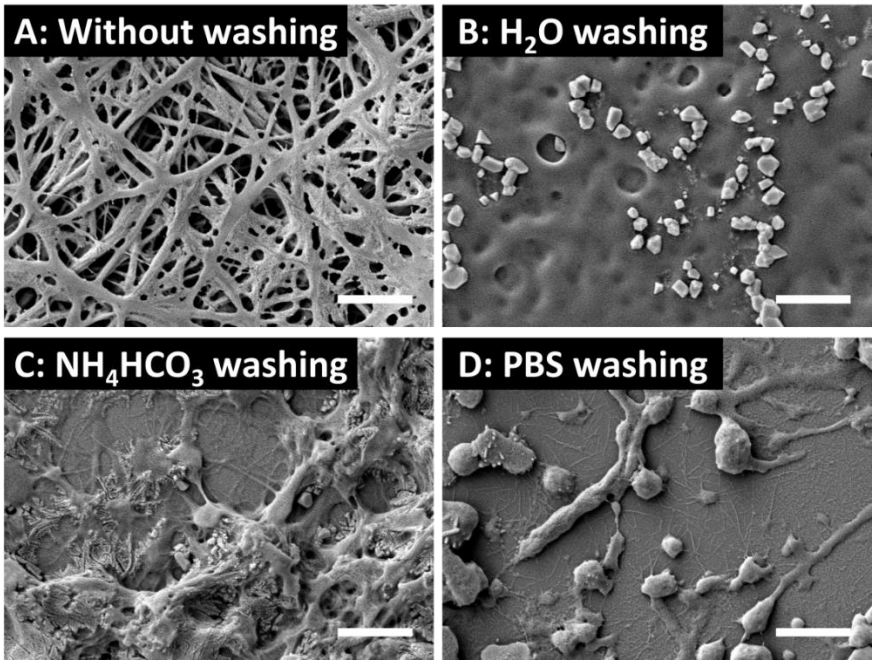

Figure 42: Washing of self-assembled fibrinogen scaffolds
5 mg/ml fibrinogen in 5 mM NH_4HCO_3 were dried in the presence of 2.5x PBS. SEM images were recorded without washing (A), after washing with ultrapure water two times (B), after washing with 10 mM NH_4HCO_3 (C) or after washing with PBS (D) and subsequent drying. All washing procedures redissolved the self-assembled fibrinogen nanofibers. Scale bars represent 2 µm.

The washing experiments revealed that self-assembled fibrinogen fibers were not stable upon rehydration. Without washing the fibrinogen scaffold showed the fibrous star-shaped morphology that was previously observed (Figure 42 A). Washing twice in ultrapure water was sufficient to completely dissolve all fibrinogen fibers and only aggregates and planar structures remained on the sample (Figure 42 B). After one washing step with NH_4HCO_3 or PBS, some remains of the fibrous scaffold were still observable but most fibrinogen was aggregated in globular structures (Figure 42 C and D).

Since untreated fibrinogen fibers were not stable upon rehydration, different approaches to increase the stability after self-assembly were investigated. Fibrinogen scaffolds were incubated in methanol vapor, treated with UV light or with a combination of riboflavin and UV light. After the stabilization treatment, the samples were washed in ultrapure H_2O.

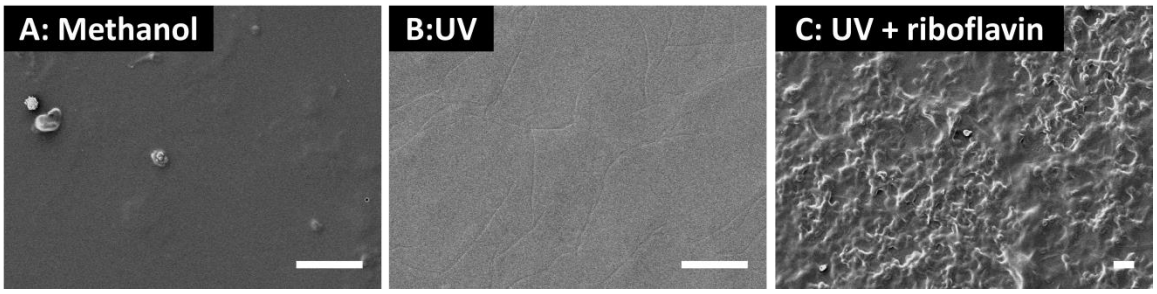

Figure 43: Stabilization of self-assembled fibrinogen scaffolds
For methanol vapor treatment 10 mg/ml fibrinogen in 5 mM NH_4HCO_3 were dried in the presence of 2.5x PBS. The sample was incubated overnight in a methanol vapor atmosphere and subsequently washed with ultrapure H_2O (A). For UV treatment samples were prepared by drying 5 mg/ml fibrinogen in 5 mM NH_4HCO_3 in the presence of 2.5x PBS. For riboflavin and UV incubation, the riboflavin was present during the drying process. The samples were exposed to UV light for 1 h and subsequently washed using ultrapure water (B and C). All scale bars represent 10 µm.

It was shown that all stabilization treatments failed to preserve the fibrous morphology of self-assembled fibrinogen scaffolds. After washing SEM analyses revealed that all fibrous structures were redissolved during the washing even with samples exposed to methanol vapor overnight or UV irradiation for 1 h (Figure 43 A and B). After UV irradiation in the presence of riboflavin a rough topography of the sample was maintained after washing, but single fibers were not found (Figure 43 C).

Crosslinking of fibrinogen scaffolds

Since the stabilization treatments were not sufficient to preserve the fibrous morphology after washing, different methods to chemically crosslink and thereby increase their stability were analyzed.

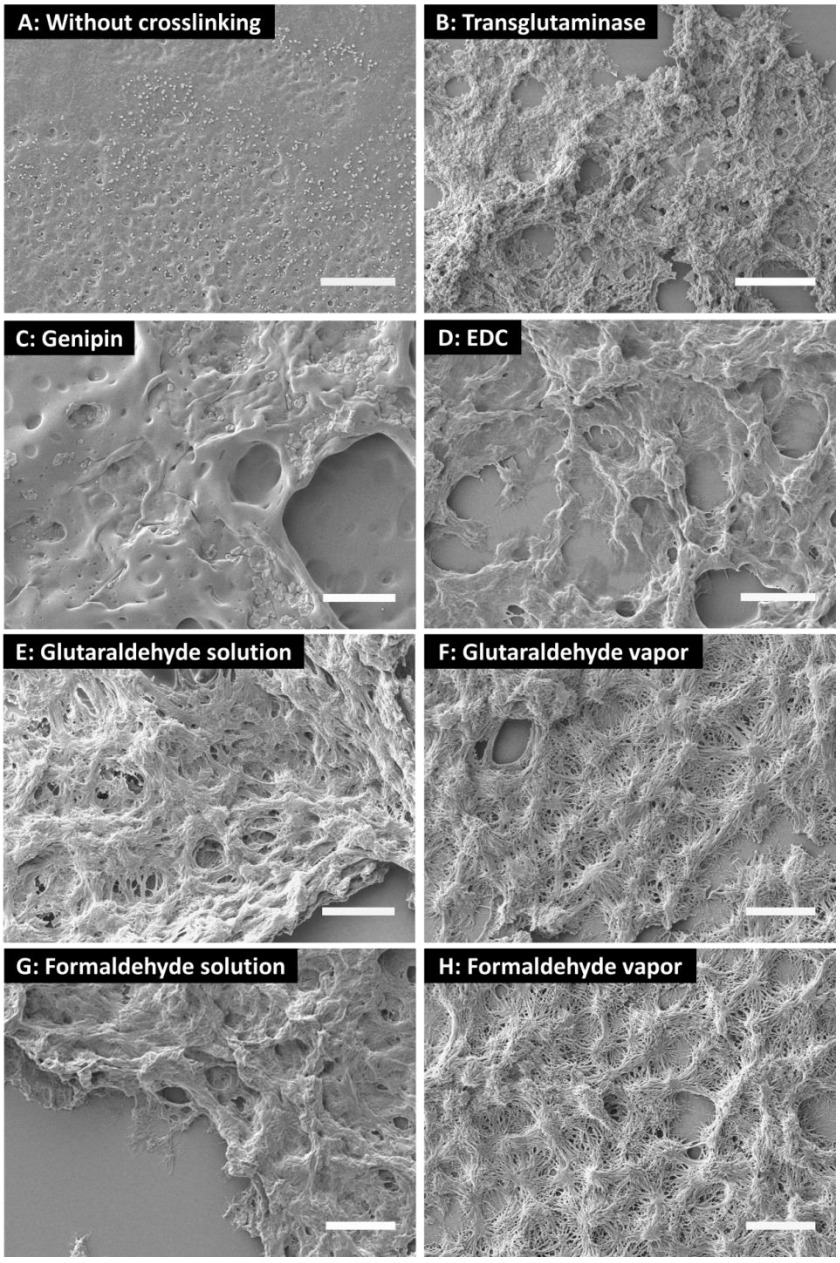

Figure 44: Crosslinking of self-assembled fibrinogen scaffolds
After drying of 5 mg/ml fibrinogen in 5 mM NH_4HCO_3 in the presence of 2.5x PBS the self-assembled scaffolds were crosslinked by incubation in a solution of the described crosslinking agent (A-E and G) or by exposure to a vapor of the crosslinking agent (F and H). Subsequently, the scaffolds were washed in ultrapure water, dried and analyzed using SEM. Scale bars represent 10 µm.

When fibrinogen scaffolds were washed without crosslinking, the fibrinogen fibers dissolved and only a planar molten like surface was observed (Figure 44 A). After washing of fibrinogen scaffolds crosslinked with transglutaminase, genipin or EDC, a similar effect was detected. Hardly any fibers were observed in the SEM and only a molten like topography of the fibrinogen scaffolds remained after washing (Figure 44 B-D).

Crosslinking with glutaraldehyde or formaldehyde solutions for 30 min was more efficient for the preservation of the nanofibrous fibrinogen scaffold. When fibrinogen nanofiber scaffolds were crosslinked in formaldehyde or glutaraldehyde solution, that morphology was largely preserved and define fibers were visible after washing. Only in some parts of the sample, the fibers had redissolved and some gaps in the scaffold were visible especially when glutaraldehyde solution was used (Figure 44 E and G).

The best crosslinking result was achieved when glutaraldehyde or formaldehyde were applied as vapor. The overall morphology of the crosslinked fibrous scaffold was maintained with even fewer gaps and well defined fibers (Figure 44 F and H). Therefore, formaldehyde vapor treatment was chosen as crosslinking method for further experiments that required a rehydration of the fibrinogen scaffolds.

5.1.9. Free-standing and immobilized fibrinogen scaffolds

An additional observation during the crosslinking experiments was that the self-assembled fibrinogen scaffolds, which were prepared on piranha cleaned glass slides and crosslinked using formaldehyde vapor, easily detached form the piranha-cleaned substrate. Therefore, the detachment of crosslinked scaffolds was further investigated using piranha cleaned substrates and APTES modified substrates.

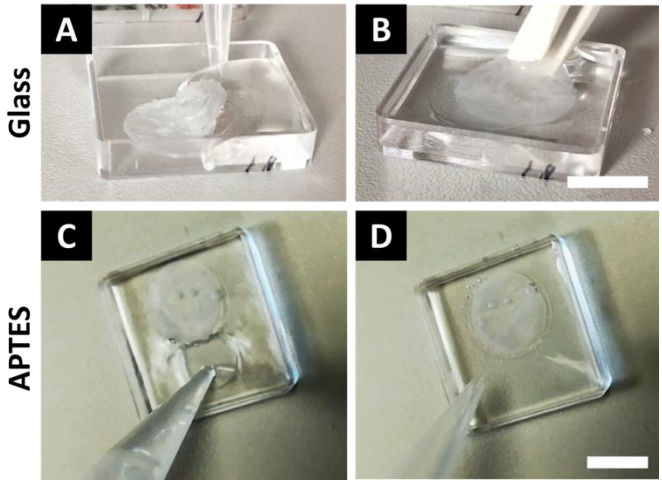

Figure 45: Detachment or immobilization of crosslinked fibrinogen scaffolds
Scaffolds were prepared drying 5 mg/ml fibrinogen in 5 mM NH_4HCO_3 in the presence of 2.5x PBS. After crosslinking in formaldehyde vapor and washing with water, scaffolds on glass substrates detached immediately (A and B), whereas on APTES-modified substrates fibrinogen scaffolds stayed immobilized (C and D). Scale bars represent 1 cm. Image from (Stapelfeldt et al., 2019a).

It was shown that fibrinogen scaffolds crosslinked on a piranha-cleaned substrate completely detached from the substrate when washed with water. However, the detached scaffold did not break or dissolve and stayed intact as a free floating scaffold (Figure 45 A and B). When fibrinogen scaffolds were prepared and crosslinked on APTES modified substrates, the fibrinogen scaffolds stayed immobilized on the substrate material upon rehydration. Even vigorous washing did not detach the scaffold from the surface (Figure 45 C and D).

Upscaling of the fibrinogen self-assembly process

For a future application as a biomaterial, scaffolds in the size range of several cm^2 are required. So far, the fibrinogen scaffolds were prepared on slides with a diameter of 15 mm. Therefore, it was studied whether the size of fibrinogen scaffolds could be increased by upscaling the self-assembly process on 24 x 24 mm glass slides, on which the double volume of the fibrinogen solution and PBS were dried.

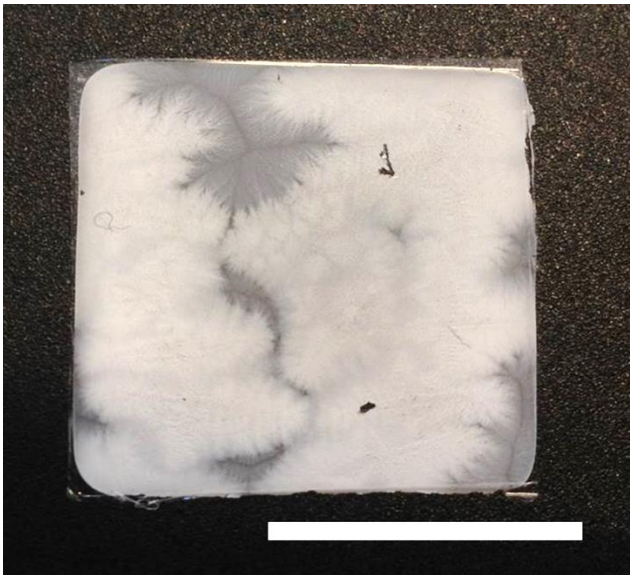

Figure 46: Large self-assembled fibrinogen scaffold on a 24 x 24 mm slide
5 mg/ml fibrinogen in 5 mM NH_4HCO_3 solution were dried in the presence of 2.5x PBS on a piranha-cleaned 24 x 24 mm glass slide. After drying the complete glass slide was covered with a self-assembled fibrinogen scaffold. Scale bar represents 15 mm. Image published in the supplementary information of (Stapelfeldt et al., 2019a).

By doubling the volume and using glass substrates with bigger dimensions, it was possible to obtain a self-assembled fibrinogen scaffold with a total surface area of almost 6 cm^2. The

scaffold showed only few defects and some gaps where no salt crystals had formed (Figure 46). Thereby it was shown that an upscaling of the fibrinogen self-assembly process is possible.

5.2. Conformational changes in self-assembled fibrinogen nanofibers

Established fibrinogen self-assembly approaches like exposure to hydrophobic surfaces and acid or ethanol-induced self-assembly are accompanied by changes in the secondary structure of the fibrinogen molecule. Changes in the conformation of the fibrinogen molecule are also discussed to occur during electrospinning of fibrinogen fibers. Especially for a potential application of fibrinogen fibers as a biomaterial the conformational integrity of the fibrinogen molecules in the produced fibers is crucial. Even a small change of fibrinogen native secondary structure could hamper the desired biological activity and biocompatibility of the material.

A second important reason for a detailed analysis of changes in secondary structure is the understanding of the mechanism of fibrinogen self-assembly itself. If a change in the conformation of fibrinogen molecules during self-assembly is detected, it might explain how fibrinogen molecules assemble in and organize into fibers.

Therefore, the secondary structure of fibrinogen fiber scaffolds obtained by drying in the presence of PBS was analyzed in this thesis using circular dichroism spectroscopy. The results obtained were additionally validated by Fourier-transform infrared spectroscopy as published in (Stapelfeldt et al., 2019b). Although the total values of single structural components differed between the two methods, the overall changes of secondary structures showed similar tendencies and results were in good agreement.

5.2.1. Secondary structure of fibrinogen in solution and fibrin

To investigate the structure of fibrinogen molecules in self-assembled fibers, the structural composition of fibrinogen in solution and of fibrin were analyzed for comparison. Fibrinogen solution was directly measured. However, in a fibrin hydrogel the residual residues of thrombin and the cleaved off fibrinopeptides are still present. Therefore, the spectra of fibrinopetides A and B as well as thrombin were recorded and subtracted from

the initially measured fibrin spectrum. From the spectra of fibrinogen solution and fibrin the secondary structure content was calculated using the BeStSel web server.

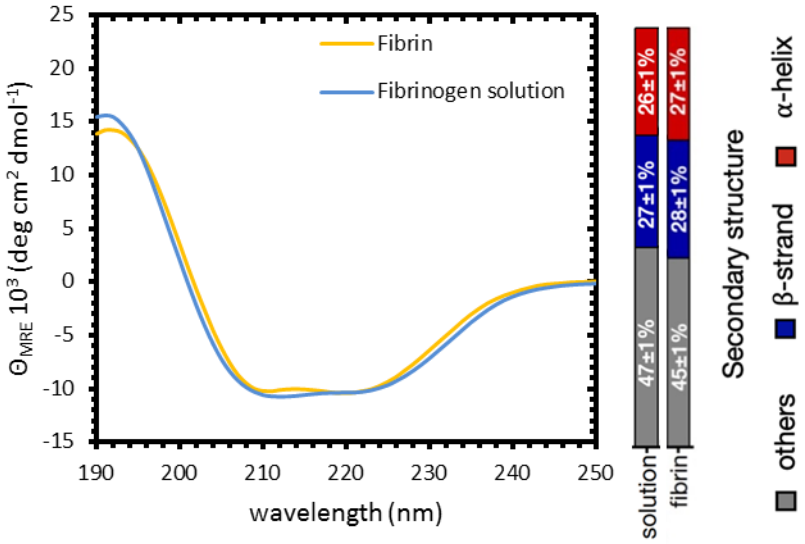

Figure 47: Circular dichroism spectra of fibrin and fibrinogen in solution
The spectrum of 5 mg/ml fibrinogen in 5 mM NH_4HCO_3 solution was measured in a 0.01 mM path length cuvette. Fibrin was prepared and measured in a 0.01 mm path length cuvette by incubating 5 mg/ml fibrinogen 5 mM NH_4HCO_3 solution with 25 U/ml thrombin for 15 min. The secondary structure content of fibrinogen in solution and fibrin was calculated using the BeStSel web server.

The spectra of fibrinogen in solution and fibrin are almost overlaying with the same maximum below 195 nm and the two minima at 210 and 222 nm. This results in a very similar secondary structure content calculated by the BeStSel. Fibrinogen in solution showed 26 ± 1% α-helical and 27 ± 1 % β-sheet structures. Fibrin showed 27 ± 1% α-helical and 28 ± 1% β-sheet structures (Figure 47). These findings are in rough agreement with the conformation reported for fibrinogen and fibrin (Dutta et al., 2018) and show that the fibrinogen molecules maintain their native conformation when assembled into a fibrin scaffold.

5.2.2. Structural analysis of nanofibrous and planar fibrinogen

Planar fibrinogen layers and self-assembled fibrinogen nanofiber scaffolds were directly prepared in 0.01 mm path length quartz cuvettes by drying fibrinogen solution without any addition or in the presence of PBS. The circular dichroism spectra of both dried samples

were recorded and the secondary structure content was calculated using the BeStSel web server.

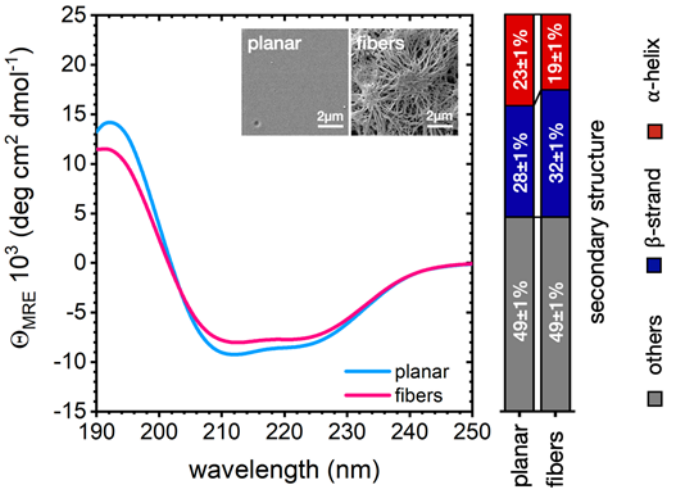

Figure 48: Circular dichroism spectra of planar fibrinogen layers and self-assembled fibrinogen fibers
Both scaffold types were prepared by drying 5 mg/ml fibrinogen in 5 mM NH_4HCO_3 directly in a 0.01 mm path length cuvette. For fibrinogen nanofibers 2.5x PBS at pH 7.4 was present during the drying process. Insets show the morphological differences using SEM analysis. The secondary structure contents shown in the bar chart were calculated from the spectra using the BeStSel web server. Image modified from (Stapelfeldt et al., 2019b).

Interestingly, the circular dichroism spectra of planar fibrinogen layers and self-assembled fibrinogen fibers differed. The local minimum around 210 nm was less distinct for fibrous scaffolds than for planar fibrinogen while the local minimum at 222 nm was in a similar range. This also results in a difference in the analyzed secondary structure content. While planar fibrinogen layers showed 23 ± 1% α-helical and 28 ± 1 % β-sheet structures, which is in the range of native fibrinogen in solution, self-assembled fibrinogen fibers showed 19 ± 1% α-helical and 32 ± 1 % β-sheet structures (Figure 48). During the self-assembly process in the presence of PBS upon drying, a transition of α-helical structures to β-sheets took place.

Thioflavin T staining of self-assembled fibrinogen scaffolds.

In comparison to fibrinogen in solution or planar fibrinogen layers, fibrinogen fiber scaffolds prepared by drying in the presence of PBS showed a higher content of β-sheet structures. For the self-assembly of other proteins into fibers an increased content of β-sheet structures has previously been reported, which was associated with the formation of β-amyloid structures, which are affiliated with various diseases.

To investigate whether the increased content of β-sheets in self-assembled fibrinogen fibers occurred due to the formation of β-amyloid structures, fiber scaffolds were prepared in the presence of thioflavin T (ThT). Thioflavin T is a dye, which changes its emission from 450 nm to 480 nm when bound to β-amyloid structures.

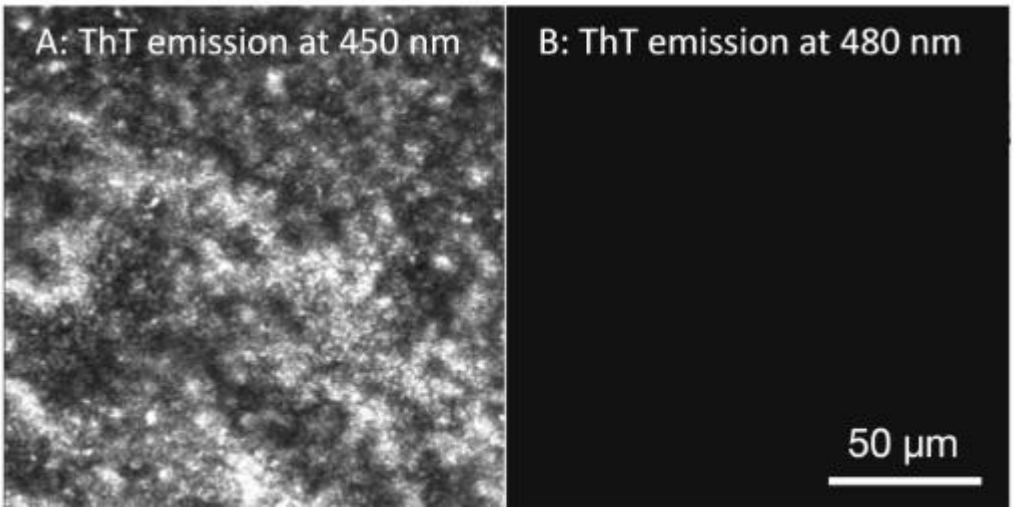

Figure 49: Thioflavin T staining of fibrinogen fiber scaffolds
Nanofibrous scaffolds were prepared by drying 5 mg/ml fibrinogen in 5 mM NH_4HCO_3 and 2.5x PBS in the presence of 5 mM Thioflavin (ThT). The ThT containing scaffolds were excited at 405 nm and the emission imaged at 450 nm (A) or they were excited at 450 nm and the emission was imaged at 480 nm (B). Image from the supplementary material of (Stapelfeldt et al., 2019b).

After the drying process, the thioflavin T dye was present throughout the scaffold as indicated by the emission at 450 nm (Figure 49 A). However, no emission was observed at 480 nm (Figure 49 B).

5.2.3. Concentration dependence of fibrinogen fiber secondary structure

In the previous section, it was shown that alongside the drying process in the presence of PBS, the fibrinogen concentration had a strong effect on fiber formation and showed clear thresholds, which had to be overcome to induce fiber formation. Below this threshold, only globular aggregates were observed after drying. Therefore, it was interesting to determine whether those observed threshold of fibrinogen concentration also had an influence on the content of different secondary structures.

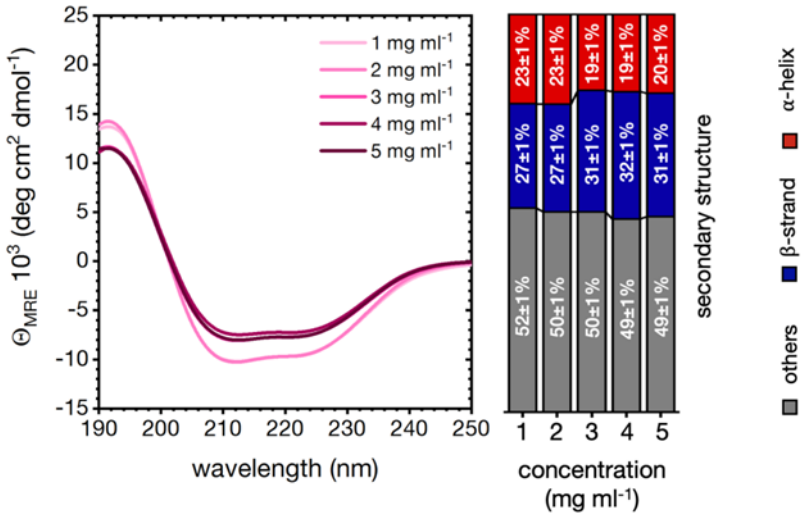

Figure 50: Secondary structure of fibrinogen scaffolds prepared by self-assembly of different fibrinogen concentrations
1 to 5 mg/ml fibrinogen in 5 mM NH_4HCO_3 were dried in 0.01 mm quartz cuvettes in the presence of 2.5x PBS and subsequently analyzed using circular dichroism spectroscopy. The circular dichroism spectra were converted into secondary structure content represented in the bar chart using the BeStSel web server. Image modified from (Stapelfeldt et al., 2019b).

When 1 or 2 mg/ml fibrinogen were dried in the presence of PBS, the corresponding circular dichroism spectra almost overlapped with a strong maximum at 195 nm and local minima at 210 and 222 nm. The BeStSel analyses showed that scaffolds prepared by drying 1 or 2 mg/ml fibrinogen had a content of 23 ± 1 % α-helical structures and 27 ± 1 % β-sheet structures (Figure 50). Scaffolds prepared with 3, 4 or 5 mg/ml fibrinogen showed similar circular dichroism spectra, which had a lower intensity compared to the spectra of 1 or 2 mg/ml especially for the maximum at 195 nm. In addition, the local minimum around 210 nm was less distinct for scaffolds prepared with 3, 4 or 5 mg/ml. The BeStSel analysis of the circular dichroism spectra revealed an increased content of β-sheet structures of 31 ± 1 % for 3 mg/ml, 32 ± 1 % for 4 mg/ml and 31 ± 1 % for 5 mg/ml. The content of α-helical structures, on the other hand, was decreased to 19 ± 1 %, 19 ± 1 % or 20 ± 1 % for 3, 4 or 5 mg/ml, respectively (Figure 50).

5.2.4. Secondary structure of fibrinogen nanofibers under varying pH conditions

Similar to the concentration threshold of fibrinogen fiber formation, a clear pH threshold, which had to be overcome for fiber formation, was observed in the previous section. When

the pH was below a threshold of 7 only globular aggregates of fibrinogen were observed after drying. Therefore, it was determined whether the pH thresholds of fibrinogen fiber formation also had an influence on the content of different secondary structures.

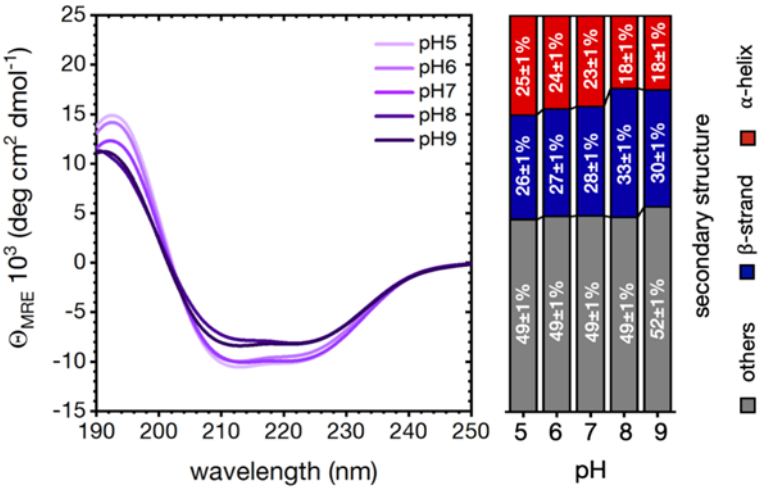

Figure 51: Secondary structure of fibrinogen scaffolds prepared by self-assembly at different pH values
Scaffolds were prepared by drying 5 mg/ml fibrinogen in the presence of 2.5x PBS with varying pH in 0.01 mm quartz cuvettes and subsequently analyzed using circular dichroism. The circular dichroism spectra were converted into secondary structure content represented in the bar chart using the BeStSel web server. Image modified from (Stapelfeldt et al., 2019b).

The circular dichroism spectra of fibrinogen scaffolds prepared with a pH of 5, 6 or 7 partially overlapped and had a high intensity while the spectra of scaffolds prepared with a pH of 8 or 9 had a lower intensity. The two minima were observed at wavelengths of 210 and 222 nm for the spectra and were not affected by the pH during fiber formation. The secondary structure content calculated using the BeStSel sever was in a similar range for pH 5, 6 and 7 with an α-helical content of 25 ± 1 %, 24 ± 1 % or 23 ± 1 % and a β-sheet content of 26 ± 1 %, 27 ± 1 % or 28 ± 1 %, respectively. When scaffolds were prepared at pH 8 or 9, a higher content of β-sheet structures was observed. Scaffolds prepared at pH 8 showed 18 ± 1 % α-helical and 33 ± 1 % β-sheet structures. Scaffolds prepared at pH 9 had a content 18 ± 1 % α-helical and 30 ± 1 % β-sheet structures (Figure 51).

5.2.5. Influence of humidity on the secondary structure of fibrinogen nanofibers

High humidities during drying resulted in fibrinogen scaffolds with a planar fibrinogen layer on top but with a fiber scaffold beneath the planar layer, which was confirmed by cross-sectional SEM analysis. Hence, the influence of different humidities during the drying process on the secondary structure of the fibrinogen scaffolds was additionally investigated.

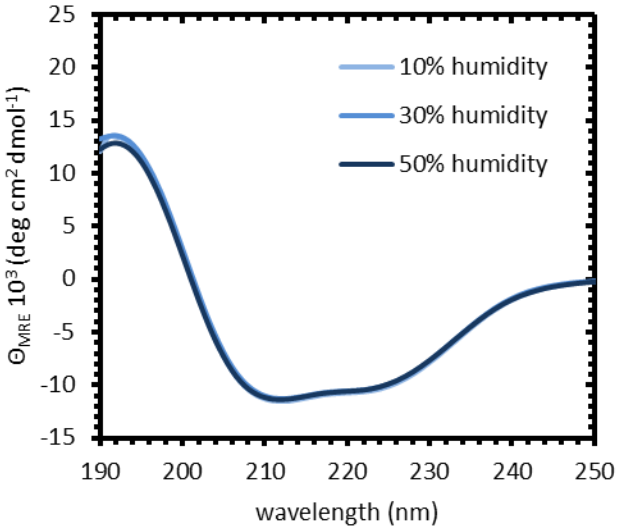

Figure 52: Secondary structure of fibrinogen scaffolds prepared by self-assembly at different pH values
Scaffolds were prepared by drying 5 mg/ml fibrinogen in the presence of 2.5x PBS with varying pH in 0.01 mm quartz cuvettes and subsequently analyzed using circular dichroism.

The circular dichroism spectra of fibrinogen scaffolds prepared by drying at different humidities almost perfectly overlapped. The local minima at 210 and 222 nm were not affected and the intensities did not change due to the humidity. The humidity during scaffold preparation had no influence on the circular dichroism of the samples (Figure 52).

5.2.6. Effect of crosslinking on the secondary structure of nanofibrous fibrinogen scaffolds

In the previous section, it was shown that the fibrinogen scaffolds prepared by drying in the presence of PBS were not stable upon rehydration. This drawback was overcome by a crosslinking step in formaldehyde vapor. Since further experiments for a potential future

biomaterial application require crosslinked scaffolds, prepared for example on glass or APTES substrates, the influence of these two substrate materials on the secondary structure of scaffolds was investigate with circular dichroism spectroscopy. It was shown that the substrate material had no influence on the secondary structure of self-assembled fibrinogen fibers.

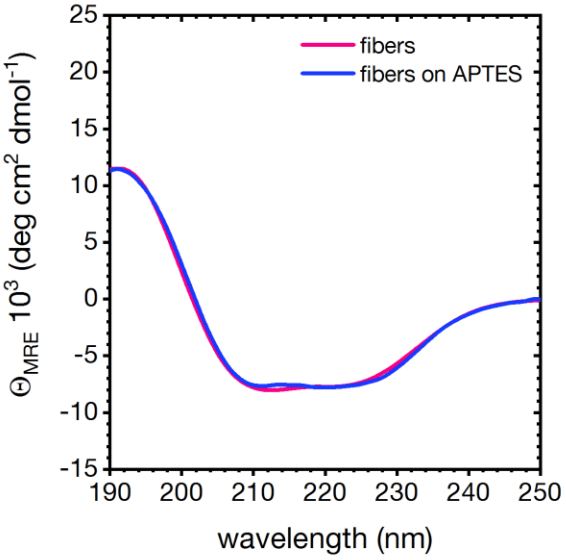

Figure 53: Secondary structure of self-assembled fibrinogen fiber scaffolds in APTES modified cuvettes
Fibers were prepared by drying 5 mg/ml fibrinogen in the presence of 2.5x PBS. The samples were either prepared in 0.01 mm cuvettes or in 0.01 mm cuvettes, which had been modified with APTES. Image was published in the supplementary material of (Stapelfeldt et al., 2019b).

The circular dichroism spectra of fibrinogen fiber scaffolds prepared in untreated or in APTES modified cuvettes overlaid almost completely. Only a minor shift in intensity and the minimum position at 210 nm was detected for the spectrum of the scaffold prepared on APTES. This shows that the fibrinogen fibers in scaffolds prepared on both different substrates have the same conformation (Figure 53); therefore, a further calculation of secondary structure components using the BeStSel software was not carried out.

Secondary structure of crosslinked fibrinogen scaffolds

In a second experiment, fibers were crosslinked using formaldehyde vapor and subsequently analyzed using circular dichroism. It was shown that an additional crosslinking of fibrinogen fibers did not affect the observed secondary structure.

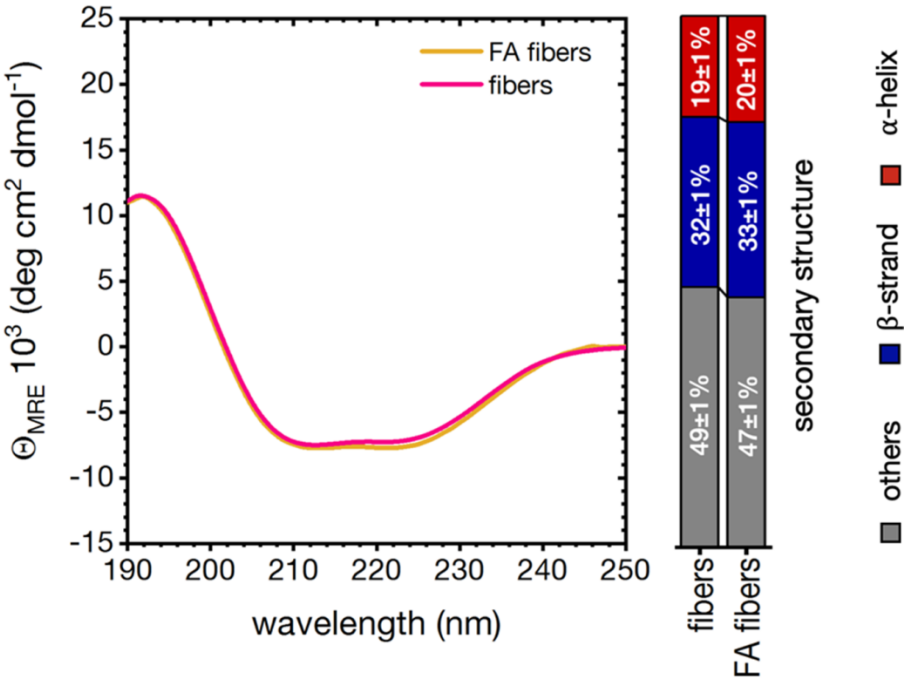

Figure 54: Secondary structure of self-assembled fibrinogen scaffold before and after crosslinking
Fibrinogen scaffolds were prepared by drying 5 mg/ml fibrinogen in the presence of 2.5x PBS in 0.01 mm cuvettes. The circular dichroism spectra were recorded either directly or after crosslinking in formaldehyde vapor. Spectra were converted into secondary structure content represented in the bar chart using the BeStSel web server. Image modified from (Stapelfeldt et al., 2019b).

The circular dichroism spectra of untreated fibrinogen scaffolds and of scaffolds crosslinked in formaldehyde vapor were overlaying with a slightly stronger minimum at 222 nm for the formaldehyde crosslinked fibers. The local minimum at 210 nm and the maximum at 195 nm as well as the overall intensity were similar for crosslinked and noncrosslinked fibers. Hence, the untreated and crosslinked scaffolds have a similar content of secondary structures. Untreated fibrinogen scaffolds showed 19 ± 1 % α-helical and 32 ± 1 % β-sheet structures. Crosslinked fibrinogen scaffolds showed 20 ± 1 % α-helical and 33 ± 1 % β-sheet content (Figure 54).

5.2.7. Secondary structure of dried and rehydrated fibrinogen nanofibers

In the third experiment, the secondary structure of the crosslinked fibrinogen fibers was analyzed after rehydration in water to investigate whether the changes in secondary

structure observed during the fiber formation were persistent. Surprisingly, the rehydration experiments revealed that crosslinked fibers change their conformation upon rehydration. The secondary structure of crosslinked fibers after rehydration returned into α-helical and β-sheet contents close to native fibrinogen or fibrin.

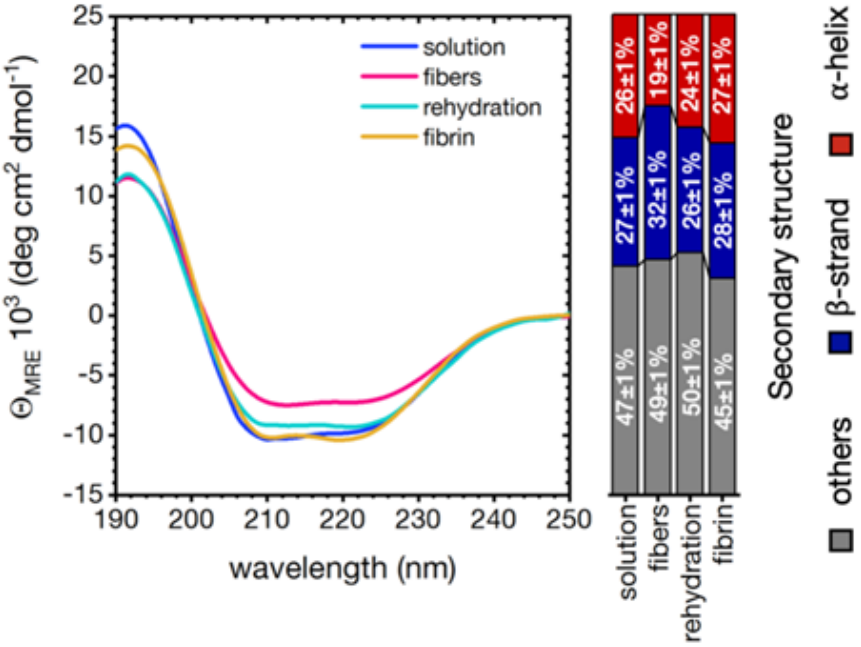

Figure 55: Effect of rehydration on the secondary structure of crosslinked fibrinogen fibers
CD spectra for fibrinogen in solution, fibrinogen nanofibers prepared by drying in the presence of PBS, formaldehyde vapor crosslinked fibrinogen nanofibers, which were subsequently rehydrated, and fibrin. The circular dichroism spectra were converted into secondary structure content represented in the bar chart using the BeStSel web server. Image modified from (Stapelfeldt et al., 2019b).

For comparison, the spectra and structure composition of fibrinogen solution and fibrin shown above were added to the graph. The spectra of dried and of rehydrated fibers showed similar minima at 210 and 222 nm; however, the spectrum of rehydrated fibers had a higher intensity. Interestingly, the spectrum of rehydrated fibers had an intermediate intensity between the spectra of dried fibers and the spectra of fibrin or fibrinogen in solution. In addition, the calculated secondary structure content returned to values similar to fibrinogen solution or fibrin. While crosslinked fibrinogen still showed an increased β-sheet content of 32 ± 1 % and 19 ± 1 % α-helical content, the rehydrated fibrinogen showed a β-sheet content of only 26 ± 1 % and a α-helix content 24 ± 1 %. This is close to the 27 ± 1 % or 28 ± 1 % of β-sheets and the 26 ± 1 % or 27 ± 1 % of α-helix content calculated for fibrinogen in solution and fibrin.

5.3. Bioactivity of self-assembled fibrinogen scaffolds

For further research and a potential future application of self-assembled fibrinogen fibers, a crosslinking step to increase the stability of the fiber scaffold in solution is inevitable. Cell culture or *in vivo* applications will expose the crosslinked fibrinogen scaffold to aqueous solution for several weeks. Therefore, the stability of self-assembled fibrinogen in solution was tested *in vitro* for a time course of five weeks. Since in a cell culture or *in vivo* situation the crosslinked fibrinogen scaffold will be additionally exposed to enzymes that could increase the scaffold degradation, the enzymes thrombin, plasmin and plasmin activated by urokinase were additionally studied in the long-term degradation experiments. The fibrinogen released from the scaffold into the supernatant was determined using UV spectroscopy. The degradation studies are good indicators for the usefulness of the self-assembled fibrinogen scaffold for future applications. A scaffold, which is for example used in a wound healing application, should not degrade rapidly, however some degradation should occur especially catalyzed by enzymes to assure a remodeling regeneration of the replaced tissue. Moreover, a study on the enzymatic degradability of self-assembled fibrinogen scaffolds can also reveal whether the fibrinogen remained biologically active during the drying and crosslinking process and whether it is still susceptible to its native reaction partners.

Another approach to investigate whether the fibrinogen is still biologically active after the self-assembly and crosslinking process is to study the binding of ligands that naturally bind to fibrinogen. In these experiments, the binding of fibrinogen or heparin to the crosslinked fibrinogen scaffolds was studied using a fluorimeter. The scaffolds were incubated with fluorescently labeled fibrinogen or heparin and the decrease in concentrations in the supernatant was determined.

5.3.1. Enzymatic degradation of fibrinogen in solution

To study the degradation of fibrinogen by the enzymes plasmin, urokinase or a combination of both, the degradation of fibrinogen solutions in DMEM or in HEPES buffer was

analyzed. After fibrinogen was incubated in the presence of these enzymes overnight at 37°C, the products of the enzymatic digestion were analyzed using SDS-PAGE.

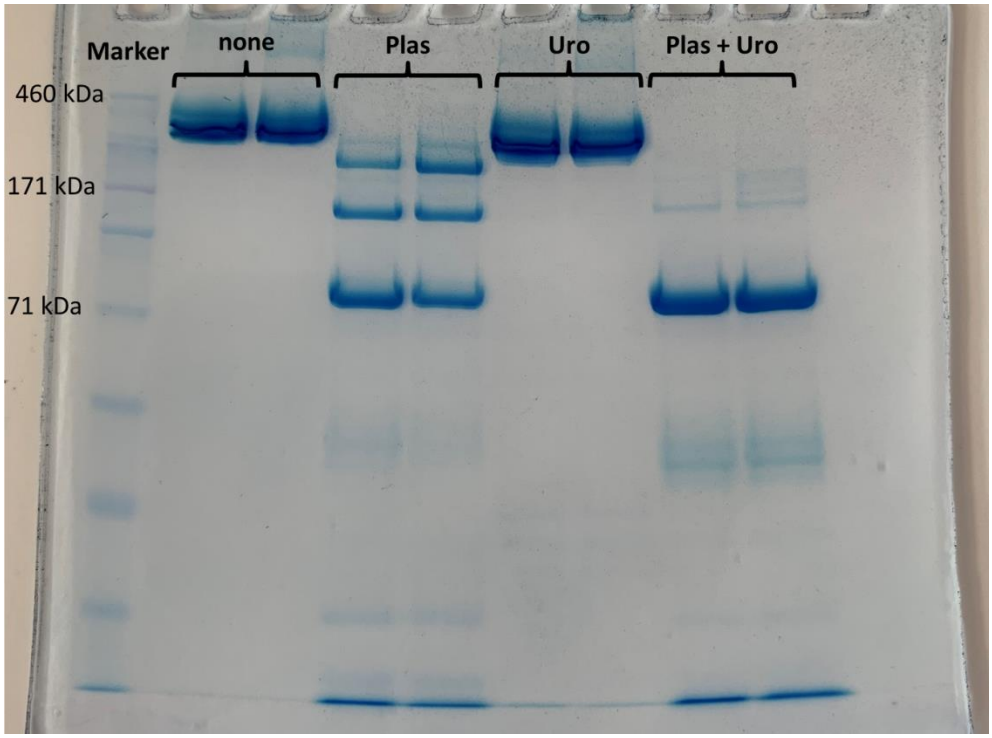

Figure 56: Enzymatic digestion of fibrinogen solution
1 mg/ml fibrinogen was incubated overnight at 37°C either with no enzyme present (none) or in the presence of the enzymes plasmin (Plas), urokinase (Uro) or a combination of both (Plas + Uro). The left lane for each condition represents a test in DMEM, the right lane represents a test in 10 mM HEPES buffer at pH 7.4 with addition of 150 mM NaCl and 5 mM $CaCl_2$. As a marker a HighMark protein standard was used.

The use of DMEM or the described HEPES buffer system did not affect the outcome of the enzymatic degradation experiments. Without any enzymes present, the fibrinogen was not degraded overnight and maintained the native molecular weight of approximately 340 kDa. In the presence of plasmin, fibrinogen was digested into three large fragments with molecular weights of approximately 260, 160 and 80 kDa. Fibrinogen was not degraded by incubation in the presence of urokinase alone, where only the native 340 kDa band was observed. However, the combination of plasmin and urokinase showed a stronger band at 80 kDa than the incubation of fibrinogen with plasmin alone and hardly any band of a higher molecular weight (Figure 56).

Since the enzymatic degradation worked in the HEPES buffer system, which has substantially less components than DMEM, it was applied in long-term degradation experiments with the crosslinked fibrinogen scaffolds.

5.3.2. Long-term enzymatic degradation of self-assembled fibrinogen scaffolds

The long-term stability of fibrinogen scaffolds prepared by self-assembly was investigated in solution or in the presence of the enzymes thrombin, urokinase or plasmin, since these enzymes are interacting with fibrin or fibrinogen in the *in vivo* environment. Planar or nanofibrous fibrinogen scaffolds were crosslinked in formaldehyde vapor for one or two hours, respectively, and were subsequently incubated in the presence of different enzymes for 35 days at 37°C. To measure whether degraded fragments of fibrinogen were released into the supernatant, each week the total protein amount in the supernatant was determined by spectroscopy.

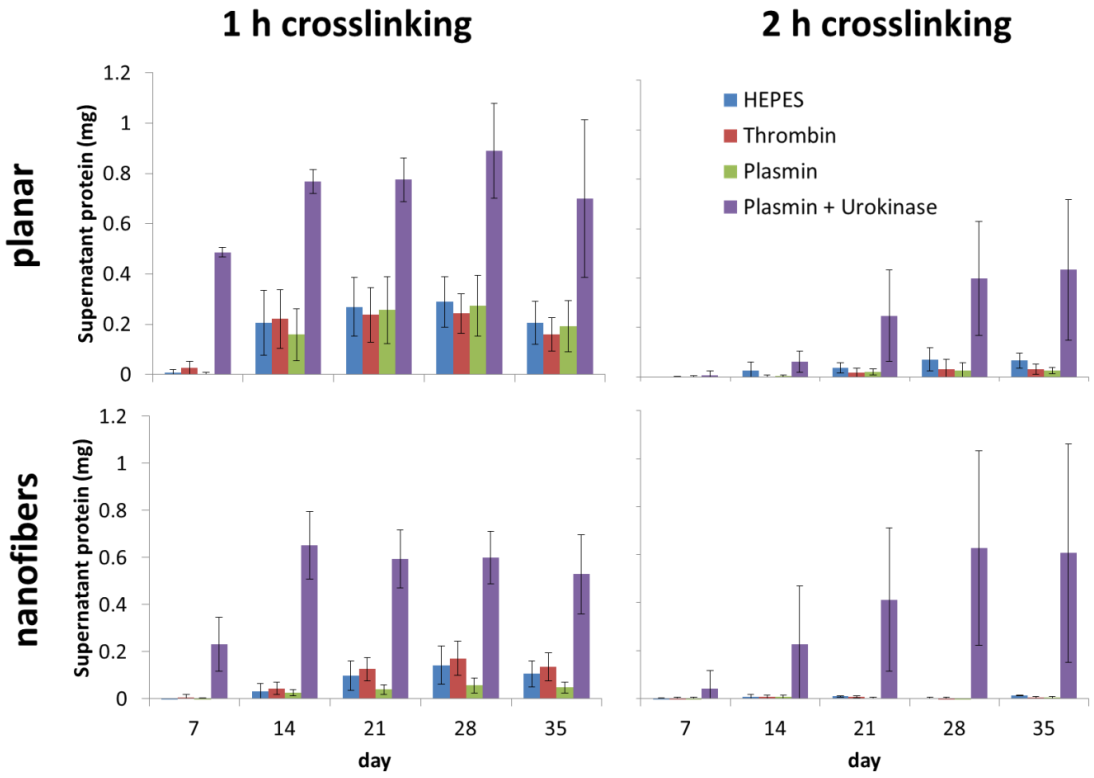

Figure 57: Long-term degradation of fibrinogen scaffolds
Scaffolds were prepared by drying a 5 mg/ml fibrinogen solution. For the induction of nanofiber formation 2.5x PBS were present. The scaffolds were crosslinked by exposing them to formaldehyde vapor for 1 or 2 h. After washing, the scaffolds were exposed to the indicated enzymes or HEPES buffer at 37°C for 35 days and the total protein amount in the supernatant was determined each week. The data displayed for HEPES, thrombin, plasmin and plasmin + urokinase represent means and standard deviation of three independent experiments. The data of thrombin and plasmin for each time point were analyzed for significant differences in respect to the HEPES buffer data of that condition by two way ANOVA and a Tukey's multiple comparison test. No significant differences between the protein amount of HEPES and the protein amounts of thrombin or plasmin were found.

From the amount of fibrinogen measured in the supernatant and the known total amount of 1 mg per sample, the remaining percentage of fibrinogen present on the samples was calculated and is shown in Table 5 and Table 6.

Table 5: Percentage of remaining fibrinogen on 1 h crosslinked scaffolds.
After 35 days of incubation of 1 h crosslinked fibrinogen scaffolds in the presence of different enzymes, the percentage of remaining fibrinogen on the sample was determined based on the measured amount of fibrinogen released into the supernatant.

	Planar				Nanofibrous			
Day	HEPES	Thrombin	Plasmin	Plasmin + Urokinase	HEPES	Thrombin	Plasmin	Plasmin + Urokinase
7	99 ± 1	98 ± 3	100 ± 1	51 ± 2	101 ± 1	100 ± 1	100 ± 0	77 ± 12
14	79 ± 13	78 ± 12	84 ± 10	23 ± 5	97 ± 3	96 ± 3	98 ± 1	35 ± 14
21	73 ± 12	76 ± 11	74 ± 13	23 ± 9	90 ± 6	87 ± 5	96 ± 2	41 ± 12
28	71 ± 10	76 ± 8	73 ± 12	11 ± 19	86 ± 8	83 ± 7	94 ± 3	40 ± 11
35	79 ± 8	84 ± 7	81 ± 10	30 ± 31	89 ± 5	87 ± 6	95 ± 2	47 ± 17

Table 6: Percentage of remaining fibrinogen on 2 h crosslinked scaffolds.
After 35 days of incubation of 2 h crosslinked fibrinogen scaffolds in the presence of different enzymes, the percentage of remaining fibrinogen on the sample was determined based on the measured amount of fibrinogen released into the supernatant.

	Planar				Nanofibrous			
Day	HEPES	Thrombin	Plasmin	Plasmin + Urokinase	HEPES	Thrombin	Plasmin	Plasmin + Urokinase
7	101 ± 1	101 ± 1	99 ± 1	99 ± 2	100 ± 1	100 ± 1	100 ± 1	96 ± 7
14	97 ± 3	100 ± 1	79 ± 13	94 ± 4	99 ± 1	99 ± 1	99 ± 1	77 ± 24
21	96 ± 2	98 ± 2	73 ± 12	75 ± 19	99 ± 0	99 ± 0	100 ± 0	59 ± 30
28	93 ± 5	97 ± 4	71 ± 10	60 ± 23	100 ± 0	100 ± 1	101 ± 1	37 ± 41
35	93 ± 3	97 ± 2	79 ± 8	57 ± 28	99 ± 0	100 ± 0	100 ± 0	39 ± 46

When 1 h crosslinked fibrinogen scaffolds were incubated for 35 days, an increase in protein concentration in the supernatant was detected (Figure 57). This indicates a loss of fibrinogen from the sample, which was converted to the percentage of fibrinogen remaining on the sample (Table 5). For planar scaffolds crosslinked for 1 h, the amounts of fibrinogen in the supernatant and the corresponding values of remaining fibrinogen on the sample were in a similar range for HEPES buffer, thrombin and plasmin. After 7 days almost all fibrinogen remained on the sample (99 ± 1%, 98 ± 3 % and 100 ± 1%, respectively). After incubation for 35 days, the amount of fibrinogen had decreased to ¾ of the initial amount on the sample (79 ± 8 %, 84 ± 7 % and 81 ± 10 %, respectively),(Table 5). Only when a combination of plasmin and urokinase was applied the release of fibrinogen into the

supernatant was accelerated. Even after 7 days, a substantial amount of fibrinogen was detected in the supernatant and only 51 ± 2 % of fibrinogen remained on the sample (Figure 57, Table 5). Fibrous scaffolds showed a similar degradation behavior but with a lower release of fibrinogen into the supernatant. After 35 days incubation in HEPES buffer thrombin or plasmin 89 ± 5%, 87 ± 6% and 95 ± 2 % of fibrinogen remained on the scaffold, respectively (Table 5). Here the combination of plasmin and urokinase resulted in a stronger release of fibrinogen into the supernatant, too. After 7 days 77 ± 12 % of fibrinogen was still present on the sample, while after 35 only 47 ± 17% were present, when the samples were incubated with plasmin and urokinase (Figure 57, Table 5).

The release of fibrinogen into the supernatant was overall lower when planar of nanofibrous fibrinogen scaffolds were crosslinked for 2 h (Figure 57). When planar scaffolds crosslinked for 2 h were incubated in HEPES buffer, thrombin or plasmin 93 ± 3 %, 97 ± 2% or 79 ± 8% of the fibrinogen were still present on the sample after 35 days (Table 6). Incubation with a combination of plasmin and urokinase resulted in a higher content of fibrinogen into the supernatant while 57 ± 28% remained on the planar samples after 35 days (Figure 57, Table 6).

Nanofibrous samples crosslinked for 2 h showed an even lower release of fibrinogen into the supernatant (Figure 57). When the scaffolds were incubated in HEPES buffer, thrombin or plasmin hardly any fibrinogen was detected in the supernatant and almost all fibrinogen remained on the sample. Only incubation in the presence of plasmin and urokinase resulted in a release of fibrinogen into the supernatant and after 35 days 39 ± 46 % remained on the sample (Figure 57, Table 6).

Morphology of self-assembled fibrinogen scaffolds after 35 days of degradation

After 35 days of incubation, the samples of the long-term experiment were dried and the morphology was analyzed in the SEM.

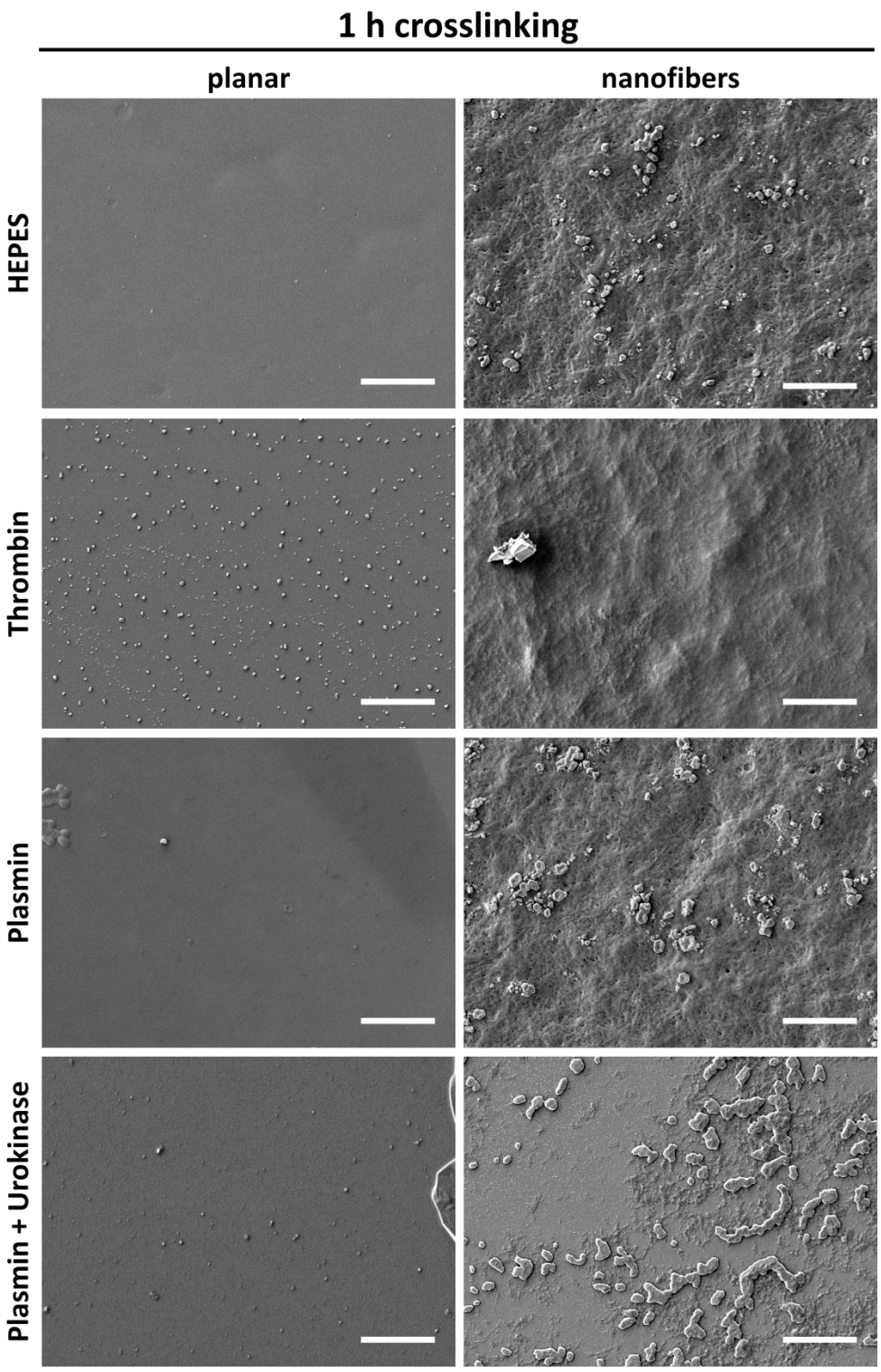

Figure 58: Fibrinogen scaffolds crosslinked for 1 h after 35 days of degradation
Planar fibrinogen layers and nanofibrous fibrinogen scaffolds were crosslinked in formaldehyde vapor for 1 h. After washing, the scaffolds were incubated in the presence of different enzymes for 35 days. After drying, the samples were analyzed using scanning electron microscopy. Scale bars represent 10 µm.

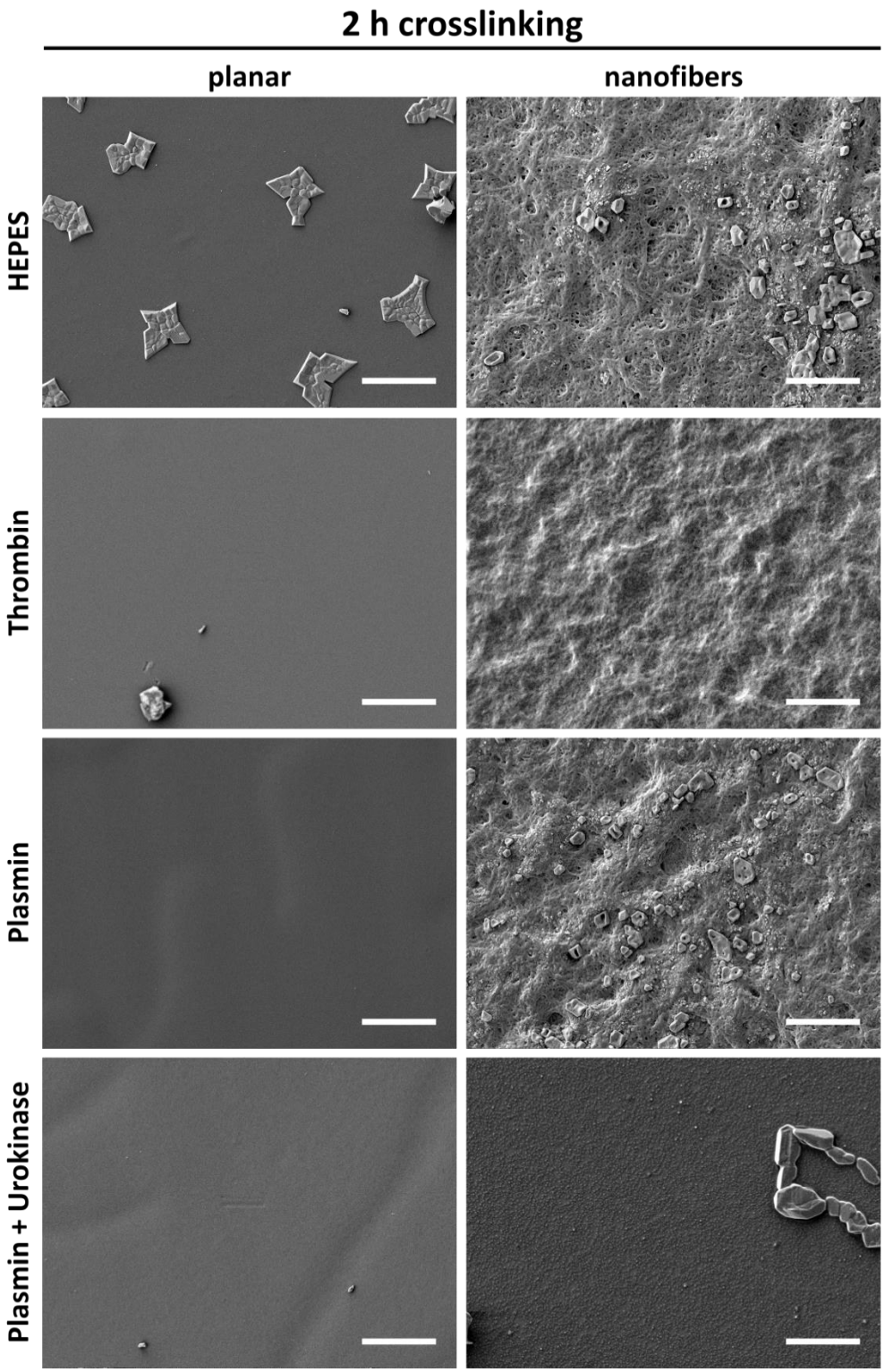

Figure 59: Fibrinogen scaffolds crosslinked for 2 h after 35 days of degradation
Planar fibrinogen layers and nanofibrous fibrinogen scaffolds were crosslinked in formaldehyde vapor for 2 h. After washing, the scaffolds were incubated in the presence of different enzymes for 35 days. After drying, the samples were analyzed using scanning electron microscopy. Scale bars represent 10 µm.

Scanning electron microscopy revealed that the planar samples crosslinked for 1 h maintained a planar morphology after 35 days of incubation with HEPES buffer, thrombin, plasmin or a combination of plasmin and urokinase. Some salt crystals were observed, especially on thrombin treated samples (Figure 58). Fibrous samples crosslinked for 1 h showed some remains of the nanofiber scaffolds after 35 days of incubation in the presence of HEPES buffer, thrombin or plasmin. However, the scaffolds showed a poor fiber morphology and appeared in a molten like shape, especially after incubation with thrombin (Figure 58). After incubation of a 1 h crosslinked nanofiber scaffold with plasmin and urokinase on the other hand only a few aggregated remains of the fibrinogen scaffold were observed under the SEM (Figure 58).

Planar samples that were crosslinked for 2 h remained planar after 35 days of incubation in HEPES buffer, thrombin, plasmin or a combination of plasmin and urokinase. On samples incubated in HEPES buffer, additional crystal formation was observed (Figure 59). When fibrous samples crosslinked for 2 h were incubated in HEPES buffer, intact scaffold morphology with defined fibers was still observed under SEM. After incubation in the presence of thrombin or plasmin, the overall scaffold morphology was not affected but the fibers of the scaffold showed a molten like topography. However, after 35 days incubation in the presence of plasmin and urokinase only patchy aggregates of fibrinogen remained on the surface of the 2 h crosslinked samples (Figure 59).

Overall, the long-term experiments indicate that crosslinked fibrinogen scaffolds prepared by self-assembly slowly degraded over time. This trend is stronger for planar as for fibrous samples. The crosslinking time had a strong impact on the scaffold morphology after 35 days, which is in agreement with the measured amounts of fibrinogen in the supernatant. With 1 h formaldehyde vapor crosslinking, more fibrinogen is released into the supernatant and fibrinogen scaffolds showed fewer nanofibers, whereas with 2 h crosslinking, less fibrinogen was released into the supernatant and some fibrous structures remained on the samples. Incubation with a combination of plasmin and urokinase resulted in high amounts of protein in the supernatant. Consistent with these findings the morphology of the fibrinogen scaffolds incubated with plasmin and urokinase showed only a few patchy scaffold remains. The data indicate a slow degradation that is present in all buffers

dependent on the crosslinking time. This degradation was accelerated by the combination of plasmin and urokinase.

5.3.3. Binding of fibrinogen and heparin to self-assembled fibrinogen scaffolds

In order to analyze if crosslinked planar layers or self-assembled fibrous scaffolds of fibrinogen are still able to interact with some of their native ligands, binding experiments were conducted using fibrinogen or heparin in solution as potential binding partners for the crosslinked fibrinogen. Planar layers of self-assembled fibrous scaffolds of fibrinogen were prepared on APTES slides and crosslinked in formaldehyde vapor for 1 h, because 1 h crosslinking showed the highest susceptibility to enzymatic degradation in the previous experiments. In a second step, fluorescently labeled fibrinogen or heparin solution was added upon the samples. After 1 h incubation at room temperature, the concentration of labeled fibrinogen or heparin in the supernatant was measured to analyze how much fibrinogen or heparin had bound to the sample. The samples were washed and the fibrinogen or heparin concentration in the washing fraction was measured to exclude unbound fibrinogen or heparin.

To compare the amount of bound fibrinogen or heparin, the experiment was also carried out on APTES surfaces or on BSA surfaces that were prepared in the presence or absence of PBS. With these control experiments, the unspecific binding to APTES surfaces and unspecific protein interactions of the labeled fibrinogen or heparin was determined.

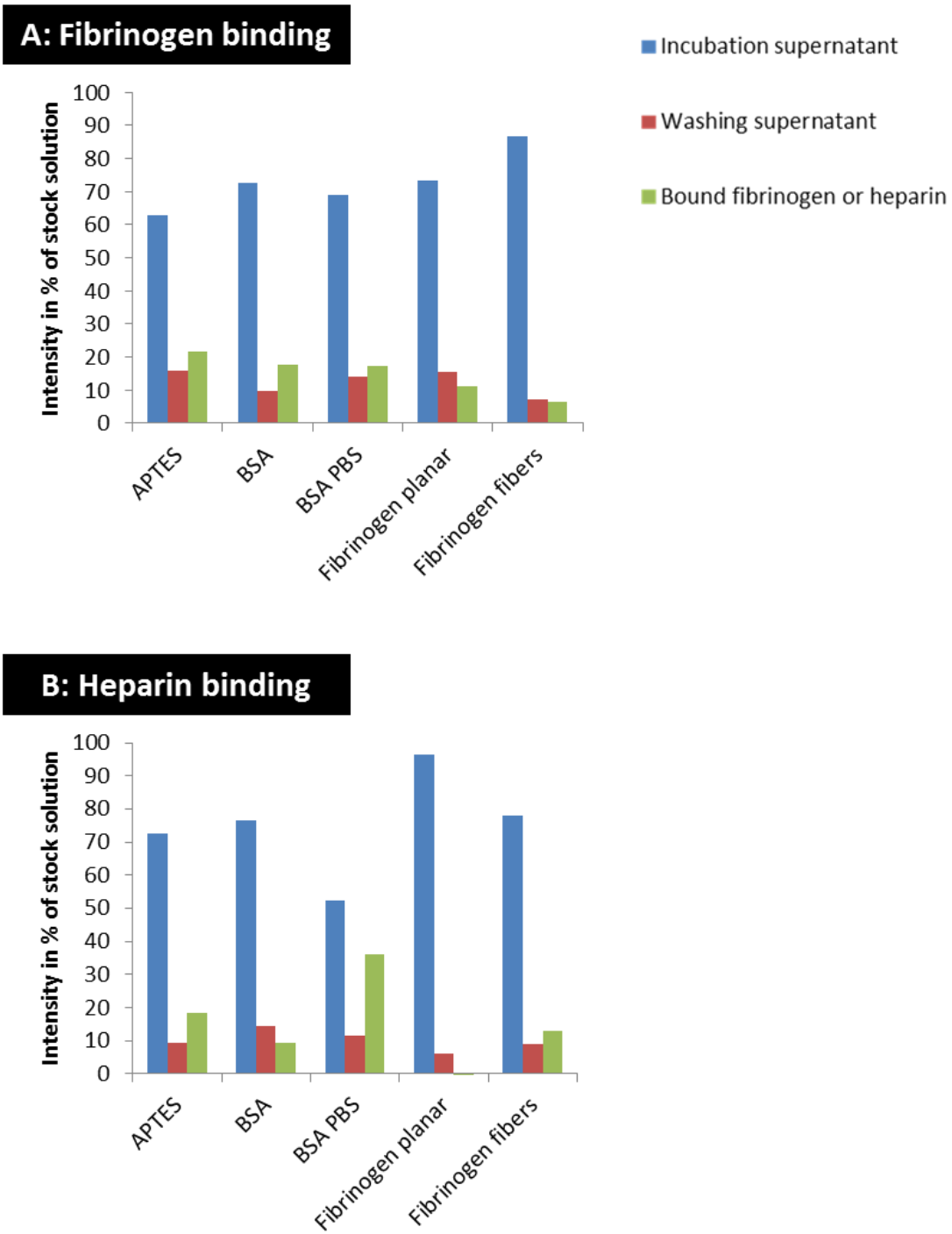

Figure 60: Binding of fibrinogen or heparin to planar or nanofibrous fibrinogen
Planar fibrinogen layers and nanofibrous fibrinogen scaffolds were prepared on APTES surfaces and crosslinked in formaldehyde vapor for 1 h. Similar to planar and nanofibrous fibrinogen, BSA control samples were prepared and crosslinked. The binding to APTES surfaces was analyzed without further crosslinking. Alexa 488-labeled fibrinogen or heparin were incubated on the samples and after 1 h, the remaining concentration in the supernatant was measured using fluorimetry. The samples were washed and the concentration of labeled fibrinogen or heparin in the washing fraction was determined. With the remaining concentration and the concentration redissolved into the supernatant the concentration of bound fibrinogen was calculated.

The binding experiments revealed that most of the labeled fibrinogen (60 to 90 %) remained in the incubation supernatant and was not bound to any of the substrates. In addition, 10 to 15% of the labeled fibrinogen, which had not bound to the substrates, was observed in the washing fraction. Only 22, 18, 17, 11 or 6 % of the labeled fibrinogen had bound to APTES, BSA, BSA and PBS, planar fibrinogen scaffolds or fibrous fibrinogen scaffolds, respectively.

In addition, the binding of heparin to the substrates was low. The majority of the labeled heparin was detected in the incubation supernatant (50 to 95 %) and roughly 10% were additionally found in the washing fraction. This resulted in a percentage of fibrinogen bound to APTES, BSA, BSA and PBS, planar fibrinogen scaffolds or fibrous fibrinogen of 18, 9, 36, 0 or 13 %, respectively.

Overall, planar and nanofibrous fibrinogen scaffolds showed the lowest binding of labeled fibrinogen and of labeled heparin, while the unspecific binding to APTES or to BSA substrates was higher.

6. Discussion

6.1. Morphology of self-assembled fibrinogen scaffolds

When fibrinogen solutions were dried in the presence of citrate, phosphate buffer or PBS the SEM analysis revealed that networks of fibrinogen nanofibers had formed. The fiber networks had similar fiber diameters and showed a characteristic star-shaped morphology. However, when fibrinogen was dried in the presence of NH_4HCO_3 solution without any additions only planar fibrinogen layers were observed.

The possibility to prepare planar fibrinogen layers is one major advantage of the newly discovered fibrinogen self-assembly. This allows to prepare planar 2D fibrinogen controls in addition to the 3D fibrinogen fiber scaffolds. The preparation of planar fibrinogen layers as reference samples has been neglected by other methods described for fabrication of fibrinogen nanofibers (Koo et al., 2010; Wei et al., 2008b; Wnek et al., 2003). Planar control samples are a useful tool to design experiments, which investigate and distinguish the effects of fibrinogen biochemistry and the morphology of the fibrinogen substrate, especially concerning cellular interactions. Moreover, planar samples might also prove useful for an application as a biomaterial because they have different structural properties and therefore provide a different interface for biological interactions.

During the drying, the NH_4HCO_3 solution completely evaporated in the form of ammonia carbon dioxide and water. In contrast, citrate, phosphate buffer or PBS contain ions that do not evaporate during the drying process. Apparently, the combination of drying and the presence of ions are crucial for the self-assembly of the fibrinogen into fiber scaffolds.

Fibrinogen fiber formation due to drying in the presence of ions has not been described before. However, Reichert and coworkers, who investigated fibrinogen assembly on hydrophobic surfaces, discussed that the presence of positively charged potassium and sodium ions might have an additional effect on fiber formation (Reichert et al., 2009). However, Reichert and coworkers considered the exposure of fibrinogen to hydrophobic surfaces as the main driving force of fiber formation and did not further investigate their hypothesis about the effect of ions. In contrast, the presence of ions during drying seems to be the main driving force for the self-assembly mechanism discovered in this thesis.

Planar fibrinogen prepared by drying in the presence of NH_4HCO_3 solution was transparent, while the fibrinogen fiber formation during the drying in the presence of ions was accompanied by a change in turbidity. A change of turbidity is also observed during the formation of fibrin fibers and is frequently used to quantify the thrombin catalyzed conversion of fibrinogen into fibrin (Davis et al., 2011) as well as the formation of other fibrous protein networks, like for example collagen (Zhu and Kaufman, 2014). However, these changes in turbidity already occur in solution. Nevertheless, the change in turbidity observed during late stages of fibrinogen self-assembly raises one of the main initial questions about the newly found mechanism of fibrinogen fiber formation; if the fibrous scaffolds consist of fibrinogen fibers or if they are actual fibrin fibers formed by the reaction of fibrinogen and some thrombin contamination.

Although the fibrinogen used in this thesis had a purity of 99%, it is important to prove that the observed fiber formation is not due to some trace contaminations of thrombin. A first indication that the fibers prepared by drying in the presence of ions are no fibrin fibers, are the morphological differences. Although the fibers prepared by drying in the presence of ions had diameters in the range of fibrin fiber diameters, the overall morphology of the fibrinogen scaffolds was different compared to fibrin. While fibrin fibers show a homogenous network, the fibrinogen fibers prepared by drying formed a fibrous network with local star-shaped center points of a higher fibrinogen density (Figure 26). A further strong indicator that the fiber formation relied on an unknown and thrombin-independent mechanism is the fact that planar fibrinogen layers can be prepared by drying fibrinogen in NH_4HCO_3 solution. A trace contamination of thrombin in the fibrinogen stock would have induced fiber formation in all samples including those where fibrinogen was dried in NH_4HCO_3 solution without additional ions present.

To fully exclude any possible involvement of thrombin residues in the fiber formation, fibrinogen was dried in the presence of PBS with an addition of 4-(2-aminoethyl)benzenesulfonyl fluoride hydrochloride (AEBSF). AEBSF is a strong inhibitor for serine proteases, which covalently binds to the active center and thereby inactivates any potential trace amounts of thrombin (Markwardt et al., 1973).

The self-assembly studies with the thrombin inhibitor AEBSF showed that fiber formation still occurred even when high concentrations of AEBSF were present. Therefore, it can be concluded that thrombin is not involved in the formation of fibrinogen fibers and that the salt-induced self-assembly is based on an enzyme-independent mechanism.

An additional indication that the fibrinogen fiber scaffolds are not fibrin is the fact that fibrin is stable in solution while the fibrinogen fibers prepared by drying in the presence of ions were not stable without further crosslinking treatment.

The findings of this thesis show that drying of fibrinogen in the presence of PBS induces fiber formation. Since PBS contains different salts, fibrinogen was also dried in the presence of the single components of PBS. Drying with high concentrations of NaCl or KCl was sufficient to induce fibrinogen fiber formation, but with less abundant fibers and a less distinct fiber morphology as compared to drying with PBS. With a low concentration of KCl no fiber formation was observed, which could indicate that KCl has a lower potential to initiate self-assembly and that a KCl concentration threshold has to be overcome obtain fibrinogen fiber networks.

Interestingly, a recent study by Hämisch and coworkers investigated the aggregation of fibrinogen in solutions of with different ion compositions and different ionic strengths and found an opposite effect of the fiber formation observed in this thesis. Hämisch and coworkers observed an aggregation of fibrinogen when the concentration of ions was diluted, which was confirmed by an increase in hydrodynamic diameter. This was interpreted as a form of self-assembly, although it is unclear if this assembly leads to fibrinogen fibers. AFM images presented by Hämisch rather indicate an assembly into globular aggregates (Hämisch et al., 2019).

In contrast, the fibrinogen self-assembly of fibrinogen observed in this thesis resulted in aggregation of fibrinogen into fibers and was initiated by an increasing ion concentration during the drying process.

High concentrations of certain salts can be used to precipitate proteins by salting them out. The potential of ions to precipitate proteins has been described in the Hofmeister series, which categorizes ions as chaotropic or kosmotropic. Chaotropic ions disrupt hydrogen

bridges and therefore have a low potential to precipitate proteins. Strong chaotropic ions can even denature protein structures by reducing the order in of hydrogen bridges. Kosmotropic ions, on the other hand, stabilize hydrogen bridges and have a great potential to precipitate proteins (Baldwin, 1996; Zhang and Cremer, 2006).

All ion species used for the preparation of fibrinogen networks are classified somewhere in the middle of the Hofmeister series. Remarkable is the fact that KCl, which showed less potential to form fibrinogen fibers, has a slightly higher potential to precipitate proteins compared to NaCl. Even more remarkable, the NH_4HCO_3 solution, which resulted in planar fibrinogen layers, has an even higher potential for protein aggregation, since NH_4^+ ions and CO_3^- ions are even less chaotropic than NaCl or KCl (Baldwin, 1996; Zhang and Cremer, 2006).

During drying the concentration of each ion increases up to the point, where fibrinogen began to precipitate. It is counterintuitive that the most chaotropic salt NaCl resulted in organized fibrinogen fibers, while salts with a better potential to aggregate fibrinogen resulted in planar or globular structures. This indicates that planar fibrinogen layers formed under drying conditions where fibrinogen has a low solubility, while fibrinogen fibers formed during drying under conditions where fibrinogen had a high solubility. Probably planar layers prepared in the presence of NH_4HCO_3 form during an early stage within the drying process since the point where the NH_4HCO_3 concentration is sufficient to precipitate is reached quicker in comparison to fibrinogen, which is dried in the presence of ions. Here, the point of fibrinogen precipitation will be reached in a very late stage because higher concentrations of sodium or potassium ions are needed to precipitate the fibrinogen. Nevertheless, the formation of planar and fibrous fibrinogen scaffolds is not directly induced and both events happen most likely at the end of the drying process. It also has to be taken into account that the NH_4HCO_3 evaporated during the drying process, which leads to a lower potential for protein aggregation. Nevertheless, to fully understand the influence of chaotropic agents, the fibrinogen drying experiments should be continued with even more chaotropic salts from the Hofmeister series like nitrate or iodide salts. In addition, charge effects could be investigated using divalent ions like calcium or magnesium. However, this approach would be challenging and the results would be hard to interpret, due to two reasons. Calcium and magnesium have a high potential to form complexes with

proteins, which might interfere with the fiber formation observed in the presence of monovalent cations. Secondly, it has been shown that different ion species of the same charge (like sodium or potassium) show a different fibrinogen precipitation behavior. This indicates that charge effects are not the main factor during fibrinogen fibrillogenesis and that the Hofmeister effects have a stronger influence like describe for other proteins (Moreira et al., 2006).

The precipitation of proteins by different salts is not completely understood. Less chaotropic salts are known to stabilize hydrogen bridges between protein molecules thereby allowing aggregation. On the other hand, the presence of ions also has an influence on the hydration shell of the protein molecules in solution, which is even higher for more chaotropic salts. Since more chaotropic salts showed a slightly higher effect on fibrinogen fiber formation, it seems likely that the effect on the hydration shell of the protein is involved in the formation of fibrinogen fibers. Interactions and even aggregation of fibrinogen molecules with a weaker hydration shell, induced by chaotropic salts seems plausible. It has been shown that the hydrodynamic diameter of fibrinogen changes dependent on the pH and on the ionic strength, which makes a similar effect due to the presence of chaotropic salts likely (Wasilewska et al., 2009).

It also has to be considered that the pH value of pure NaCl and KCl solutions differs from the pH value of PBS. The influence of the pH is an important aspect of fiber formation. Fiber formation was also observed, when potassium phosphate buffer (pH 7.4) was used but with a lower fiber density and less distinct fiber morphology as compared to fibers prepared with sodium phosphate buffer. This is an additional indication that buffer containing potassium has a lower potential to induce self-assembly of fibrinogen fiber because potassium ions are not as chaotropic as sodium ions.

Overall, the findings show that a high concentration of monovalent ions during drying alone is sufficient to induce fibrinogen fiber formation and that the chaotropic potential of the used ions has an influence. Nevertheless, the following experiments were conducted using PBS and sodium phosphate buffer, because drying in the presence of those buffers resulted in the most defined fibrinogen fiber morphology and those buffers allow an accurate adjustment of the pH.

The thresholds of fibrinogen fiber formation were analyzed with regard to fibrinogen concentration, buffer concentration and pH. The determination of conditions under which fiber formation does occur or does not occur allows to gain insight into the mechanism of fiber formation.

Formation of fibrinogen fibers was observed with all applied concentrations of phosphate buffer or PBS. Apparently, fiber formation during drying is even induced when only low concentrations of ions are present. The phosphate buffer or PBS concentration also had no effect on the fiber diameter. However, the used buffer concentration was correlated to total substrate coverage of the fibrinogen scaffold on the glass slides. With low concentrations of phosphate buffer or PBS the fibrinogen fiber scaffolds were only observed in a small part in the center of the sample. This indicates that with low buffer concentrations the required conditions are reached in a very late stage of the drying process, but are reached due to a concentration of the buffer during drying.

During the drying process, water evaporates and the fibrinogen concentration increases, therefore, the concentration independent behavior observed for the buffers should be similar for the starting concentration of fibrinogen, but interestingly it is not. The experiments, which analyzed the fiber formation with different fibrinogen starting concentrations showed that with concentrations lower than 2 mg/ml no fiber formation was observed at all in both buffer systems. It is remarkable that the increase in fibrinogen concentration during the drying process is not sufficient to induce at least some fiber formation when the starting concentration is too low. Interestingly, the useful initial concentrations for salt-induced self-assembly of fibrinogen fibers are in the range of the concentration of fibrinogen in the blood plasma (Mosesson, 2005; Stein et al., 1978). Other investigations of fibrinogen self-assembly, for example on hydrophobic surfaces, observed fibrinogen fibers with concentration of even 1 µg/ml (Wei et al., 2008a) or 200 µg/ml (Koo et al., 2010). The use of electrospinning for the fabrication of fibrinogen fibers on the other hand requires fibrinogen high concentrations of up to 167 g/ml (Wnek et al., 2003).

The fibrinogen concentration of 2 mg/ml, which is required for salt induced self-assembly is an interesting observation, especially since the threshold for fiber formation seems to be much lower for the self-assembly of fibrinogen on hydrophobic surfaces. This could

indicate that either both self-assembly methods rely on different mechanisms or that the presence of a hydrophobic surface strongly enhances the self-assembly of fibrinogen fibers.

An additional observation of the concentration experiments was the fact that total scaffold thickness increased when higher starting concentrations were used. The scaffolds reached thicknesses up to 10 µm, while the studies that used low fibrinogen concentrations only resulted in single fibers. The findings in this thesis also show that fibrinogen fibers are present throughout the whole scaffold thickness. This indicates that none of the used fibrinogen concentration was too high and had an inhibitory effect on fibrinogen self-assembly. It can be presumed that even higher concentrations of fibrinogen or a layer-by-layer approach could be used to prepare thicker scaffolds. The scaffold thickness will be an important factor for wound healing applications of fibrinogen scaffolds, because the scaffolds should be thick enough to withstand the blood pressure and the mechanical stress of a wound. A thick scaffold is also easier to handle during application. However, the thicker the fibrinogen scaffolds the longer the integration time and the replacement of fibrinogen with regenerated tissue. Therefore, the suggested layer-by-layer approach might be useful to create scaffolds with applicable mechanic and a low scaffold thickness.

Other approaches like fibrinogen fiber formation on hydrophobic surfaces (Koo et al., 2010; Reichert et al., 2009), ethanol-induced fibrinogen fiber formation (Wei et al., 2008b), acidic fibrinogen denaturation (Wei et al., 2008a) or fibrinogen extrusion (Raoufi et al., 2016) only yielded in scarce fibrinogen fibers or had a poor reproducibility, which makes the application of these methods impractical. The only other reproducible method to fabricate self-supporting fibrinogen fiber scaffolds with a high density of fibers and dimensions in the centimeter range is electrospinning. However, obtaining an electrospun fibrinogen scaffold with similar dimensions requires several ml of a 100 to 167 mg/ml fibrinogen solution (Sell et al., 2008a; Wnek et al., 2003), while for salt-induced self-assembly 200 µl of a 5 mg/ml solution was sufficient. In contrast to the electrospinning, for salt-induced fiber formation, no high voltage equipment is necessary and only aqueous solutions are required instead of organic solvents. Therefore, salt-induced fiber formation is a more gentle process and also more cost efficient.

The formation of fibrinogen fibers upon drying in the presence of salt ions was investigated with phosphate buffer or PBS prepared with a pH of 5 to 9. A correlation of pH and fiber formation was found. For both buffers a pH value of 7 or higher resulted in fibrinogen fibers, while at pH values lower than 7 no fiber formation was observed.

The isoelectric point of fibrinogen is 5.8. Fibrinogen at higher pH is negatively charged, while fibrinogen at lower pH is positively charged (Wasilewska et al., 2009). The absence of fiber formation with pH values around or under the isoelectric point strongly indicates that a negative net charge of the fibrinogen molecule is required for fiber formation. However, the pH cannot be considered as the main driving force of fiber formation, because fibrinogen in NH_4HCO_3 buffer did not form fibers even though NH_4HCO_3 buffer has a pH of roughly 8.6, which should be in the pH range required for fiber formation.

Wei and coworkers used an acidic pH of 2 to induce the formation of fibrinogen fibers (Wei et al., 2008b). In this thesis, no fibrinogen fiber formation was observed with pH values lower than 7, with pH 5 being the lowest value. It is likely that the fiber formation observed by Wei and coworkers was due to a different mechanism than the salt-induced fiber formation investigated in this study. Especially since fibrinogen starts to denature at pH values lower than 5 (Marguerie, 1977), it is likely that Wei and coworkers observed a denaturation-induced aggregation of fibrinogen.

It also has to be taken into account that phosphate buffer or PBS have a different ionic strength when they are prepared with different pH values. With a pH of 5 or 6 the ionic strength of both buffers is lower as compared to higher pH. Nevertheless, the ionic strength is probably not the reason for the absence of fiber formation at pH 5 or 6, since the differences in ionic strength in phosphate buffer and PBS are even larger, but both show the same pH threshold for fibrinogen fiber formation (see Table 4).

The pH also has an influence on the solubility of fibrinogen. It was shown that fibrinogen has the lowest solubility in PBS with a pH of 5.8 (Leavis and Rothstein, 1974). The trend that fibrinogen forms no fibers at pH values where it has a low solubility is consistent with the influence of ions on solubility, which was discussed above. It seems that low fibrinogen solubility leads to planar or globular fibrinogen aggregates while a high solubility results in the formation of fibrinogen fibers. These findings indicate that the formation of fibrinogen

fibers or planar fibrinogen layers might occur at different time points during the drying process. It can be presumed that under conditions wherein the pH or the ion composition result in a low solubility of fibrinogen, the threshold for fibrinogen precipitation is reached quickly during the drying process, which might lead to planar layers or globular aggregates. Under conditions where fibrinogen has a high solubility, the threshold of precipitation will be reached later. Interestingly, this delayed precipitation of fibrinogen may be the reason for the formation of nanofibrous structures.

A recent study by Helbing and coworkers has shown that fibrinogen forms fibers on a polyethylene surface at pH 7.4. However, at a pH of 9.2 no fiber formation was observed. This is in contrast to our finding of fiber formation over a brought pH range during self-assembly (pH 7 to 9). However, Helbing and coworkers used different buffers for the experiments. Samples at a pH 7.4 were prepared in a buffer containing Na^{+}-ions, while for the preparation of samples at a pH of 9.2 a Ca^{2+}-ion containing buffer was used (Helbing et al., 2016). The presence of monovalent or divalent ions possibly had a strong influence on the experiment conducted by Helbing and therefore an interpretation of the pH as a solely reason for the observed fiber formation seems farfetched.

During the experiments in the self-made humidity chamber it occurred that fibrinogen dried in the presence of PBS at high relative humidities of 50%, showed no fibers in the top view SEM analysis. Only a later cross-sectional SEM analysis of the same samples revealed that just the topmost layer of the sample was planar while fibrinogen fibers were present throughout most of the sample thickness. This shows that the self-assembly of fibrinogen by drying in the presence of salts is humidity independent. The reason for the planar top layer that occurs when the samples are dried at high humidities is most likely condensation of water on top of the sample, which results in a partial redissolving of the top fibrinogen layer. Samples that contain fibers but also a planar top layer might not be suited for follow up experiments. Therefore, it is advisable to carry out the fibrinogen self-assembly at relative humidities of 30% to obtain fibrous scaffolds throughout the whole sample thickness.

Many different publications described surface-induced self-assembly of fibrinogen nanofibers, especially on hydrophobic surfaces (Dubrovin et al., 2019; Feinberg and Parker,

2010; Koo et al., 2010; Reichert et al., 2009; Zhang et al., 2017). Since the salt-induced self-assembly of fibrinogen nanofibers was first discovered on piranha-cleaned glass, which in contrast is very hydrophilic, it was of great interest to test the influence of surface chemistry on the self-assembly process.

The self-assembly of fibrinogen on gold substrates resulted in planar or nanofibrous scaffolds similar to those observed on glass substrates. Drying of fibrinogen in NH_4HCO_3 resulted in planar fibrinogen layers while drying in the presence of PBS resulted in scaffolds of fibrinogen fibers. The fibrinogen scaffolds prepared on gold show a similar star-shaped morphology as scaffold prepared on glass. Moreover, the threshold concentration of fibrinogen and the pH threshold required for fiber formation were the same on gold and on glass. These findings show that the self-assembly process of fibrinogen self-assembly upon drying is possible on a more hydrophobic surface as well and that the mechanism of fiber formation is largely independent of the surface chemistry of the substrate. In other studies, the self-assembly of fibrinogen on gold coated substrates has been observed as a surface reaction. However, these experiments were conducted in solution containing 1 mg/l fibrinogen and the fiber formation was analyzed in solution without a further drying step (Chen et al., 2009). The single fibrinogen fibers observed in these studies strongly differed from the fibrinogen fiber scaffold prepared by drying on a gold-coated surface in this thesis.

A gold-coated surface is more hydrophobic than a piranha-cleaned glass surfaces. Nevertheless, most polymer surfaces are even more hydrophobic. Therefore, in addition to glass and gold surfaces the fibrinogen fiber formation upon drying in the presence of PBS was also studied on APTES modified glass, PLA, PS, PBAT, on parafilm and on PDMS. The wide range of different substrates with distinct surface chemistry and hydrophobicity that can be used as a substrate for fibrinogen fiber formation by drying in the presence of PBS leads to the conclusion that the discovered fibrinogen self-assembly process is largely independent of the used substrate. This is in contrast to many studies that investigated fibrinogen self-assembly on hydrophobic surfaces and concluded that the observed fiber formation was a surface-induced process (Dubrovin et al., 2019; Koo et al., 2010; Reichert et al., 2009). The fibers, which were observed on hydrophobic surfaces in those studies, had a low fiber yield and no dense fibrous scaffolds were formed. In contrast, the self-assembly

process established in this thesis yielded fibrous scaffolds with overall thicknesses of up to 10 µm. It seems unlikely that the bulk of fibrinogen assembled into fibers because of a surface interaction, although it might be possible that the substrate had an influence in the lowermost layer of fibrinogen fibers.

The possible mechanism of the fibrinogen self-assembly on hydrophobic surfaces is not completely understood, like the mechanism studied in this thesis. Although the drying of fibrinogen in the presence of PBS worked on all investigated surfaces and the fiber yield is much higher than the yield of fibers formed by interaction on hydrophobic surfaces, it has to be considered that both self-assembly processes might occur due to a similar or related underlying mechanism. For instance, one main driving force of the PBS induced fiber formation is the drying process. During drying water is evaporated and the fiber formation occurs in an environment, which gradually becomes water free. A hydrophobic surface likewise provides a two-dimensional partially water free environment. The exclusion of water might be one underlying principle that is crucial for salt-induced self-assembly as well as for surface-induced self-assembly of fibrinogen. This could possibly indicate that these two ways of self-assembly are actually relying on the same mechanism, but that the surface induced self-assembly takes place in a two-dimensional water free environment while the salt induced self-assembly takes place in three-dimensional environment, that become gradually water free.

The necessary absence of water for fiber formation is a factor that has not been discussed in detail in other publications concerning the self-assembly of fibrinogen, but it seems to be a crucial factor since fibrinogen fibers prepared by self-assembly could also easily redissolve in water. Only Reichert and coworkers shortly discussed that the change of chemical conditions, which occurs during the drying of the sample, might be related to fiber formation (Reichert et al., 2009).

Fibrinogen fiber scaffolds prepared by drying in the presence of ions were not stable upon rehydration and rapidly dissolved in aqueous buffers. Therefore, different approaches were studied to increase the stability of fibrinogen scaffolds in aqueous environment. A stabilization of the fibrinogen scaffolds is required since further research and a potential future application will take place in aqueous conditions. Furthermore, an understanding of

the rapid redissolving of fibrinogen scaffolds gives some additional insight in the mechanism of fiber formation.

When fibrinogen scaffolds prepared by drying in the presence of PBS were exposed to water, NH_4HCO_3 solution or PBS, the scaffolds were completely dissolved even after incubations as short as 5 min. The rapid dissolving of the fibrinogen scaffolds is an additional indicator that the scaffolds are actually fibrinogen and not fibrin. Fibrin monomers would aggregate due to the knob hole interactions, which makes a fibrin scaffold stable in water even without additional crosslinking (Kolehmainen and Willerth, 2012). Although it has been assumed for a long time that the knob hole interactions of fibrin are irreversible, newer studies suggest a slow dissolving and turnover rate even for knob hole interactions. However, the dissociation of knob hole interactions is a slow process that mostly takes place at the ends of fibrin protofibrils and does not affect the overall stability of fibrin in solution (Chernysh et al., 2012).

The poor stability of fibrinogen scaffolds in water shows that fibrinogen fibers prepared by drying in the presence of PBS are not fibrin. Additionally, this is a strong indication that the binding of fibrinogen molecules involves different sequences than the knob hole domains on the fibrinogen molecules, which results in an aggregation that is strongly susceptible to dissolution in water. It seems likely that these unknown noncovalent binding sites of fibrinogen include ionic bonds or hydrogen bridges, which are affected by competing water molecules. This could also be a possible explanation for the inevitability of the drying step for the formation of fibrinogen fibers.

The fist approaches that were tested to increase the stability of fibrinogen scaffolds were UV irradiation and treatment with methanol. UV-irradiation for 1 h was not sufficient to stabilize the self-assembled fibrinogen scaffold. This is an interesting observation since UV irradiation is commonly used for stabilization of biomaterials and for example has been shown to increase the mechanical stability of fibrin threads (Cornwell and Pins, 2007).

During UV exposure, the irradiation generates radicals, which should crosslink the substrate. The process of radical generation can be accelerated by addition of riboflavin, a method that is often applied for the crosslinking of collagen. The combination of UV

irradiation and riboflavin is also used for cornea crosslinking during some treatments of corneal ectatic diseases (Raiskup and Spoerl, 2013).

Interestingly, the combination of UV light and riboflavin was also not sufficient to crosslink the fibrinogen scaffolds prepared by drying in the presence of PBS. It has to be considered that the intensity of the used UV lamp might have been too low to efficiently crosslink the fibrinogen scaffolds.

As an alternative to UV irradiation different chemical crosslinking agents were investigated. Fibrinogen scaffolds, which were treated with transglutaminase, genipin or EDC were not stable upon rehydration. Incubation with glutar- or formaldehyde solution on the other hand preserved some of the fibrinogen fibers, but with an overall poor fiber and scaffold morphology. It is interesting that no solution-based crosslinking procedure was sufficient to completely crosslink the fibrinogen scaffold. Electrospun fibrinogen scaffolds can be crosslinked by solutions of EDC or genipin (Sell et al., 2008b), but incubation in EDC or genipin solution did not preserve the morphology of self-assembled fibrinogen. This shows that the dissolving of the fibrinogen scaffold is a rapid process. The water molecules in the respective crosslinking solution dissolved the fibrinogen with a higher rate than the rate covalent bonds were formed between fibrinogen molecules by the crosslinkers. This effect is especially visible for transglutaminase, genipin and EDC. These crosslinkers were used in concentrations, which have been reported to have a low toxicity and no negative effect on the biocompatibility of the crosslinked product (Azeredo and Waldron, 2016). However, this treatment also resulted in a very slow crosslinking, which is apparently completely outcompeted by the dissolution of fibrinogen fibers in water.

Especially the failure of the transglutaminase treatment to maintain the fibrinogen fiber scaffold is an interesting observation. Transglutaminase is the enzyme that covalently crosslinks the fibrin monomers of the fibrin clot *in vivo* (Ariëns et al., 2002). Therefore, one would expect transglutaminase to be an optimal crosslinker for fibrinogen fibers that consist of fibrinogen molecules with the same groups for binding. In addition to the rehydration and dissolving that is introduced during the transglutaminase crosslinking, the unsuccessful transglutaminase incubation might also indicate that the fibrinogen molecules in the self-assembled fibrinogen fibers are ordered in an arrangement that differs from the

arrangement of the fibrin monomers in fibrin fibers. In fibrin fibers, the fibrin monomers are oriented in a half staggered arrangement, which allows the close contact of the D-domains of two adjacent monomers. At this position, the first crosslink between two fibrin monomers is catalyzed by transglutaminase. Only in later stages other domains of the molecule especially the α-C domains are crosslinked (Ariëns et al., 2002). If the fibrinogen molecules in self-assembled fibrinogen fibers have a different orientation, transglutaminase crosslinking of the D-domains would not be possible, which could explain the inefficiency of transglutaminase incubation observed for self-assembled fibrinogen.

In contrast to the three rather mild crosslinkers the harsher treatments with glutar- or formaldehyde were more successful. Although aldehyde crosslinking is not ideal for biomaterials, because aldehydes show high toxicity and change the mechanics of biomaterials (Heck et al., 1990), glutar- or formaldehyde solution were able to preserve some of the fibrinogen fibers upon rehydration. However, the aldehyde crosslinked scaffolds still showed a less defined morphology. Since the dissolving of the scaffolds even outcompeted the aldehyde solution crosslinking, glutar- or formaldehyde vapor treatment was investigated afterwards. Crosslinking with aldehyde vapor was also used in studies that crosslinked electrospun fibrinogen scaffolds. By applying glutar- or formalaldehyde as a vapor an additional exposure to water during the crosslinking procedure was circumvented. Both, crosslinking with glutar- and formaldehyde vapor preserved the fibrinogen fiber morphology and stabilized self-assembled fibrinogen scaffolds completely. Even after multiple washing steps, the fibrinogen scaffolds maintained their fiber structure. Although aldehyde treatment is harsh, it was the most efficient way to stabilize self-assembled fibrinogen scaffolds. When aldehyde vapor crosslinking will be used to crosslink scaffolds for applications involving cells or living tissue, a prolonged washing procedure has to be considered, since formaldehyde is cytotoxic and mutagenic (Heck et al., 1990). With extensive washing and shorter time for the vapor incubation, it should be possible to lower the concentration of unbound aldehyde in the samples to a non-toxic level. Eukaryotic cells have mechanisms to metabolize aldehydes and for example have been shown to endure formaldehyde concentrations of up to 1 mM without a loss in cellular viability (Heck et al., 1990; Nilsson et al., 1998).

An additional surprising observation that was made during the washing of aldehyde crosslinked fibrinogen scaffolds was the partial detachment of fibrinogen scaffolds from the underlying glass. With some agitation, the crosslinked scaffolds completely detached and floated on top of the washing solution. The freestanding scaffolds prepared that way could be removed with forceps and dried without damage of the scaffold. The possibility to prepare freestanding scaffolds is especially promising for a future biomaterial application of the self-assembled fibrinogen scaffolds. As a biomaterial, the fibrinogen should be applied without other materials that might have different effects on the living tissue or have mechanical properties that complicate the handling. It was possible to detach intact scaffolds with a size of several cm^2, although only a few µm in thickness. These freestanding scaffolds could be easily handled and for example be applied to a wound. After removal from the surface and handling with forceps, the fibrinogen scaffold still showed its original fiber morphology. In addition, crosslinking planar fibrinogen scaffold could be detached from piranha cleaned substrate, but the washing had to be even more vigorously and took longer to detach planar scaffolds completely.

The only other described method that was able to produce freestanding fibrinogen fiber scaffolds so far is electrospinning (Wnek et al., 2003). However, the scaffolds produced by electrospinning had thicknesses of several hundred µm and required lager amounts of fibrinogen.

The detachment of fibrinogen is promising for future applications of self-assembled fibrinogen scaffolds. However, for the *in vitro* studies that have to precede a future application of fibrinogen scaffolds, a freestanding scaffold might be hard to handle. Therefore, fibrinogen scaffolds were prepared on APTES-modified substrate and immobilized by crosslinking in formaldehyde vapor. Scaffolds crosslinked on APTES did not detach even after vigorous washing. Since the modification with APTES introduces amino groups on the glass surface, the aldehyde treatment does not only crosslink amino groups of different fibrinogen molecules but also crosslinks the fibrinogen fibers with the amino groups of the APTES substrate. It can be assumed that the fibrinogen scaffolds were immobilized to the APTES modified surface after crosslinking, because the fibrinogen was covalently bound to the amino groups of the APTES. The immobilized fibrinogen scaffolds on APTES are a useful additional class of fibrinogen scaffolds, especially for research

purposes like for example cell compatibility experiments or degradation studies. An immobilization of crosslinked fibrinogen samples has also been observed on gold substrates (Stamboroski, personal communications). However since a gold substrate lacks amino groups it can be assumed that the immobilization on gold is due to a different mechanism.

It was also possible to prepare fibrinogen scaffolds by drying in the presence of PBS on a 24 x 24 mm glass slide. The resulting fibrinogen scaffolds of several cm^2 showed that an upscaling of the fibrinogen self-assembly process is possible by adjusting the volume of the fibrinogen and the salt solution.

6.2. Changes of secondary structure accompanying fibrinogen self-assembly

In many other studies investigating fibrinogen assembly *in vitro*, changes in the secondary structure of fibrinogen are used as an hypothesis to explain fiber formation (Feinberg and Parker, 2010; Koo et al., 2012; Wei et al., 2008a). The idea that a conformational change makes binding sites of the fibrinogen molecule available, which are blocked in a native conformation, seems plausible. Nevertheless, none of the aforementioned publications included detailed investigation of the changes in fibrinogen secondary structure that could confirm this hypothesis. Therefore, it is an interesting question whether and to what extent conformational changes play a role during fiber formation by salt-induced self-assembly.

The secondary structure of planar and nanofibrous fibrinogen layers was analyzed using solid state circular dichroism and the content of different secondary structure components was calculated using the BeStSel server (Micsonai et al., 2018). The results discussed in this section are one main part of the publication (Stapelfeldt et al., 2019b), in which the structural data acquired using circular dichroism spectroscopy were additionally validated by Fourier transformed infrared spectroscopy. Overall, the changes of the secondary structure analyzed with both methods were in good accordance. However, the absolute content of different secondary structure motives derived from these methods sometimes differed.

Fibrinogen in solution and fibrin sowed a similar content of α-helical and β-sheet structures. This is in agreement with other studies that reported no change in secondary

structure during the conversion of fibrinogen into fibrin (Dutta et al., 2018). Moreover, the structural data obtained for fibrinogen solution and fibrin are in good agreement with the BeStSel analyses of the x-ray crystallography structure reported for fibrinogen (Kollman et al., 2009). In planar fibrinogen scaffolds prepared by drying in the presence of NH_4HCO_3 without additional ions, the content of α-helical and β-sheet structures was similar to the ones determined for fibrinogen in solution and fibrin. This indicates that during the drying and the formation of the planar fibrinogen layer no change of fibrinogen secondary structure occurred. Furthermore, this shows that none of the experimental conditions like the drying or the used surface material affected the fibrinogen conformation per se.

Interestingly, the circular dichroism spectra of the dried planar and nanofibrous fibrinogen scaffolds differed, which resulted in a difference in the secondary structure content calculated by the BeStSel server. Fibrinogen nanofiber scaffolds showed an increased content of β-sheet structures while a lower content of α-helical structures was observed. This finding shows that the formation of fibrinogen fibers is accompanied by a conformational change of the fibrinogen molecule. It is unclear if this conformational change is responsible for fiber formation or just a side effect of fiber formation by salt-induced self-assembly. However, since the conformational change is rather small (4%), it can be concluded that the overall structure of fibrinogen is maintained during fiber formation and no major denaturation is occurring. Other studies investigating structural changes of fibrinogen during fiber formation are scarce, but one circular dichroism study was carried out on the changes of fibrinogen when it is prepared in the organic solvent for electrospinning (Carlisle et al., 2009). In this study a 30% change of secondary structure was observed upon dissolving fibrinogen in hexafluoropropanol, unfortunately the secondary structure was not analyzed after the fibrinogen had been spun into fibers. Interestingly, the change observed when fibrinogen was dissolved in the hexafluoropropanol was an increase of α-helical structures. In contrast, the structural change observed during self-assembly of fibrinogen was a conversation of α-helical into β-sheet structures, which seems to be minor in comparison.

Recent studies investigating self-assembly of peptides or proteins into fibers found increased content of β-sheets linked to the formation of β-amyloid structures (Wei et al., 2017). To investigate if the observed increase in β-sheet structures was due to the formation

of β-amyloid structures during the self-assembly, fibrinogen scaffolds were prepared in the presence of thioflavin T (ThT). ThT changes its emission spectrum to 480 nm when it is bound to β-amyloid structures. (Biancalana and Koide, 2010). Since the ThT staining showed no emission at 480 nm, it was concluded that the observed change in secondary structure was not correlated with a transition into β-amyloid structures. This was also indicated by the low stability of fibrinogen scaffolds in aqueous environment without additional crosslinking. In contrast, protein fibers, which form due to the aggregation of β-amyloids were reported to have a high stability (Makin et al., 2005; Toyama and Weissman, 2011).

β-amyloid structures have been attributed to various protein misfolding diseases (Chiti and Dobson, 2006). A genetic mutation of fibrinogen can result in a pathogenic misfolding of fibrinogen into β-amyloid structures. The misfolded fibrinogen can accumulate in the liver and other organs, which leads to a condition called fibrinogen amyloidosis (Picken, 2010). However, this change in secondary structure requires a mutation of the primary amino acid sequence of fibrinogen, which makes such transitions highly unlikely for samples prepared with native fibrinogen. In accordance with this the absence of β-amyloid transitions during the fibrinogen self-assembly was confirmed in the ThT staining, which makes a misfolding related pathogenicity of the fibrinogen scaffolds unlikely.

The formation of fibrinogen fibers shows a clear fibrinogen concentration threshold. When 2 mg/ml or higher fibrinogen concentrations were dried in the presence of PBS, fiber formation was observed while with 1 mg/l or lower fibrinogen no fiber formation was observed. Remarkably, the analysis of secondary structure and the analysis of morphology revealed the same fibrinogen concentration threshold for fiber formation.

An increase in β-sheet structures accompanied by a decrease of α-helical structures was only observed when fibrinogen concentrations were used, which were sufficient to induce fiber formation. When fibrinogen was present in concentrations too low to induce fiber formation, the secondary structure was similar to the conformation of planar fibrinogen, even though PBS was present during the drying process. This shows that only fiber formation is accompanied by a conformational change and that the presence of PBS alone is not sufficient to induce a conformational change of fibrinogen. These results show that

the observed conformational change is not the driving force but rather a result of fiber formation. The conformational change only seems to occur in the presence of PBS and a fibrinogen concentration sufficient for fiber formation. A PBS induced conformational change that leads to the formation of fibers was not confirmed since such a change in secondary structure would also be measurable with low fibrinogen concentrations. An additional mechanism seems to be the reason for the observed conformational change when the fibrinogen concentration is sufficient for fiber formation.

Other studies that hypothesized about an involvement of changes in secondary structure, were carried out using fibrinogen concentrations that were substantially lower than the lowest concentration used in this thesis (Koo et al., 2010; Wei et al., 2008b). However, in this thesis no structural changes where observed when low concentrations of fibrinogen were used, which makes the structural changes postulated by Koo or Wei seem unlikely.

Another observed threshold of fiber formation is a pH threshold. While fibers are formed, when fibrinogen was dried in the presence of PBS with a pH of 7 or higher, with a pH below 7 no fiber formation is observed. The pH threshold of fiber formation is also a threshold for the transition of secondary structure.

When the PBS had a pH higher than 7 during the drying of fibrinogen solution, a transition of α-helical structures to β-sheets was observed. However, with pH 7 or lower fibrinogen showed a conformation similar to the one observed for planar fibrinogen. The isoelectric point of fibrinogen is 5.8. At a pH higher than 7 fibrinogen will be negatively charged (Wasilewska et al., 2009). It seems likely that the negative net charge due to deprotonated glutamic or aspartic acid residues of the fibrinogen is required for fibrinogen fiber formation and that ionic interactions are involved in the assembly of fibrinogen molecules.

For the protein serum albumin it has been shown that changes in the pH resulted in changes in the protonation state of glutamic and aspartic acid residues. The protonated acids can form additional hydrogen bonds, which disrupted some α-helical structures in the albumin molecule. However, the experiments on pH induced changes of secondary structure were carried out in solution (Murayama et al., 2001). The conformational changes observed in this thesis do not necessarily indicate that the observed conformational change is pH dependent or even is a driving force of the fiber formation process. It seems likely that no

fibrinogen fibers form at low pH because acidic residues are protonated and inhibit fiber formation. The observed conformational change does not necessarily have to be a result of the pH. It could also be due to the drying process of the fibers that formed under certain pH conditions.

In addition to the fibrinogen concentration and to the pH, the effects of the humidity during the drying process were analyzed. It was shown that the planar layer of fibrinogen, which forms on top of the scaffold when the drying process is carried out at high relative humidities only affects the topmost layer of fibrinogen while the bulk scaffold underneath stays in its fibrous form. Therefore, it is not surprising, that all circular dichroism spectra of fibrinogen scaffolds prepared at different humidities were similar to the spectra of fibrous fibrinogen prepared with a standard humidity of 30%. Apparently, the planar top layer, which forms while drying at a humidity of 50% has no observable effect on the circular dichroism spectrum of the fibrinogen scaffold, which becomes clear when morphological cross-sections are analyzed. Only a thin layer at the top has planar appearance, while the majority of fibrinogen contributing to the pathway is fibrous. Since the contribution of fibrous fibrinogen is higher to the CD signal, the resulting spectrum is characteristic for self-assembled fibrinogen fibers.

When fibrinogen scaffolds prepared by drying in the presence of PBS were crosslinked in formaldehyde vapor, the secondary structure remained the same. The increased content of β-sheet structures and the decreased content of α-helical structures were still observable. The crosslinking treatment alone did not affect the conformation of the fibrinogen molecules. However, the secondary structure of crosslinked fibrinogen scaffold changed when they were rehydrated.

The secondary structure analysis revealed that rehydration of fibrinogen nanofibers reversed the transition of α-helical structures into β-sheets. After rehydration, the crosslinked fibers showed a secondary structure composition, which was closer to native fibrinogen solution or even fibrin as to the structure observed for dried fibers. The content of α-helical and β-sheet structures after rehydration was in the range that was reported for fibrinogen (Kollman et al., 2009) or even fibrin fibers (Dutta et al., 2018). Apparently, the change in secondary structure that was observed after drying of fibrinogen fibers was not

permanent. This result strongly supports the hypothesis that the changes in secondary structure observed in fibrinogen, which was dried in the presence of high ion concentration, are a result of the drying process. The return to an almost native structure after rehydration shows that the conformational changes were not permanent and therefore a crucial role in the self-assembly process seems most unlikely.

For the point of cell experiments or even a future biomedical application, the results are promising. The structural analysis showed no indications of any pathogenic β-amyloid transitions during the fibrinogen self-assembly process. Furthermore, crosslinked and rehydrated fibrinogen showed a conformation close to native fibrinogen solution or even fibrin. Hence, it can be assumed that the crosslinked fibrinogen fibers prepared by salt-induced self-assembly mostly contain fibrinogen with correctly folded secondary structure, which is a promising indication that the fibrinogen fibers maintained their bio-activity and -compatibility during the self-assembly process.

6.3. Bioactivity of self-assembled fibrinogen scaffolds

In the application of biomaterials, the persistence of the material which is introduced into the living organism has to be considered. While for some applications, like for example bone replacements or artificial heart valves a long durability is desired, other applications like soft tissue engineering or wound healing materials are aiming for a temporary persistence of the material. A biomaterial applied for wound healing purposes should be able to disintegrate on its own or to be degraded by cellular enzymes during later stages of the regeneration process.

The natural mechanism for the degradation of the fibrin clot during later stages of wound healing relies on the serum protease plasmin, which is able to cleave fibrin (Rijken and Sakharov, 2001; Walker and Nesheim, 1999) as well as fibrinogen (Pizzo et al., 1972). Plasmin can be activated from its precursor plasminogen by the enzyme urokinase (Blasi et al., 1987). If a fibrinogen-based biomaterial is applied in tissue engineering, especially as a wound healing material it will be exposed to the same plasmin-based degradation mechanism. On the other hand, a fibrinogen-based biomaterial in such a scenario would also be exposed to the present thrombin, which might even have a stabilizing effect by

converting the fibrinogen material into fibrin. To assess whether fibrinogen scaffolds prepared by salt-induced self-assembly are suitable substrates for those enzymes and will be integrated in the enzymatic *in vivo* processes, enzyme experiments were performed. The potential of plasmin or urokinase to degrade fibrinogen was tested in soulton in the first experiment. In the second long-term experiment crosslinked fibrinogen scaffolds were exposed thrombin, plasmin and a combination of plasmin and urokinase. In addition, the capacity of fibrinogen scaffolds to bind other fibrinogen molecules or heparin molecules was studied to assess if the fibrinogen scaffolds were able to bind to *in vivo* interaction partners of fibrin.

The fibrinogen degradation was analyzed in DMEM or HEPES buffer, both solutions did not affect the outcome of the enzymatic degradation experiments. Without any enzymes present, fibrinogen was not degraded overnight and maintained the native molecular weight of approximately 340 kDa. In the presence of plasmin, however, fibrinogen was digested into three large fragments with molecular weights of approximately 260, 160 and 80 kDa. This finding is consistent with the data reported for *in vitro* fibrinogen digestion by plasmin (Pizzo et al., 1972). Fibrinogen was not degraded by incubation in the presence of urokinase and only the native 340 kDa band was observed. However, the combination of plasmin and urokinase showed a stronger band at 80 kDa than the incubation with plasmin alone, and hardly any band of a higher molecular weight was observed. This observation indicates an acceleration of the plasmin activity by urokinase, which is remarkable, since urokinase was originally reported to convert the precursor plasminogen into active plasmin (Blasi et al., 1987). The acceleration of the plasmin activity could indicate that not all of the used plasmin was actually in its active form. Gel electrophoresis could elucidate if some plasminogen of larger molecular weight is present in the plasmin stock.

For a long-term investigation planar or nanofibrous fibrinogen scaffolds were crosslinked in formaldehyde vapor and incubated in the presence of different enzymes for 35 days. Fibrinogen scaffolds, which were crosslinked for 1 h, showed degradation over time when incubated in HEPES buffer. When scaffolds were crosslinked for 2 h, only slow degradation was observed in HEPES buffer. Apparently, a long crosslinking time resulted in a scaffold stable in solution, while after 1 h crosslinking a slow hydrolysis of the fibrinogen scaffold was still possible.

A similar hydrolysation behavior in solution was shown for the *in vitro* degradation of fibrin. Fibrin gels prepared with high fibrinogen and calcium concentrations only showed slow degradation over a time course of three weeks. However, fibrin gels prepared with a low fibrinogen concentration or a low content of calcium almost completely dissolved within three weeks (Eyrich et al., 2007).

Some studies have been carried out on the degradation behavior of electrospun fibrinogen scaffolds, but those studies investigated the degradation of fibrinogen by cells and failed to analyze a potential hydrolization of the scaffold in the solvent alone. Furthermore, these studies did not investigate a degradation of the scaffold by single enzymes without the presence of cells (McManus et al., 2007b; McManus et al., 2007a).

In contrast, the self-assembled fibrinogen scaffolds prepared in this thesis were analyzed to potentially degrading or stabilizing enzymes. Interestingly, the presence of thrombin had no effect on the stability of the scaffold. If thrombin still cleaves off the fibrinopeptides of the fibrinogen molecules in the crosslinked scaffolds, an additional stabilization should occur via the possible knob hole interactions (Mosesson, 2005). However, no indication of such a thrombin stabilization was observed in this thesis. Interestingly SEM analysis revealed that a thrombin treatment influenced the surface morphology especially visible on fibrous scaffolds. After 35 days of thrombin incubation, the samples showed a poorer fiber morphology, which could indicate some degradation of fibrin fibers by thrombin. Another possible explanation would be a binding of thrombin molecules, which covers the fiber scaffold by a layer of thrombin molecules.

Even more remarkably, the presence of plasmin during the 35 days of incubation had no effect on the fibrinogen scaffold stability, even though the previous experiments had confirmed the activity of plasmin in the HEPES buffer system. After 35 days of incubation in the presence of plasmin the fibrinogen content in the supernatant of 1 or 2 h crosslinked scaffolds was similar to the one measured from samples exposed to buffer without any enzyme. Either the activity of plasmin was not high enough to degrade the crosslinked fibrinogen or the targeted amino acid sequence, which is cleaved by plasmin, was modified by the crosslinking procedure.

It was shown for collagen fibers that a scaffold, which was exposed to high concentrations of a crosslinking agent, could not be degraded by collagenase anymore. A collagen fiber scaffold, which was crosslinked using low concentrations of crosslinking agent, on the other hand was still susceptible to enzymatic degradation and was completely degraded after four weeks. Also in this study the crosslinking density was correlated to a resistance against enzymatic degradation and with the highest crosslinking density tested no degradation was observed during the four week experiment (Kishan et al., 2015). It seems likely that even when fibrinogen scaffolds are crosslinked for 1 h, the resulting crosslinking density is too high for efficient plasmin degradation. This idea is supported by SEM observation of almost intact fiber scaffold after plasmin treatment of 2 h crosslinked scaffolds. However, the scaffolds crosslinked for only 1 h showed a poorer fiber morphology, which indicates that at least some effect of plasmin.

The combination of plasmin with the plasmin activator urokinase resulted in an accelerated degradation under all tested conditions during both experimental trials. In contrast to all other enzymes or buffer controls, which showed that 90 % of the 1 h crosslinked and 100 % of the 2 h crosslinked fibrinogen scaffolds were still intact after 35 days, a treatment with plasmin and urokinase resulted in a degradation, which only left roughly 40% of the 1 and 2 h crosslinked scaffolds intact. The strong degradation by plasmin and urokinase was also confirmed by SEM analysis of the samples, which in contrast to the other tested buffers or enzymes showed only a few patchy scaffold remains after 35 days. The accelerated degradation of the scaffold by plasmin and urokinase is an interesting observation, which like the accelerated degradation in solution is hard to explain.

Urokinase was originally described as an activator of the plasmin precursor plasminogen, but no effect of urokinase on the already active plasmin was described (Blasi et al., 1987). The findings of this thesis indicate that the capacity of plasmin to degrade crosslinked fibrinogen fibers is strongly increased when urokinase is present. An older publication discussed some combined effect of urokinase and plasmin during fibrin degradation, but this effect was not observed when fibrinogen was used (Müllertz, 1974). One possible explanation for the additional effect of urokinase is the digestion of fibrinogen by urokinase itself. It was shown that urokinase itself has a direct catalytic activity towards fibrinogen and is able to cleave of fibrinopeptide B (Weitz and Leslie, 1990). The degradation

experiment using urokinase and fibrinogen in solution in this thesis did not indicate a cleavage of fibrinopeptide B, however fibrinopeptide B is only a 12 amino acid fragment, which would not have been detected by the used gel electrophoresis (Mosesson, 2005).

If fibrinopeptide B was cleaved during the incubation with urokinase and plasmin, two explanations of the accelerated degradation are possible. The cleavage of fibrinopeptide B from the crosslinked fibrinogen fibers would make those fibers at least partially fibrin, therefore a combined effect of plasmin and urokinase like described above is maybe possible, since the scaffolds present a fibrin-like substrate.

Another possible explanation would be an initial cleavage of the fibrinogen by urokinase and a subsequent cleavage by plasmin. If the cleavage of fibrinopeptide B by urokinase makes additional plasmin cleavage sites available that are usually blocked in the crosslinked fibrinogen, this could result in a plasmin degradation. That would not be possible in fibrinogen scaffolds that still contain fibrinopeptide B. In this hypothesis, an initial cleavage of the small fibrinopeptide B is needed to allow the subsequent main degradation by plasmin. One simple way to test this hypothesis would be an experiment where crosslinked fibrinogen fibers are incubated in a combination of plasmin and thrombin. Since thrombin should also cleave of fibrinopeptide B, a combination of thrombin and plasmin should also result in an accelerated degradation of the fibrin scaffold.

Overall, single enzymes had hardly any effect on the degradation kinetics of crosslinked scaffolds, while combinations of enzymes were able to accelerate the degradation. In an *in vivo* system the fibrinogen scaffolds will be exposed to a variety of enzymes and other factors at the same time, therefore more experiments with combinations of different enzyme are needed to make a profound assessment of the stability of fibrinogen scaffolds.

Based on the degradation experiments, future cell culture experiments will be the next important step to study further, whether, for instance, fibroblasts will be able to degrade and remodel the fibrinogen scaffolds under *in vitro* conditions. Moreover, the degradation experiments are an additional indicator that the structure and bioactivity of fibrinogen were maintained during salt-induced fiber formation and that the binding sites and activity of the fibrinogen degrading *in vivo* enzymes was not compromised.

When the interaction of fluorescently labeled ligands with self-assembled fibrinogen was studied it was observed that neither fibrinogen nor heparin bind to the fibrinogen scaffolds. It was shown that fibrinogen had a stronger affinity towards control samples prepared with BSA or even bare APTES surfaces than to fibrinogen scaffolds. This observation shows that even the unspecific binding to BSA or APTES was higher than the fibrinogen-fibrinogen interaction. Apparently, no further fibrinogen is able to attach to the crosslinked fibrinogen scaffolds, as they were prepared in this study. This could indicate that an incorporation of the crosslinked fibrinogen scaffold into a living tissue might be difficult. However, *in vivo* there are more binding partners like for example fibronectin, which bridges fibrin with other ECM molecules during wound healing (Laurens et al., 2006). Furthermore, it has to be considered that the used methods in this study might not elucidate the dynamic binging and unbinding that occurs *in vivo*.

Interestingly, also heparin showed a much lower affinity towards fibrinogen scaffolds than to BSA samples or to bare APTES surface. This is surprising since fibrinogen was expected to bind to heparin. Heparin is a known binding partner of fibrin that binds to the central E-domain and partially to the α-C-domains (Fredenburgh et al., 2013). The lack of heparin binding to crosslinked fibrinogen fibers could be explained by the fact that the main binding site, to which heparin binds to fibrin, is located at the central E domain close to the site where fibrinopeptide A and B are cleaved off during fibrin formation. This binding site is not accessible without cleavage of the fibrinopeptides (Odrljin et al., 1996b). Since the fibrinogen scaffolds prepared in this study most likely still comprise both fibrinopeptides, the main heparin binding site is not available. Some heparin binding also has been reported to occur at the α-C domains of fibrinogen (Fredenburgh et al., 2013). This could indicate that also the α-C domains in self-assembled fibrinogen are not accessible for binding.

The observed differences in fibrinogen or heparin binding might also be due to the use of fluorimetry as an endpoint-based method. Like for most biological molecules the binding of fibrinogen to the crosslinked fibrinogen scaffolds will occur with certain on and off rates like for example the binding of intergins to fibrinogen (Litvinov et al., 2012b). However, the approach used in this study only detected the final concentration of bound fibrinogen and was not suited to determine the kinetics of binding or unbinding. A much more detailed investigation of the binding characteristics would be possible with other techniques, for

example, a quartz crystal microbalance based approach, which would allow kinetic studies of the binding processes. The dynamics of the formation of fibrin for example have been studied using a quartz crystal microbalance approach. In the same study the influence and the kinetics of heparin binding during the fibrin formation have been studied (Vikinge et al., 2000). In addition to quartz crystal microbalance this study also used surface plasmon resonance, which shows that both methods are useful to study dynamic binding events (Vikinge et al., 2000). Therefore, it is to assume that the methods hold the potential for an in depth investigation of the binding events occurring on self-assembled fibrinogen as well.

6.4. Mechanism of fibrinogen self-assembly

When all the analyzed factors that were found to influence the fibrinogen self-assembly in the first main experimental part of this thesis are taken into consideration, it is possible to formulate some conclusions about the potential mechanism of fibrinogen fiber formation. Additionally, the results of the second main experimental part give some indication on the structural changes and their role in the mechanism of fibrinogen self-assembly.

The binding sites, which facilitate the assembly of fibrinogen molecules into fibrin, so called knob hole interactions, are normally blocked by the fibrinopeptides, which *in vivo* are cleaved off by the enzyme thrombin (Mosesson, 2005). The results of this thesis clearly show that the self-assembled fibers do not consist of fibrin and that thrombin is not involved in the fiber formation process. This is strongly supported by the results, which showed that fibrinogen fibers also formed in the presence of the thrombin inhibitor AEBSF. However, fiber formation might also involve the same knob hole interactions without the presence of thrombin and lead to fibrinogen molecules oriented in a half staggered way with interactions between the D-domains and the E-domains like in fibrin. Other studies on self-assembly of fibrinogen, for example by fibrinogen denaturation in ethanol (Wei et al., 2008b) or by surface induced self-assembly (Koo et al., 2012), also discussed that an interaction of D-and E-domains plays a major role in the investigated assembly processes. Nevertheless, they avoided to declare the same knob hole interactions, which occur after thrombin activation as the single mechanism.

In the case of the self-assembly mechanism an involvement of the knob hole interactions seems unlikely for two reasons. First of all, the knob hole interactions are blocked by the fibrinopeptides and there is no indication that the drying or the presence of ions could hydrolyze the fibrinopeptides or change the conformation of the molecules to make them available. An antibody staining of the fibrinopeptides could reveal if they are still present in a self-assembled fibrinogen scaffold.

Second, the fibrinogen fibers formed by self-assembly were not stable in aqueous solution. The noncovalent knob hole interactions are a combination of an ionic bond between a positively charged arginine residue at the knob domain and a negatively charged hole domain, which are surrounded by hydrophobic interactions (Mosesson, 2005). This makes the knob hole interactions highly resistant to redissolving in water and is the reason why fibrin does not dissolve in water. Therefore, it seems unlikely that the fibrinogen fiber formation during drying in the presence of ions relies on knob hole interactions. The binding during self-assembly possibly occurs via a different binding mechanism which is weaker and water sensitive.

One additional experiment to prove that self-assembly of fibrinogen does not involve knob hole interactions and is not similar to fibrin, would be the use of fibrinogen including point mutations at the knob or hole binding sites. If fibrinogen molecules without the knob hole binding site would still self-assemble into fibers upon drying in the presence of salts, this would confirm other cryptic binding sites, which are responsible for self-assembly. Some mutations of knob hole sequences are known to result in impaired fibrin formation and could be utilized for such an experiment (Bowley and Lord, 2009; Hogan et al., 2001).

The fibrinogen domain with the highest conformational flexibility is the α-C domain (Protopopova et al., 2015; Weisel and Medved, 2001). The flexible α-C domain was associated with accumulation and self-assembly of fibrinogen in many publications (Collet et al., 2005; Weisel and MEDVED, 2001; Williamson, 1994; Zuev et al., 2017). It might be possible that the salt-induced self-assembly takes place in the α-C domains and allows the organization of fibrinogen molecules. The flexible poly-proline helix of the α-C domain is stabilized by hydrogen bridges involving adjacent water molecules (Weisel and MEDVED,

2001). Therefore, it is to assume that the α-C domain is strongly affected by the drying process and the effects that ions have on the hydration shell of the molecule.

The removal of water is one of the main driving forces of the fibrinogen self-assembly. It would be interesting to investigate, if other approaches, which remove the water instantly, would also result in fiber formation. Possible approaches would be to mix an aqueous fibrinogen solution with an organic solvent or to even overlay an organic phase with an aqueous phase of fibrinogen solution. At the interface of the two phases the fibrinogen should be converted from a hydrated to a dehydrated state instantly, which might also lead to self-assembly. Similar approaches have been described for the extraction of proteins from an aqueous phase into an organic solvent (Chin et al., 1994).

The second main driving force of fibrinogen fiber formation is the presence of salts. During drying, bulk waters evaporate until the fibrinogen starts to precipitate. However, for fiber formation the additional presence of ions is required, since without the presence of ions only planar fibrinogen layers are formed. If high concentrations of ions are present, surface charges of the fibrinogen molecules will be compensated. Moreover, the presence of high ion concentrations has direct influence on the first hydration shell of the fibrinogen molecules (Zhang and Cremer, 2006). During the drying in solutions with high ion concentrations the point where the hydration shells are weakened and the fibrinogen starts to precipitate, will be reached faster as in solutions with low ion concentrations. This allows Van der Waals forces, hydrogen bridges and possibly ionic interactions between molecules of fibrinogen, which might allow a self-organization of adjacent fibrinogen molecules into fibers (Baldwin, 1996). During drying without the presence of high ion concentrations the hydration shell of fibrinogen will be maintained until the very end of the drying process and interactions of fibrinogen molecules will be prohibited by repulsion of the hydration shells (Baldwin, 1996). Therefore, only planar layers will form under those conditions.

The fiber formation during drying in the presence of salts relies on noncovalent interactions between fibrinogen molecules, which can be interfered by the presence of water. Although hydrogen bridges and ionic interactions seem to be possible candidates to enable the assembly of fibrinogen into nanofibers, most likely, both kinds of interactions contribute to

the fibrinogen assembly. Based on the results of this thesis, there is a strong indication that ionic interactions are crucial for the self-assembly of fibrinogen fibers. A correlation of pH and fiber formation was observed. A pH value of 7 or higher resulted in fibrinogen fibers, while at pH values lower than 7 no fiber formation was observed. This indicates that the charge of fibrinogen side chains plays a role in fiber assembly. Presumably charged amino acids of fibrinogen molecules form ionic bonds during the fiber formation process.

The isoelectric point of fibrinogen is 5.8. Fibrinogen at higher pH is negatively charged, while fibrinogen at lower pH is positively charged (Wasilewska et al., 2009). The absence of fiber formation with pH values around or under the isoelectric point strongly indicates that a negative net charge of the fibrinogen molecule is required for fiber formation. Most likely aspartic and glutamic acid resides are involved in this ionic interaction since they have a negative charge at physiological and high pH and are not charged at low pH.

However, the pH cannot be considered as the main driving force of fiber formation, because fibrinogen in NH_4HCO_3 buffer did not form fibers even though NH_4HCO_3 buffer has a pH of roughly 8.6, which should be in the pH range required for fiber formation. It is also possible that the negative net charge of the fibrinogen is required for the interaction with positively charged ions in the solution. A contribution of the presence of positively charged ions was also discussed for other observed mechanism of fibrinogen self-assembly but was not identified as one of the main driving forces (Reichert et al., 2009) .

The fibrinogen fiber self-assembly relies on a water removal during drying and on the presence of ions. During precipitation, noncovalent interactions, which are most likely ionic bonds, between single fibrinogen molecules allow an arrangement into fibers. This arrangement is reversible, and the ionic bonds can be disrupted by introducing water again. Interestingly, this proposed mechanism relies on the arrangement of fibrinogen molecules and the modification of the fibrinogen hydration shell. A change of secondary structure of the fibrinogen molecules is not necessarily involved in the self-assembly.

It was hypothesized in many publications that fibrinogen self-assembly is based on a change in the fibrinogen secondary structure, which makes cryptic binding sites accessible (Feinberg and Parker, 2010; Koo et al., 2012; Wei et al., 2008a). In these publications, it is assumed that a change in secondary structure is the driving force of fiber formation, which

allows fibrinogen to aggregate and form fibers. Although a minor change in conformation was observed for fibrinogen fibers prepared by drying in the presence of PBS, the results obtained using circular dichroism spectroscopy show that this change in secondary structure is rather a result of the drying process of the fibers than a crucial driving force of the self-assembly. The formation and aggregation of fibrinogen in fiber form allow the small change in secondary structure. Two of the main findings support this interpretation: The absence of conformational changes when low fibrinogen concentrations are used and the reversibility of the conformational change when crosslinked fibers were rehydrated.

The observed conversion of α-helical into β-sheet structures only occurred under conditions that allowed fiber formation. If this conformational change of fibrinogen molecules would be a prerequisite for fiber formation, it would occur even at low fibrinogen concentrations. But no conformational change of the fibrinogen was detected when low fibrinogen concentrations were exposed to the same concentrations of PBS and the same drying process, therefore it seems unlikely that a conformational change is initiated by the initial reaction and drying conditions. It is more likely that the conformational change occurs after the formation of fibers, possibly due to the shrinking of fibers during the drying.

The fact that crosslinked fibers returned to an almost native conformation after rehydration also indicates that the conformational change is not a driving force of fibrinogen fiber formation. If the conformational change would expose some cryptic binding sites that are involved in the aggregation of fibrinogen fibers, a reversibility of that change would be highly unlikely. The results indicate that the observed small change in secondary structure occurs in a domain of the fibrinogen that is of some conformational flexibility but is not involved in the fiber formation during self-assembly.

The domains with the highest content of α-helical motives in the fibrinogen molecule are the coiled coil domains, which link the E-domain and the two D-domains (Mosesson, 2005). It is likely that the observed conversion of α-helical motives into β-sheet takes place in these domains.

Actually, Litvinov and coworkers observed a very similar α-helix to β-sheet transition in the coiled coil regions of fibrin monomers in a fibrin gel. If strain was applied to a fibrin

gel a transition of α-helical to β-sheet structures was observed, which was interpreted as a refolding of the α-helical coiled coil linker domains into β-sheet structures (Litvinov et al., 2012a). The coiled coil domains function like springs, which elongate by refolding α-helical domains into β-sheets and thereby give fibrin its high elasticity (Litvinov and Weisel, 2017). It seems likely that a similar strain-induced transition of α-helices into β-sheets could also occur during the drying process of self-assembled fibrinogen fibers, since the fibrinogen molecules have a similar structure to the fibrin monomers. A possible mechanism would be that during the self-assembly of fibrinogen strain is induced in the fibers. During an early stage of the drying process where some water is still present, the fibers are in a relaxed state. However, as more water evaporates during the final stage of the drying process the fibers might shrink, which creates strain. It is possible that such an induced strain in the fibers would be compensated by partially refolding the coiled coil α-helices into β-sheets as it was shown in fibrin.

It was shown using atomic force microscopy that crosslinked fibers swell again upon rehydration (Stapelfeldt et al., 2019b). This indicates that at least crosslinked fibrinogen fibers in a dried state could be under strain due to shrinkage during the drying. The swelling upon rehydration results in a relaxation of the fibers, which perfectly explains the observed refolding into an almost native state, which was observed for rehydrated fibers.

Moreover, the idea that fibrinogen fibers change their conformation because of the strain created during drying, could also explain why no conformational changes were observed when fibrinogen concentrations were not sufficient to form fibers.

Therefore, it can be concluded that changes in the secondary structure are not a driving force of the newly discovered fibrinogen self-assembly. However, a minor conformational change occurs in the fibrinogen fibers, which might be due to strain induced in the fibers during the drying process. The conformational change most likely occurred in the α-helical coiled coil domains and is reversible upon rehydration. This indicates that the formed fibrinogen fibers are a conformational flexible material, which was able to refold during rehydration similar to the well-understood fibrin.

Overall the findings of this thesis strongly indicated that the self-assembly of fibrinogen is due to noncovalent interaction of fibrinogen, which occur during the drying process in the

presence of ions. The potential of ions to interfere with the hydration shell of the fibrinogen seems to play an important role for the fiber formation. Since the self-assembly is a reversible process it seems likely that the arrangement of fibrinogen occurs due to ionic interaction, which is also supported by the fact that the self-assembly only occurs in a certain pH regime. Some changes in secondary structure have been observed to result of fiber formation, which were possible induced by the drying process. However, the presented results do not indicate a direct involvement of conformational changes in the mechanism of fibrinogen self-assembly itself.

7. Conclusion and Outlook

The results of this thesis lead to many conclusions, which imply future experiments. During the first main part of this thesis, a novel *in vitro* self-assembly mechanism of fibrinogen into nanofibers was introduced. When fibrinogen solution was dried in the presence of high ion concentrations, dense fibrinogen nanofiber networks were obtained. Interestingly, the morphological analysis revealed that without high ion concentration no fibrinogen fibers had formed. The presence of different ions species during the drying were able to induce fibrinogen self-assembly, however, the resulting fiber morphology was dependent on the chaotropic potential of the used ions. Crucial factors for the fibrinogen self-assembly seem to be the drying process and the influence that chaotropic ions have on the hydration shell of the fibrinogen molecule. To gain a better understanding of the relation of hydration shell and fibrinogen self-assembly, future experiments with salts from the Hofmeister series are a good option. Especially, more chaotropic salts like lithium chloride or even guanidinium hydrochloride should have a higher potential to form fibers while salts with a high potential to precipitate fibrinogen like ammonium sulfate should result in planar layers. Further experiments with divalent cations like calcium or magnesium could bring some additional insight into fiber formation upon drying. However, it has to be taken into account that fibrinogen binding sites for divalent ions or potential complex formation with divalent ions might have some additional influence on the self-assembly process. Closely related to the effect of ions is the observed pH threshold of fibrinogen fiber self-assembly. Fibrinogen fibers only formed when the pH was higher than the isoelectric point of fibrinogen, which

shows that a negative net charge of fibrinogen is required for fiber formation. The pH threshold is a major challenge for the design of future experiments because an investigation of other factors combined with pH would require a buffer system out of components, which allows different pH values, but do not contribute to the formation of fibers themselves.

In this thesis, it was shown for the first time that fibrinogen self-assembly can occur surface independent on different substrate materials. This is contrast to many other publications, which identified fibrinogen self-assembly as a surface induced mechanism. It has to be clarified if the self-assembly described in this thesis is due to a completely different mechanism or if the surface induced self-assembly described by others relies on similar factors like for example water exclusion and changes of the fibrinogen hydration, which might take place at certain surface materials.

In the second main part of this thesis it was confirmed that the self-assembly of fibrinogen fibers is accompanied by a small change in secondary structure. When the results of the morphological analysis were correlated to the investigation of fibrinogen conformation, it became clear that the changes in secondary structure are a result of the fiber formation. However, a crucial role of changes in secondary structure for the mechanism of fibrinogen self-assembly, like it was proposed in many other studies, could not be confirmed. Most likely, the observed conversion of α-helical into β-sheet structures was due to strain induced in the fibers during the drying process. This is also indicated by the return of those secondary structure motives into a native state when fibrinogen fibers were rehydrated. To fully understand the conformational changes during fibrinogens self-assembly a real time investigation of secondary structure during the drying process would be required. A potential method that could yield some structural data in such a challenging setting, which includes a transition from a liquid to a dried state, could be nuclear magnetic resonance spectroscopy.

The structural analysis also revealed that no potentially pathogenic formation of β-amyloid structures took place during the self-assembly of fibrinogen. This and the reversibility of the changes in fibrinogen secondary structure upon rehydration are first indicators that the fibrinogen stayed biologically active during the self-assembly process.

The biofunctionality of self-assembled fibrinogen scaffolds was confirmed in the final part of this thesis. Although an *in vitro* degradation of crosslinked fibrinogen scaffolds was not possible when single enzymes were used, a combination of different enzymes resulted in an enzymatic degradation of the scaffolds. Additionally, it was shown that the crosslinking time had a strong influence on the scaffold stability in aqueous solution or in the presence of enzymes. The findings of the thesis provide a good foundation for future cell culture experiments. It can be assumed that the fibrinogen in self-assembled fibers has a high biocompatibility and is still a biologically active substrate, they were susceptible to degradation by plasmin, the same enzymatic reaction utilized by fibroblasts to remodel fibrin. For cell culture experiments, a careful selection of fibrinogen scaffold samples and a number of control samples has to be made. To avoid a detachment during cell culture, fibrinogen samples crosslinked to APTES should be used. Therefore, a control with cells on the bare APTES substrate is inevitable. In addition to salt-induced fibrinogen fibers, the process described in this thesis also allows the fabrication of planar fibrinogen scaffolds, which for comparison should be analyzed in cell culture as well. With planar reference samples, it will be possible to distinguish, if an observed cell behavior is due to the biochemical environment presented by crosslinked fibrinogen or a specific result of the fibrous three-dimensional morphology of fibrinogen fibers.

The most important control samples for cell experiments will be fibrin samples, which are prepared with the same fibrinogen concentration as the self-assembled scaffolds. It is advisable to use non-crosslinked fibrin samples as well as fibrin samples that were additionally crosslinked in formaldehyde vapor for comparison with the fibrinogen fibers.

Although the self-assembly process is not completely understood, it resulted in fibrinogen scaffolds with dimensions up to several cm^2, which could also be prepared as freestanding scaffolds. This holds some potential for an application as a biomaterial, especially as a wound dressing material similar to the desired use of electrospun fibrinogen mats or the already used fibrin-based materials. With degradation times of roughly one month the self-assembled fibrinogen would be a suitable wound dressing material, which would provide a provisional extracellular matrix and could be absorbed during later stages of the wound healing process.

With a further investigation of the newly found salt-induced fibrinogen self-assembly in combination with cell culture tests, it will be possible to make a concluding assessment for the future application of self-assembled fibrinogen scaffolds as a biomaterial. From the results obtained in this thesis, self-assembled fibrinogen scaffolds seem to be a promising undenatured alternative to electrospun fibrinogen scaffolds. To determine how useful self-assembled fibrinogen will be in comparison to fibrin is up to future research studies.

8. References

Albala, D.M., Lawson, J.H., 2006. Recent clinical and investigational applications of fibrin sealant in selected surgical specialties. Journal of the American College of Surgeons 202, 685–697. 10.1016/j.jamcollsurg.2005.11.027.

Ambrus, C.M., Back, N., Ambrus, J.L., 1962. On the Mechanism of Thrombolysis by Plasmin. Circulation Research 10, 161–165. 10.1161/01.RES.10.2.161.

Amento, E.P., Ehsani, N., Palmer, H., Libby, P., 1991. Cytokines and growth factors positively and negatively regulate interstitial collagen gene expression in human vascular smooth muscle cells. Arterioscler Thromb 11, 1223–1230. 10.1161/01.ATV.11.5.1223.

Andree, C., Munder, B.I.J., Behrendt, P., Hellmann, S., Audretsch, W., Voigt, M., Reis, C., Beckmann, M.W., Horch, R.E., Bach, A.D., 2008. Improved safety of autologous breast reconstruction surgery by stabilisation of microsurgical vessel anastomoses using fibrin sealant in 349 free DIEP or fascia-muscle-sparing (fms)-TRAM flaps: A two-centre study. Breast (Edinburgh, Scotland) 17, 492–498. 10.1016/j.breast.2008.03.010.

Annemie Collen, Pieter Koolwijk, Marielle Kroon, Victor W. M. van Hinsbergh, 1998. Influence of fibrin structure on the formation and maintenance of capillary-like tubules by human microvascular endothelial cells. Angiogenesis 2, 153–166. 10.1023/A:1009240522808.

Ariëns, R.A.S., Lai, T.-S., Weisel, J.W., Greenberg, C.S., Grant, P.J., 2002. Role of factor XIII in fibrin clot formation and effects of genetic polymorphisms. Blood 100, 743–754. 10.1182/blood.v100.3.743.

Azeredo, H.M.C., Waldron, K.W., 2016. Crosslinking in polysaccharide and protein films and coatings for food contact – A review. Trends in Food Science & Technology 52, 109–122. 10.1016/j.tifs.2016.04.008.

Baldwin, R.L., 1996. How Hofmeister ion interactions affect protein stability. Biophysical Journal 71, 2056–2063. 10.1016/S0006-3495(96)79404-3.

Berg, J.M., Tymoczko, J.L., Stryer, L., 2012. Biochemistry: [this edition is for use outside the USA and Canada], 7th ed. Freeman Palgrave Macmillan, New York, NY.

Bergel, S., 1909. Ueber Wirkungen des Fibrins. Dtsch med Wochenschr 35, 663–665. 10.1055/s-0029-1201395.

Berova, N., Nakanishi, K., Woody, R.W. (Eds.), 2000. Circular dichroism: Principles and applications, 2nd ed. Wiley-VCH, New York, NY, 877 pp.

Biancalana, M., Koide, S., 2010. Molecular mechanism of Thioflavin-T binding to amyloid fibrils. Biochimica et Biophysica Acta (BBA) - Proteins and Proteomics 1804, 1405–1412. 10.1016/j.bbapap.2010.04.001.

Bjarkam, C.R., Jorgensen, R.L., Jensen, K.N., Sunde, N.A., Sørensen, J.-C.H., 2008. Deep brain stimulation electrode anchoring using BioGlue((R)), a protective electrode covering, and a titanium microplate. Journal of neuroscience methods 168, 151–155. 10.1016/j.jneumeth.2007.09.008.

Blasi, F., Vassalli, J.D., Danø, K., 1987. Urokinase-type plasminogen activator: Proenzyme, receptor, and inhibitors. The Journal of cell biology 104, 801–804. 10.1083/jcb.104.4.801.

Blombäck, B., Blombäck, M., 1972. The molecular structure of fibrinogen. Annals of the New York Academy of Sciences 202, 77–97. 10.1111/j.1749-6632.1972.tb16323.x.

Bosman, F.T., Stamenkovic, I., 2003. Functional structure and composition of the extracellular matrix. J. Pathol. 200, 423–428. 10.1002/path.1437.

Bowley, S.R., Lord, S.T., 2009. Fibrinogen variant BbetaD432A has normal polymerization but does not bind knob "B". Blood 113, 4425–4430. 10.1182/blood-2008-09-178178.

Braiman-Wiksman, L., Solomonik, I., Spira, R., Tennenbaum, T., 2016. Novel Insights into Wound Healing Sequence of Events. Toxicol Pathol 35, 767–779. 10.1080/01926230701584189.

Brown, A.C., Barker, T.H., 2014. Fibrin-based biomaterials: Modulation of macroscopic properties through rational design at the molecular level. Acta biomaterialia 10, 1502–1514. 10.1016/j.actbio.2013.09.008.

Caen, J.P., Michel, H., 1972. Platelet Shape Change and Aggregation. Nature 240, 148–149. 10.1038/240148a0.

Carlisle, C.R., Coulais, C., Namboothiry, M., Carroll, D.L., Hantgan, R.R., Guthold, M., 2009. The mechanical properties of individual, electrospun fibrinogen fibers. Biomaterials 30, 1205–1213.

Castiglioni, E., Biscarini, P., Abbate, S., 2009. Experimental aspects of solid state circular dichroism. Chirality 21 Suppl 1, E28-36. 10.1002/chir.20770.

Catelas, I., Sese, N., Wu, B.M., Dunn, J.C.Y., Helgerson, S., Tawil, B., 2006. Human mesenchymal stem cell proliferation and osteogenic differentiation in fibrin gels in vitro. Tissue engineering 12, 2385–2396. 10.1089/ten.2006.12.2385.

Chaudhari, A.A., Vig, K., Baganizi, D.R., Sahu, R., Dixit, S., Dennis, V., Singh, S.R., Pillai, S.R., 2016. Future Prospects for Scaffolding Methods and Biomaterials in Skin Tissue Engineering: A Review. International journal of molecular sciences 17. 10.3390/ijms17121974.

Chen, G., Ni, N., Wang, B., Xu, B., 2009. Fibrinogen Nanofibril Growth and Self-Assembly on Au (1,1,1) Surface in the Absence of Thrombin. Chemphyschem 11, 565–568.

Chernysh, I.N., Nagaswami, C., Purohit, P.K., Weisel, J.W., 2012. Fibrin Clots Are Equilibrium Polymers That Can Be Remodeled Without Proteolytic Digestion. Nature Publishing Group 2, 1–6.

Chin, J.T., Wheeler, S.L., Klibanov, A.M., 1994. On protein solubility in organic solvent. Biotechnol. Bioeng. 44, 140–145. 10.1002/bit.260440120.

Chiti, F., Dobson, C.M., 2006. Protein misfolding, functional amyloid, and human disease. Annual review of biochemistry 75, 333–366. 10.1146/annurev.biochem.75.101304.123901.

Clark, R.A.F., 2001. Fibrin and Wound Healing. Annals of the New York Academy of Sciences 936, 355–367. 10.1111/j.1749-6632.2001.tb03522.x.

Collet, J.-P., Moen, J.L., Veklich, Y.I., Gorkun, O.V., Lord, S.T., Montalescot, G., Weisel, J.W., 2005. The alphaC domains of fibrinogen affect the structure of the fibrin clot, its physical properties, and its susceptibility to fibrinolysis. Blood 106, 3824–3830. 10.1182/blood-2005-05-2150.

Cornwell, K.G., Pins, G.D., 2007. Discrete crosslinked fibrin microthread scaffolds for tissue regeneration. Journal of biomedical materials research. Part A 82, 104–112. 10.1002/jbm.a.31057.

Cumming, B.D., McElwain, D.L.S., Upton, Z., 2009. A mathematical model of wound healing and subsequent scarring. Journal of The Royal Society Interface 7, 19–34. 10.1098/rsif.2008.0536.

Dahlbäck, B., 2000. Blood coagulation. The Lancet 355, 1627–1632. 10.1016/S0140-6736(00)02225-X.

Dascombe, W.H., Dumanian, G., Hong, C., Heil, B.V., Labadie, K., Hessel, B., Blombäck, B., Johnson, P.C., 1997. Application of thrombin based fibrin glue and non-thrombin based batroxobin glue on intact human blood vessels: Evidence for transmural thrombin activity. Thrombosis and haemostasis 78, 947–951.

Debelle, L., Tamburro, A.M., 1999. Elastin: Molecular description and function. The International Journal of Biochemistry & Cell Biology 31, 261–272. 10.1016/S1357-2725(98)00098-3.

Diegelmann, R.F., Cohen, I.K., McCoy, B.J., 1979. Growth kinetics and collagen synthesis of normal skin, normal scar and keloid fibroblasts in vitro. Journal of cellular physiology 98, 341–346. 10.1002/jcp.1040980210.

Dubrovin, E.V., Barinov, N.A., Schäffer, T.E., Klinov, D.V., 2019. In Situ Single-Molecule AFM Investigation of Surface-Induced Fibrinogen Unfolding on Graphite. Langmuir : the ACS journal of surfaces and colloids 35, 9732–9739. 10.1021/acs.langmuir.9b01178.

Dutta, B., Vos, B.E., Rezus, Y.L.A., Koenderink, G.H., Bakker, H.J., 2018. Observation of Ultrafast Vibrational Energy Transfer in Fibrinogen and Fibrin Fibers. J. Phys. Chem. B 122, 5870–5876. 10.1021/acs.jpcb.8b03490.

Eyrich, D., Brandl, F., Appel, B., Wiese, H., Maier, G., Wenzel, M., Staudenmaier, R., Goepferich, A., Blunk, T., 2007. Long-term stable fibrin gels for cartilage engineering. Biomaterials 28, 55–65. 10.1016/j.biomaterials.2006.08.027.

Feinberg, A.W., Parker, K.K., 2010. Surface-initiated assembly of protein nanofabrics. Nano letters 10, 2184–2191. 10.1021/nl100998p.

Fisher, M.B., Mauck, R.L., 2013. Tissue Engineering and Regenerative Medicine: Recent Innovations and the Transition to Translation. Tissue Engineering Part B: Reviews 19, 1–13. 10.1089/ten.teb.2012.0723.

Forget, J., Awaja, F., Gugutkov, D., Gustavsson, J., Gallego Ferrer, G., Coelho-Sampaio, T., Hochman-Mendez, C., Salmeron-Sánchez, M., Altankov, G., 2016. Differentiation

of Human Mesenchymal Stem Cells Toward Quality Cartilage Using Fibrinogen-Based Nanofibers. Macromol. Biosci. 16, 1348–1359. 10.1002/mabi.201600080.

Fortelny, R.H., Schwab, R., Glaser, K.S., Puchner, K.U., May, C., König, F., Redl, H., Petter-Puchner, A.H., 2008. The assessment of quality of life in a trial on lightweight mesh fixation with fibrin sealant in transabdominal preperitoneal hernia repair. Hernia : the journal of hernias and abdominal wall surgery 12, 499–505. 10.1007/s10029-008-0365-1.

Foster, J.J., Temple, S.E., How, M.J., Daly, I.M., Sharkey, C.R., Wilby, D., Roberts, N.W., 2018. Polarisation vision: Overcoming challenges of working with a property of light we barely see. Die Naturwissenschaften 105, 27. 10.1007/s00114-018-1551-3.

Fowkes, F.G.R., Housley, E., Rattray, A., Lowe, G.D.O., Rumley, A., Elton, R.A., MacGregor, I.R., Dawes, J., 1993. Cross-linked fibrin degradation products, progression of peripheral arterial disease, and risk of coronary heart disease. The Lancet 342, 84–86. 10.1016/0140-6736(93)91288-W.

Fowler, W.E., Erickson, H.P., 1979. Trinodular structure of fibrinogen. Journal of Molecular Biology 134, 241–249. 10.1016/0022-2836(79)90034-2.

Fredenburgh, J.C., Leslie, B.A., Stafford, A.R., Lim, T., Chan, H.H., Weitz, J.I., 2013. Zn 2+ Mediates High Affinity Binding of Heparin to the αC Domain of Fibrinogen. J. Biol. Chem. 288, 29394–29402. 10.1074/jbc.M113.469916.

Goldstein, J.I., Newbury, D.E., Echlin, P., Joy, D.C., Fiori, C., Lifshin, E., 1981. Preparation of Biological Samples for Scanning Electron Microscopy, in: Goldstein, J.I., Newbury, D.E., Echlin, P., Joy, D.C., Fiori, C., Lifshin, E. (Eds.), Scanning Electron Microscopy and X-Ray Microanalysis. A Text for Biologist, Materials Scientist, and Geologists. Springer US, Boston, MA, pp. 495–539.

Greenfield, N.J., 1996. Methods to estimate the conformation of proteins and polypeptides from circular dichroism data. Analytical biochemistry 235, 1–10. 10.1006/abio.1996.0084.

Greenfield, N.J., 2006. Using circular dichroism spectra to estimate protein secondary structure. Nature protocols 1, 2876–2890. 10.1038/nprot.2006.202.

Gugutkov, D., Gustavsson, J., Ginebra, M.P., Altankov, G., 2013. Fibrinogen nanofibers for guiding endothelial cell behavior. Biomaterials Science 1, 1065–1069.

Guo, S., DiPietro, L.A., 2010. Factors Affecting Wound Healing. Journal of dental research 89, 219–229. 10.1177/0022034509359125.

Hämisch, B., Büngeler, A., Kielar, C., Keller, A., Strube, O., Huber, K., 2019. Self-Assembly of Fibrinogen in Aqueous, Thrombin-Free Solutions of Variable Ionic Strengths. Langmuir : the ACS journal of surfaces and colloids 35, 12113–12122. 10.1021/acs.langmuir.9b01515.

Harada, T., Kuroda, R., 2002. Circular Dichroism Measurement of a Protein in Dried Thin Films. Chem. Lett. 31, 326–327. 10.1246/cl.2002.326.

Heck, H.D., Casanova, M., Starr, T.B., 1990. Formaldehyde toxicity--new understanding. Critical reviews in toxicology 20, 397–426. 10.3109/10408449009029329.

Helbing, C., Stoeßel, R., Hering, D.A., Arras, M.M.L., Bossert, J., Jandt, K.D., 2016. pH-Dependent Ordered Fibrinogen Adsorption on Polyethylene Single Crystals. Langmuir : the ACS journal of surfaces and colloids 32, 11868–11877. 10.1021/acs.langmuir.6b03110.

Helms, C.C., Ariëns, R.A.S., Uitte de Willige, S., Standeven, K.F., Guthold, M., 2012. α−α Cross-Links Increase Fibrin Fiber Elasticity and Stiffness. Biophysical Journal 102, 168–175. 10.1016/j.bpj.2011.11.4016.

Hinsbergh, V.W.M., Collen, A., Koolwijk, P., 2001. Role of Fibrin Matrix in Angiogenesis. Annals of the New York Academy of Sciences 936, 426–437. 10.1111/j.1749-6632.2001.tb03526.x.

Hogan, K.A., Bolliger, B., Okumura, N., Lord, S.T., 2001. The Formation of β Fibrin Requires a Functional a Site. Annals of the New York Academy of Sciences 936, 219–222. 10.1111/j.1749-6632.2001.tb03509.x.

Hogg, P.J., Jackson, C.M., 1989. Fibrin monomer protects thrombin from inactivation by heparin-antithrombin III: Implications for heparin efficacy. Proceedings of the National Academy of Sciences 86, 3619–3623. 10.1073/pnas.86.10.3619.

Hornyak, T.J., Shafer, J.A., 2002. Interactions of factor XIII with fibrin as substrate and cofactor. Biochemistry 31, 423–429. 10.1021/bi00117a017.

Hotary, K.B., Yana, I., Sabeh, F., Li, X.-Y., Holmbeck, K., Birkedal-Hansen, H., Allen, E.D., Hiraoka, N., Weiss, S.J., 2002. Matrix Metalloproteinases (MMPs) Regulate Fibrin-invasive Activity via MT1-MMP–dependent and –independent Processes. Journal of Experimental Medicine 195, 295–308. 10.1084/jem.20010815.

Huang, S., Cao, Z., Davie, E.W., 1993. The role of amino-terminal disulfide bonds in the structure and assembly of human fibrinogen. Biochemical and biophysical research communications 190, 488–495. 10.1006/bbrc.1993.1074.

Janmey, P.A., Winer, J.P., Weisel, J.W., 2009. Fibrin gels and their clinical and bioengineering applications. Journal of the Royal Society, Interface 6, 1–10. 10.1098/rsif.2008.0327.

Kattula, S., Byrnes, J.R., Wolberg, A.S., 2017. Fibrinogen and Fibrin in Hemostasis and Thrombosis. Arteriosclerosis, thrombosis, and vascular biology 37, e13-e21. 10.1161/ATVBAHA.117.308564.

Kelly, S.M., Jess, T.J., Price, N.C., 2005. How to study proteins by circular dichroism. Biochimica et biophysica acta 1751, 119–139. 10.1016/j.bbapap.2005.06.005.

Kemp, J.C., 1969. Piezo-Optical Birefringence Modulators: New Use for a Long-Known Effect. J. Opt. Soc. Am. 59, 950. 10.1364/JOSA.59.000950.

Kishan, A.P., Nezarati, R.M., Radzicki, C.M., Renfro, A.L., Robinson, J.L., Whitely, M.E., Cosgriff-Hernandez, E.M., 2015. In situ crosslinking of electrospun gelatin for improved fiber morphology retention and tunable degradation. Journal of materials chemistry. B 3, 7930–7938. 10.1039/c5tb00937e.

KK Kane, 1984. Fibrinolysis--a review. Ann Clin Lab Sci 14, 443–449.

Kolehmainen, K., Willerth, S.M., 2012. Preparation of 3D fibrin scaffolds for stem cell culture applications. Journal of visualized experiments : JoVE, e3641. 10.3791/3641.

Kollman, J.M., Pandi, L., Sawaya, M.R., Riley, M., Doolittle, R.F., 2009. Crystal structure of human fibrinogen. Biochemistry 48, 3877–3886. 10.1021/bi802205g.

Koo, J., Galanakis, D., Liu, Y., Ramek, A., Fields, A., Ba, X., Simon, M., Rafailovich, M.H., 2012. Control of Anti-Thrombogenic Properties: Surface-Induced Self-Assembly of Fibrinogen Fibers. Biomacromolecules 13, 1259–1268.

Koo, J., Rafailovich, M.H., Medved, L., Tsurupa, G., Kudryk, B.J., Liu, Y., Galanakis, D.K., 2010. Evaluation of fibrinogen self-assembly: role of its \alphaC region. Journal of Thrombosis and Haemostasis 8, 2727–2735.

Kuipers, B.J.H., Gruppen, H., 2007. Prediction of molar extinction coefficients of proteins and peptides using UV absorption of the constituent amino acids at 214 nm to enable quantitative reverse phase high-performance liquid chromatography-mass spectrometry analysis. Journal of agricultural and food chemistry 55, 5445–5451. 10.1021/jf070337l.

Kular, J.K., Basu, S., Sharma, R.I., 2014. The extracellular matrix: Structure, composition, age-related differences, tools for analysis and applications for tissue engineering. J Tissue Eng 5, 204173141455711. 10.1177/2041731414557112.

Kundu, A., Kishore, N., 2004. 1,1,1,3,3,3-hexafluoroisopropanol induced thermal unfolding and molten globule state of bovine alpha-lactalbumin: Calorimetric and spectroscopic studies. Biopolymers 73, 405–420. 10.1002/bip.20014.

Kuroda, R., Honma, T., 2000. CD spectra of solid-state samples. Chirality 12, 269–277. 10.1002/(SICI)1520-636X(2000)12:4<269:AID-CHIR13>3.0.CO;2-P.

Laurens, N., Koolwijk, P., Maat, M.P.M. de, 2006. Fibrin structure and wound healing. Journal of thrombosis and haemostasis : JTH 4, 932–939. 10.1111/j.1538-7836.2006.01861.x.

Lenselink, E.A., 2015. Role of fibronectin in normal wound healing. Int Wound J 12, 313–316. 10.1111/iwj.12109.

Li, D., Xia, Y., 2004. Electrospinning of Nanofibers: Reinventing the Wheel? Advanced Materials 16, 1151–1170. 10.1002/adma.200400719.

Lim, B.B.C., Lee, E.H., Sotomayor, M., Schulten, K., 2008. Molecular Basis of Fibrin Clot Elasticity. Structure 16, 449–459. 10.1016/j.str.2007.12.019.

Litvinov, R.I., Faizullin, D.A., Zuev, Y.F., Weisel, J.W., 2012a. The α-Helix to β-Sheet Transition in Stretched and Compressed Hydrated Fibrin Clots. Biophysical Journal 103, 1020–1027. 10.1016/j.bpj.2012.07.046.

Litvinov, R.I., Mekler, A., Shuman, H., Bennett, J.S., Barsegov, V., Weisel, J.W., 2012b. Resolving two-dimensional kinetics of the integrin αIIbβ3-fibrinogen interactions using binding-unbinding correlation spectroscopy. The Journal of biological chemistry 287, 35275–35285. 10.1074/jbc.M112.404848.

Litvinov, R.I., Weisel, J.W., 2017. Fibrin mechanical properties and their structural origins. Matrix Biology 60-61, 110–123. 10.1016/j.matbio.2016.08.003.

Lorand, L., 2001. Factor XIII: Structure, activation, and interactions with fibrinogen and fibrin. Annals of the New York Academy of Sciences 936, 291–311. 10.1111/j.1749-6632.2001.tb03516.x.

Lorand, L., Downey, J., Gotoh, T., Jacobsen, A., Tokura, S., 1968. The transpeptidase system which crosslinks fibrin by γ-glutamyl-ε-lysine bonds. Biochemical and biophysical research communications 31, 222–230. 10.1016/0006-291X(68)90734-1.

Lutolf, M.P., Hubbell, J.A., 2005. Synthetic biomaterials as instructive extracellular microenvironments for morphogenesis in tissue engineering. Nat Biotechnol 23, 47–55. 10.1038/nbt1055.

Makin, O.S., Atkins, E., Sikorski, P., Johansson, J., Serpell, L.C., 2005. Molecular basis for amyloid fibril formation and stability. Proceedings of the National Academy of Sciences 102, 315–320. 10.1073/pnas.0406847102.

Makogonenko, E., Tsurupa, G., Ingham, K., Medved, L., 2002. Interaction of Fibrin(ogen) with Fibronectin: Further Characterization and Localization of the Fibronectin-Binding Site †. Biochemistry 41, 7907–7913. 10.1021/bi025770x.

Marguerie, G., 1977. The binding of calcium to fibrinogen: Some structural features. Biochimica et Biophysica Acta (BBA) - Protein Structure 494, 172–181. 10.1016/0005-2795(77)90145-3.

Mark, H., 1991. Principles and practice of spectroscopic calibration. Wiley, New York, NY, 170 pp.

Markwardt, F., Hoffmann, J., Körbs, E., 1973. The influence of synthetic thrombin inhibitors on the thrombin-antithrombin reaction. Thrombosis Research 2, 343–348. 10.1016/0049-3848(73)90044-3.

Matthews, J.A., Wnek, G.E., Simpson, D.G., Bowlin, G.L., 2002. Electrospinning of Collagen Nanofibers. Biomacromolecules 3, 232–238. 10.1021/bm015533u.

Mazlyzam, A.L., Aminuddin, B.S., Fuzina, N.H., Norhayati, M.M., Fauziah, O., Isa, M.R., Saim, L., Ruszymah, B.H.I., 2007. Reconstruction of living bilayer human skin equivalent utilizing human fibrin as a scaffold. Burns : journal of the International Society for Burn Injuries 33, 355–363. 10.1016/j.burns.2006.08.022.

McManus, M., Boland, E., Sell, S., Bowen, W., Koo, H., Simpson, D., Bowlin, G., 2007a. Electrospun nanofibre fibrinogen for urinary tract tissue reconstruction. Biomedical Materials 2, 257–262.

McManus, M.C., Boland, E.D., Koo, H.P., Barnes, C.P., Pawlowski, K.J., Wnek, G.E., Simpson, D.G., Bowlin, G.L., 2006. Mechanical properties of electrospun fibrinogen structures. Acta Biomater 2, 19–28.

McManus, M.C., Boland, E.D., Simpson, D.G., Barnes, C.P., Bowlin, G.L., 2007b. Electrospun fibrinogen: Feasibility as a tissue engineering scaffold in a rat cell culture model. Journal of Biomedical Materials Research Part A 81A, 299–309.

Micsonai, A., Wien, F., Bulyáki, É., Kun, J., Moussong, É., Lee, Y.-H., Goto, Y., Réfrégiers, M., Kardos, J., 2018. BeStSel: A web server for accurate protein secondary

structure prediction and fold recognition from the circular dichroism spectra. Nucleic acids research 46, W315-W322. 10.1093/nar/gky497.

Micsonai, A., Wien, F., Kernya, L., Lee, Y.-H., Goto, Y., Réfrégiers, M., Kardos, J., 2015. Accurate secondary structure prediction and fold recognition for circular dichroism spectroscopy. Proceedings of the National Academy of Sciences of the United States of America 112, E3095-103. 10.1073/pnas.1500851112.

Min, B.-M., Lee, G., Kim, S.H., Nam, Y.S., Lee, T.S., Park, W.H., 2004. Electrospinning of silk fibroin nanofibers and its effect on the adhesion and spreading of normal human keratinocytes and fibroblasts in vitro. Biomaterials 25, 1289–1297. 10.1016/j.biomaterials.2003.08.045.

Mirzaei-Parsa, M.J., Ghanizadeh, A., Ebadi, M.T.K., Faridi-Majidi, R., 2018. An alternative solvent for electrospinning of fibrinogen nanofibers. BME 29, 279–287. 10.3233/BME-181736.

Mittermayr, R., Wassermann, E., Thurnher, M., Simunek, M., Redl, H., 2006. Skin graft fixation by slow clotting fibrin sealant applied as a thin layer. Burns : journal of the International Society for Burn Injuries 32, 305–311. 10.1016/j.burns.2005.10.010.

Monroe, D.M., Hoffman, M., Roberts, H.R., 2002. Platelets and thrombin generation. Arteriosclerosis, thrombosis, and vascular biology 22, 1381–1389. 10.1161/01.atv.0000031340.68494.34.

Moreira, L.A., Boström, M., Ninham, B.W., Biscaia, E.C., Tavares, F.W., 2006. Hofmeister effects: Why protein charge, pH titration and protein precipitation depend on the choice of background salt solution. Colloids and Surfaces A: Physicochemical and Engineering Aspects 282-283, 457–463. 10.1016/j.colsurfa.2005.11.021.

Mosesson, M.W., 2005. Fibrinogen and fibrin structure and functions. Journal of thrombosis and haemostasis : JTH 3, 1894–1904. 10.1111/j.1538-7836.2005.01365.x.

Müllertz, S., 1974. Different molecular forms of plasminogen and plasmin produced by urokinase in human plasma and their relation to protease inhibitors and lysis of fibrinogen and fibrin. The Biochemical journal 143, 273–283. 10.1042/bj1430273.

Murayama, K., Wu, Y., Czarnik-Matusewicz, B., Ozaki, Y., 2001. Two-Dimensional/Attenuated Total Reflection Infrared Correlation Spectroscopy Studies on Secondary Structural Changes in Human Serum Albumin in Aqueous Solutions: PH-Dependent Structural Changes in the Secondary Structures and in the Hydrogen Bondings of Side Chains. J. Phys. Chem. B 105, 4763–4769. 10.1021/jp004537a.

Muszbek, L., Yee, V.C., Hevessy, Z., 1999. Blood Coagulation Factor XIII. Thrombosis Research 94, 271–305. 10.1016/S0049-3848(99)00023-7.

O'Brien, F.J., 2011. Biomaterials & scaffolds for tissue engineering. Materials Today 14, 88–95. 10.1016/S1369-7021(11)70058-X.

Odrljin, T.M., Francis, C.W., Sporn, L.A., Bunce, L.A., Marder, V.J., Simpson-Haidaris, P.J., 1996a. Heparin-Binding Domain of Fibrin Mediates Its Binding to Endothelial Cells. ATVB 16, 1544–1551. 10.1161/01.ATV.16.12.1544.

Odrljin, T.M., Shainoff, JR, Lawrence, S.O., Simpson-Haidaris, P.J., 1996b. Thrombin cleavage enhances exposure of a heparin binding domain in the N-terminus of the fibrin beta chain. Blood 88, 2050–2061. 10.1182/blood.V88.6.2050.bloodjournal8862050.

Ohkawa, K., Cha, D., Kim, H., Nishida, A., Yamamoto, H., 2004. Electrospinning of Chitosan. Macromol. Rapid Commun. 25, 1600–1605. 10.1002/marc.200400253.

Palta, S., Saroa, R., Palta, A., 2014. Overview of the coagulation system. Indian journal of anaesthesia 58, 515–523. 10.4103/0019-5049.144643.

Pechik, I., Yakovlev, S., Mosesson, M.W., Gilliland, G.L., Medved, L., 2006. Structural Basis for Sequential Cleavage of Fibrinopeptides upon Fibrin Assembly †,‡. Biochemistry 45, 3588–3597. 10.1021/bi0525369.

Pfützner, H., 2012. Angewandte Biophysik, 2nd ed. Springer, Vienna, 321 pp.

Picken, M.M., 2010. Fibrinogen amyloidosis: The clot thickens! Blood 115, 2985–2986. 10.1182/blood-2009-12-236810.

Pizzo, S.V., Schwartz, M.L., Hill, R.L., McKee, P.A., 1972. The effect of plasmin on the subunit structure of human fibrinogen. The Journal of biological chemistry 247, 636–645.

Protopopova, A.D., Barinov, N.A., Zavyalova, E.G., Kopylov, A.M., Sergienko, V.I., Klinov, D.V., 2015. Visualization of fibrinogen αC regions and their arrangement during fibrin network formation by high-resolution AFM. Journal of thrombosis and haemostasis : JTH 13, 570–579. 10.1111/jth.12785.

Raiskup, F., Spoerl, E., 2013. Corneal crosslinking with riboflavin and ultraviolet A. I. Principles. The ocular surface 11, 65–74. 10.1016/j.jtos.2013.01.002.

Rajangam, T., An, S.S.A., 2013. Fibrinogen and fibrin based micro and nano scaffolds incorporated with drugs, proteins, cells and genes for therapeutic biomedical applications. International Journal of Nanomedicine 8, 3641–3662. 10.2147/IJN.S43945.

Ramakrishnan, C., Ramachandran, G.N., 1965. Stereochemical Criteria for Polypeptide and Protein Chain Conformations. Biophysical Journal 5, 909–933. 10.1016/S0006-3495(65)86759-5.

Raoufi, M., Aslankoohi, N., Mollenhauer, C., Boehm, H., Spatz, J.P., Bruggemann, D., 2016. Template-assisted extrusion of biopolymer nanofibers under physiological conditions. Integrative biology : quantitative biosciences from nano to macro 8, 1059–1066. 10.1039/c6ib00045b.

Raoufi, M., Das, T., Schoen, I., Vogel, V., Bruggemann, D., Spatz, J.P., 2015. Nanopore Diameters Tune Strain in Extruded Fibronectin Fibers. Nano letters 15, 6357–6364. 10.1021/acs.nanolett.5b01356.

Reichert, J., Wei, G., Jandt, K.D., 2009. Formation and Topotactical Orientation of Fibrinogen Nanofibrils on Graphite Nanostructures. Advanced Engineering Materials 11, B177-B181.

Reimer, L., 1998. Scanning Electron Microscopy: Physics of Image Formation and Microanalysis. Springer Berlin Heidelberg, Berlin, Heidelberg, s.l., 529 pp.

Rosenberg, R.D., 1989. Biochemistry of heparin antithrombin interactions, and the physiologic role of this natural anticoagulant mechanism. The American Journal of Medicine 87, S2-S9. 10.1016/0002-9343(89)80523-6.

Santoro, E., Agresta, F., Buscaglia, F., Mulieri, G., Mazzarolo, G., Bedin, N., Mulieri, M., 2007. Preliminary experience using fibrin glue for mesh fixation in 250 patients undergoing minilaparoscopic transabdominal preperitoneal hernia repair. Journal of laparoendoscopic & advanced surgical techniques. Part A 17, 12–15. 10.1089/lap.2006.0107.

Schatten, H., 2011. Low voltage high-resolution SEM (LVHRSEM) for biological structural and molecular analysis. Micron (Oxford, England : 1993) 42, 175–185. 10.1016/j.micron.2010.08.008.

Schatten, H., Pawley, J.B. (Eds.), 2008. Biological Low-Voltage Scanning Electron Microscopy. Springer Science+Business Media LLC, New York, NY.

Sell, S., Barnes, C., Simpson, D., Bowlin, G., 2008a. Scaffold permeability as a means to determine fiber diameter and pore size of electrospun fibrinogen. Journal of Biomedical Materials Research Part A 85A, 115–126.

Sell, S.A., Francis, M.P., Garg, K., McClure, M.J., Simpson, D.G., Bowlin, G.L., 2008b. Cross-linking methods of electrospun fibrinogen scaffolds for tissue engineering applications. Biomedical Materials 3, 45001–45012.

Shireman, P.K., Greisler, H.P., 1998. Fibrin sealant in vascular surgery: A review. Journal of long-term effects of medical implants 8, 117–132.

Sierra, D.H., 1993. Fibrin sealant adhesive systems: A review of their chemistry, material properties and clinical applications. Journal of biomaterials applications 7, 309–352. 10.1177/088532829300700402.

Sporn, L.A., Bunce, L.A., Francis, C.W., 1995. Cell proliferation on fibrin: Modulation by fibrinopeptide cleavage. Blood 86, 1802–1810.

Spraggon, G., Everse, S.J., Doolittle, R.F., 1997. Crystal structures of fragment D from human fibrinogen and its crosslinked counterpart from fibrin. Nature 389, 455–462. 10.1038/38947.

Stapelfeldt, K., Stamboroski, S., Mednikova, P., Brüggemann, D., 2019a. Fabrication of 3D-nanofibrous fibrinogen scaffolds using salt-induced self assembly. Biofabrication 11, 25010. 10.1088/1758-5090/ab0681.

Stapelfeldt, K., Stamboroski, S., Walter, I., Suter, N., Kowalik, T., Michaelis, M., Brüggemann, D., 2019b. Controlling the Multiscale Structure of Nanofibrous Fibrinogen Scaffolds for Wound Healing. Nano letters 19, 6554–6563. 10.1021/acs.nanolett.9b02798.

Stein, T.P., Leskiw, M.J., Wallace, H.W., 1978. Measurement of half-life human plasma fibrinogen. The American journal of physiology 234, D504-10. 10.1152/ajpendo.1978.234.5.E504.

Teo, W.E., Ramakrishna, S., 2006. A review on electrospinning design and nanofibre assemblies. Nanotechnology 17, R89. 10.1088/0957-4484/17/14/R01.

Toyama, B.H., Weissman, J.S., 2011. Amyloid Structure: Conformational Diversity and Consequences. Annual review of biochemistry 80, 557–585. 10.1146/annurev-biochem-090908-120656.
van Kampen, C.L., Gibbons, D.F., Jones, R.D., 1979. Effect of implant surface chemistry upon arterial thrombosis. J. Biomed. Mater. Res. 13, 517–541. 10.1002/jbm.820130402.
Vikinge, T.P., Hansson, K.M., Sandström, P., Liedberg, B., Lindahl, T.L., Lundström, I., Tengvall, P., Höök, F., 2000. Comparison of surface plasmon resonance and quartz crystal microbalance in the study of whole blood and plasma coagulation. Biosensors and Bioelectronics 15, 605–613. 10.1016/S0956-5663(00)00125-1.
Vogel, V., 2018. Unraveling the Mechanobiology of Extracellular Matrix. Annu. Rev. Physiol. 80, 353–387. 10.1146/annurev-physiol-021317-121312.
Wang, J., Wang, H., Wang, Y., Li, J., Su, Z., Wei, G., 2014. Alternate layer-by-layer assembly of graphene oxide nanosheets and fibrinogen nanofibers on a silicon substrate for a biomimetic three-dimensional hydroxyapatite scaffold. J. Mater. Chem. B 2, 7360–7368. 10.1039/C4TB01324G.
Wang, S., Han, X., Wang, Y., Li, K., 2019. Dispersion of the Retardation of a Photoelastic Modulator. Applied Sciences 9, 341. 10.3390/app9020341.
Wasilewska, M., Adamczyk, Z., Jachimska, B., 2009. Structure of fibrinogen in electrolyte solutions derived from dynamic light scattering (DLS) and viscosity measurements. Langmuir : the ACS journal of surfaces and colloids 25, 3698–3704. 10.1021/la803662a.
Wei, G., Reichert, J., Bossert, J., Jandt, K.D., 2008a. Novel Biopolymeric Template for the Nucleation and Growth of Hydroxyapatite Crystals Based on Self-Assembled Fibrinogen Fibrils. Biomacromolecules 9, 3258–3267.
Wei, G., Reichert, J., Jandt, K.D., 2008b. Controlled self-assembly and templated metallization of fibrinogen nanofibrils. Chemical communications, 3903-3.
Wei, G., Su, Z., Reynolds, N.P., Arosio, P., Hamley, I.W., Gazit, E., Mezzenga, R., 2017. Self-assembling peptide and protein amyloids: From structure to tailored function in nanotechnology. Chemical Society reviews 46, 4661–4708. 10.1039/c6cs00542j.
Weisel, J.W., MEDVED, L., 2001. The structure and function of the alpha C domains of fibrinogen. Annals of the New York Academy of Sciences 936, 312–327. 10.1111/j.1749-6632.2001.tb03517.x.
Weisel, J.W., Stauffacher, C.V., Bullitt, E., Cohen, C., 1985. A model for fibrinogen: Domains and sequence. Science (New York, N.Y.) 230, 1388–1391. 10.1126/science.4071058.
Weisel, J.W., Veklich, Y., Gorkun, O., 1993. The sequence of cleavage of fibrinopeptides from fibrinogen is important for protofibril formation and enhancement of lateral aggregation in fibrin clots. Journal of Molecular Biology 232, 285–297. 10.1006/jmbi.1993.1382.
Weitz, J.I., Hudoba, M., Massel, D., Maraganore, J., Hirsh, J., 1990. Clot-bound thrombin is protected from inhibition by heparin-antithrombin III but is susceptible to inactivation

by antithrombin III-independent inhibitors. The Journal of clinical investigation 86, 385–391. 10.1172/JCI114723.

Weitz, J.I., Leslie, B., 1990. Urokinase has direct catalytic activity against fibrinogen and renders it less clottable by thrombin. The Journal of clinical investigation 86, 203–212. 10.1172/JCI114685.

Williamson, M.P., 1994. The structure and function of proline-rich regions in proteins. The Biochemical journal 297 (Pt 2), 249–260. 10.1042/bj2970249.

Wnek, G.E., Carr, M.E., Simpson, D.G., Bowlin, G.L., 2003. Electrospinning of Nanofiber Fibrinogen Structures. Nano letters 3, 213–216.

Yee, V.C., Pratt, K.P., Côté, H.C., Trong, I.L., Chung, D.W., Davie, E.W., Stenkamp, R.E., Teller, D.C., 1997. Crystal structure of a 30 kDa C-terminal fragment from the gamma chain of human fibrinogen. Structure (London, England : 1993) 5, 125–138.

Zeugolis, D.I., Khew, S.T., Yew, E.S.Y., Ekaputra, A.K., Tong, Y.W., Yung, L.-Y.L., Hutmacher, D.W., Sheppard, C., Raghunath, M., 2008. Electro-spinning of pure collagen nano-fibres - just an expensive way to make gelatin? Biomaterials 29, 2293–2305. 10.1016/j.biomaterials.2008.02.009.

Zhang, G., Wang, X., Wang, Z., Zhang, J., Suggs, L., 2006. A PEGylated fibrin patch for mesenchymal stem cell delivery. Tissue engineering 12, 9–19. 10.1089/ten.2006.12.9.

Zhang, L., Casey, B., Galanakis, D.K., Marmorat, C., Skoog, S., Vorvolakos, K., Simon, M., Rafailovich, M.H., 2017. The influence of surface chemistry on adsorbed fibrinogen conformation, orientation, fiber formation and platelet adhesion. Acta biomaterialia 54, 164–174. 10.1016/j.actbio.2017.03.002.

Zhang, Y., Cremer, P.S., 2006. Interactions between macromolecules and ions: The Hofmeister series. Current opinion in chemical biology 10, 658–663. 10.1016/j.cbpa.2006.09.020.

Zhu, J., Kaufman, L.J., 2014. Collagen I Self-Assembly: Revealing the Developing Structures that Generate Turbidity. Biophysical Journal 106, 1822–1831. 10.1016/j.bpj.2014.03.011.

Zuev, Y.F., Litvinov, R.I., Sitnitsky, A.E., Idiyatullin, B.Z., Bakirova, D.R., Galanakis, D.K., Zhmurov, A., Barsegov, V., Weisel, J.W., 2017. Conformational Flexibility and Self-Association of Fibrinogen in Concentrated Solutions. The journal of physical chemistry. B 121, 7833–7843. 10.1021/acs.jpcb.7b05654.

9. Acknowledgements

First of all, I would like to thank Prof. Dr. Dorothea Brüggemann for giving me the opportunity to join her working group for my doctoral thesis. I am thankful for her guidance, her supervision and scientific discussion.

I would like to especially thank her for her efforts allowing me to start this thesis and for her efforts making it possible to complete this thesis.

Secondly, I would like to thank Prof. Dr. Monika Fritz for agreeing to review this thesis and for her advice and ideas she contributed to this project during the Biophysics seminars.

My special thanks go to Monika Michaelis who taught me to measure and to interpret circular dichroism. I am thankful for her advice and her diplomatic skills.

I also would like to thank especially Naiana Suter for being one of the best colleagues, motivational coaches, friends and housekeepers I know. One of the other best colleagues that I would like to thank is of course Dr. Jana Markhoff. I will miss all the scientific and nonscientific discussions I had with both of you.

Thanks also to Eva Eilers who contributed to a lot of basic infrastructure, a lot of work and even more cake, without which the thesis would not have been possible.

Furthermore, I would like to thank all the other members and students of the Biophysics Institute. Thank you for the amazing times we had.

Last but not least I would like to thank all of my friends and family members who supported me during the past years.

10. Eigenständigkeitserklärung

Hiermit versichere ich, dass ich

1. die Arbeit ohne unerlaubte fremde Hilfe angefertigt habe,

2. keine anderen als die von mir angegeben Quellen und Hilfsmittel benutzt habe,

3. die, den benutzten Werken wörtlich oder inhaltlich entnommenen Stellen als solche kenntlich gemacht habe.

Des Weiteren versichere ich, dass ich mich bisher keinem Promotionsverfahren unterzogen bzw. ein solches beantragt habe.

Ich bin damit einverstanden, dass eine Überprüfung der Dissertation mit qualifizierter Software im Rahmen der Untersuchung von Plagiatsvorwürfen gestattet ist.

Datum: _____ Unterschrift: _____